Sleep-Like Neurophysiology Under

Chloral Hydrate and Urethane Anesthesia

by

Rachel Ward-Flanagan

A thesis submitted in partial fulfillment of the requirements for the degree of

Doctor of Philosophy

Neuroscience
University of Alberta

© Rachel Ward-Flanagan, 2023

Abstract

Sleep is a vital neurobiological process, yet despite its fundamental significance, delineating the endogenous neural pathways involved has been slow to progress due to a lack of diverse sleep models. Anesthesia, which has direct behavioural parallels to natural sleep, and which is often linked with endogenous sleep-wake systems on both mechanistic and physiological levels, is an obvious choice to model specific components of sleep. In particular, the research anesthetic urethane has long been regarded as an unparalleled model for the archetypical electrophysiological dynamics of natural sleep; specifically, the spontaneous alternations between both activated and deactivated forebrain states, and accompanying physiological measures.

Yet, there have remained a few drawbacks for urethane as a model for sleep. First, it remained undetermined how urethane promoted its sleep-like neurophysiological effects, and second that urethane is limited to acute experimental paradigms due to ethical considerations. Consequently, the overall aim of my thesis was twofold: to determine if any anesthetics not limited to acute experimental paradigms produced sleep-like alternations in neurophysiology at a surgical plane, and to assess if sleep and urethane had similar profiles of neural activity in known sleep-wake nuclei.

In Chapter 2, I used identical recording conditions to compare the spontaneous brain states of five common research anesthetics with urethane anesthesia. At a surgical plane of anesthesia, three of the anesthetics tested produced a coma-like brain state of burst-suppression activity (pentobarbital, isoflurane, and propofol), ketamine-xylazine produced synchronized slow-oscillatory state akin to slow-wave sleep. Critically, any changes to a state of forebrain activation under these anesthetics coincided with a loss of the surgical plane of anesthesia.

Conversely, chloral hydrate produced sleep-like spontaneous alternations of brain state, comparable to those observed under urethane. Unlike the other anesthetics, these alternations were not due to changes in anesthetic depth. Thus, I showed that chloral hydrate could provide an alternate model to urethane for sleep-like brain state alternations in non-acute experimental paradigms.

In Chapter 3, using c-Fos immunoreactivity as a proxy for neural activity, I showed that urethane anesthesia produced a similar pattern of neural activation in known sleep-wake nuclei as unpressured natural sleep. Animals engaging in pressured sleep (also referred to as recovery sleep) following sleep-deprivation had slightly different patterns of neural activation, likely due to the rebound of slow-wave sleep following sleep deprivation. Patterns of neural activity across unpressured (no sleep-deprivation) sleep, and both pressured and unpressured urethane were highly comparable. It is important to note, that all sleep and urethane groups had patterns of neural activation that were vastly divergent from the forced wake behavioural group, indicating that differences between sleep and urethane groups were not due to arousal. This study shows that neural activity under urethane is highly stereotyped, and most representative of normal sleep state architecture in rats.

In Chapter 4, I investigated the assertion that chloral hydrate provides insufficient analgesia for surgical manipulations. The majority of these claims were in reference textbooks, and were in direct conflict with the evidence in primary literature. In agreement with the primary literature, my results showed that intravenous chloral hydrate significantly increased tail withdrawal latencies to a noxious thermal stimulus. Furthermore, as some trials did result in a tail flick response, it is clear that this effect is due to analgesia, not immobility. This was also confirmed by the absence of changes in heart or respiration rate to the nociceptive stimulus. With

these experiments I showed that chloral hydrate provides sufficient analgesia to be used as a sole anesthetic, and therefore if used as a model of sleep will not require additional analgesics which could influence experimental outcomes.

In Chapter 5, I characterized in detail the strengths and weaknesses of chloral hydrate as a pharmacological model of sleep. Chloral hydrate produces an incredibly similar neurophysiological profile to both sleep and urethane, including individual brain states of forebrain activation and deactivation, the timing of the alternations between these states, and the sensitivity of these alternations to cholinergic manipulations. Furthermore, respiratory rate, respiratory variability and sighs all fluctuate as a function of brain state the same way under sleep, urethane and chloral hydrate. There are some minor differences between sleep, urethane and chloral hydrate, including an overall slowing of hippocampal theta during forebrain activation that occurs in both anesthetics, although this occurs more profoundly under chloral hydrate. Additionally, there were no discernable changes in heart rate across state under chloral hydrate. However, when these caveats are accounted for in an experimental design, chloral hydrate represents an exciting new tool to model sleep-like brain state and breathing without the constraints of an acute paradigm.

Increasingly, the overlaps and divergences between components of sleep and specific anesthetic agents are offering insight into pharmacological mechanisms and fundamental nuclei involved in the induction and maintenance of unconsciousness. The results of my thesis suggest that urethane and chloral hydrate could be invaluable tools to probe the intersections of sleep and anesthesia.

Preface

Chapter 1 of this thesis is based upon a review chapter that I wrote for the Handbook of Sleep Research, but it contains substantial changes to the original text based on important updates that have occurred since the initial publication. The original version of this chapter was published as Ward-Flanagan, R., & Dickson, C. T. (2019). Neurobiological parallels, overlaps, and divergences of sleep and anesthesia. In *Handbook of Behavioral Neuroscience* (Vol. 30, pp. 223-236). Elsevier. DOI: doi.org/10.1016/B978-0-12-813743-7.00015-3.

In addition to my own work, Chapters 2, 3 and 5 of this thesis includes important work from Alto Lo, Elizabeth Clement and Nicholas Silver. The work presented in Chapter 2 was initially a project led by Alto Lo, and contains data collected by Alto Lo, Elizabeth Clement and Trish Wolansky. This data comprised the urethane, pentobarbital, isoflurane and ketamine-xylazine experiments, as well as the initial analyses of this data. I completed the project by collecting the data for the chloral hydrate and propofol experiments, and compiling the data. I was responsible for all final analyses and writing presented in Chapter 2.

Additionally, Chapter 2 has been published as Ward-Flanagan, R., Lo, A. S., Clement, E. A., & Dickson, C. T. (2022). A comparison of brain-state dynamics across common anesthetic agents in male Sprague-Dawley rats. *International Journal of Molecular Sciences*, *23*(7), 3608. DOI: doi.org/10.3390/ijms23073608. Final analyses, figure creation and manuscript composition were conducted by me. As supervisory author, CT Dickson contributed to concept formation, methodological planning, data analysis and figure creation. All authors contributed to manuscript edits.

The work in Chapter 3 was co-authored with Nicholas Silver. I proposed the original concept for the project, but Nicholas helped me refine it, and we developed the protocol together. Nicholas performed the c-Fos immunohistochemistry, but otherwise all data and analyses were collected and performed equally. This project was an opportunity not only to answer a research question, but also to learn important mentorship skills, and I am grateful to Nicholas for the experience. In Chapter 5, Nicholas also graciously helped analyze the respiration and heart rate data.

Chapter 4 has also been published as Ward-Flanagan, R., & Dickson, C. T. (2023). Intravenous chloral hydrate anesthesia provides appropriate analgesia for surgical interventions in male Sprague-Dawley rats. *Plos one*, *18*(6), e0286504. DOI: doi.org/10.1371/journal.pone.0286504. All data collection, analyses, figure creation and manuscript composition were conducted by me. As supervisory author, CT Dickson contributed to concept formation, methodological planning, data analysis and figure creation.

Otherwise, all ideas, data and analyses presented here are my own, or have been developed in collaboration with my supervisor Dr. Clayton Dickson. This thesis is part of a larger project that received ethics approval University of Alberta Biosciences Animal Care and Use Committee (AUP00000092; project name: Cellular and Network Dynamics of Neo- and Limbic-Cortical Brain Structures).

Even a soul submerged in sleep

is hard at work and helps

make something of the world

Heraclitus, 500 BCE

From *Fragments*

Acknowledgements

The work in this thesis was supported by a Discovery grant from the Natural Sciences and Engineering Council of Canada (NSERC) awarded to Clayton Dickson (2016-06576, 2021-02926), as well as an NSERC Doctoral Postgraduate Scholarship (PGS-D), and an Alberta Graduate Excellence Scholarship (AGES) awarded to me.

I would like first and foremost, to thank my supervisor Dr. Clayton Dickson for his support and guidance throughout my many years in the lab. No matter what, I have always felt that Clay was in my corner, and that he believed in me no matter whatever endeavour I undertook, both in and outside of the lab. His passion for science and curiosity are infectious – I would go to Clay with one question, and inevitably leave with an answer that had spawned five new questions, a series of new experiments, and a page full of notes hastily scribbled in my excitement. I could not have asked for a better mentor, and lab dad. Thanks, Clay.

I would also like to thank my supervisory committee members, Dr. Greg Funk and Dr. Jesse Jackson. Throughout my degree, I benefitted from the interesting papers they suggested for reading, and the thought-provoking questions they raised about my own data. I have immensely enjoyed our conversations, even when they were in an exam setting, and I have always come away with new ideas, and a renewed appreciation for science.

I also want to extend my thanks to members of the Brain Rhythm Lab, both past and present. The community within our lab is second to none, and I am truly grateful to have made so many incredible friends during my time here. In particular, I would like to thank my mind-twin Brandon, who I met on the first day of my PhD, and who is one of my best friends to this day. Coming into work every day is a lot easier when you know you get to crack jokes, listen to

music, and maybe drink a beer with one of your best friends! I would also like to thank Aakanksha and Nick – watching both of you become the amazing scientists you are today will forever be one of my most treasured memories of my time in the lab.

Finally, I would like to thank my family and friends. To my parents, Ali and Tom, I would like to say thank you for putting up with me always asking “why?” ever since I was little, and fostering that curiosity, as it has carried me all the way through graduate school. To my partner Thorbjorn, thank you for making sure I stayed alive, and (somewhat) sane through both candidacy and preparing this thesis. I am incredibly lucky to pursue this dream and I am so thankful you’ve always supported me in chasing it.

Table of Contents

List of Tables

List of Figures

1 Introduction

Introduction

1.1 The unconscious brain

The ouroboros of the brain contemplating itself has been an inexhaustible source of artistic, philosophical and scientific discourse - we have sought to answer who we are by understanding how we think. In the pursuit to unravel the origin of conscious thought, our understanding of the brain has evolved along with our approach; from the theory of mind-body dualism in early philosophy (Descartes, 1984), to the observation of dual consciousness in split-brain patients (LeDoux et al., 1977; LeDoux et al., 2020), to probing the neural correlates of consciousness with modern neuroscientific techniques (Koch et al., 2016). With these scientific advances has also come the recognition that consciousness is only half the story, and that, given the ubiquitous nature of both sleep and the susceptibility to anesthesia across species, it is just as vital to explore the reciprocal state of unconsciousness (Kelz and Mashour, 2019).

The significance of the unconscious brain becomes obvious when considering the myriad of negative health outcomes associated with insufficient sleep, including, but not limited to: increased risk of cardiovascular disease, type 2 diabetes, depression, inflammation, chronic pain and in the event of prolonged total sleep deprivation, even death (Rechtschaffen et al., 2002; Altevogt and Colten, 2006; Irwin et al., 2016; Haack et al., 2020). What is more, the unconscious state produced by anesthesia is crucial to the success of modern medicine, enabling over 300 million life-saving surgeries annually (Brown et al., 2010; Weiser et al., 2015). However, in spite of growing awareness, research in the field of unconsciousness is still relatively emergent, meaning many of the fundamental functions and mechanisms of unconsciousness have yet to be delineated. For instance, although we spend approximately one third of our lives asleep, it is only

within the last century that sleep has gone from being regarded as merely the cessation of waking due to reduced external stimuli, to a dynamic process required for optimal physiological and psychological functioning, and ultimately survival (Aserinsky, 1965; Rechtschaffen et al., 2002; Tung and Mendelson, 2004). Consequently, the evolutionary function of sleep remains unknown, likely due in part to the absence of a universally accepted definition of (un)consciousness, which has been a matter of contention throughout scientific history, and presently remains an active topic of debate (Pal and Mashour, 2011; Seth and Bayne, 2022). This lack of consensus similarly affects studies aiming to establish a generalized theory of anesthesia; explaining how agents with disparate pharmacological effects can yield the same discrete clinical endpoints (Adapa, 2017). Despite these unknowns, the inevitable convergence of sleep and anesthesia research has provided the most promising path to understanding the neural mechanisms underlying the induction and maintenance of unconsciousness.

On the surface, the unconsciousness produced by sleep and anesthesia is near identical due to their shared behavioural parallels, including a reversible loss of consciousness, decreased sensory awareness and reduced behavioural responsiveness (Shafer, 1995; Vacas et al., 2013). These similarities are so striking that "being put to sleep" is a long-standing and universal colloquialism for anesthesia. The association is not without merit, as sleep and anesthesia respectively represent physiological and pharmacological facets of an altered state of brain operation. Increasingly, evidence of mechanistic overlaps beyond behavioural indices have been reported in sleep and anesthesia research, indicating that unconsciousness in sleep and anesthesia may arise from shared neurobiological mechanisms (Lydic and Baghdoyan, 2005; Franks, 2008; Adapa, 2017; Franks and Wisden, 2021). Some of the more compelling parallels include: that anesthetic potency is modulated by sleep deprivation (Tung et al., 2002), that total or slow-wave

sleep debt can be attenuated by specific anesthetic agents (Tung et al., 2004; Nelson et al., 2010; Pal et al., 2011) that the neuroanatomical targets of anesthetic agents are also involved in endogenous sleep pathways (Nelson et al., 2002; Franks, 2008; Leung et al., 2014; Gelegen et al., 2018), and that optogenetic activation of neurons previously activated by anesthesia promotes slow-wave sleep (Jiang-Xie et al., 2019). Consequently, it has become progressively recognised that some anesthetics may co-opt endogenous sleep-promoting circuits to produce unconsciousness (Moody et al., 2021), and that anesthesia can be used as a tool to model specific components of natural sleep (Ward-Flanagan et al., 2022).

Nonetheless, as an endogenous process, sleep is distinct from anesthesia. Most notably, sleep differs from anesthesia in that it is homeostatically regulated, reversible by external stimuli, and spontaneously occurring (Tung and Mendelson, 2004; Mashour and Pal, 2012). However, despite these differences, anesthesia offers an alternative experimental paradigm for situations where the use of a naturally sleeping preparation is problematic. For example, in instances where experimental control is vital, anesthesia affords tractable opportunities to perform manipulations which might cause a naturally sleeping subject to awaken. In addition, anesthesia can also alleviate potential ethical challenges related to experimental control in naturally sleeping animals (Clement et al., 2008; Mashour et al., 2022). Thus, a pharmacological model of sleep not only provides a means of testing sleep-like neurophysiology using experimental techniques that may not be feasible in natural sleep, but also an unconscious state to compare and contrast with natural sleep. As separate physiological and pharmacological conditions, sleep and anesthesia are essentially two sides of the same coin, namely unconsciousness. Consequently, any parity in neuroanatomical targets warrants further investigation as a potential factor in the initiation and maintenance of unconsciousness.

The deductive power provided by overlaps among multiple pharmacological mechanisms of anesthesia and the multiple endogenous elements of natural sleep cannot be ignored, as the study of sleep and anesthesia mutually inform one another, and advancement in one field precipitates advancement in the other. More specifically, understanding how sleep and anesthetic agents with disparate mechanisms of action relate to one another in terms of neurophysiology is the first step in deducing how unconsciousness is initiated and maintained, and reversed. In this chapter I will provide an overview of the current knowledge of shared neural pathways, neuromodulators and electrophysiological characteristics of sleep and anesthesia. In subsequent chapters, I will detail my own research comparing multiple anesthetics and sleep.

1.2 Sleep

Sleep is a behavioural state objectively and operationally defined by behavioral unresponsiveness and a reversible, perceptual disengagement from the environment (Carskadon and Dement, 2005). While sleep has been a topic of philosophical discussions since early human history, the lexicon surrounding it remained highly speculative until the invention of the electroencephalogram (EEG) by Hans Berger in 1924 (Gloor, 1969). This revolutionary technology allowed for the first empirical measurements of sleep states and initiated an intense research effort to describe brain activity in various states of consciousness, including sleep (Blake and Gerard, 1937; Gottesmann, 2001). The culmination of these early efforts were the seminal experiments of Aserinsky and Kleitman in 1953, which revolutionized the canonical understanding of sleep with the first description of rapid-eye movement (REM) sleep: a desynchronized brain state characterized by low-voltage, fast cortical EEG activity antithetical to the synchronized high-voltage, low-frequency cortical activity of which sleep was previously thought to be solely comprised (Aserinsky and Kleitman, 1953; Gottesmann, 2001; Pal and

Mashour, 2011). Critically, it became understood that sleep is not a unitary, deactivated state, but an active neurobiological process with dynamic alternations between two distinct states: REM and non-REM.

REM sleep - also known as paradoxical sleep for its electrophysiological resemblance to an alert, wakeful state, despite the high arousal threshold to evoke wakefulness - is characterized by low-voltage, high-frequency cortical activity, concomitant with larger amplitude, rhythmic activity in the hippocampus of both humans (~2 – 7 Hz) and rodents (~6 – 9 Hz) (Bland, 1986; Bodizs et al., 2001; Buzsaki, 2002; Cantero et al., 2003). Elevated sympathetic activity associated with this activated EEG state affects physiological correlates, resulting in: increased heart rate; a reduction in thermal regulation; increased brain metabolism and cerebral blood flow; and an almost complete atonia of skeletal muscles, including upper airway respiratory musculature, resulting in increased irregular respiration (Rechtschaffen and Siegel, 2000; Horner, 2008; Pagliardini et al., 2013a). Physiological activity in REM sleep can further be dissociated into two sub-categories: tonic features, which are primarily comprised of the archetypical REM-induced muscle atonia; and phasic features which are comprised of the hallmark rapid saccadic eye movements of REM, and muscle twitches in both extremities and middle ear muscles (Aserinsky, 1965; Rechtschaffen and Siegel, 2000; Mashour and Pal, 2012). Both tonic and phasic events occur in a typical REM epoch (Pagliardini et al., 2013a).

All other sleep falls under the broad classification of non-REM (NREM) sleep, which is a state characterized by high-voltage, low-frequency electrophysiological activity (Rechtschaffen and Siegel, 2000). Non-REM in humans is comprised of three stages of increasingly deep sleep, with transitions following a stereotyped progression from light NREM (stages N1 and N2) to deep NREM (stage N3) and back through light NREM stages to REM. This cycle takes

approximately 90 minutes and repeats 4-5 times over a full sleep sequence (Carskadon and Dement, 2005). Light NREM onset is marked by the amplified EEG activity in lower frequency bands, increased spindle activity, and K-complexes; whereas deep NREM is typified by the large amplitude, synchronized slow oscillations of slow-wave sleep (SWS) in both the neocortex and hippocampus (Wolansky et al., 2006; Brown et al., 2012). Physiologically, NREM is relatively quiescent in comparison to REM, with depressed, but stable cardiovascular, respiratory, and metabolic activity. Additionally, body temperature and skeletal muscle tone are reduced during NREM sleep in comparison to wake (Carskadon and Dement, 2005). Thus, REM and NREM represent two distinct electrophysiological states that are also discrete in terms of other physiological variables.

1.2.1 Sleep-wake circuitry

The first insight into the discrete nuclei underlying sleep-wake regulation came almost a century ago, when Constantin von Economo observed differences in the post-mortem neuropathology of patients with encephalatica lethargica, which depended on the presentation of their symptoms: either extreme lethargy or insomnia. These observations led him to propose that the anterior hypothalamic area was involved in sleep regulation, while the posterior hypothalamic and brainstem areas regulated wakefulness (von Economo, 1930). His hypothesis was confirmed by the identification of one of the most potent sleep-promoting brain nuclei, the ventrolateral pre-optic area (VLPO) in the anterior hypothalamus, and the wake-promoting histaminergic tuberomammillary nucleus (TMN) in the posterior hypothalamus (Yang and Hatton, 1997; Steriade and McCarley, 2005). Over time, the theories regarding the central

control of sleep and arousal have consistently been refined and revised, reflecting the ever evolving knowledge base of sleep-wake nuclei and associated neuromodulators.

As a brief overview of the prevailing ideas regarding sleep-wake circuitry over the last 30 years (for an excellent review of earlier landmarks in the history of sleep research see Pelayo and Dement (2017)), sleep-promoting influences were thought to predominantly arise from nuclei in the VLPO area of the hypothalamus through GABAergic inhibition of wake-promoting nuclei (Sherin et al., 1998). Monoaminergic neurons in the locus coeruleus (LC - noradrenergic), dorsal raphe nuclei (DRN - serotonergic), and TMN (histaminergic), in conjunction with cholinergic neurons in the pedunculopontine tegmentum (PPT) and laterodorsal tegmentum (LDT), were accepted as the main wake-promoting system (Saper et al., 2005). This wake-promoting ascending arousal system (sometimes called the ascending reticular activating system) was thought to exert global effects to the cortex through the innervation of the thalamus, hypothalamus, and basal forebrain (BF) (Saper and Fuller, 2017). However, lesion studies targeting these assumed wake-promoting neurons revealed that monoaminergic and cholinergic neuromodulatory influences may not be the driving forces behind wakefulness, as once thought. In fact, lesioning individual components of the ascending arousal system, such as the noradrenergic neurons in the LC (Gompf et al., 2010), cholinergic neurons in the BF (Fuller et al., 2011), or both systems concurrently (Blanco-Centurion et al., 2007), appears to have no clear effect on the amount of sleep-wake states (Saper and Fuller, 2017).

Thus, a novel hypothesis arguing that shifts in brain state, including arousal, NREM and REM sleep are driven primarily by the fast neurotransmitters glutamate and GABA has steadily gained momentum (Luppi et al., 2006; Saper and Fuller, 2017; Yu et al., 2019; Jones, 2020). Classic monoaminergic and cholinergic neuromodulatory systems are still considered to have a

strong influence on sleep-wake states (McCormick et al., 2020), but their role is considered secondary to the fast neurotransmitter systems (Saper and Fuller, 2017). The sleep-wake glutamate and GABA neurons are distributed throughout the brain and electrophysiologically categorized into four functional cell types based on their maximal firing rate across sleep-wake states: wake/REM-, NREM-, REM- or wake-max (Jones, 2017). Importantly, the relative distribution of these functional cell types within discrete sleep-wake nuclei may offer insight into the role of nuclei that are heterogeneous, either in function, molecular determinants or both (Jones, 2020).

This model of sleep regulation is also an excellent fit for studies examining the influence of anesthetics on states of consciousness, as a majority of the current anesthetics used are $GABA_A$ receptor agonists. For example, the discovery that GABAergic anesthetics markedly increased c-FOS expression (a marker of neuronal excitation) in the lateral habenula - a glutamatergic thalamic nucleus involved in reward pathways (Matsumoto and Hikosaka, 2007; Lu et al., 2008), led to further research using the classic GABAergic anesthetic propofol; these studies demonstrated that the lateral habenula was not only important for gating GABAergic anesthetic action, but also for natural NREM sleep consolidation (Gelegen et al., 2018). Going forward, studies combining the use of neurochemically specific anesthetics with novel techniques, such as calcium-imaging, optogenetics and other methods with high spatio-temporal resolution, will offer new insights into the molecular mechanisms underlying the complex system of sleep-wake circuitry that controls consciousness.

1.3 Anesthesia

The introduction of general anesthesia modernised surgical practices by allowing anesthesiologists to manipulate the level of consciousness, eliminating sensitivity to pain, and ensuring that the patient would have no memory of a painful procedure (Prys-Roberts, 1987). Consequently, general anesthesia is one of the most prevalent neurobiological manipulations currently in use, both in neuroscientific research, and in clinical practice with almost 60,000 surgical procedures conducted under general anesthesia every day in the United States alone (Brown et al., 2010). Yet, while the choice of an anesthetic agent can have a significant impact on experimental neurophysiological outcomes, the brain state produced by anesthesia often remains ignored as a variable in animal research (Piccitto, 2018). Furthermore, despite a growing body of literature elucidating agent-specific electrophysiological signatures of unconsciousness in humans, such as: the shift from occipital to frontal alpha coherence, increases in low-frequency power, and cross-frequency phase amplitude peak-max coupling between alpha rhythms (8-14 Hz) and low-frequency activity (0.1 – 2 Hz) observed under propofol-induced unconsciousness; brain-state monitoring using agent-specific spectral features remains an uncommon practice in anesthesiology (Purdon et al., 2013; Mukamel et al., 2014).

Instead, anesthesiologists typically rely on a simplified unidimensional index mathematically derived from the EEG, which represents the depth of unconsciousness as a value between 0-100 (Sigl and Chamoun, 1994). The range of values indicating a safe depth of unconsciousness is supposed to remain the same across anesthetics when using these indices, however it is well-documented that these estimations of anesthetic depth are often inaccurate under atypical anesthetics such as nitrous oxide, ketamine and dexmedetomidine (Barr et al., 1999; Hans et al., 2004; Abel et al., 2021). As a result, it is increasingly clear that although anesthetics yield an identical clinical endpoint, the agent-specific pharmacological properties

play a much larger role in both research and clinical outcomes than previously thought. However, the mechanisms that allow disparate pharmacological agents to produce unconsciousness remain largely unknown (Leung et al., 2014; Adapa, 2017).

1.3.1 Anesthetic action

While general anesthesia is characterized by a composite of clinical endpoints including decreased muscle tone, amnesia, and a reduction of responsiveness to external stimuli, the most important feature also constitutes the closest parallel to natural sleep – hypnosis (Scharf and Kelz, 2013). Clinically, hypnosis is referred to as a loss of consciousness (LOC); in humans, it is often operationally defined as a lack of response to sensory cues (e.g., verbal, visual, painful) (Sanders et al., 2012). The equivalent behavioural measure in animal research is a loss of the righting reflex (LORR), where upon losing consciousness, the intrinsic drive of an animal to correct its body orientation to a normal, upright posture is lost (Leung et al., 2014). It has been demonstrated that, across a wide range of anesthetic doses, the latency to human LOC correlates exceptionally well with the latency to animal LORR, confirming that both measures serve as a valid index of anesthetic induction (Campagna et al., 2003; Franks, 2008).

Though the exact mechanisms of anesthetic action remain elusive, progress has been made in understanding some of the molecular determinants. Initially, the influential Meyer-Overton theory of anesthesia suggested that, due to the positive correlation between lipid solubility and anesthetic potency of a compound, anesthetics act to modify neuronal membrane properties at the lipid bilayer. However, the discovery of stereoselective optical isomers with identical lipid solubility but reduced potency led to a shift away from this theory, and to focus

instead upon protein ion channels as the most likely molecular site of anesthetic action (Franks, 2008). Over the last 20 years, this focus typically converged upon three receptor-ion channel complexes that are considered important to the induction of anesthetic LOC: 1) γ-aminobutyric-acid type A ($GABA_A$) receptors, 2) two-pore-domain potassium (K_{2P}) channels, and 3) *N*-methyl-D-aspartate (NMDA) receptors. Almost all clinical anesthetics act upon $GABA_A$ receptors, either by potentiating GABA-induced chloride currents, or by agonizing the receptor directly (Franks, 2008). As such, $GABA_A$ receptors are a valuable entry point for understanding anesthetic action. For some anesthetic agents, a net decrease in neural activity is also thought to be mediated by the antagonism of glutamatergic NMDA receptors, or hyperpolarization caused by the opening of K_{2P} channels (Franks, 2008).

Despite their importance, anesthetic action is certainly not limited to $GABA_A$, NMDA and K_{2P} channels (Kelz and Mashour, 2019). Anesthetics have also been found to modulate the following: intrinsic calcium channels (Orestes et al., 2009), intrinsic sodium channels (Herold and Hemmings Jr, 2012), mechanisms for pre-synaptic neurotransmitter release (Nagele et al., 2005), and mitochondrial cellular respiration (Jung et al., 2022). To add an additional layer of complexity, structural studies in prokaryotic models of ligand gated channels have demonstrated that anesthetics can bind to multiple modulatory sites of a single channel, and either potentiate or inhibit the channel depending on the binding site and functional alignment (Hemmings et al., 2019). The promiscuity of anesthetic binding means that, at anesthetic doses, many anesthetics are likely not selective for a single target and can act at multiple ion channels in various agent-specific permutations (Garcia et al., 2010). Consequently, the pharmacokinetic and pharmacodynamic effects of a single anesthetic agent can shift dramatically based on dosage, weight, and species (Flecknell, 2016a). In order to contend with this Gordian knot of potential

mechanisms, anesthetics will be categorized based on their proposed primary pharmacological actions for the purposes of this chapter. However, it is clear that this mesoscopic comparison is only the first step in unravelling the intricacies of pharmacologically-induced unconsciousness.

1.3.2 General anesthesia vs. sedatives

Sedatives (sometimes referred to as hypnotics) are substances designed to depress the central nervous system to induce anxiolysis and increase sleepiness (Wisden et al., 2017). Often, sedatives can induce a state similar to natural NREM sleep, characterized by increased delta oscillations, reduced respiratory rate, and lowered body temperature (Yu et al., 2018). As such, sedatives are frequently employed in clinical settings, such as intensive care units, to reduce post-operative delirium and promote sleep in an inhospitable environment (Skrobik et al., 2018; Yu et al., 2018). While sedatives differ from general anesthesia in that it is usually possible to be aroused from a sedative state, certain sedative agents share anesthetic molecular targets ($GABA_A$ receptors) and even act as general anesthetics at elevated dosages (i.e., propofol and barbituates) (Franks, 2008; Yu et al., 2018). Accordingly, discerning the neural mechanisms essential to exerting a sedative effect can give insight to the processes of sleep and general anesthesia. Therefore, the literature evaluating the neurobiological overlaps of specific sedative compounds and natural sleep will also be included in this review.

1.4 The shared-circuit hypothesis

Another theory for deciphering anesthetic action came roughly 30 years ago, when due to the shared behavioural phenotypes of anesthesia and sleep, it was proposed that the loss of

consciousness associated with anesthesia is likely controlled by activity in the sub-cortical nuclei associated with sleep-wake regulation (Lydic and Biebuyck, 1994). Since then, the shared-circuit hypothesis has been a very active, and at times divisive topic of debate (Eikermann et al., 2020). For although there is an abundance of compelling evidence of mechanistic overlaps (which will be discussed in greater detail in section 1.6), there have also been some recent studies which have called the shared-circuit hypothesis into question. These criticisms were based on divergent outcomes that were observed across conditions of sleep and anesthesia when GABA or glutamatergic neurons in the sleep-promoting areas of the hypothalamus were manipulated using pharmacogenetic techniques (Vanini et al., 2020; Luo et al., 2023).

At the surface, the question of the shared-circuit hypothesis seems relatively simple: *does anesthesia co-opt endogenous sleep-wake wake circuitry to produce unconsciousness?* It is human nature to want a categorical answer, a black and white "yes" or "no". However, the seeming simplicity of the question belies its innumerable complexities, meaning that the answer most likely lies in the grey with "it depends". First and foremost, this stems from a philosophical issue: when an exogenous drug is applied to a complex living being, it is difficult to dissociate where "co-opting" an endogenous system ends, and where a whole new process begins. This is because when viewed from a reductionist standpoint, the nervous system is effectively a closed-system processor designed to produce output (e.g. behaviour, brain state, or physiological response) in response to an input (e.g stimulation, or drug), meaning that any input that produces an appreciable output response, invariably must act upon the endogenous pathways of the closed system to some degree.

The difficulty of this dissociation is not limited to anesthesia. For example, exogenous opioids modulate endogenous pain pathways to produce analgesia, arguably co-opting the

physiological pathways of endogenous opioid neuropeptides. Certain modes of neurostimulation also promote analgesia through mechanisms that are not yet fully understood, but that likely modulate endogenous opioidergic circuits (Lubejko et al., 2022). Thus, although these different exogenous stimuli both produce analgesia, in the absence of a fully delineated endogenous process, it remains difficult to quantify the extent to which each approach "co-opts" the endogenous pain pathways. Nevertheless, external stimuli such as opioids, and anesthesia have been invaluable tools in refining our collective understanding of endogenous pain pathways (Hua et al., 2020; Casely and Laycock, 2022).

Accordingly, as parallel but distinct processes within a closed system resulting in a similar output (i.e unconsciousness), some "shared circuits" across sleep and anesthesia are inevitable, and indeed have already been demonstrated (Gelegen et al., 2018; Jiang-Xie et al., 2019). However, as previously described, sleep and anesthesia have fundamental differences, such as homeostatic regulation, and rousability. Moreover, since anesthesia is comprised of multiple agents with diverse pharmacology, and the endogenous sleep-wake system is comprised of multiple neuromodulatory systems and diverse neuroanatomical sites, it is extremely unlikely that all anesthetics and all sleep-wake neuroanatomical sites will correspond. Consequently, rather than approaching the shared-circuit hypothesis as theory that should apply universally to all anesthetics, and all sleep-wake circuitry, a Venn diagram paradigm of overlapping, but also divergent states more accurately encompasses the complexities of both sleep and anesthesia.

1.5 Arousal and anesthetic emergence

Arguably, the most important shared trait of unconsciousness during sleep and anesthesia is that it is reversible. Recently, there has been a major shift in the canonical understanding of anesthetic emergence from a passive reversal of anesthetic induction, to an active, and more importantly, tractable process (Chemali et al., 2012; Kelz et al., 2019; Hu et al., 2023). Some of the mechanisms driving anesthetic emergence appear to be functionally distinct from the mechanisms for induction and maintenance of unconsciousness, however there is a growing body of literature demonstrating that endogenous arousal circuits facilitate anesthetic emergence (Moody et al., 2021; Reitz and Kelz, 2021). The commonalities between arousal and anesthetic emergence have further highlighted the importance of anesthesia as a tool to probe the mechanisms of reversible unconsciousness, especially as the advancement and refinement of scientific techniques provide increasingly finer resolution of molecularly heterogeneous sleep-wake nuclei (Bao et al., 2021; Cai et al., 2021; Reitz and Kelz, 2021).

As elucidated in a previous section, the ablation of discrete components of the ascending arousal system, such as the orexinergic or histaminergic neurons in the hypothalamus (Gerashchenko et al., 2001; Gerashchenko et al., 2004), or even multiple arousal-related nuclei concurrently (Blanco-Centurion et al., 2007), did not significantly alter daily wake levels in rodents. These studies serve to highlight the close-to failsafe redundancies in the organization of sleep-wake systems that serve to maintain consciousness even in the event of localized brain injury (Pal and Mashour, 2011). Consequently, it is unlikely that a single, discrete locus is sufficient to produce a state of sleep or arousal; rather, it appears that a diffuse network comprising of multiple neuroanatomical sites and neuromodulatory systems is responsible for orchestrating states of consciousness (Sulaman et al., 2023). Therefore, it follows that there likely is a similarly distributed system underlying both anesthetic induction and emergence, and

that the anesthetic state is not mediated by a single structure (Pal and Mashour, 2011; Leung et al., 2014; Moody et al., 2021). To that end, the next section of this chapter will explore the sub-cortical nuclei implicated in the functional network of unconsciousness, with emphasis on the intersection of functions in both sleep and anesthetic states.

1.6 Subcortical interfaces of sleep and anesthesia

1.6.1 Anterior hypothalamus

Reported symptoms of insomnia in patients with damage to the anterior hypothalamus led to the discovery of the preoptic area (POA) as one of the first brain loci to have a role in sleep-wake regulation (von Economo, 1930). To confirm these clinical case descriptions, a subsequent experimental study used systematic lesioning in discrete hypothalamic sections of the rat brain and concluded that the POA is a "sleep center" (Nauta, 1946). This hypothesis gained traction with the development of neurobiological techniques, starting with successive lesion (Sallanon et al., 1989) and inactivation studies (Lin et al., 1989), and was further substantiated by elevated c-FOS (a marker of neuronal activation) immunohistochemistry following sleep episodes. This c-FOS staining was found in a population of GABAergic neurons in the ventrolateral preoptic area (VLPO) and median preoptic nucleus (MnPO), defining these regions and cells as prominent sleep-promoting units (Sherin et al., 1996; Szymusiak et al., 1998; Gong et al., 2004).

The POA also plays an important role in the homeostatic functions of regulating blood pressure, electrolytic balance, sexual behaviour, and most importantly thermoregulation, which intersects with sleep regulation and brain state (Szymusiak et al., 2007; Takahashi et al., 2009;

Harding et al., 2018). The POA is well situated as a hub for sleep promotion, as it sends inhibitory projections which target some of the major wake-promoting centres of the brain, such as the orexinergic-rich perifornical area of the lateral hypothalamus (LH) (Yoshida et al., 2006), the noradrenergic locus coeruleus (LC), the serotonergic dorsal and medial raphe nuclei (DRN; MRN), and the tuberomammillary nucleus (TMN) in the posterior hypothalamus, which is the sole source of histamine in the central nervous system (Sherin et al., 1998; Steininger et al., 1999; Steininger et al., 2001; Lin et al., 2011). In turn, these areas often provide reciprocal innervation of the POA subnuclei which can inhibit sleep-promoting POA neurons, and activate wake-promoting POA neurons, leading to rapid arousal as demonstrated by activation of GABAergic terminals from the LH, or noradrenergic terminals from the LC in the VLPO (Venner et al., 2019; Liang et al., 2021). Similarly, the VLPO-TMN circuit is hypothesized to be a mutually inhibitory loop that likely plays a particularly important role in sleep generation, as inactivation of the TMN can reverse symptoms of insomnia associated with POA lesions, and promote sleep (Liu et al., 2010b; Thakkar, 2011; Weber and Dan, 2016; Chung et al., 2017). This mutually inhibitory interaction is also supported by the observation that systemic injection of the anesthetic $GABA_A$ receptor agonists propofol and pentobarbital simultaneously significantly increased and decreased c-FOS expression in the VLPO and the TMN, respectively (Nelson et al., 2002).

A similar pattern of elevated VLPO c-FOS activation was not observed with ketamine, an anesthetic that antagonizes NMDA receptor function, but has been reported with a variety of other anesthetics, including isoflurane and the sedative dexmedetomidine (DEX) (Nelson et al., 2003; Lu et al., 2008; Moore et al., 2012). As a selective α_2 adrenergic agonist, the primary effects of DEX are on metabotropic α_2 G_i–protein coupled receptors (Jasper et al., 1998), which

are abundant in the noradrenergic LC (Correa-Sales et al., 1992). Consequently, it has long been presumed that the main sedative effect of DEX arose from direct inhibition of the LC through α_2 autoreceptors and the subsequent loss of excitatory noradrenergic output (Yu et al., 2018). However, while the LC is indeed inhibited by DEX through α_2 receptors (Lakhlani et al., 1997), NREM-like sedation still occurs when DEX is administered to α_2A receptor knockout animals (Gilsbach et al., 2009), indicating that the sedative effect of DEX is unlikely to be solely mediated by inhibition of the LC via these receptors. This hypothesis initially gained traction with a study that demonstrated elevated c-FOS levels in the VLPO following administration of DEX, implicating the VLPO in DEX-induced sedation (Nelson et al., 2003). More recently, it has been demonstrated that, through a pharmacogenetic technique known as TetTagging (Reijmers et al., 2007; Garner et al., 2012), the experimental reactivation of neurons that became c-FOS positive during a low, systemic dose of DEX or during recovery sleep following a period of sleep deprivation, induced NREM-like sleep and strong hypothermia (Zhang et al., 2015). Importantly, these effects were mediated by neurons in the POA, indicating that a subcortical structure other than the LC was sufficient to produce the sedative response associated with DEX (Yu et al., 2018).

However, while the POA plays a pivotal role in the regulation of NREM sleep, it is also important to note that the POA is highly heterogeneous, and thus is not exclusively somnergic (Moffitt et al., 2018; Sulaman et al., 2023). This molecular and functional complexity has led to some perplexingly inconsistent outcomes in studies assessing the role of the POA in promoting unconsciousness or arousal in sleep and anesthesia. For instance, activation of POA tachykinin 1 neurons promoted sleep in one study (Chung et al., 2017), but both strongly consolidated wakefulness, and produced partial resistance to isoflurane and sevoflurane induced

unconsciousness in another (Reitz et al., 2021). Similarly, isoflurane has been demonstrated to directly depolarize sleep-promoting VLPO neurons (Moore et al., 2012), and optogenetic or chemogenetic activation of VLPO GABA neurons co-expressing galanin has been shown to increase NREM sleep (Kroeger et al., 2018), yet another study did not show changes in sleep-wake architecture or isoflurane induction or recovery time following chemogenetic activation of VLPO GABA neurons (Vanini et al., 2020). Taken together, these conflicting results suggest that fully elucidating the specific contributions of the heterogenous neuronal populations of the POA to the regulation of unconsciousness will take both time, and potentially the development of more precise methods for distinguishing these populations *in vivo*, as a single molecular marker may not be sufficient (Reitz and Kelz, 2021).

1.6.2 Posterior Hypothalamus

In the posterior hypothalamus, the TMN appears to have a pivotal role in endogenous sleep-wake circuitry, given the trifecta of: 1) the role of histamines in regulating aspects of wakefulness, such as cortical activation and behavioural arousal (Anaclet et al., 2009; Zant et al., 2012); 2) the widespread projections throughout the brain of histaminergic neurons solely originating in TMN (Kohler et al., 1985; Staines et al., 1987); and 3) the strong inhibitory inputs to the TMN from the sleep-active and sleep-promoting GABAergic POA neurons discussed above (Chung et al., 2017). Almost a decade ago, the TMN was postulated to have a fundamental role in transitions between unconsciousness and arousal, which was thought to occur through inhibition of the TMNs wake-promoting histaminergic drive to the rest of the brain by the increased inhibitory GABA input from either the VLPO, or through GABAergic agonism via

hypnotic actions using anesthetics such as propofol (Zecharia et al., 2009; Saper et al., 2010). However, when it was found that selective genetic ablation of $GABA_A$ receptors from histamine-containing neurons had no influence on basal sleep-wake architecture or propofol-induced LORR, this hypothesis was called into question (Zecharia et al., 2012). Notwithstanding, subsequent studies demonstrated that acute *in vivo* optogenetic silencing of histamine neurons induced a transition to NREM sleep in waking mice (Fujita et al., 2017), and that targeted pharmacogenetic inhibition of histamine neurons with the GABAergic sedative zolpidem (Ambien) significantly reduced latency to, and increased time spent in NREM sleep (Uygun et al., 2016). In light of this recent evidence, the authors of Zecharia et al. (2012) have interpreted the incongruity of their results to be due to the inherent compensatory drive of the central nervous system in response to the chronic loss of histaminergic $GABA_A$ receptors (Yu et al., 2018). Thus, while it appears that the TMN, or its inhibition thereof may not induce arousal or sleep *per se*, it undoubtedly plays a role in the endogenous sleep-wake circuit (Takahashi et al., 2009; Yu et al., 2018).

1.6.3 Lateral Hypothalamus

The perifornical area of the lateral hypothalamus is recognized as being predominantly populated by orexinergic (also called hypocretinergic) neurons, which are highly active during waking behaviours and have diffuse projections throughout the brain, including monoaminergic brainstem nuclei and cholinergic BF targets (Lee et al., 2005a; Mileykovskiy et al., 2005; Arrigoni et al., 2010; Lin et al., 2011). Loss of orexinergic influence results in narcolepsy (Lee and Dan, 2012), whereas optogenetic stimulation of orexinergic neurons induces wakefulness

(Adamantidis et al., 2007). The wake-promoting influence of orexin is also speculated to have an integral role in facilitating emergence from anesthesia, as ablation of orexinergic neurons does not affect the induction of isoflurane anesthesia (a GABAergic volatile anesthetic), but significantly delays emergence from anesthesia (Kelz et al., 2008). A similar effect has been observed with sevoflurane, wherein chemogenetic activation of orexinergic projections from the LH to the lateral habenula, which is a nuclei known to consolidate NREM sleep and mediate hypnosis in propofol anesthesia, both reduced anesthetic depth and facilitated emergence (Zhou et al., 2023).

The promotion of emergence from anesthesia is not limited to volatile anesthetics, propofol decreases c-FOS expression in orexinergic LH neurons, while intracerebroventricular (ICV) or intra-nucleus basalis microinjection of orexin-A both expedite emergence from propofol-induced anesthesia (Shirasaka et al., 2011; Zhang et al., 2012). Furthermore, a decreased time in the unconscious LORR state was observed for both propofol and DEX following ICV orexin injection (Zecharia et al., 2009). However, a similar effect is not observed in ketamine anesthesia (Zecharia et al., 2009), suggesting that the primary pharmacological mechanism of this anesthetic agent intercedes the properties of orexinergic potentiation of arousal from anesthesia.

1.6.4 Basal Forebrain

Based on the organization of anatomical connections alone, it is clear that the basal forebrain (BF) likely has a central role in coordinating behavioural states of consciousness. The BF receives input from other arousal-related nuclei, including monoaminergic efferents from the

LC, dorsal and medial raphe, substantia nigra (SN), and ventral tegmental area (VTA); cholinergic and glutamatergic efferents from the penduculopontine nucleus and laterodorsal tegmental nucleus; and orexinergic and histaminergic efferents from the hypothalamus (Vertes, 1988; Zaborszky et al., 1991; Zaborszky and Duque, 2000). In turn, BF neurons project to the neocortex, thalamus, hippocampus and entorhinal cortex (Mesulam et al., 1983; Vertes and Kocsis, 1997; Semba, 2000). While the BF contains both sleep-promoting and wake-promoting neuronal populations that are spatially intermingled (Xu et al., 2015), the BF plays a crucial role in cortical activation (Sulaman et al., 2023), subsequently this section will focus on the arousal-related cholinergic BF neurons.

High acetylcholine (ACh) levels in the CNS are associated with active EEG states, as cholinergic BF neurons fire maximally during wakefulness and REM sleep (Lee et al., 2005b). These neurons may serve as a target for the sedative-hypnotic effects of anesthesia, as the intrinsic excitability of BF cholinergic neurons is significantly decreased following the *in vitro* application of propofol (Chen et al., 2019). Accordingly, pharmacogenetic activation of BF cholinergic neurons reduced the anesthetic potency of propofol and isoflurane, whereas selective lesioning of cholinergic neurons in the BF amplified the anesthetic potency of propofol, pentobarbital, and isoflurane resulting in increased delta power and LORR duration (Leung et al., 2011; Luo et al., 2020). However, this effect is not observed with halothane (another volatile anesthetic), which suggests that the observed effects of anesthesia on the cholinergic system are likely dependent on agent-specific pharmacological mechanisms (Leung et al., 2011). Other anesthetic studies have shown that infusion of histamine into the BF, mimicking the inputs from the LH, decreased the burst-suppression EEG ratio and latency to emergence from LORR under isoflurane (Luo and Leung, 2009), with similar results observed with infusion of norepinephrine,

mimicking BF input from the LC, under desflurane anesthesia (Pillay et al., 2011). As such, it is possible that some arousal-promoting influences affecting sleep and anesthesia from disparate nuclei of the sleep-wake system may be critically mediated by the BF as the interface with cortical and thalamocortical circuitry.

Additionally, adenosine, a purine nucleoside that acts as a neuromodulator, shows increased concentration in the BF following sleep deprivation and is implicated in the homeostasis of sleep-wake architecture, particularly the induction of unconsciousness (Porkka-Heiskanen et al., 1997; McCarley, 2007; Sulaman et al., 2023). Indeed, an anesthetic study found that, while latency to LORR under anesthesia was shortened when animals were sleep-deprived, local infusion of an adenosine antagonist into the BF of sleep-deprived animals both increased the latency to LORR, and decreased emergence from anesthesia (Tung et al., 2005). Furthermore, systemic administration of adenosine (which may act at adenosine receptors outside of the basal forebrain) reduced induction time and enhanced anesthetic potency for thiopental (a barbiturate) and propofol (Kaputlu et al., 1998), whereas caffeine, a potent adenosine antagonist, has been demonstrated to accelerate emergence from isoflurane anesthesia (Fong et al., 2017). This bidirectional effect has also been observed using systemic administration of adenosine 2A receptor agonists, which resulted in increased anesthetic potency and antagonists, which resulted in decreased anesthetic potency under propofol anesthesia (Guo et al., 2023). Thus, the hypnogenic influences of anesthesia and sleep are likely modulated by adenosine.

1.6.5 Thalamus

As the main gateway for sensory input to the cortex, with strong neuromodulatory influences from nuclei in the sleep-wake network such as the BF, and extensive reciprocal projections to the cortex, the thalamus has also been suggested to play a pivotal role in global brain state regulation; specifically, wake generation and wake-related processing (Levey et al., 1987; Steriade, 2005; Sulaman et al., 2023). This is reflected by the inhibition of thalamocortical neurons by a variety of general anesthetics, including propofol, isoflurane and pentobarbital (Wan et al., 2003; Ying and Goldstein, 2005; Ying et al., 2009). However, as the thalamus is a functionally heterogeneous structure (Hudetz, 2012; Hauer et al., 2019), specific thalamic nuclei likely play different roles in the control of sleep-wake states, with higher order and midline thalamic structures ostensibly playing a larger role in the regulation of consciousness (Baker et al., 2014; Mease et al., 2016; Gent and Adamantidis, 2017).

One such nucleus, the paraventricular thalamus (PVT) has been recently demonstrated to contribute not only to the control of transitions of consciousness under propofol anesthesia, and promote emergence from isoflurane anesthesia, but also to be critical in the promotion and persistence of physiological wakefulness (Ren et al., 2018; Wang et al., 2023). In accordance with the wake-promoting role of the thalamus, removal of the inhibitory influence of the GABAergic thalamic reticular nucleus on other specific thalamic nuclei resulted in an emergence from an anesthetic state (Herrera et al., 2016), an effect also observed with pharmacological or electrical stimulation (Alkire et al., 2007; Bastos et al., 2021). Furthermore, a recent study found that genetic blockade of glutamate release from the lateral habenula, an epithalamic nucleus, diminished sensitivity to the anesthetic properties of propofol and severely fragmented natural NREM sleep (Gelegen et al., 2018), again demonstrating that the unconsciousness of sleep and anesthesia are often modulated by the same nodes of the sleep-wake network. Taken together,

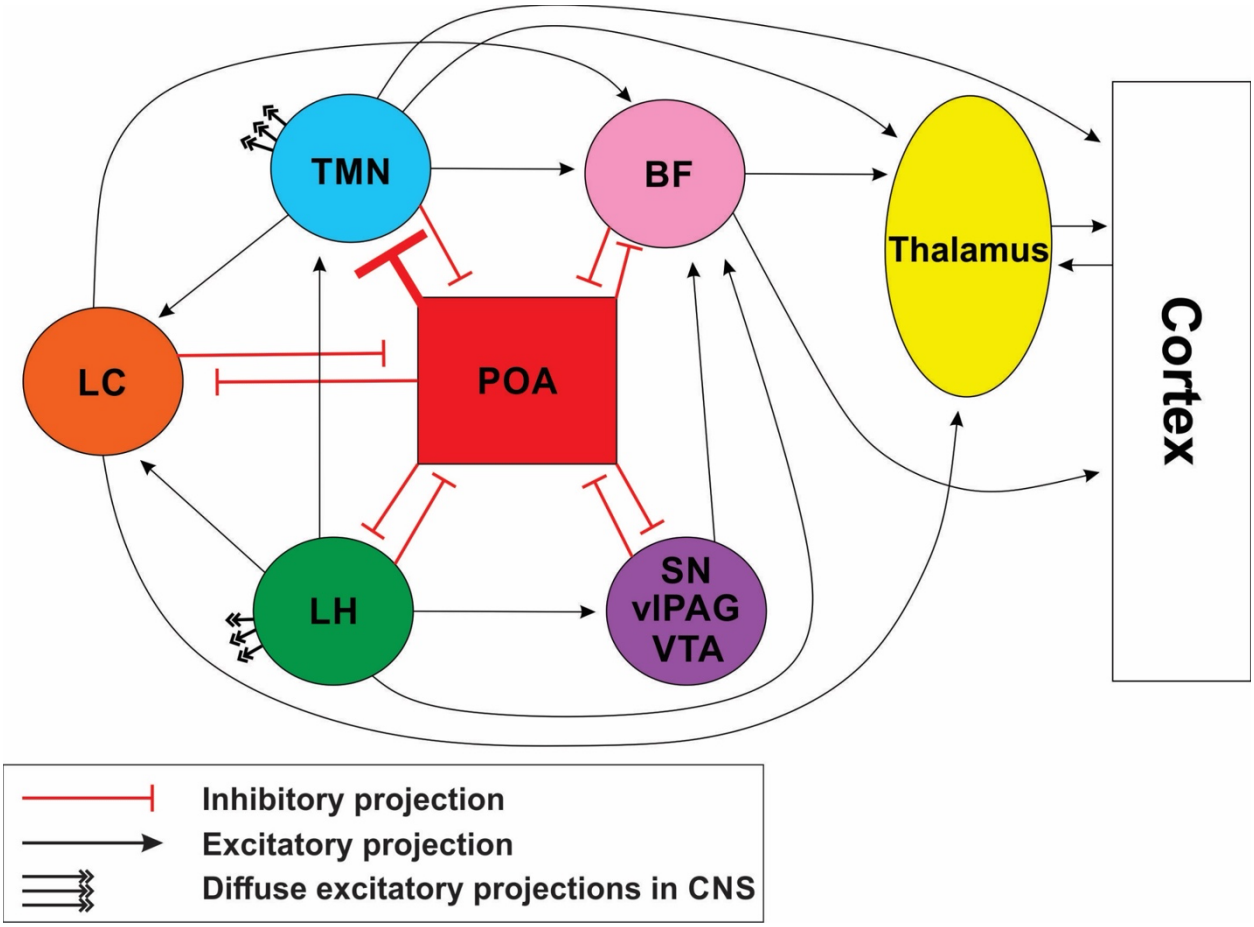

Figure 1.1 Selected excitatory and inhibitory pathways integral to induction and maintenance of unconsciousness in sleep and anesthesia.

LC: Locus coeruleus, LH: Lateral hypothalamus, TMN: Tubomammillary nucleus, POA: Preoptic area, BF: Basal forebrain, SN: Substantia nigra, vlPAG: ventrolateral periaqueductal gray, VTA: Ventral tegmental area.

these studies suggest that the thalamus and the related nuclei thereof, are highly involved in the regulation of states of consciousness (and perhaps even states of awareness), although it has yet to be fully elucidated how these changes in state occur.

1.6.6 Brainstem

Despite vacillations in the hypothesized role of specific monoaminergic brainstem nuclei in sleep and anesthesia, these loci are undoubtedly imperative in modulating states of conscious arousal. While (as previously discussed) the LC does not appear to be the sole mediator of the sedative effects of DEX, as initially hypothesized (Zhang et al., 2015), nor absolutely necessary for wakefulness, it has been consistently implicated in contributing to the regulation of arousal, given its role as the largest source of noradrenergic neurons in the brain, with projections to a vast array of targets in the CNS (Aston-Jones and Bloom, 1981; Espana and Berridge, 2006; Sulaman et al., 2023). This is perhaps best illustrated by the rapid termination of sleep by direct optogenetic stimulation of either the LC, or LC noradrenergic projections to the VLPO (Carter et al., 2010; Liang et al., 2021). Indeed, release of noradrenaline and neuronal firing in the LC were both reported to increase upon emergence from halothane anesthesia (Saunier et al., 1993) and, more recently, it has been determined that the excitatory noradrenergic pathway from the LC to the central medial thalamic nucleus accelerates emergence from propofol anesthesia (Fu et al., 2017). Thus, it is feasible that the noradrenergic system works in synchrony with the orexinergic system to promote arousal and emergence from an anesthetic state – an idea that is also supported by the inability to elicit orexin-induced awakening when the LC is inhibited (Carter et al., 2012). Interestingly, the anesthetic action of ketamine (an NMDA-receptor antagonist) may

be facilitated by the LC, as lesions to the LC actually decreased the duration of LORR under ketamine, in contrast to the increased duration of LORR observed with thiopental (Kushikata et al., 2011). These observations suggest that the LC is involved in mediating anesthetic action depending on pharmacological specificity, as well as promoting arousal in the sleep-wake system.

There is growing evidence that the central dopaminergic system of the VTA, SN and ventrolateral periacquaductal gray (vlPAG) also plays a central role in mediating anesthetic hypnosis. Dopaminergic neurons in the VTA are mainly active during wakefulness and REM sleep, and appear to be wake-promoting as pharmacogenetic activation induces and maintains wakefulness (Monti and Jantos, 2008; Oishi et al., 2017; Sulaman et al., 2023). In the context of anesthesia the effects are similar, inactivation or lesion of the VTA prolonged LORR induced by pentobarbital or propofol, respectively (Ma and Leung, 2006; Zhou et al., 2015), and optogenetic stimulation of the dopaminergic VTA neurons induced emergence and reanimation from isoflurane anesthesia (Taylor et al., 2016). Analogously, lesions to the dopaminergic neurons in the SN significantly increased the latency to recovery from propofol-induced anesthesia (Shi et al., 2017), and targeted lesions of the dopaminergic neurons in the vlPAG both reduced induction time and prolonged emergence from propofol anesthesia (Li et al., 2018). VTA GABAergic neurons are also a region of interest for the control of transitions of consciousness, because when they are chemogenetically activated they produce an NREM-like state of unconsciousness, and similarly enhance the effects of isoflurane anesthesia (Yin et al., 2019; Yu et al., 2019) Collectively, these results indicate that the VTA, SN and vlPAG play an important role in the reversible unconsciousness of sleep and anesthesia.

It is important to note that there is an alternative theory to the contemporary models of coordinated systems of disparate sleep-wake nuclei with failsafe redundancies. This theory, based on the "dedicated pathways" hypothesis of Moruzzi and Magoun (1949), postulates that anesthetics act to inhibit the mesopontine reticular activating system which then produces cortical and behavioural suppression. Specifically, this model suggests that anesthetic action is mediated by a single locus, the mesopontine tegmental anesthesia area (MPTA), which has both ascending and descending afferents in the CNS to key effector structures that themselves induce hypnosis, as well as analgesia and immobility secondarily (Devor and Zalkind, 2001). Bilateral injection of pentobarbital into the MPTA invoked a transient anesthesia-like state in rats, and the MPTA has been demonstrated to be differentially sensitive to other GABAergic anesthetics such as thiopentone (Voss et al., 2005). Furthermore, MPTA lesions decreased the sensitivity to the GABAergic anesthetics pentobarbital, propofol and etomidate (Minert and Devor, 2016; Minert et al., 2020), prolonged periods of wakefulness, and increased total time spent awake (Lanir-Azaria et al., 2018). However, the lack of clear histological markers for this region likely impacts lesioning specificity. Moreover, despite improved localization, the immediate proximity of other arousal-related nuclei, such as the vlPAG, laterodorsal tegmental nucleus, and pendunculopontine tegmental nucleus, suggests these results require replication and further investigation (Minert et al., 2017). Nevertheless, the MPTA may represent a new node in the sleep-wake circuitry and, if so, further implicates the anesthetic appropriation of endogenous mechanisms of unconsciousness.

1.7 Behavioural and electrophysiological commonalities

Sleep and anesthesia align at more than just neuroanatomical targets; functional intersections also occur for specific behavioural and electrophysiological features. Among the most compelling evidence for the symbiotic relationship between sleep and anesthesia is the amelioration of total sleep debt following sleep deprivation by propofol (Tung et al., 2004), and the modulation of anesthetic potency by sleep deprivation, which significantly decreased latency to anesthetic induction and prolonged time to emergence from isoflurane and propofol (Tung et al., 2002). Similar results have been observed for sevoflurane, with reduced latency to induction of LORR and dissipation of NREM, but not REM sleep debt following sleep deprivation (Pal et al., 2011). These and similar results suggest that the reciprocity between sleep and anesthesia in terms of homeostasis may be both agent- and sleep state-specific (Mashour and Pal, 2012). If this is indeed the case, understanding the differences in the pharmacological and physiological actions of different anesthetics may offer insight into both endogenous sleep homeostatic processes and the functional relevance of NREM and REM states.

It has long been held that anesthesia is not a suitable surrogate for the cyclic alternations of state that are observed in natural sleep, due to the unitary, coma-like burst-suppression activity, or NREM-like brain activity observed under most anesthetics (Tung and Mendelson, 2004; Lydic and Baghdoyan, 2005; Adapa, 2017; Ward-Flanagan et al., 2022). However, spontaneous and cyclical alternations between an activated state of cortical desynchronization concomitant with hippocampal theta (~4 Hz), and a deactivated state of synchronous large amplitude, slow oscillations in the cortex and hippocampus has been observed under urethane anesthesia in both rats and mice (Clement et al., 2008; Pagliardini et al., 2013b). Interestingly, for urethane, the often lengthy transitional period between activated and deactivated states shows properties of light NREM states (i.e., prominent cortical spindling), while the transition from

deep slow-wave states to activated REM-like patterns is more rapid; both of these features of urethane anesthesia are similar to the state transition present in natural sleep cycles. While urethane is similar in nature to other anesthetics, in that at higher doses it has multiple sites of action, including, but not limited to GABA, NMDA, and AMPA receptors (Hara and Harris, 2002); it differs in its primary pharmacological mechanism, which is to potentiate resting potassium conductance, subsequently inducing hyperpolarization of central neurons (Sceniak and MacIver, 2006). This distinct mechanism is illustrated by the initial reduction of tonic firing, and subsequent potentiation of bursting activity in ventrobasal thalamocortical neurons in mice anesthetized with urethane (Huh and Cho, 2013), and likely contributes to the unique anesthetic effects of urethane.

In addition to the cyclic alternations between REM-like and NREM-like states that have periods similar to those typically observed in natural sleep, other physiological changes (e.g., heart rate, respiration, and muscle tone) that occur in relation to the stages of natural sleep show almost identical relations to the different stages present under urethane anesthesia (Clement et al., 2008; Whitten et al., 2009; Pagliardini et al., 2012). As such, urethane is already in use as a model in rodent studies of sleep-like neurophysiological processes, including, but not limited to: activity-dependent scaling of neuroplasticity in slow-wave sleep (Gonzalez-Rueda et al., 2018), sudden, unexpected death in epilepsy (Goldman et al., 2017), the role of astrocytes in changing cortical brain states (Poskanzer and Yuste, 2016), and urodynamic functions associated with changes in brain state (Crook and Lovick, 2016).

Despite these numerous, and compelling overlaps, it should also be stressed that urethane is not *identical* to natural sleep. Besides the obvious need for pharmacological as opposed to

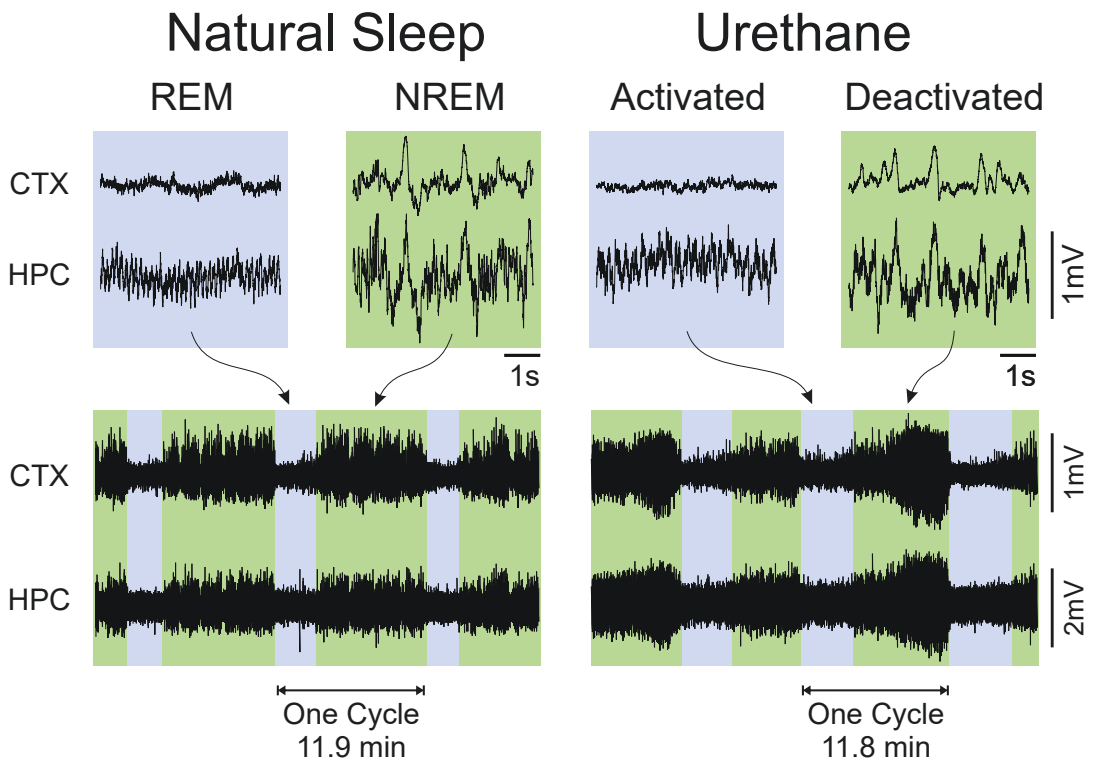

Figure 1.2 Comparison of electrographic features of natural sleep and urethane anesthesia.

Traces are from separate recording sessions within the same rat. Both conditions demonstrate: 1) an activated state of cortical low-voltage fast activity concomitant with theta (~ 4 Hz) activity in the hippocampus, and 2) a deactivated state of slow (~ 1 Hz) synchronous activity in both the cortex and hippocampus. Importantly both conditions demonstrate spontaneous, cyclic alternations between these states that are also analogous in time frame.

physiological induction and lack of rousability, urethane also differs from sleep in that it does not produce the saccadic rapid-eye movements archetypical of REM sleep, and that it produces an overall slowing of forebrain activity, especially in hippocampal theta from ~ 6-9 Hz in naturally sleeping rats to ~ 4 Hz under urethane (Bland, 1986; Clement et al., 2008). These differences are undoubtedly important to keep in mind when using urethane as a model of sleep, especially as they require specific accommodations in analysis (i.e accounting for the frequency slowing) in order to fairly interpret results (Mondino et al., 2022; Ward-Flanagan et al., 2023). However, these differences do not preclude urethane from providing an excellent model of sleep-like neurophysiology, for in addition to the consistencies in neurophysiology outlined above, urethane also is also synonymous with natural sleep in terms of: 1) bidirectional sensitivity to central cholinergic neuromodulation, with agonism promoting REM sleep, and a REM-like activated state under urethane, and antagonism promoting NREM sleep and an NREM-like deactivated state under urethane (Clement et al., 2008; Arrigoni and Fuller, 2019), 2) the laminar and current source density profile of hippocampal theta during the tonic phase of REM sleep, and although slower, the activated state under urethane (Bland, 1986; Wolansky et al., 2006), and 3) changes in brain state in response to manipulations of forebrain-projecting cholinergic nuclei in the brainstem (Clement et al., 2008).

Thus, urethane offers a unique experimental model to interrogate the mechanisms underlying sleep-like brain states and their alternations, and to further identify the roles of specific neuronal populations in promoting different states during unconsciousness (Walczak and Blasiak, 2017). However, while urethane provides a long-acting, stable anesthetic effect, the drawback associated with this stability is systemic toxicity, which ethically limits the use of urethane to terminal experiments (Maggi and Meli, 1986; Silver et al., 2021). As such, for

chronic experimental manipulations that require an anesthetic surrogate of slow-wave sleep, ketamine-xylazine is commonly used. Nonetheless, there are also caveats for ketamine-xylazine, including an elevated power in the gamma frequency (30 – 100 Hz; (Chauvette et al., 2011), and a unitary state of NREM-like slow oscillations evoked at a surgical plane of anesthesia (Sharma et al., 2010). This raised the question of whether other anesthetics could produce the same sleep-like neurophysiology and surgical depth of anesthesia as urethane, without being limited to acute experimental preparations, especially in light of the growing focus on overlaps between arousal and anesthetic emergence.

1.8 Pharmacological models of sleep – summary of findings

In Chapter 2, I use identical recording conditions to compare the spontaneous brain activity of urethane with that of five other commonly used research anesthetics at a surgical plane of anesthesia. Based on previous work in our lab, which showed that urethane produced sleep-like brain state alternations (Clement et al., 2008), and that ketamine-xylazine produced a unitary state of NREM-like global slow-oscillatory activity (Sharma et al., 2010), I hypothesized that urethane alone could provide a pharmacological model of the neurophysiological dynamics of natural sleep, while other anesthetics could provide adequate models of specific components of unconscious states. I show that, at a surgical plane of anesthesia, propofol, pentobarbital, and isoflurane all produced a coma-like brain state of burst-suppression, and that ketamine-xylazine produced the NREM-like state of global slow oscillations that had been previously observed. Surprisingly though, I show that not only urethane, but also chloral hydrate produced spontaneous, sleep-like alternations of brain state, which were not associated with a decrease in

anesthetic depth. To my knowledge, this is the first demonstration of these sleep-like brain state alternations under chloral hydrate anesthesia, which has important implications for modelling both brain state alternations, and anesthetic emergence, as unlike urethane, chloral hydrate is not limited to acute experimental paradigms.

The aim of Chapter 3 is to explore the mechanistic overlaps between sleep and urethane anesthesia, which potentially give rise to their well-documented parallels in measures of EEG and peripheral physiology. To that end, I measured the relative activation of ten sub-cortical nuclei within the endogenous sleep-wake circuit in rats using c-Fos as a marker of neuronal activity, across five behavioural conditions: 1) rats engaged in recovery sleep following sleep deprivation (i.e pressured sleep), 2) rats engaged in regular sleep without sleep deprivation (i.e unpressured sleep), 3) rats under urethane anesthesia following sleep-deprivation (i.e pressured anesthesia), 4) rats under urethane anesthesia without sleep-deprivation (i.e unpressured anesthesia), and 5) wake. When the patterns of activation across these ten sleep-wake nuclei was compared across these conditions, rats in the urethane conditions had near identical profiles to those in the unpressured sleep condition, irrespective of prior sleep deprivation. Consequently, it appears that urethane not only mimics sleep-like neurobiological measures, but also produces similar patterns of activity in neuroanatomical targets. However, it also seems that the state produced by urethane is highly stereotyped, and supersedes any internal homeostatic changes that typically occur in response to sleep debt. Urethane then, is similar to physiological sleep in terms of physiological correlates, but unlike sleep in terms of sensitivity to sleep pressure.

Chapter 4 assesses the assertion that chloral hydrate anesthesia does not provide adequate analgesia to serve as a sole anesthetic for surgical manipulations. If chloral hydrate is to serve as a pharmacological model of sleep, it is imperative that it can produce adequate analgesia for both

ethical considerations, as well as to limit the potential confounds of having to administer additional analgesics. I demonstrate that, in alignment with previous reports from the primary literature, chloral hydrate produces significant analgesia, and that importantly, this effect is not due to paralytic immobility.

In Chapter 5, I characterize a number of neurophysiological measures under chloral hydrate anesthesia to assess its utility as a pharmacological model of natural sleep. I show that chloral hydrate produces cyclic alternations of brain state that are strikingly similar to natural sleep in terms of individual components, the timing of the alternation cycles, as well as the sensitivity to cholinergic manipulations. Furthermore, I demonstrate that respiration co-varies with the brain state alternations in a sleep-like pattern, namely with increased respiration rate, respiratory variability and an increased incidence of sighs during forebrain activation. However, heart rate and temperature fluctuations under chloral hydrate did not correspond with the changes typically observed in natural sleep. Therefore, at present, urethane offers a more comprehensive pharmacological model of sleep, however chloral hydrate presents an exciting new tool to probe sleep-like brain state changes, and importantly, to explore anesthetic emergence – which are experiments that are not ethically feasible using urethane.

The overlaps and parallels between sleep and anesthesia cannot and, indeed, should not be ignored, as progress in one of these areas is often mutually informative of the other. The endogenous sleep-wake system is complex and intricate, and the value of having an additional model system to unravel the anatomical connectivity, neuromodulators and electrophysiology involved in eliciting and maintaining an unconscious state is immeasurable. From the ability of dexmedetomidine to promote sleep and reduce delirium (Skrobik et al., 2018), to the capacity of propofol as a substitute for specific aspects of natural sleep (Tung and Mendelson, 2004), and the

ability to model the dynamics of natural sleep using urethane in rodents (Pagliardini et al., 2013a), the intersection of sleep and anesthesia offers exciting new opportunities to explore the shared neurobiological pathways of unconsciousness. While there has been exponential growth in this field, there is still much to understand, and it is clear that progress in this area of research will yield further important insights into the optimization of clinical approaches to sleep disorders, enhance surgical anesthesia interventions and, ultimately define consciousness.

2 A comparison of brain state dynamics across common anesthetic agents in male Sprague-Dawley rats

Rachel Ward-Flanagan [1], Alto S. Lo [2], Elizabeth A. Clement [1] and Clayton T. Dickson[1,2,3,4]

[1] Neuroscience and Mental Health Institute, University of Alberta, Canada, T6G 2E1

[2] Department of Psychology, University of Alberta, Canada, T6G 2R3

[3] Department of Physiology, University of Alberta, Canada, T6G 2H7

[4] Department of Anesthesiology and Pain Medicine, University of Alberta, Canada, T6G 2G3

Acknowledgements: This work was supported by a Natural Sciences and Engineering Research Council of Canada (NSERC) Discovery grant 2016-06576 to C.T.D. R.W-F was supported by an NSERC Doctoral Postgraduate Scholarship, as well as an Alberta Graduate Excellence Scholarship.

https://doi.org/10.3390/ijms23073608

2.1 Abstract

Anesthesia is a powerful tool in neuroscientific research, especially in sleep research where it has the experimental advantage of allowing surgical interventions that are ethically problematic in natural sleep. Yet, while it is well documented that different anesthetic agents produce a variety of brain states, and consequently have differential effects on a multitude of neurophysiological factors, these outcomes vary based on dosages, the animal species used, and the pharmacological mechanisms specific to each anesthetic agent. Thus, our aim was to conduct a controlled comparison of spontaneous electrophysiological dynamics at a surgical plane of anesthesia under six common research anesthetics using a ubiquitous animal model, the Sprague-Dawley rat. From this direct comparison, we also evaluated which anesthetic agents may serve as pharmacological proxies for the electrophysiological features and dynamics of unconscious states such as sleep and coma. We found that at a surgical plane, pentobarbital, isoflurane and propofol all produced a continuous pattern of burst-suppression activity, which is a neurophysiological state characteristically observed during coma. In contrast, ketamine-xylazine produced synchronized, slow-oscillatory activity, similar to that observed during slow-wave sleep. Notably, both urethane and chloral hydrate produced the spontaneous, cyclical alternations between forebrain activation (REM-like) and deactivation (non-REM-like) that are similar to those observed during natural sleep. Thus, choice of anesthesia, in conjunction with continuous brain state monitoring, are critical considerations in order to avoid brain-state confounds when conducting neurophysiological experiments.

2.2 Introduction

Anesthesia is one of the most common tools used in neuroscientific research. Its prevalence is unsurprising given the exceptional experimental control that it affords, granting researchers the ability to perform surgical manipulations that would otherwise be technically or ethically impossible (Ward-Flanagan and Dickson, 2019). Yet, despite the predominance of anesthesia in animal research, the appropriate choice of an anesthetic agent can be difficult, as neurophysiological effects vary by anesthetic agent (Purdon et al., 2015; Bonhomme et al., 2019), dosage (Ferron et al., 2009a; Brown et al., 2010), animal model (Flecknell, 2016a), and pharmacological mechanisms (Krasowski et al., 1998; Franks, 2008; Aggarwal et al., 2019). Furthermore, while the agent-specific brain states produced by anesthetics can significantly impact experimental outcomes (Piccitto, 2018), often neither the choice of anesthetic agent is rationalized, nor the brain state reported in many neurophysiological studies using anesthesia.

Consequently, our aim was to conduct a controlled comparison of the ongoing electrographic activity evoked at a surgical plane of anesthesia, under six common research anesthetics, using a ubiquitous research model, the Sprague-Dawley rat. Though at clinical doses, most anesthetics act at multiple molecular targets, for the sake of brevity we mainly focused on the primary pharmacological mechanisms of our chosen agents. In order for our comparison to serve as a preliminary guide for researchers in choosing a suitable anesthetic, we tested easily accessible, commonly used anesthetics with a variety of primary pharmacological actions, including: ketamine-xylazine (KET-XYL) which acts as an NMDA receptor antagonist (Harrison and Simmonds, 1985) and an alpha-2 adrenergic agonist (Greene and Thurmon, 1988), respectively; pentobarbital (PTB), isoflurane (ISO), propofol (PRO), and chloral hydrate (CH), which are all reported to share a primary pharmacological mechanism - potentiating GABAergic

activity (Nakahiro et al., 1989; Akaike et al., 1990; Hara et al., 1993; Lovinger et al., 1993; Hall et al., 1994). We also tested urethane (ethyl carbamate), which potentiates a resting potassium conductance in order to decrease membrane input resistance, thus hyperpolarizing excitatory neocortical pyramidal neurons as its primary pharmacological mechanism (Hara and Harris, 2002; Sceniak and MacIver, 2006).

We also reasoned that our direct comparison would serve to determine which, if any, anesthetic agents tested could act as pharmacological proxies for altered states of unconsciousness, such as sleep and coma (Brown et al., 2011). Previous work from our research group using rodents has established that urethane anesthesia produces EEG activity characterized by spontaneous, cyclical alternations between: 1) a state of forebrain activation (i.e., low-voltage fast activity in the cortex, concurrent with theta activity in the hippocampus; ~4 Hz), and 2) a deactivated state characterized by global, synchronous slow oscillatory activity (~1 Hz; (Wolansky et al., 2006; Clement et al., 2008)). These brain state dynamics closely resemble the spontaneous EEG fluctuations between rapid-eye movement (REM) and non-REM (nREM) in natural sleep in terms of periodicity, duration, and concomitant changes in physiology such as heart rate, breathing rate and temperature (Whitten et al., 2009; Pagliardini et al., 2012; Pagliardini et al., 2013a). Due to these previous findings, and the unusual primary pharmacological mechanism of urethane, we hypothesized that when compared to other commonly used anesthetics, only urethane anesthesia would serve as a viable pharmacological proxy for the full neurophysiological dynamics of natural sleep.

Using identical recording conditions to enable direct comparisons, we monitored ongoing brain state dynamics via intracranial electrodes placed in the neocortex and hippocampus, as well as any associated changes in the plane of anesthesia either following bolus doses of the

anesthetic, or conversely during subsequent metabolism of the anesthetic agent. We evaluated consistencies and divergences in brain activity across our tested anesthetic agents at a surgical plane of anesthesia, using spectral analysis of the EEG recordings. Our comparison revealed that three different states could be observed: coma-like burst-suppression (PTB, ISO, PRO), nREM-like slow-oscillatory activity (KET-XYL), and sleep-like cyclical oscillations between an REM-like and NREM-like state (urethane, CH).

2.3 Methods

2.3.1 Subjects

Thirty-six naïve male Sprague-Dawley rats (Charles River, and University of Alberta Science Animal Support Services) weighing on average 287.4±8.5 g (mean±SEM) were randomly assigned to one of the following anesthetic groups for acute electrophysiological recordings: urethane (n=10), KET-XYL (n=5), ISO (n=5), PTB (n=6), PRO (n=5), or CH (n=5). Animals were kept on a 12 hour light/dark cycle at 20±1°C, and housed in cages with no more than 4 rats per cage. All surgical procedures outlined herein conform to our animal use protocol (092) that was approved by the Biological Sciences Animal Care and Use Committee of the University of Alberta, in accordance with the guidelines of the Canadian Council on Animal Care.

2.3.2 Surgery and anesthesia

Initial induction of animals occurred in a plexiglass anesthetic chamber using 4% ISO in medical (100%) oxygen. Upon the loss of righting reflexes (Leung et al., 2014), animals were transferred to a nose cone and maintained at 1.5–2.5% ISO. All rats, except those assigned to the ISO anesthetic group, were subsequently implanted with a jugular catheter to allow for intravenous (i.v.) administration of their assigned anesthetic. Including knock-down time, the procedure to implant the jugular catheter took approximately 10-12 minutes, so rats in drug groups other than ISO received only a short exposure to ISO. Rats in the ISO anesthetic group were continuously administered anesthesia in gaseous form via a nose cone and were maintained at a surgical plane of anesthesia using 2% ISO, unless manipulated to evaluate changes in EEG dynamics associated with anesthetic depth. For all other animals, ISO was immediately discontinued following the implantation of the jugular catheter, and they were switched to i.v. administration of their respective anesthetic. Additionally, stereotaxic and surgical procedures outlined below took a minimum of 1 hour, so animals not in the ISO group had ample time to exhale and metabolize any excess ISO prior to EEG recordings.

To ensure animals were maintained at a surgical level of anesthesia, changes in anesthetic state were continuously monitored by observing for any changes in heart or breathing rates, particularly when changes in brain state were observed, and subsequently verified by administering a hind paw pinch. If a reflexive withdrawal was observed, then supplemental bolus doses (2% of the original dose) of the assigned anesthetic were administered until a stable plane of surgical anesthesia was restored. The dosages used to establish a surgical plane for each i.v. anesthetic group were as follows: urethane (1.70 g/kg); KET-XYL (93.8 mg/kg, 9.24 mg/kg); PTB (65.0 mg/kg); PRO (8.00 mg/kg bolus, 60.0 $mg \cdot kg^{-1} \cdot hr^{-1}$ continuous infusion); CH (200.0 mg/kg bolus, 150.0 $mg \cdot kg^{-1} \cdot hr^{-1}$ continuous infusion). Additional bolus doses of anesthetic were

only delivered either when evaluating the effects of an increased dose of anesthetic on ongoing EEG measures, or if the animal exhibited a loss of surgical plane as evidenced by a reflexive withdrawal to a hind paw pinch.

2.3.3 Stereotaxic and recording procedures

Following the initial surgical procedures, rats were secured in a stereotaxic frame (Kopf Instruments, Tujunga, CA, USA). Core body temperature was monitored and maintained at 37°C for the duration of the experiment using a servo-driven system connected to a heating pad and rectal probe (TR-100, Fine Sciences Tools, Vancouver, BC, Canada). For three of the drug groups (ISO, PRO, and CH) rats received continuous delivery of the anesthetic. This was achieved using a modified nose cone attached to the stereotaxic frame in the ISO anesthetic group, and a continuous infusion pump (Harvard Apparatus, Holliston, MA) in the PRO, and CH anesthetic groups.

Teflon-coated stainless steel wire was used to construct all recording electrodes (bare diameter 125 μm; A-M Systems Inc., Sequim, WA), and placement of recording electrodes was conducted using stereotaxic coordinates measured in relation to bregma. These electrodes were placed in the frontal neocortex (AP: +2.8 mm; ML: ±2.0 mm) in either superficial (DV: -0.1 to –0.5 mm) or deep layers (DV: -1.0 to –1.3 mm), and the hippocampus (AP: -3.3 to -3.5 mm; ML: ±2.3 to 2.5 mm; DV: -2.4 to –3.3 mm) to confirm any observed changes in forebrain state.

Based on previous work from our lab (Wolansky et al., 2006), recorded field potential signals from the cortex and hippocampus were either: 1) measured against an electrically neutral

reference point, which was typically the grounded stereotaxic frame but in a few cases was a low-resistance uninsulated teflon wire ~2mm long placed vertically through the layers of frontal cortex, or 2) were differentially amplified by referencing one tip of a staggered bipolar electrode to another. Field potential recordings were then amplified at a gain of 1000, and then filtered between 0.1 to 500 Hz using a differential AC amplifier (Model 1700, A-M Systems Inc.; Sequim, WA, USA). Recorded signals were digitized online (at sampling frequency of 1 kHz) using either a Digidata 1322A A-D board in conjunction with the acquisition program AxoScope (Axon Instruments; Union City, CA, USA), or a PowerLab Pro combined with Lab Chart 8 software (AD Instruments; Colorado Springs, CO, USA).

2.3.4 Experimental design

Cortical and hippocampal field potential activity was recorded for a minimum of 70 minutes for all animals regardless of anesthetic group. For the purposes of this study, a surgical plane of anesthesia was operationally defined as a loss of reflexive withdrawal from a nociceptive stimulus (i.e., withdrawal of a paw when pinched) and an absence of reactivity while in the stereotaxic frame. All animals were maintained at surgical plane of anesthesia at the average effective dosage of the designated anesthetic. Changes in electrophysiological activity in response to discontinuation of supplementary doses of anesthesia were recorded for 10–40 minutes depending on when the animal responded to the nociceptive stimulus. Subsequently, the animal was restored to a surgical plane using supplementary doses of anesthetic. Following termination of the EEG recording, rats were euthanized by transcardial perfusion with saline.

2.3.5 Statistical analyses

Analyses were conducted offline on the previously acquired digitized files. Visual inspection of raw EEG signals was used to segment data based on recorded bolus i.v administrations of anesthetics, or tagged reports of changes in anesthetic state. Data was segmented into two groups: 40 minute epochs at a given anesthetic dose, to characterize changes in spectral power over time using a spectrogram, and 2-5 minute epochs to assess differences in spectral power at specific time points in the recording. Spectral power was computed using Welch's periodogram method on Hanning-windowed data of 6-second epochs with a 2-second overlap (MATLAB: Mathworks, Natick, MA) for analysis. Spectrograms were computed using 30 second epochs separated by 10 seconds across the analysed segment. The computation of spectral power also included an estimate of the upper and lower 95% confidence limits which enabled us to calculate significant changes in power across our manipulations. Plots of the analyzed data were subsequently created using Origin software (Microcal Software, North Hampton, MA). Averages were computed as arithmetic means and include the standard error of the mean.

Both state changes, and cycle duration in urethane and CH were characterized by first extracting the peak frequency of slow oscillatory power in the cortex either alone, or along with the peak frequency of theta in the hippocampus to create a ratio of slow oscillatory power compared to theta power across time. Then the state change threshold was established by determining the saddle point of the bimodal power distribution, allowing for calculation of cycle duration and the proportion of time spent in deactivated or activated states on a cycle by cycle basis. In CH, where rats spent 100% of time in deactivated patterns following bolus doses, and

no threshold crosses occurred, cycles were estimated based on any small changes observed in the raw EEG traces or spectrograms.

Changes in the duration of inter-burst intervals during burst-suppression activity in the PTB, ISO and PRO groups were compared over a span of 3 minutes both pre- and post-bolus administration for each anesthetic using a 2-way ANOVA. Since we were only interested in the effect of dose, only this component of the analysis was reported. The threshold for detection of burst activity was set at half of the peak amplitude over the six minutes assessed per animal, with an average threshold of 0.18 mV±0.01 mV (n=9). Statistical significance was set at α=0.05.

2.4 Results

2.4.1 Urethane

As with our previous studies (Wolansky et al., 2006; Clement et al., 2008), rats in the urethane anesthetized group exhibited robust cyclical and spontaneous alternations of forebrain state during long-term neocortical and hippocampal local field potential recordings (Figure 2.1A,B). Two electrographically distinct states were observed: an activated pattern, consisting of low-voltage fast activity in the neocortex, concomitant with rhythmic theta activity (3.90±0.13 Hz) in the hippocampus; and a deactivated state characterized by large amplitude, slow oscillatory (~ 1 Hz: CTX: 1.18±0.07 Hz; HPC: 0.96±0.09 Hz) activity in both the neocortex and the hippocampus (Figure 2.1C). The average period for these highly rhythmic state alternations was 11.6±1.0 min (n=10).

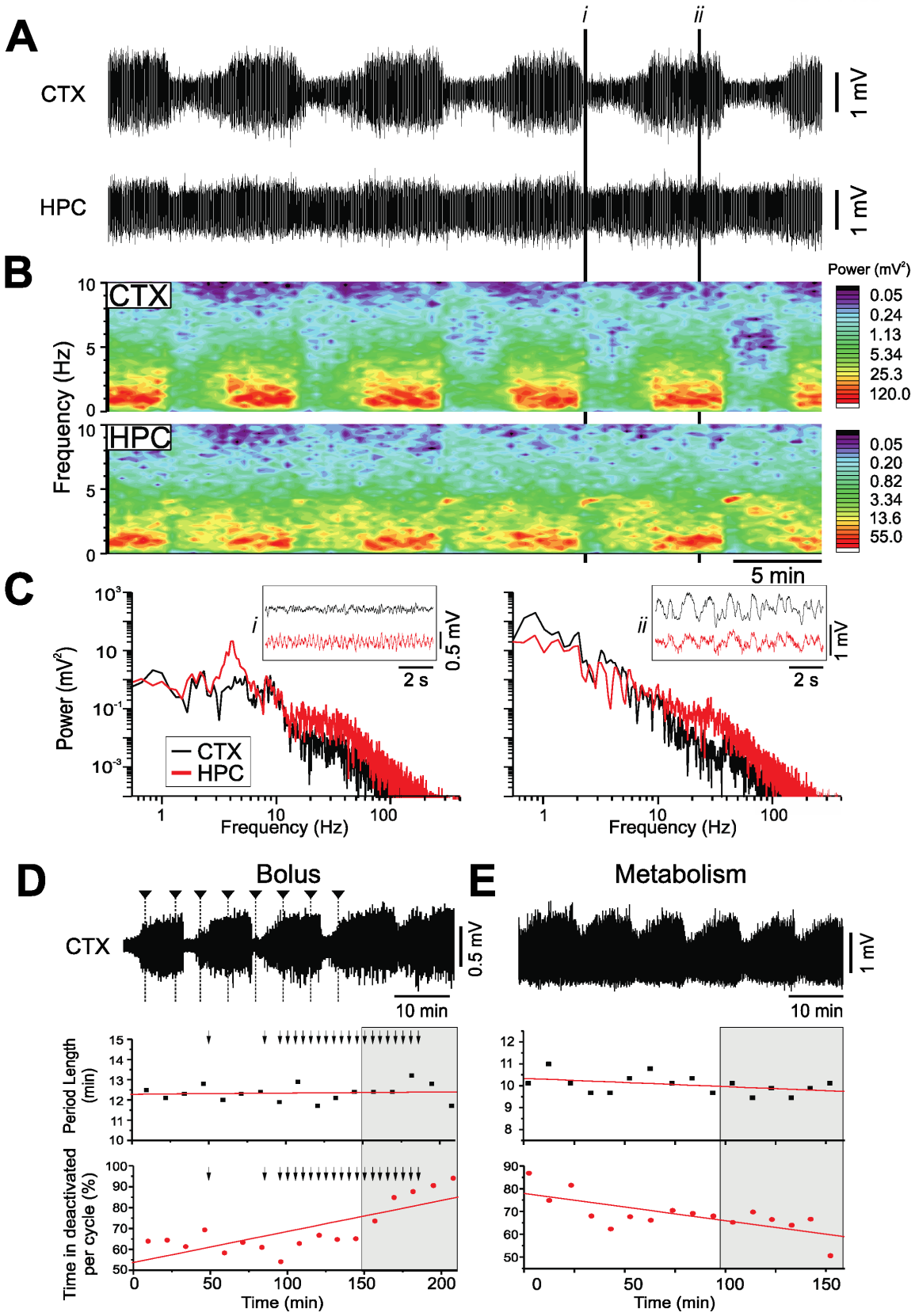

Figure 2.1 Spontaneous and cyclic alternations of brain state under urethane anesthesia.

Figure 2.1 Spontaneous and cyclic alternations of brain state under urethane anesthesia. **A**, Continuous, 40-minute duration cortical (CTX) and hippocampal (HPC) EEG traces. 10-second samples of activated (i) and deactivated (ii) states are expanded in C. **B**, Spectrograms of CTX (top) and HPC (bottom) EEG traces in A. **C**, Power spectra for the CTX and HPC during an activated state (left), and a deactivated state (right), with insets of 10-second raw traces representative of each state. **D,** A 60-minute cortical EEG sample (top). Arrows indicate administration of supplemental doses of urethane in increments of 0.01 ml. The sample trace is denoted by the grey box in both the scatterplots of the period length of cycles across time (linear fit, n=17, p=0.74) and the percentage of time spent in deactivated per cycle (linear fit, n=17, $p<0.01$). **E**, A 60-minute cortical EEG sample (top) of metabolism of urethane over time. The sample trace is denoted by the grey box in both the scatterplots of the period length of cycles across time (linear fit, n=16, p=0.11) and the percentage of time spent in deactivated per cycle (linear fit, n=16, $p<0.01$).

Furthermore, additional bolus doses of urethane did not change the rhythmicity nor the periodicity of state changes, although they did change the proportion of time spent in the two states. In a subset of urethane anesthetized rats, supplemental doses of urethane (0.52±0.14 g/kg; n=4) decreased the proportion of time spent in the activated state (42.2±12.0% per cycle; Figure 2.1D). However, in the subset of rats that were not administered supplemental doses of urethane, the gradual metabolism of urethane (over an average time period of 2.46±0.28 hours; n=6) increased the proportion of time spent in the activated state (29.83±6.62% per cycle; Figure 2.1E).

During these long-term recordings, anesthetic plane was monitored via a nociceptive stimulus to the hind paw. However, consistent with our previous observations (Clement et al., 2008), no reflexive withdrawal response was observed in any of the urethane anesthetized animals regardless of brain state, indicating that the observed changes in brain state were not due to a decline in anesthetic plane.

2.4.2 Ketamine-xylazine

In accordance with our previous research (Sharma et al., 2010), KET-XYL anesthesia was found to evoke a particularly stable and unitary state of large amplitude, slow oscillatory activity in both the neocortex and hippocampus (Figure 2.2A,B) at an average peak frequency of 1.6±0.07 Hz (n=5; Figure 2.2C). We also observed some slow-oscillation coupled beta activity in the cortex with a wide bandwidth range between 10-25 Hz (the 10 Hz peak in 2C is an exemplar such activity). Over a 40-minute period of metabolism, there was a gradual decrease in the

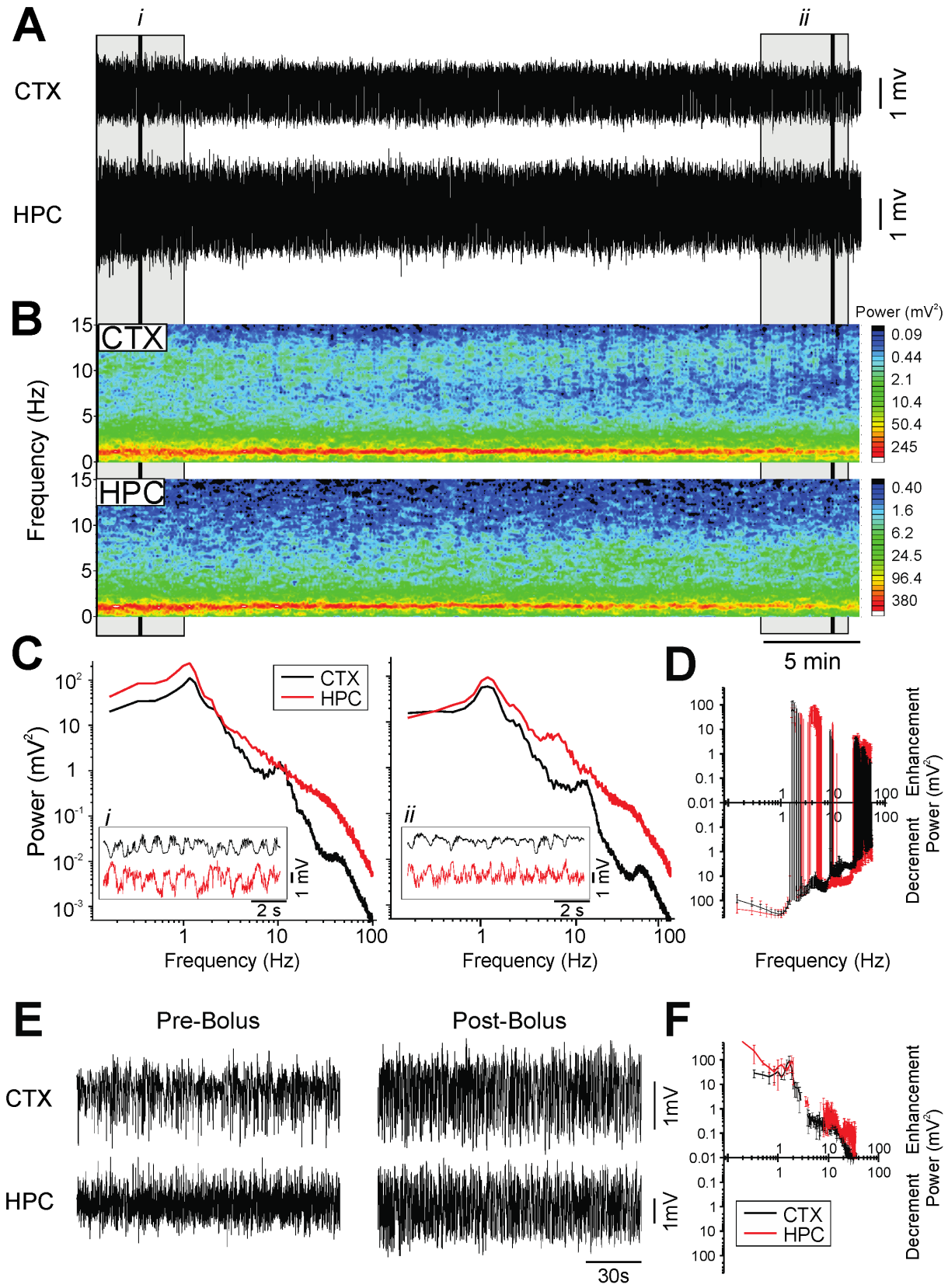

Figure 2.2 Global slow-oscillatory activity under ketamine-xylazine anesthesia.

Figure 2.2 Global slow-oscillatory activity under ketamine-xylazine anesthesia. A, Continuous, 40-minute duration cortical (CTX) and hippocampal (HPC) EEG traces. 5-minute (grey box) and 10-second (black line) samples from the beginning (i) and end (ii) of the are further analyzed in in C **B**, Spectrograms of CTX and HPC traces from A. **C**, Power spectra of a 5-minute selection (grey box) from the EEG traces in A, with an inset of a 10-second raw CTX and HPC EEG trace (black line) from the beginning of A (left panel, i) and end of A (right panel, ii) **D**, The average difference in spectral power over a 40 minute metabolism period, plotted using 2-minute samples pre and post-metabolism to denote the average increment or decrement of power (n=3). **E**, *Pre-bolus:* A 2-minute sample of CTX and HPC traces during a surgical plane of ketamine-xylazine anesthesia. *Post-bolus*: A 2-minute sample of CTX and HPC traces following a bolus infusion of ketamine-xylazine (16.6±1.9 mg/kg and 1.5±0.1 mg/kg; n=5). **F**, The average difference in spectral power following bolus infusion, plotted using 2-minute samples pre and post bolus to denote average increment or decrement of power (n=5).

amplitude of slow oscillatory local field potentials in the raw neocortical and hippocampal recordings, which could also be observed in the power spectra in the 0.5–2 Hz bandwidth (Figure 2.2D). While this state of synchronized slow oscillatory activity resembled the activity observed during the deactivated state under urethane, KET-XYL anesthetized rats did not exhibit any cyclical alternations in brain state while at a surgical plane.

Supplemental i.v. bolus doses of KET-XYL (16.6±1.9 mg/kg and 1.5±0.1 mg/kg; n=5), consistently and rapidly increased the amplitude of the slow oscillatory activity in the neocortex and hippocampus (Figure 2.2E,F). In spectral analyses, these increases were observed in the power of the slow oscillatory signal (~1 Hz) and gamma bandwidth (30–40 Hz; Figure 2.2F). The differential pharmacodynamic and pharmacokinetic profiles of ketamine and xylazine likely have a role in the brain state effects we observed following bolus doses and metabolism of the drugs, as each drug would exert a more powerful influence dependent on time from administration.

On the other hand, when animals were left to metabolize the drug over long periods (> 40 minutes), a shift in both brain and physiological state (i.e., increased respiration rate) could suddenly occur. Brain state during this time period exhibited patterns of neocortical low-voltage fast activity, and hippocampal theta similar to the activity observed in the activated state in urethane anesthetized rats and during REM sleep. However, in contrast with the stable anesthetic plane produced by urethane, these electrophysiological changes in KET-XYL coincided with a reflexive withdrawal to a hind paw pinch. This key difference indicates that the observed shifts in EEG state were reflective of a loss of surgical plane, rather than a neurophysiological state analogous to REM in natural sleep or the activated state under urethane. Accordingly, when animals exhibited these shifts, they were promptly administered a supplementary dose of KET-

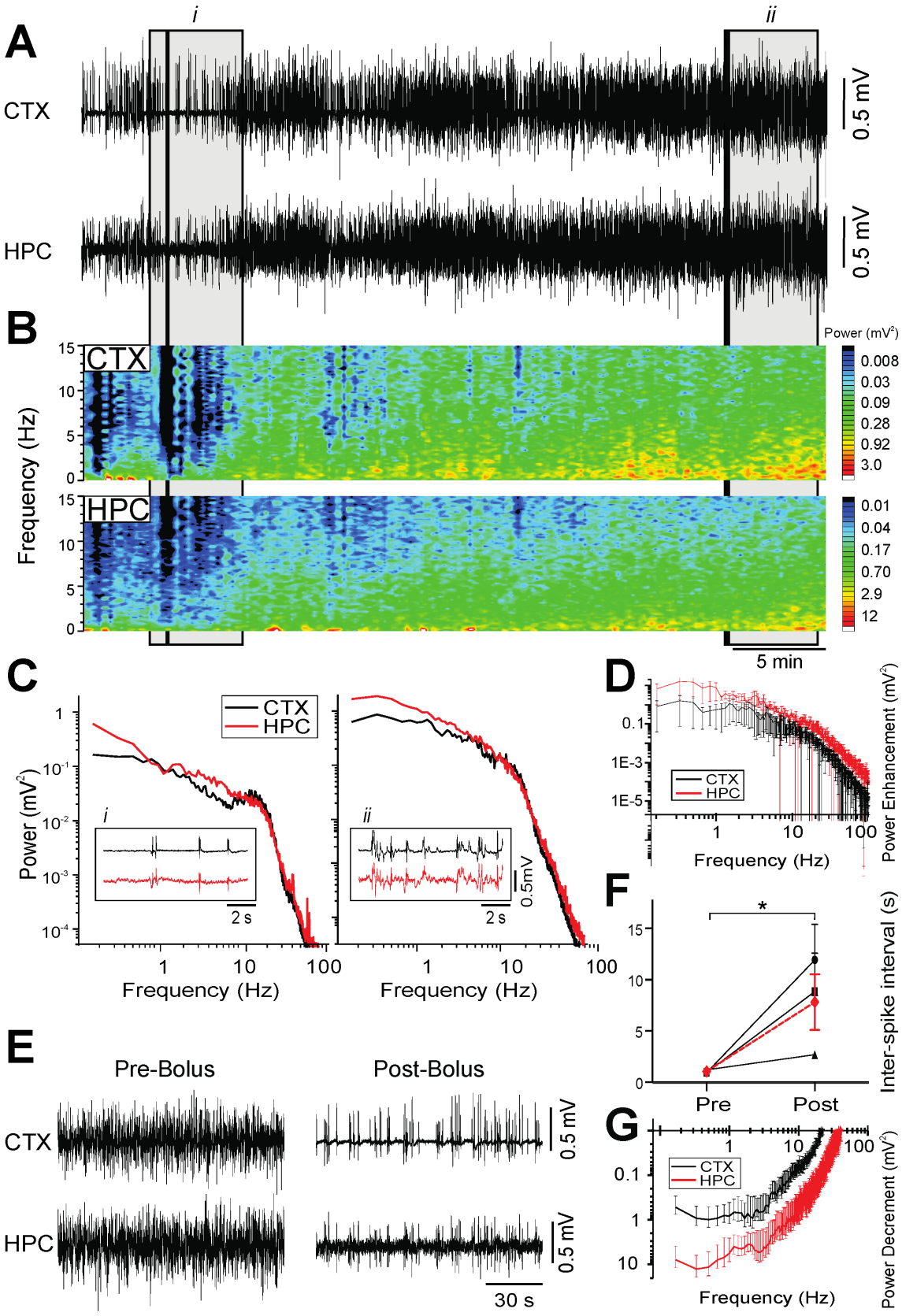

Figure 2.3 Burst-suppression activity under pentobarbital anesthesia.

Figure 2.3 Burst-suppression activity under pentobarbital anesthesia. A, Continuous, 40-minute duration cortical (CTX) and hippocampal (HPC) EEG traces. 5-minute (grey box) and 10-second (black line) samples from the beginning (i) and end (ii) of the are further analyzed in in C. **B**, Spectrograms of CTX and HPC EEG traces in A. **C**, Power spectra of a 5-minute selection (grey box) from the EEG traces in A, with an inset of a 10-second raw CTX and HPC EEG trace (black line) from the beginning of A (left panel, i) and end of A (right panel, ii). **D,** The average difference in spectral power over a 40 minute metabolism period, plotted using 2-minute samples pre and post-metabolism to denote the average increment or decrement of power (n=3). **FE**, *Pre-bolus:* A 2-minute sample of raw CTX and HPC traces during surgical plane of pentobarbital anesthesia. *Post-bolus*: A 2-minute sample of activity following a bolus infusion of pentobarbital (6.5 mg). **F,** The duration of isoelecticity (ISI) in pentobarbital anesthetized rats significantly increased by 6.8±2.8 s (n=3; $F_{(1,503)}$ =163.5; $P < 0.0001$) following a 6.5 mg bolus dose of pentobarbital (individual animals are represented in black, average in red). **G,** The average difference in spectral power pre to post-bolus infusion, plotted using 2-minute samples pre and post-metabolism to denote increment or decrement of power (n=3).

XYL to restore a surgical plane of anesthesia. This promptly restored the slow-wave pattern that was characteristic of the baseline anesthetized recordings.

2.4.3 Pentobarbital

Burst-suppression activity was consistently observed at a surgical plane in both the neocortex and hippocampus of PTB anesthetized rats (Figure 2.3A,B). Burst-suppression is a pattern of activity characterized by isoelectricity interspersed with high-amplitude spikes and typically serves as an indicator of very deep levels of anesthesia (Derbyshire et al., 1936; Swank and Watson, 1949). It is also associated with brain activity observed in patients with brain damage or coma (Brown et al., 2010).

Across neocortical and hippocampal sites, bursts occurred with a high degree of coincidence (Figure 2.3C). However, during periods of isoelectricity in the neocortex, the hippocampus showed low-voltage, faster activity with a peak amplitude in the 11–18 Hz bandwidth (Figure 2.3C). Over 40-minute periods of recording, without supplemental infusions of PTB, we observed a near-linear increase in electrographic amplitude in both the neocortex and the hippocampus (Figure 2.3A-D). Correspondent with these increases in amplitude was a gradual return of spectral power for all frequencies, with a preferential increase in lower frequency bandwidths (0–10 Hz; Figure 2.3D).

A subset of this group of rats was administered bolus increases of PTB. At baseline, in the pre-bolus phase, we observed an average isoelectric period between bursts of 1.1±0.1 s (n=3), during a stable surgical plane of anesthesia (Figure 2.3E,F). Subsequently, when a bolus dose of PTB (6.5 mg) was administered, the duration of isoelectric periods between bursts significantly increased on average by 6.8±2.8 s (n=3; $F_{(1,503)} = 163.5$; $P < 0.0001$; Figure 2.3F). The

concurrent periods of isoelectricity in the cortex, and low-voltage fast activity in the hippocampus observed post-bolus infusion translated to a decrease in spectral power across all frequencies, with lower frequencies (0.5–4.5 Hz) being preferentially depressed (Figure 2.3G).

When rats were allowed to metabolize the bolus dose without additional infusions, we observed a reciprocal and significant change in the isoelectric inter-burst interval; an average decrease of 6.2±3.2 s over 40 minutes (n=3; $F_{(1,459)} = 183.9$; $P < 0.0001$. While spectral power (and signal amplitude) gradually recovered to pre-infusion levels, there were no dramatic shifts in brain state, nor in anesthetic plane.

2.4.4 Isoflurane

At a surgical plane of anesthesia, ISO (2.0% in medical oxygen) also generated a burst-suppression pattern of electrographic activity in the forebrain, with remarkable similarities to the pattern of burst-suppression activity observed under PTB (Figure 2.4A,B). As with PTB, bursts tended to occur concomitantly at both neocortical and hippocampal sites, while periods of isoelectricity in cortex corresponded to low-voltage fast activity (8–15Hz; n=5) in the hippocampus (Figure 2.4C).

We also recorded EEG activity under reduced concentrations, while closely monitoring anesthetic state. At a concentration of 1.5% ISO, the average inter-burst interval was 2.9±1.7 s (n=3; Figure 2.4D-F). Subsequent changes from this to a higher concentration (2%) significantly increased the duration of the isoelectric period between bursts, which corresponded to an average

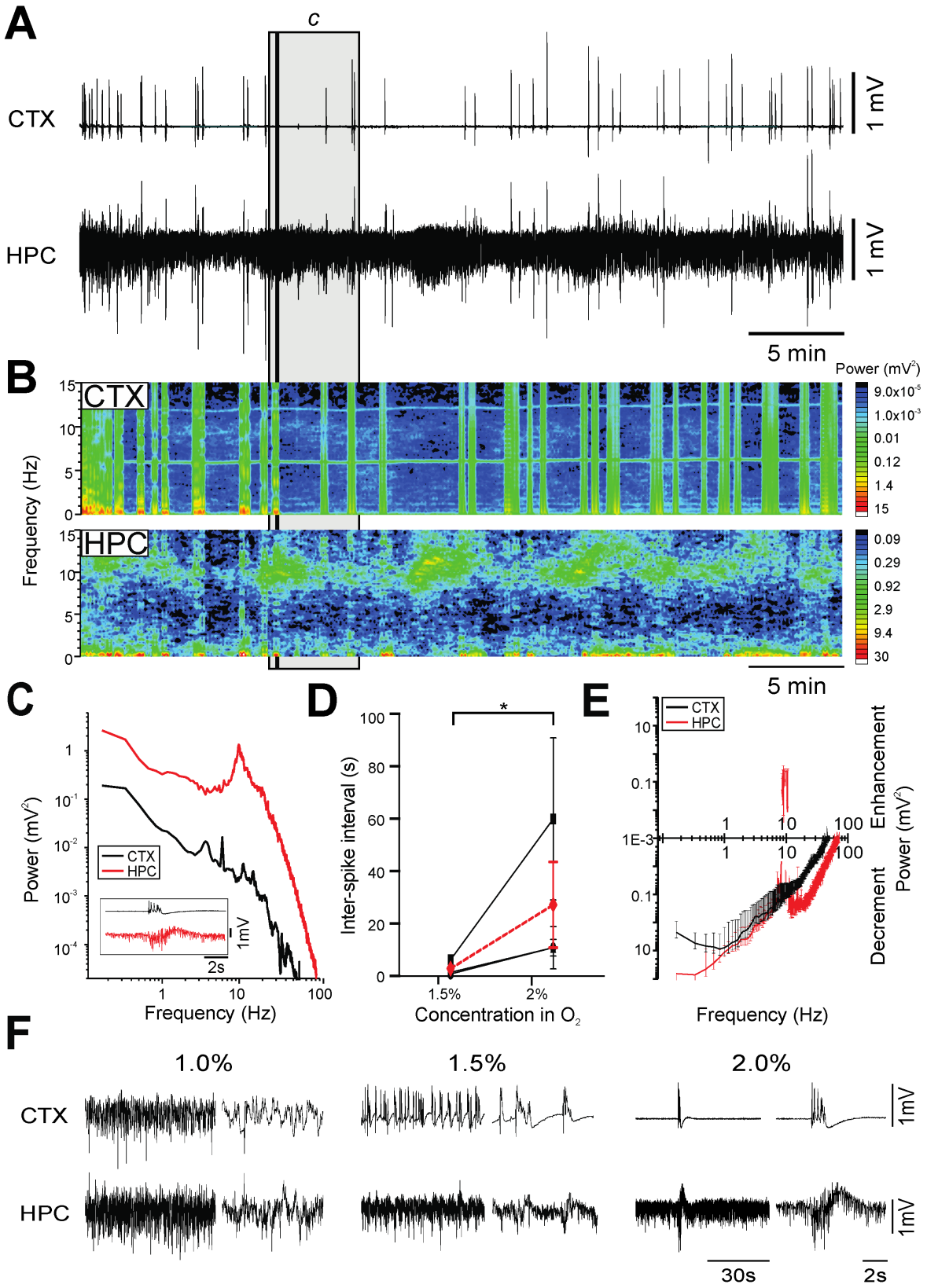

Figure 2.4 Burst-suppression activity under isoflurane anesthesia at 2%.

Figure 2.4 Burst-suppression activity under isoflurane anesthesia at 2%. A, Continuous, 40-minute duration cortical (CTX) and hippocampal (HPC) EEG traces. A 5-minute (grey box) and 10-second (black line) sample from the 40-minutes at 2% isoflurane of the are further analyzed in in C. **B**, Spectrograms of CTX and HPC EEG traces in A. **C**, Power spectra of a 5-minute selection (grey box) from the EEG traces in A, with an inset of a 10-second raw CTX and HPC EEG trace (black line) from A. **D**, Inter-spike intervals (ISI) in isoflurane anesthetized rats significantly increased by 24.4±14.6 s (n=3; $F_{(1,263)} = 96.11$; $P < 0.0001$) following a shift from 1.5% to 2% isoflurane (individual animals are represented in black, average in red). **E,** The average differences in spectral power between 2-minute samples from 1.5% and 2% isoflurane are plotted to denote average increment or decrement of power with increased isoflurane concentration (n=3). **F**, One-minute samples of CTX and HPC EEG traces at 1%, 1.5% and 2%, with 8 second expansions to the right of each 1-min trace.

increase of 24.4±14.6 s ($F_{(1,263)} = 96.11$; $P < 0.0001$; Figure 2.4D). Interestingly, at further decreased concentrations of ISO (1%), we observed changes in brain state in 3 of the 5 rats tested. Unlike the effects observed at 1.5%, these changes in brain state were marked by a shift in neocortical activity from burst-suppression to low-voltage fast irregular activity, and the appearance of theta activity (3–12 Hz) in the hippocampus. While the state produced by this transition was reminiscent of the activated state observed in urethane anesthesia and REM sleep, it was also accompanied by a reflexive withdrawal to a hind paw pinch, indicating a loss of surgical plane. This was immediately rectified with an increase in the delivered concentration of ISO to 2% in order to restore an appropriate level of anesthesia, which was accompanied by a broadband decrease in power (Figure 2.4E). Therefore, our results show that at surgical planes of anesthesia, the only form of activity apparent in the forebrain was burst-suppression, and any observed changes in state-dependent activity were reflective of a loss of surgical plane.

2.4.5 Propofol

Due to a relatively short duration of anesthetic effect, PRO is often administered via continuous infusion to ensure a stable plane of anesthesia (Flecknell, 2016c). Thus, we investigated the neurophysiological state evoked by PRO at a steady rate of infusion, and assessed differences in circulating levels of PRO by administering supplementary bolus doses, and/or by temporarily discontinuing continuous infusion until a change in brain state (or anesthetic plane) was observed.

At a continuous infusion rate of 60 $mg \cdot kg^{-1} \cdot hr^{-1}$, PRO induced a stable pattern of burst-suppression activity (Figure 2.5A-C), consistent with previous reports (Kenny et al., 2014),

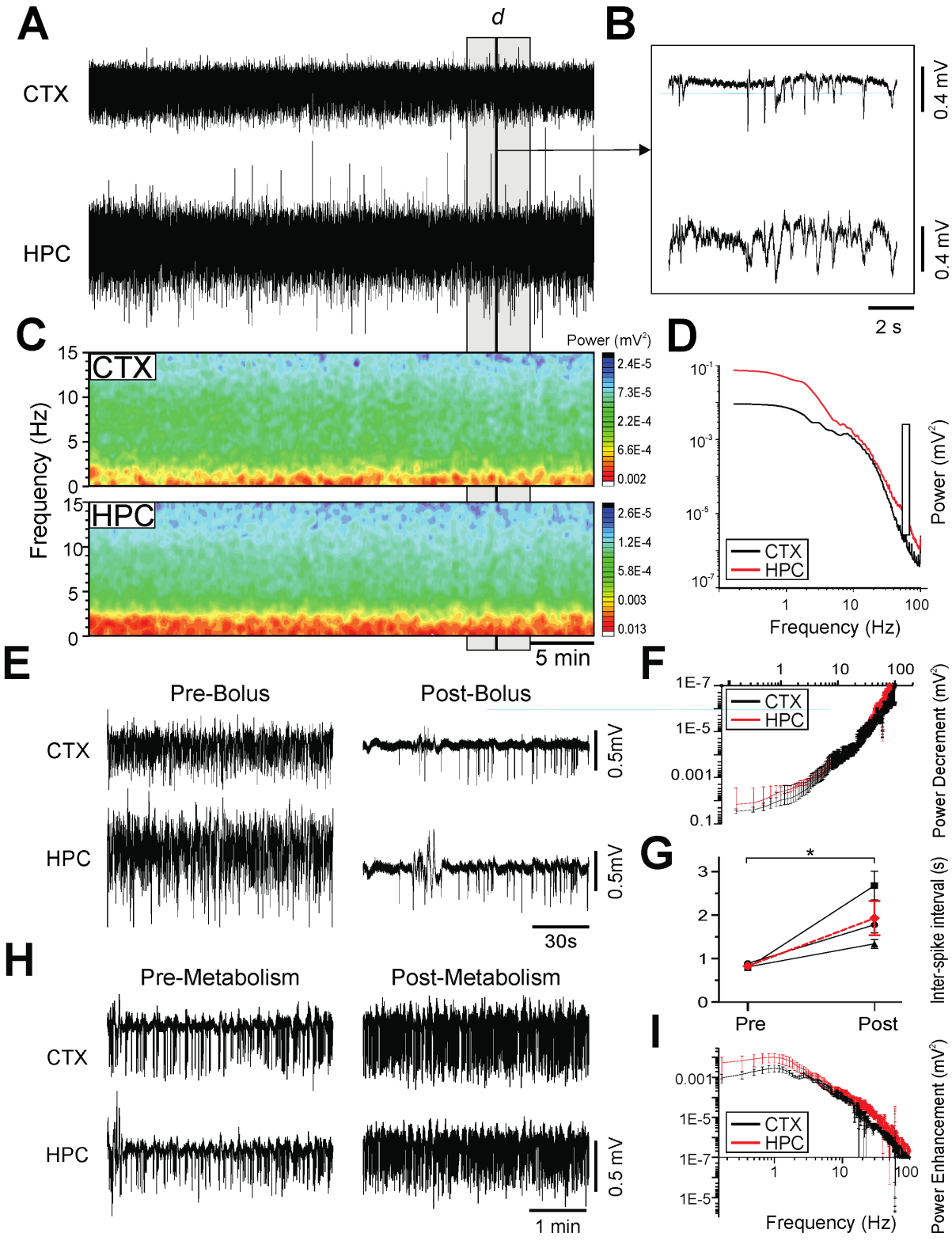

Figure 2.5 Burst-suppression activity under propofol anesthesia.

Figure 2.5 Burst-suppression activity under propofol anesthesia. **A**, Continuous, 40-minute duration cortical (CTX) and hippocampal (HPC) EEG traces. A 5-minute (grey box) sample is further analyzed in D, and a 10-second (black line) sample is expanded in B. **B**, Expanded 10-second trace of CTX and HPC from A (black line). **C,** Spectrograms of CTX and HPC traces in A. **D**, Power spectra of a 5-minute selection from A (grey box), representative of the activity observed throughout the 40-minute duration of the trace in A, due to continuous delivery of propofol. Noise at 60 Hz has been obsfucated by a white box. **E**, *Pre-bolus:* A 2-minute sample of CTX and HPC traces during a surgical plane of propofol anesthesia. *Post-bolus*: A 2-minute sample of activity following a bolus infusion of propofol (2 mg). **F**, The average difference in spectral power following a bolus (2mg) of propfol, plotted using 2-minute samples pre and post-metabolism to denote the average increment or decrement of power (n=3). **G,** Inter-spike intervals in propofol anesthetized rats significantly increased by 1.1±0.4 s ($F_{(1,574)} = 136.0$; $P < 0.0001$; n=3) following a 2 mg bolus dose of propofol. **H**, *Pre-metabolism:* A 4-minute sample of pre-metabolism activity in the CTX and the HPC during propofol anesthesia. *Post-metabolism*: A 4-minute sample of activity following 10 minute metabolism of a bolus. **I,** The average difference in spectral power over a 10 minute metabolism period, plotted using 2-minute samples pre and post-metabolism to denote the average increment or decrement of power (n=3).

which showed amplified power in the 0.5–2 Hz bandwidth (Figure 2.5C,D). This activity was similar to the burst-suppression activity observed in both PTB and ISO, albeit with a shorter average period of isoelectricity during inter-burst intervals (0.83±0.06 s; n=3). A bolus infusion (2 mg) of PRO produced a broadband decrease in power (Figure 2.5E,F), accompanied by a significant increase in the average period of isoelectric activity between bursts of 1.1±0.4 s ($F_{(1,574)} = 136.0$; $P < 0.0001$; n=3; Figure 2.5G). This observed increase in inter-burst interval was analogous to the increases in isoelectric activity observed in both ISO and PTB following supplemental doses of anesthetic.

Temporary suspension of the continuous infusion of PRO (over 10 minutes) coincided with a gradual increase of broadband power, with a preferential increase in the delta frequencybandwidth (0-3 Hz) in both the neocortex and the hippocampus (Figure 2.5H,I). Additionally, over these 10 minutes, the duration of isoelectric inter-burst intervals significantly decreased by an average of 1.1±0.2 s (n=3; $F_{(1,562)} = 87.6$; $P < 0.0001$). However, this transition coincided with a reflexive withdrawal of the hind paw to a nociceptive stimulus indicating a loss of surgical plane, and was subsequently rectified by returning the animal to continuous infusion of PRO. Hence, PRO, PTB and ISO all appear to evoke a similar burst-suppression pattern of altered brain activity during surgical planes of anesthesia.

2.4.6 Chloral hydrate

Similar to the PRO group, we administered CH at a constant rate of infusion (150 $mg \cdot kg^{-1} \cdot hr^{-1}$), following an initial bolus dose of 200 mg/kg. Perhaps surprisingly, especially based on its similar pharmacological profile to PTB, ISO and PRO; CH anesthetized rats exhibited

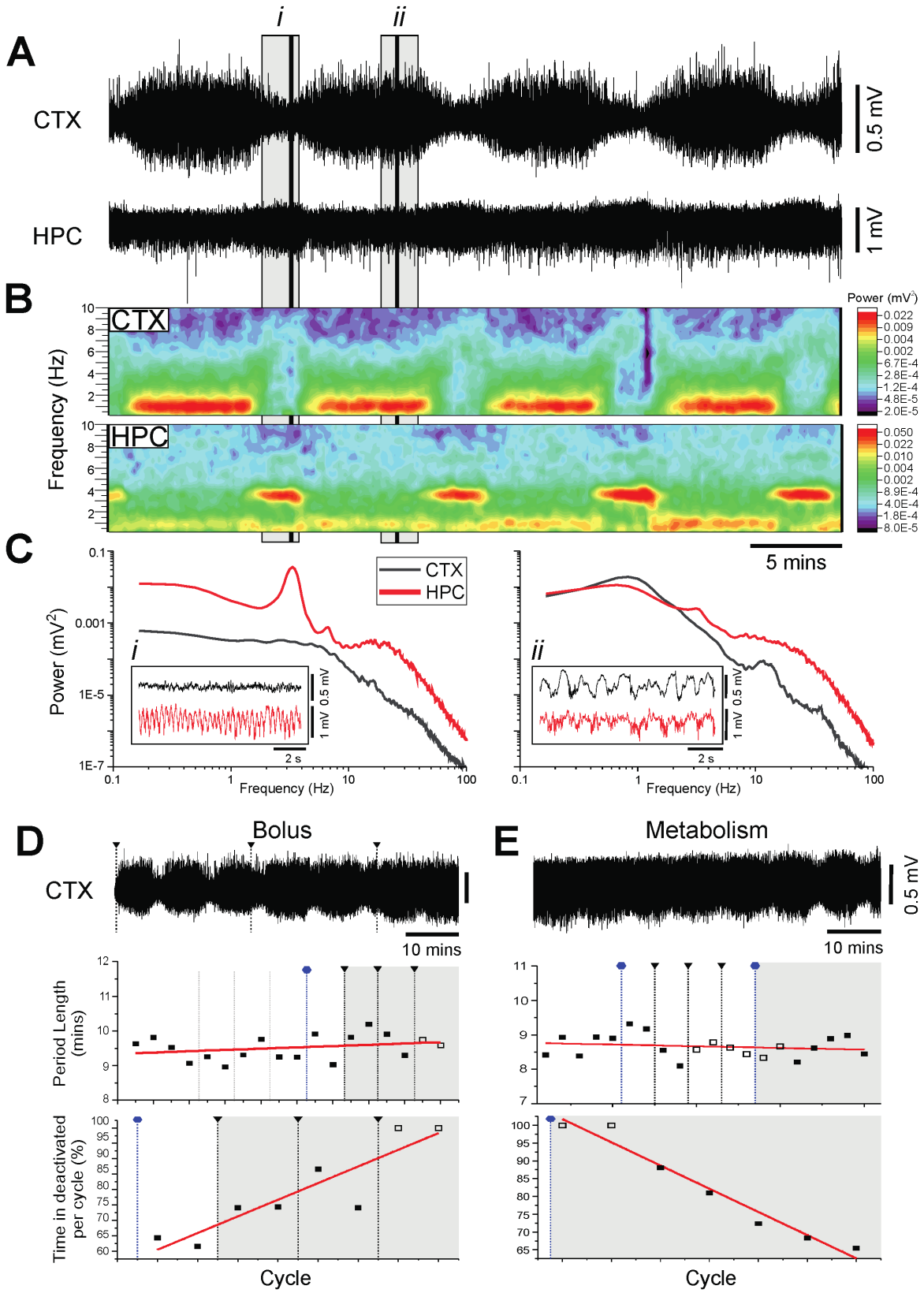

Figure 2.6 Spontaneous and cyclic alternations of brain state under chloral hydrate anesthesia.

Figure 2.6 Spontaneous and cyclic alternations of brain state under chloral hydrate anesthesia. **A**, Continuous, 40-minute duration cortical (CTX) and hippocampal (HPC) EEG traces. 10-second samples of activated (i) and deactivated (ii) states are further analyzed in C. **B**, Spectrograms of CTX (top) and HPC (bottom) EEG traces in A. **C**, Power spectra for the CTX and HPC during an activated state (left, i), and a deactivated state (right, ii), with insets of 10-second raw traces representative of each state. **D,** A 65-minute cortical EEG sample (top). Black lines indicate administration of supplemental doses of chloral hydrate in increments of 15 mg (0.15 mL). The sample trace is denoted by the grey box in both the scatterplots of the period length of cycles across time (linear fit, n=18, p=0.26) and the percentage of time spent in deactivated per cycle (linear fit, n=8, p=0.003). Grey lines indicate supplemental doses of 5 mg of chloral hydrate (0.5 mL), and blue lines indicate a stoppage of continuous infusion of chloral hydrate. Continuous infusion resumed with the next black line and bolus infusion. Unfilled boxes are estimated cycles (see methods). **E**, A 65-minute cortical EEG sample (top) of metabolism of chloral hydrate over time. The sample trace is denoted by the grey box in both the scatterplots of the period length of cycles across time (linear fit, n=20, p=0.44) and the percentage of time spent in deactivated per cycle (linear fit, n=7, p<0.001). Blue lines indicate a stoppage of continuous infusion of chloral hydrate. Continuous infusion resumed with the next black line and bolus infusion. Unfilled boxes are estimated cycles (see methods).

spontaneous, and cyclically occurring alternations between two distinct forebrain states, remarkably like those observed during urethane anesthesia (Figure 2.6A-C and Figure 2.1A-C). We observed both a state of forebrain activation that consisted of low-voltage, fast activity in the cortex, coinciding with a prominent theta (3.30±0.11 Hz) oscillation in the hippocampus, alternating with a deactivated state consisting of large amplitude slow oscillatory activity in both the cortex (0.73±0.07 Hz) and hippocampus (0.64±0.03 Hz; Figure 2.6B,C). The average period of these cyclical alternations was also highly similar to the period observed in urethane, at 10.12±0.58 minutes per cycle.

Further overlaps with urethane were observed when a subset of rats were given supplemental bolus doses of CH in addition to the continuous infusion (total supplemental dose: 50.0±5.0 mg, n=3; Figure 2.6D). During the first two 15mg i.v. bolus infusions, the proportion of time spent in the activated state decreased by an average of 16.65±4.14% per cycle, with an inverse increase in the proportion of time spent in the deactivated state (Figure 2.6D). We did not include the change in proportion of time spent in the activated state from the second to third 15 mg bolus in our calculations, since 2 of the 3 animals reached a ceiling after the second bolus infusion, spending 100% of the cycle in the deactivated state, meaning that no change was observed from the second to third bolus infusion.

When continuous infusion of CH was discontinued in the same rats (Figure 2.6E), we observed an average increase of 12.47±3.68% in the proportion of time spent in the activated state per cycle, once a distinguishable change in proportion of time spent in the activated state was observed. Importantly, neither additional doses of CH, nor metabolism altered the period length of each cycle (Figure 2.6E).

In a final parallel to urethane anesthesia, these electrophysiological dynamics do not appear to be due to a lessening of anesthetic state. During baseline recordings, all rats in the CH condition were receiving a continuous infusion of the drug, and we also observed no reflexive withdrawal response to a hind paw pinch, irrespective of brain state.

2.5 Discussion

Under identical recording conditions, each of the six anesthetic agents tested produced one of three distinct patterns of EEG activity at a surgical plane of anesthesia:

1. Burst-suppression, which is a brain state characterized by short periods of high-amplitude, high-frequency bursts interspersed with longer periods of isoelectric activity, and is typically associated with brain damage, hypothermia or coma (Brown et al., 2010). This pattern of EEG activity was observed during PTB (Van Ness, 1990), ISO (Adamantidis et al., 2007), and PRO (Kenny et al., 2014) anesthesia.
2. A unitary state of synchronized, slow-oscillatory activity similar to the rhythmic on-off (up/down) field fluctuations observed during NREM sleep (Sheroziya and Timofeev, 2014) was observed during KET-XYL anesthesia.
3. Spontaneous, cyclical alternations between activated and deactivated brain states analogous to the REM/NREM cycle during natural sleep, in terms of both electrographic features and dynamics, was observed during both urethane (Clement et al., 2008) and CH anesthesia.

The agent-specific diversity of these brain states highlights how crucial an appropriate choice of anesthetic is within an experimental paradigm, and indeed the necessity to report brain state in order to accurately interpret *in vivo* neurophysiological experimental outcomes (Piccitto, 2018).

It is important to note that any major deviations of forebrain activity towards more activated patterns, from either the patterns of burst suppression produced by PTB, ISO, and PRO, or from the slow-oscillatory activity observed during KET-XYL following periods of metabolism (or in the case of ISO, a lower gaseous concentration) were associated with a loss of surgical plane of anesthesia. In these cases, the loss of a clinical plane of anesthesia was indicative of an imminent return to consciousness. Consequently, continuous observation of brain state not only contextualizes neurophysiological experimental outcomes, but also serves as an online index of depth of anesthesia when agent-specific EEG signatures are monitored appropriately (Purdon et al., 2015).

In contrast to the metabolically coupled changes in brain state observed in PTB, ISO, PRO and KET-XYL, we have previously demonstrated that brain state alternations under urethane anesthesia are not associated with a lessening of anesthetic plane (Clement et al., 2008), nor are they significantly altered over long recording periods (Silver et al., 2021). Here, we further demonstrate that not only in urethane, but also in CH, that no reflexive withdrawal to a hind paw pinch was observed in either the activated or the deactivated brain state, and furthermore, that bolus infusions or metabolism of urethane or CH did not alter the periodicity of brain state alternations, only the proportion of time spent in either the activated or deactivated state per cycle. These data indicate that the alternations between dichotomous brain states under the two anesthetics were not attributable to changes in anesthetic plane. In this respect, both urethane and continuous i.v. administration of CH provide extremely stable and tractable

experimental models for the alternating electrophysiological features and dynamics of sleep, while also allowing for surgical manipulations that might not be technically or ethically feasible in naturally sleeping animals.

2.5.1 Anesthesia as a model for the brain states associated with altered states of consciousness

The dose-dependent, and agent-specific control of brain state that is afforded by anesthesia provides an unparalleled pharmacological analog to mimic the brain states observed in many altered states of consciousness, such as specific components of natural sleep, and coma (Sharma et al., 2010; Brown et al., 2011). As we demonstrate here, KET-XYL has applications for modelling the large-amplitude, rhythmic slow-oscillatory activity, archetypical of NREM sleep. KET-XYL also provides the added experimental advantage of brain state stationarity, since the highly transient nature of natural sleep makes cohesive analysis of a single brain state technically challenging (Sharma et al., 2010). Accordingly, the stability of the forebrain slow oscillation under KET-XYL provides a useful means to explore aspects of NREM such as the hippocampal slow oscillation (Wolansky et al., 2006), and intracellular thalamocortical dynamics (Sheroziya and Timofeev, 2014).

Anesthesia is also an excellent tool for replicating brain states associated with coma. This is perhaps best evidenced by its clinical use for inducing medical coma in order to manage conditions such as refractory status epilepticus and in treating traumatic brain injuries (Selman et al., 1981; Yang et al., 2019). Our data shows that surgical plane levels of PTB, ISO, and PRO all provide effective models to probe the mechanistic complexities of the coma-like brain state of

burst-suppression, such as cortical hyperexcitability (Ferron et al., 2009a), neurovascular coupling (Liu et al., 2010a), and local cortical spatiotemporal dynamics (Lewis et al., 2013). Indeed, ISO was recently shown to exhibit the same dysregulation in homeostatic neural firing rates as NREM in pre-symptomatic mouse models of familial Alzheimer's disease (Zarhin et al., 2022), indicating that ISO may serve as a useful model to explore the connection between subclinical epileptiform activity and network hyperexcitability observed in some models of Alzheimer's disease (Kroeger and Amzica, 2007; Brown et al., 2018).

However, it is important for researchers choosing any of these anesthetics to be aware that PTB, ISO and PRO produce agent-specific differences in both burst-suppression architecture, and duration of suppression (Akrawi et al., 1996; Fleischmann et al., 2018), which may arise from differential pharmacological mechanisms, such as distinct binding sites on GABA-A receptors (Krasowski et al., 1998). Likewise, KET-XYL has its own experimental caveats, as it has been reported to elicit highly elevated power in the gamma bandwidth (30–100 Hz; (Chauvette et al., 2011)), which we also observed when we administered supplementary bolus doses of KET-XYL. Consequently, further considerations may need to be taken into account based on agent-specific neurophysiological characteristics, and findings in these models would likely need to be replicated in the endogenously occurring altered state of consciousness. In addition, researchers employing any of these anesthetics to model specific brain states would need to continuously monitor brain state (Piccitto, 2018). Nonetheless, when the limitations of a pharmacological agent are accounted for in both experimental design and analysis, these agents provide an invaluable analogs to probe the altered states of arousal of coma and slow-wave sleep (Brown et al., 2011; Bonhomme et al., 2019).

2.5.2 Anesthesia and sleep

Anesthesia shares a number of mechanistic overlaps with sleep. First, and foremost anesthesia co-opts endogenous sleep-related circuits by recruiting sleep-promoting nuclei such as the lateral habenula, and the ventrolateral preoptic area, and simultaneously suppressing arousal-promoting nuclei such as the tuberomammillary nucleus and the dorsal raphe (Franks, 2008; Gelegen et al., 2018; Hemmings et al., 2019). More recently, it has been demonstrated that the optogenetic reactivation of a population of neuroendocrine anesthesia-activated neurons in the supraoptic nucleus promoted slow-wave sleep, and that ablation of these same cells conversely led to a significant loss of both slow-wave and REM sleep, and shorter duration of general anesthesia (Jiang-Xie et al., 2019). Furthermore, sleep and anesthesia have a reciprocal influence on one another, Sleep deprivation affects both the induction and recovery from anesthesia (Tung et al., 2002), and sleep debt induced by sleep deprivation can be attenuated by specific anesthetics (Tung et al., 2004; Pal et al., 2011). These commonalities imply that there are shared neurobiological processes across the two conditions. As such, while anesthesia may not be a perfect replication of physiological sleep (Akeju and Brown, 2017), the many mechanistic and behavioural overlaps between these two state of unconsciousness, combined with the comprehensive experimental control granted by anesthesia makes it is an optimal tool for the unravelling the intricacies of the spontaneous EEG dynamics of sleep.

Of all the anesthetics we tested, at a consistent and deep surgical plane of anesthesia only urethane and CH produced the spontaneous, cyclic alternations between a REM-like activated state and NREM-like deactivated state consistent with the quintessential EEG features and dynamics observed in natural sleep. Urethane has long been recognized as an unusual anesthetic in terms of the EEG patterns it produces (Lincoln, 1969; Robinson et al., 1977; Détári and

Vanderwolf, 1987), and its primary mechanism for inducing unconsciousness – which is to hyperpolarize central nervous system neurons by potentiating resting potassium conductance, thus decreasing membrane input resistance (Sceniak and MacIver, 2006). Moreover, the exceptionally slow pharmacokinetics of urethane induces a long lasting, stable plane of surgical anesthesia with minimal depression of both the autonomic nervous system and neurotransmission in the central nervous system (Maggi and Meli, 1986; Dringenberg and Vanderwolf, 1995; Silver et al., 2021). Unfortunately, this prolonged metabolism of urethane also contributes to the sustained exposure to its carcinogenic effects (Maggi and Meli, 1986; Hara and Harris, 2002). Due to these ethical considerations, urethane anesthesia is typically limited to acute animal experimental preparations (Maggi and Meli, 1986).

Consequently, it is of great interest that CH anesthesia produced a pattern of EEG activity remarkably similar to urethane as CH is considered an acceptable anesthetic for recovery surgeries (Field et al., 1993; Flecknell, 2016b), and indeed is still in use as a clinical sedative primarily for pediatric patients (Lian et al., 2020). This suggests that CH could provide researchers an avenue to perform controlled neurophysiological manipulations under a sleep-like state of CH anesthesia, and then assess behavioural outcomes. Such a paradigm would be especially useful in assessing the role of brain state in memory consolidation, and may also provide an ethical alternative to methods currently employed to bias brain state like sleep deprivation which inevitably induce stress. Yet, the extent to which CH mimics the dynamic physiological measures observed in both urethane and sleep remains unknown, and may not be identical, as it has been reported to dose-dependently depress cardiovascular and respiratory functions (Field et al., 1993). Nonetheless, there are several pharmacological similarities between CH and urethane that suggest a greater overlap in neurophysiology may exist.

2.5.3 Pharmacological mechanisms influencing brain state

We theorize two potential reasons for the inconsistencies in brain state evoked by CH and the other GABAergic anesthetics. First, at the dosages required to produce a surgical plane of anesthesia, all of the anesthetic agents we tested are acting at multiple neurophysiological targets in addition to potentiating GABAergic activity (Hara and Harris, 2002; Garcia et al., 2010; Hemmings et al., 2019). Secondly, CH is unique from the other GABAergic anesthetics, as it is first metabolized into 2,2,2-trichloroethanol, which then exerts the anesthetic effects that potentiate GABA-A receptor mediated activity (Butler, 1948; Krasowski and Harrison, 2000; Hemmings et al., 2019). Interestingly, urethane is also metabolized into ethanol and carbamic acid (Maggi and Meli, 1986), albeit, much more slowly (Nomeir et al., 1989; Sotomayor and Collins, 1990). Both ethanol and urethane are considered to have a diffuse spectrum of action, with actions that modestly enhance activity at glycine, GABA-A and nicotinic acetylcholine receptors, while simultaneously inhibiting AMPA and NMDA receptors (Hara and Harris, 2002; Teppema and Baby, 2011). Subsequently, the metabolism of CH into a chlorinated ethanol isomer may partially elucidate the parallels in EEG activity and dynamics we observed during both CH and urethane anesthesia, in addition to the inconsistencies with the pattern of burst-suppression activity evoked by other GABAergic anesthetics.

2.6 Conclusions

While the concept of agent-specific effects on brain state such as those we observed in the current study may be considered common knowledge to many researchers in the field of anesthesia, often the effects of a chosen anesthetic on brain state and related evaluations can be overlooked when conducting neurophysiological experiments (Piccitto, 2018). Our results clearly demonstrate why the choice of anesthetic agent is a crucial element for researchers to take into consideration when designing and conducting neurophysiological experiments under anesthesia, as the evoked brain state can significantly impact experimental output. Furthermore, as EEG becomes a more prevalent tool clinically for measuring depth of unconsciousness in both anesthesia and coma, it will be paramount to explore the pharmacological mechanisms of action driving agent-specific differences in EEG signatures between anesthetics (Hemmings et al., 2019), in order to improve clinical perioperative outcomes (Brown et al., 2014).

A better understanding of the intricacies of both the neural targets and pathways that interplay to induce and maintain unconsciousness in anesthesia not only has implications for the refinement and optimization of anesthetic interventions, but also for understanding the neurobiological causes of sleep disorders (Kelz and Mashour, 2019). The overlap with natural sleep of electrophysiological dynamics observed in CH, in addition to the physiological overlaps observed in urethane suggest that these anesthetics are unprecedented tools for probing unconsciousness and the extent to which anesthesia co-opts endogenous sleep pathways. This is because the intertwined pharmacological and physiological unconscious states of sleep and anesthesia are mutually informative, and ultimately offer novel opportunities to explore the mechanisms responsible for unconsciousness (Ward-Flanagan and Dickson, 2019).

3 Urethane anesthesia produces a parallel pattern of c-Fos expression in sleep-wake nuclei to behaviourally-defined unpressured sleep

Nicholas R.G. Silver[1#], Rachel Ward-Flanagan[1#], Silvia Pagliardini[2,3] & Clayton T. Dickson[1,2,3,4]

#Co-first authorship. These authors contributed equally to this work.

[1] Neuroscience and Mental Health Institute, University of Alberta, Canada, T6G 2E1

[2] Department of Psychology, University of Alberta, Canada, T6G 2R3

[3] Department of Physiology, University of Alberta, Canada, T6G 2H7

[4] Department of Anesthesiology and Pain Medicine, University of Alberta, Canada, T6G 2G3

Acknowledgements: This work was supported by Discovery from the Natural Sciences and Engineering Research Council of Canada (NSERC) to CTD (2016-06576), and SP (435843; 2021-02551). R.W-F was supported by an NSERC Doctoral Postgraduate Scholarship, as well as an Alberta Graduate Excellence Scholarship, and NS was supported by an NSERC-USRA.

3.1 Abstract

Investigations into the neural mechanisms that govern the physiological processes underlying unconsciousness during sleep are hindered by its fragility in terms of arousal. Consequently, the highly tractable nature of unconsciousness produced by anesthetics provides a powerful tool to unravel the potentially shared neural pathways of unconsciousness in sleep and anesthesia. Urethane anesthesia, in particular, shows marked parallels to sleep in terms of the spontaneous, cyclical alternations of central brain state and correlated peripheral physiological measures. In order to more critically evaluate the extent of this overlap within known sleep-wake circuitry, we designed a preliminary study that compared levels of neural activation using c-Fos immunohistochemistry in various brain areas known to differentiate sleep versus wake conditions across both urethane anaesthesia and natural sleep, in both sleep deprived and non-sleep deprived conditions. Both natural sleep and urethane anesthetized groups were also compared to a forced wake condition. Our results show that the pattern of neural activation across unpressured natural sleep and urethane anesthesia conditions were highly comparable.

3.2 Significance statement

Research over the past 30 years has made it increasingly clear that sleep and anesthesia can share neural pathways in producing an unconscious state. Consequently, understanding how sleep and anesthesia intersect within the brain can lead to significant insights about the neural correlates responsible for the initiation and maintenance of unconsciousness. Urethane, an acute research anesthetic, produces a behavioural and neurophysiological condition remarkably akin to natural sleep. By comparing markers of neural activity within 10 well-established sleep-wake nuclei, we observed parallel patterns of activation between behaviourally-defined natural sleep, and urethane anesthesia. Our results indicate that urethane anesthesia may co-opt endogenous sleep pathways, and therefore is an important analog to investigate further.

3.3 Introduction

Though sleep is undeniably vital for optimal neurobiological functioning, identifying the neural mechanisms necessary for inducing and maintaining unconsciousness has remained a difficult enterprise due to the complex and fragile nature of sleep (Opp and Toth, 2003; Taveras et al., 2008; Iranzo, 2016; Ward-Flanagan and Dickson, 2019). As the pharmacological counterpart to physiological unconsciousness, anesthesia shares not only clear behavioural parallels to sleep, but also many mechanistic overlaps that suggest shared endogenous pathways for eliciting unconsciousness (Tung et al., 2004; Lydic and Baghdoyan, 2005; Gelegen et al., 2018; Jiang-Xie et al., 2019). Furthermore, anesthesia has the experimental advantage of allowing surgical manipulations, alleviating many of the technical and ethical challenges present in experimental protocols that study natural sleep (Ward-Flanagan and Dickson, 2019). In this respect, anesthesia constitutes a powerful tool for advancing our knowledge of the mechanisms underlying unconscious states, including sleep.

Yet, despite behavioural and mechanistic similarities to natural sleep, at a surgical plane most anesthetics elicit a physiological state that *in toto*, does not resemble sleep. Specifically with respect to brain-derived neurophysiological measures, most anesthetics produce either a unitary state of slow oscillatory electroencephalographic (EEG) activity, or a coma-like state of burst-suppression, neither of which resembles the full and complex dynamics of natural sleep (Ferron et al., 2009b; Sharma et al., 2010; Chauvette et al., 2011). In contrast to other anesthetics, the acute laboratory anesthetic urethane produces spontaneous, cyclical alternations between: 1) an NREM-like deactivated state of large amplitude, slow oscillatory activity (~1 Hz), and 2) a REM-like activated state of low-voltage fast cortical activity, concurrent with theta (~ 4Hz) activity in the hippocampus (Wolansky et al., 2006; Clement et al., 2008). Moreover, the

periodic cycling observed between these states in urethane is not only consistent with the average REM/NREM time period observed in natural sleep, but also covaries with physiological changes, such as respiratory rate/variability, heart rate, core temperature, urodynamics, and pupillary diameter, again in a manner parallel to natural sleep (Whitten et al., 2009; Blasiak et al., 2013; Pagliardini et al., 2013a; Crook and Lovick, 2016). Thus, urethane anesthesia provides an unparalleled pharmacological model for natural sleep in terms of behavioural, electrographic and physiological elements.

As such, our aim was to conduct a preliminary comparison of the levels of neural activation between the sleep-like pharmacological state of urethane anesthesia and natural sleep itself, in order to assess the extent to which they intersect within known sleep-wake circuitry. To that end, we measured the expression of c-Fos, an immediate early gene that has been extensively used to anatomically assess neuronal activity in *in vivo* experiments (Dragunow and Faull, 1989; Chaudhuri, 1997; Chaudhuri et al., 2000; Szyndler et al., 2009; Kawashima et al., 2014). We examined five different experimental groups of rats for differences in c-Fos expression: 1) a sleep deprived group that subsequently received urethane for a 2 hour experimental period (SD-urethane), 2) a sleep deprived group that later received saline for the experimental period (SD-saline), 3) a non-sleep deprived group that later received urethane for the experimental period (nonSD-urethane), 4) a non-sleep deprived group that then received saline for the experimental period (nonSD-saline), and 5) a non-sleep deprived group that were subsequently maintained awake for the experimental period (nonSD-wake).

We chose these conditions as the five groups allowed us to directly compare the patterns of c-Fos expression across multiple manipulations: 1) groups experiencing normal, unpressured sleep and pressured, recovery sleep (nonSD-saline and SD-saline, respectively); 2) groups

undergoing urethane anesthesia following sleep deprivation or not (SD-urethane and nonSD-urethane); 3) both urethane groups to pressured, and unpressured natural sleep groups; and 4) the awake group (nonSD-wake) to all other groups.

Within these five experimental groups, we investigated cFos expression in ten established sleep-wake nuclei, including: the ventrolateral preoptic area (VLPO); the lateral habenula (LHb); the tubomammillary nucleus (TMN); the locus coeruleus (LC); the dorsal raphe (DR); the ventrolateral periaqueductal grey (vlPAG); the laterodorsal tegmentum (LDT); the pedunculopontine tegmentum (PPT); the lateral hypothalamus (LH); and the basal forebrain (BF). A summary of the evidence supporting the role of these regions of interest (ROI) in endogenous sleep-wake circuitry can be found in Table 1. In the present study, we demonstrate that urethane anesthesia produces highly similar patterns of activation in sleep-wake ROI to unpressured sleep (nonSD-saline), irrespective of whether urethane is delivered to rats in either sleep deprived or non-sleep deprived conditions.

3.4 Methods

3.4.1 Subjects

Data were obtained from 20 male Sprague-Dawley rats weighing between 248 and 370g, averaging 305.2 ± 9.24g. The rats used were exclusively male to ensure consistency with our previous studies using urethane anesthesia (Clement et al., 2008; Whitten et al., 2009; Pagliardini et al., 2013a; Pagliardini et al., 2013b). Animals were kept on a 12-hour light/dark cycle at 20 ± 1ºC, and housed in cages containing no more than 4 rats per cage. Cages were polycarbonate

Region of Interest	In Sleep	In Recovery Sleep/Sleep Deprivation	In Anesthetics
		Wake-Related Nucleus	
TMN	Strongly implicated in the generation of wakefulness based on inhibition, firing rate, and c-Fos studies (Lin et al., 1989; Ko et al., 2003; Takahashi et al., 2006)	Increased c-Fos immunoreactivity following forced wakefulness (sleep deprivation with no recovery sleep) (Ko et al., 2003; Takahashi et al., 2006)	Low levels of c-FOS immunoreactivity in dexmedetomidine, propofol, and pentobarbital (Nelson et al., 2002; Nelson et al., 2003)
		NREM-Related Nuclei	
VLPO	Strongly implicated in the generation of NREM sleep based on lesion, firing rate, and c-Fos data (McGinty and Sterman, 1968; Koyama and Hayaishi, 1994; McGinty et al., 1994; Alam et al., 1995; Sherin et al., 1996; Szymusiak et al., 1998; Lu et al., 2000; Gong et al., 2004)	Increased c-Fos immunoreactivity in recovery sleep correlated to increase NREM percentage (Gong et al., 2004)	c-Fos immunoreactivity correspond to volatile anaesthetic induce unconsciousness (Moore et al., 2012)
LHb	Implicated in the consolidation of NREM sleep (Gelegen et al., 2018)	N/A	c-Fos immunoreactivity seen in propofol anesthesia (Gelegen et al., 2018)
vlPAG	Strongly implicated in the generation of NREM and termination of REM sleep based on chemogenetic, optogenetic, and c-Fos studies (Sapin et al., 2009; Hsieh et al., 2011; Clement et al., 2012; Weber et al., 2018b; Zhong et al., 2019)	Increased c-Fos expression following REM-sleep deprivation (Sapin et al., 2009; Clement et al., 2012)	N/A
		REM-Related Nuclei	
LDT	Strongly implicated in the generation of REM sleep based on activation, lesion, optogenetic, and c-Fos studies (Thakkar et al., 1996; Maloney et al., 1999; Lu et al., 2006; Van Dort et al., 2015)	Decreased c-Fos expression following REM-sleep deprivation (Maloney et al., 1999)	N/A
PPT	Strongly implicated in the generation of REM sleep based on activation, lesion,	Decreased c-Fos expression following	N/A

	optogenetic, and c-Fos studies (Shouse and Siegel, 1992; Datta et al., 1997; Maloney et al., 1999; Lu et al., 2006; Petrovic et al., 2013; Van Dort et al., 2015)	REM-sleep deprivation (Maloney et al., 1999)	
LH	Likely involved in REM sleep production based up firing rate, inhibition and c-Fos studies (Alam et al., 2002; Hsieh et al., 2011; Clement et al., 2012; Choudhary et al., 2014; Khanday and Mallick, 2015)	Increased c-Fos expression following recovery sleep from REM-SD (Clement et al., 2012)	Implicated in the induction and emergence from anesthetics (Shirasaka et al., 2011; Zhang et al., 2012)
LC	Strongly implicated in the generation of wakefulness based on activation, firing rate, and c-Fos studies (Aston-Jones and Bloom, 1981; Cirelli et al., 1996; Berridge and Waterhouse, 2003; Nelson et al., 2003; Carter et al., 2010; Vazey and Aston-Jones, 2014; Zhang et al., 2015)	Increased c-Fos immunoreactivity following forced wakefulness (sleep deprivation with no recovery sleep) (Cirelli et al., 1996; Nelson et al., 2003)	Low levels of c-FOS immunoreactivity in dexmedetomidine, propofol, and pentobarbital (Cirelli et al., 1996; Nelson et al., 2003)
DR	Implicated in the generation of wakefulness based on firing rate and c-Fos studies (Jacobs and Fornal, 1991; Cirelli et al., 1995)	Increased c-Fos immunoreactivity following forced wakefulness (sleep deprivation with no recovery sleep) (Cirelli et al., 1995)	N/A
BF	Diverse firing patterns, optogenetic effect, and c-Fos expression based on behavioural state of the animal and neurotransmitter phenotype: primarily wake-promoting (Greco et al., 2000b; McKenna et al., 2009; Hassani et al., 2010; Xu et al., 2015)	N/A	N/A

Table 3.1 Overview of the regions of interest (ROI).

The involvement of the 10 investigated ROI in spontaneous sleep, recovery sleep and anesthetics where possible.

shoe-boxed shaped with wire tops, aspen wood chip bedding, and a PVC tube for enrichment. Standard rat chow and water were provided *ad libitum*. Welfare checks were preformed daily while animals were housed prior to experiments. All methods used in this study conform to the animal use protocol approved by the Biological Sciences Animal Care and Use Committee of the University of Alberta, in accordance with the guidelines established by the Canadian Council on Animal Care.

3.4.2 Power calculations

To determine if the present study was adequately powered, the minimum sample size required to detect a significant difference was calculated. As the primary goal was to ensure that the study was adequately powered to determine between the sleep deprived and non-sleep deprived groups, we used the typical differences in c-Fos expression in the VLPO, a nucleus with significant differences between recovery sleep and spontaneous sleep, to calculate sample size. Based on data from previous literature (Gong et al., 2004), given α=0.05 and β=0.20, the minimum sample size to detect differences between recovery and spontaneous sleep in the VLPO was 2 animals per group. As such, 4 animals per group is more than adequately powered to distinguish between sleep deprived and non-sleep deprived animals.

3.4.3 General methodology

All experiments began with a 3-hour habituation period on the day preceding the experiment in order to reduce stress within the experimental environment. The next day, all

animals were placed into one of two 6 h pre-experimental (i.e. day 2 at T=0) conditions consisting of either sleep deprivation or non-sleep deprivation. The pre-experimental conditions were designed to prime the animals in the sleep deprived group to have increased homeostatic sleep pressure (pressured), and to allow the animals in the non-sleep deprived group to have unaffected levels of homeostatic sleep pressure (unpressured) in the subsequent experimental (i.e. day 2 at T=6 hrs) condition. In all cases, two animals were yoked in each sleep deprived or non-sleep deprived situation. Following the pre-experimental condition, rats received a tail vein injection of either urethane or saline, and were subsequently placed into one of three 2 h experimental (i.e., day 2 at T=6 hrs) conditions. Each yoked pair was counterbalanced, with one rat receiving urethane and the other receiving saline. The animals that received urethane became the SD-urethane and nonSD-urethane groups, while the animals that received saline became the SD-saline and the nonSD-saline groups. The final experimental group received saline following the non-sleep deprived pre-experimental condition, and these rats were then placed into enforced wakefulness using the same sleep deprivation method used in the pre-experimental phase for the 2 h experimental condition. This latter group was the nonSD-wake group. Following the 2 h experimental condition all animals were euthanized by transcardial perfusion, and histology was performed on the brains. The general methodology and timeline is outlined in Figure 3.1.

3.4.4 Sleep deprivation

Rats were sleep deprived at the beginning of their light phase using the well characterized disk-over-water (DOW) method for sleep deprivation (Bergmann et al., 1989). The DOW method provides gentle, but consistent physical stimulation by placing rats on a periodically

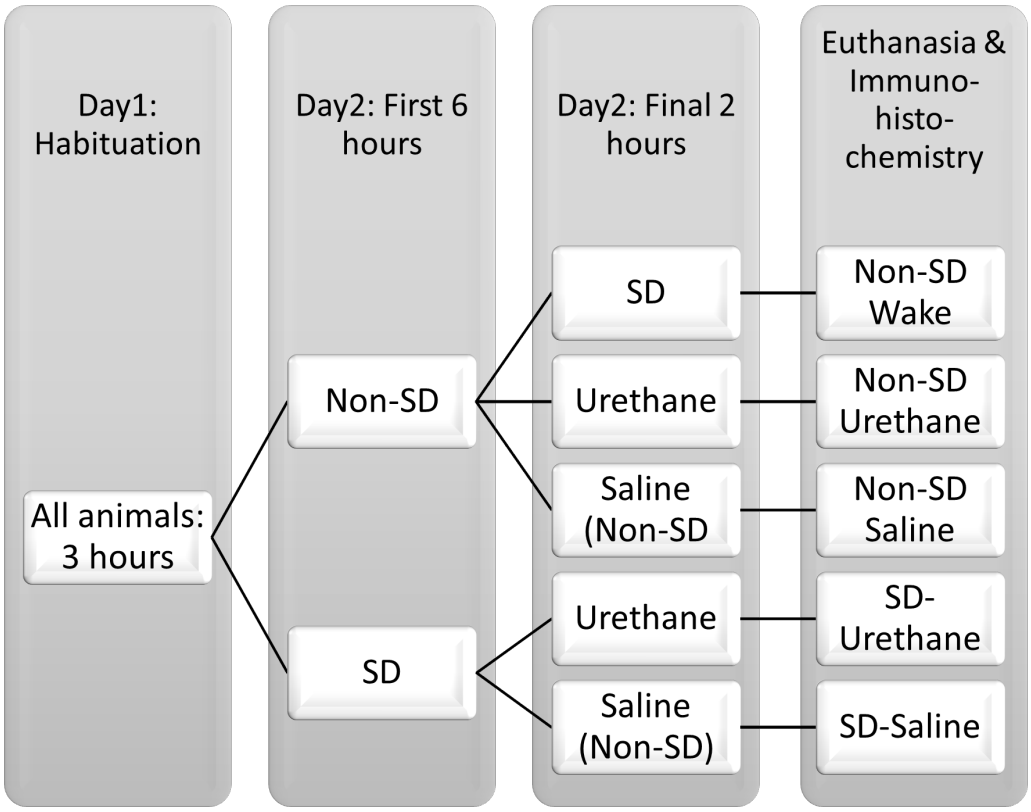

Figure 3.1 Experimental timeline.

Experiments began with a 3-hour habituation period in the stationary disk-over-water (DOW) apparatus (each condition with a blue background indicates placement in the DOW apparatus). On day 2, at the beginning of the light cycle (T=0 hours), animals were assigned to two possible pre-experimental conditions (Phase 1) in the DOW apparatus: disk spinning (i.e., sleep-deprived: SD) or disk stationary (i.e., not sleep deprived: non-SD). Following 6 hrs of either condition (T=6 hours), animals were separated into one of three experimental conditions (Phase 2). In one, animals that were previously in the non-SD group were given a tail vein injection of saline and then placed back in the DOW apparatus with disk spinning (saline + SD). In the other two groups, animals were given a tail vein injection of either urethane or saline. Urethane anesthetized animals were warmed during this period while saline-treated animals were placed in a novel cage. In all cases in

which animals were not anesthetized, they were video monitored throughout the procedures. Following 2 hrs of the experimental conditions (at T=8 hours), animals were euthanized and perfused, and immunohistochemistry (IHC) was subsequently performed following cryoprotection of brains. Animals were run 2 at a time per experiment and were yoked in the DOW apparatus as such: SD-saline and SD-urethane, as well as nonSD-saline and nonSD-urethane were paired. NonSD-wake animals were run in simultaneous yoked pairs.

rotating disk over a tray of water deep enough to ensure the rats cannot sleep in the water. The disk was situated between two separate chambers, allowing 2 rats to be sleep deprived at a time in order to ensure parallel behavioural experiences in both saline and urethane groups. The disk rotated slowly (3.75 rpm) for 8 seconds followed by a 15 second pause in alternating directions, and each chamber allowed the rat ad libitum access to both food and water (Chang et al., 2006b). To reduce stress, rats were habituated to the DOW apparatus for 3 hours in stationary mode 24 hours prior to the experiment.

Following sleep deprivation, rats were briefly anesthetized in an enclosed chamber using 4% isoflurane mixed with 100% oxygen. Upon the loss of righting reflexes, the rats were transferred to a nose cone and maintained on isoflurane (2.0 to 2.5%), while a 22G tail vein catheter was inserted for delivery of either an anesthetic dose of urethane (1.6 ± 0.06 g/kg) or an equivalent volume of saline. The SD-saline rats were returned to their home cages for 2 h to engage in recovery sleep, while the SD-urethane rats were placed on a servo-controlled heating pad (Harvard Apparatus, Holliston, MA) for 2 h to maintain a core temperature of 37°C during anesthesia. The time window of 2 hours was chosen to optimize expression and visualization of c-Fos protein during these behavioural states (Chaudhuri et al., 2000).

3.4.5 Non-sleep deprivation and wake

Animals in the non-sleep deprived and wake groups were subjected to a similar habituation protocol outlined in the sleep deprivation paradigm. However, in the non-sleep deprived and wake groups the disk did not rotate during the pre-experimental (i.e. day 2 at T=0)

6 hour period at the beginning of the light phase, thus allowing the animals to potentially sleep on the disk.

Following the 6 h in the DOW apparatus, the non-sleep deprived and wake rats were also anesthetized with 4% isoflurane and fitted with a tail vein catheter. Parallel to the sleep deprived group, rats in the non-sleep deprived group received either an anesthetic dose of urethane (1.6 ± 0.06 g/kg) or an equivalent volume of saline, and were placed on a heating pad during anesthesia, or back in their home cages, respectively, for 2 hours (day 2 at T=6 hrs). However, rats in the wake group received saline only, and then were placed back in the DOW apparatus with the disk rotation activated as above to ensure a consistent and constant wake state for the 2-hour window prior to evaluation of c-Fos expression.

3.4.6 Perfusions, extraction and tissue preparation

Following the 2 h experimental window (day 2 at T=8 hrs), rats were quickly anesthetized using a brief isoflurane exposure in a closed container, and then were immediately transcardially perfused with phosphate-buffered saline (PBS, Gibco, Fischer Scientific, Pittsburgh, Pennsylvania, USA) followed by 4% paraformaldehyde (PFA, Fischer Scientific) (see Figure 3.1 for a full timeline of experiments). Extracted brains were stored in PFA for a minimum of 48 h, and then transferred to a cryoprotective 30% sucrose-PFA solution for a minimum of 48 h. Once saturated, the brains were removed from solution and flash frozen using compressed carbon dioxide, and then cut on a sagittal plane in 60 μm sections using a rotary microtome (Leica, Germany). In total, 24 slices were taken consecutively from the same hemisphere, centered roughly 1 mm lateral of the midline (Figure 3.2).

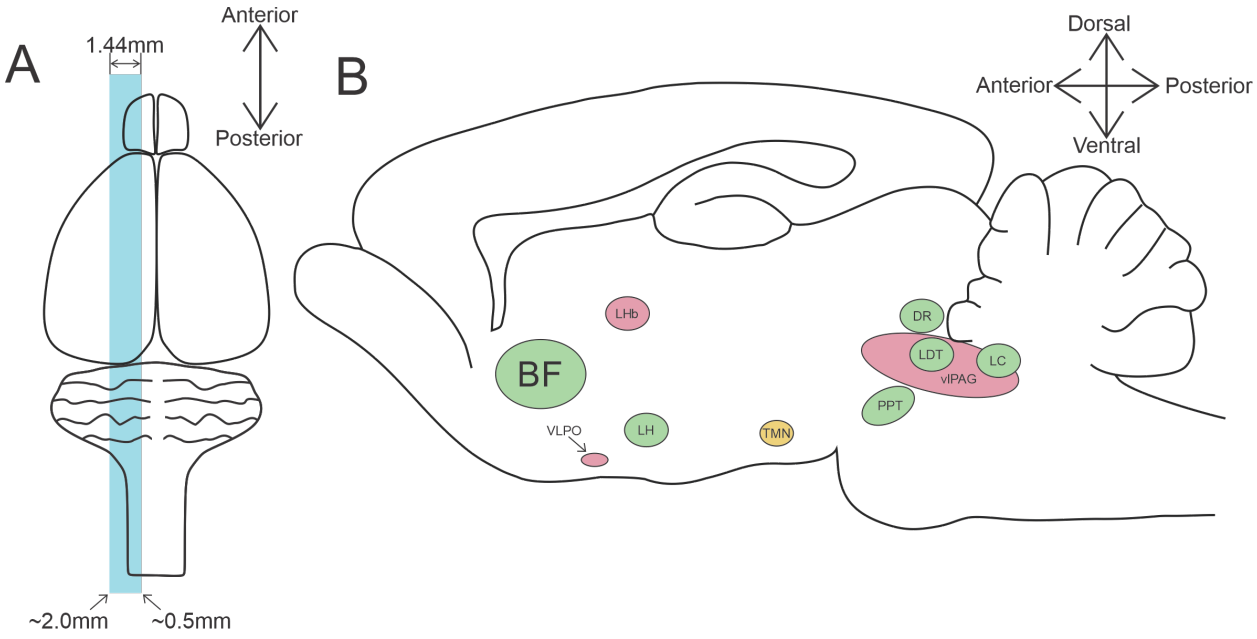

Figure 3.2 Histological illustration.

(A) A dorsal illustration of a rat brain. The section highlighted with a blue box indicates the approximate region that the twenty-four 60µm slices were taken from. The figure is not drawn to scale. (B) A sagittal illustration of a rat brain, taken from the highlighted area in A. The approximate position of NREM-related nuclei are illustrated in red, REM-related in green, and wake-related in yellow. Note: not all nuclei were found on a single slice, they are all shown here for illustrative purposes only. The section and nuclei are not drawn to scale.

3.4.7 Histology

Slices were first washed 3 times with PBS for 5 minutes each to remove any remaining PFA. Then, to reduce non-specific binding, slices were incubated with a blocking solution of 10% normal donkey serum (NDS; Jackson ImmunoResearch Laboratories, Inc., West Grove, Pennsylvania, USA), and 0.3% Triton X-100 (MP Biochemical, Inc., Irving, California, USA) in PBS for 1 hour on an orbital shaker. Once the blocking solution was removed, the primary antibodies for c-Fos (1:1000 raised in rabbit, Santa Cruz Biotechnology, Inc., Dallas, Texas, USA) and a neuronal nuclear marker (1:500 NeuN, raised in mouse, Millipore, Burlington, Massachusetts, USA) were added to a solution contain 1% NDS and 0.3% Triton, and left to incubate for 24 hours on a shaker. The following day, the slices were again washed 3 times with PBS for 5 minutes per wash, and secondary antibodies which were conjugated to a fluorescent probe were added in solution of 1% NDS in PBS, in order to visualize c-Fos (1:100 Cy3-conjugated AffiniPure Donkey Anti-Mouse IgG, Jackson ImmunoResearch Laboratories, Inc.) and NeuN (1:100 Cy5-conjgated AffiniPure Donkey Ant-Rabbit IgG, Jackson ImmunoResearch Laboratories) expressing neurons. Slices were incubated in the dark for a minimum of 2 hour on an orbital shaker, following which they were washed 3 times in PBS, mounted on a glass slide and cover slipped using a mounting medium to protect fluorescence (FluorSave, Millipore).

3.4.8 Imaging

All images were taken using a digital inverted microscope (EVOS FL, Advanced Microscopy Group, Bothell, Washington, USA), at 20x magnification in each independent fluorescent channel to allow for better visualization of the fluorescent signal while also

encompassing the nuclei of interest. Images were converted into 16-bit black and white images in ImageJ (U.S. National Institute of Health, Bethesda, Maryland, USA), and then run through the smooth function, which averages pixel brightness in order to remove single-pixel artifacts. NeuN images were first thresholded using standardized values taken from control images of the cerebellum in order to capture outlines of labeled neurons. This thresholded image was then overlaid on the corresponding c-Fos images. NeuN and c-Fos double labeled cells were counted by using the find maxima function in ImageJ to identify groups of pixels that were 10 units of intensity brighter than their surroundings within overlaid regions. A section-by-section analysis of the LC can be found in Table 3.2.

In addition to sleep-wake circuitry ROI (see Table 1, and Figure 3.2), the preBötzinger Complex (preBötC), dentate nucleus of the cerebellum and paraventricular nucleus (PVN) of the hypothalamus were imaged for c-Fos expression. The preBötC is involved in respiration and is therefore active irrespective of sleep and anaesthesia (Munoz-Ortiz et al., 2017). It served as a positive control to ensure that the c-Fos staining protocol worked. The dentate nucleus is involved in movement and is not active and thus does not express c-Fos during sleep or anaesthesia, so it served as a negative control for our staining protocol. Lastly, the PVN expresses c-Fos during periods of acute and basal stress, and as such served as a measure for the level of stress experienced by the rat (Kovacs et al., 2018). A comparison of PVN expression between groups can be found in Figure 3.3.

	SD-Saline				SD-Urethane				NonSD-Saline				NonSD-Urethane				NonSD-Wake			
1	5	9	7	7	7	8	4	3	6	8	8	1	7	10	11	8	10	5	9	12
2	12	6	9	4	8	5	6	3	14	7	6	5	8	8	8	6	11	6	9	13
3	10	10	7	9	5	12	5	8	11	9	6	7	16	9	11	2	8	8	8	8
4	6	8	9	10	6	5	7	6	12	4	5	6	14	6	11	9	10	7	14	9
5	6	5	8	14	2	5	7	8	6	5	6	5	11	12	5	8	5	9	4	11
6	7	10	8	7	5	5	6	10	11	9	6	15	9	6	7	10	6	7	6	4
7	6	9	11	9	5	3	8	9	5	6	7	15	12	8	4	6	6	13	11	8
8	5	12	11	5	3	5	5	7	7	4	6	7	9	7	9	7	9	10	5	9
Total	57	69	70	65	40	48	48	54	72	52	50	61	86	66	66	56	65	65	66	74

Table 3.2 Raw cell counts of locus coeruleus slices.

The number of cFos+/NeuN+ double labeled cells in each imaged section of the Locus Coeruleus for all experiments. Section numbers represent the order in which the sections were analyzed, representing sequential sections 60um apart.

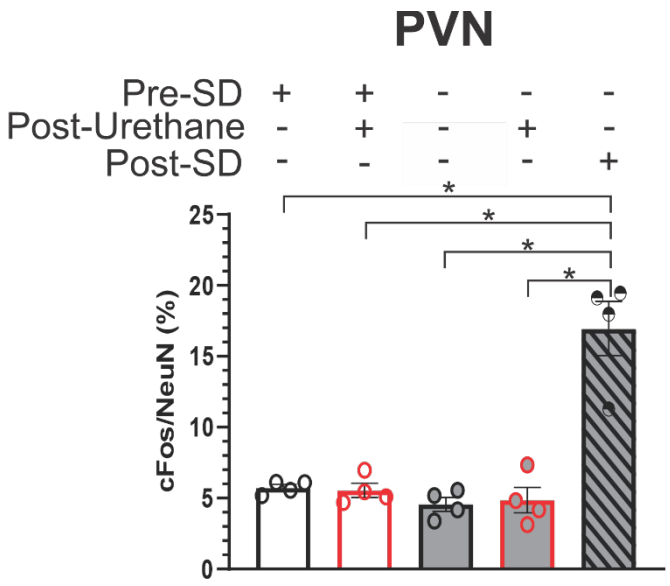

Figure 3.3 PVN cell counts.

The proportion of NeuN-cFos-IR cells for all experiments within the PVN. Each individual experiment is shown as a dot. The bars report the mean, with SEM error bars.

3.4.9 Video scoring

In order to assess the proportions of time spent in various behaviours, videos taken during the initial 6 h (sleep deprived or non-sleep deprived) pre-experimental period and the subsequent 2 h experimental period were scored by assessing behavioural states as follows: 1) active, 2) inactive but standing, or 3) inactive and laying down for periods greater than 20 seconds. The amount of time spent in each condition was converted to a percentage of total time.

In two non-sleep deprived animals (one which received saline prior to the 2 hr experimental period and one which received urethane), activity rates were more consistent with the sleep deprivation data (i.e., active for >90% of the time during the 6 h pre-experimental period). We re-classified these 2 animals as sleep deprived for the rest of the analyses. Although another rat in the nonSD-wake group was also active for >95% of the 6 hour pre-experimental period, we did not re-classify the animal since the subsequent experimental condition of enforced wakefulness was unlikely to be greatly influenced by increased sleep pressure. We also verified that these three animals were better fits for their respective groups by the comparable c-Fos expression they exhibited.

3.4.10 Data analysis

All data analysis was conducted using Prism 8 (GraphPad Prism Software Inc, San Diego, CA). All values are reported as means with standard error of the mean (SEM). A parametric two-tailed t-test was used to compare difference between two means where applicable. Analysis of Variance (ANOVA) was conducted in all cases in which multiple means

(i.e., more than two) were being compared. In situations that the ANOVA determined a significant difference, a post-hoc Tukey multiple comparison test was performed to determine which group means showed significant differences. A Shapiro-Wilk test was used to verify the normality of the distribution, and if the distribution was determined to be non-parametric, a Mann-Whitney test was used to determine if the means differed significantly.

3.5 Results

3.5.1 Pre-experimental conditions (Day 2, T=0-6h)

Twenty rats were used in the present study, with four rats in each experimental group. The mean weights were 305.2 ± 9.24g, with no significant difference in the mean weights of any of the five experimental groups ($F(4,15) = 1.69$, $p=0.20$).

As shown in Figure 3.4, the sleep deprivation protocol used in this study effectively deprived rats of sleep, with the sleep deprived groups spending only 0.48 ± 0.32% of the 6-hour period in a sleeping posture. In contrast, the non-sleep deprived groups spent 26.40 ± 3.82% of the time in a sleeping posture ($t(18)=5.47$, $p=1.01 \times 10^{-4}$). As well, the average time spent active (sleep deprived: 92.83 ± 1.48%; non-sleep deprived: 71.09 ± 3.63%), and the average time spent inactive but standing (sleep deprived: 6.69 ± 1.70%; non-sleep deprived: 2.53 ± 0.63%), also differed significantly between the sleep deprived and non-sleep deprived groups ($t(18)=4.69$, $p=3.66 \times 10^{-4}$; and $t(18)=1.58$, $p=0.02$; respectively) with inactivity being significantly higher in the non-sleep deprived group and activity being significantly higher in the sleep deprived group.

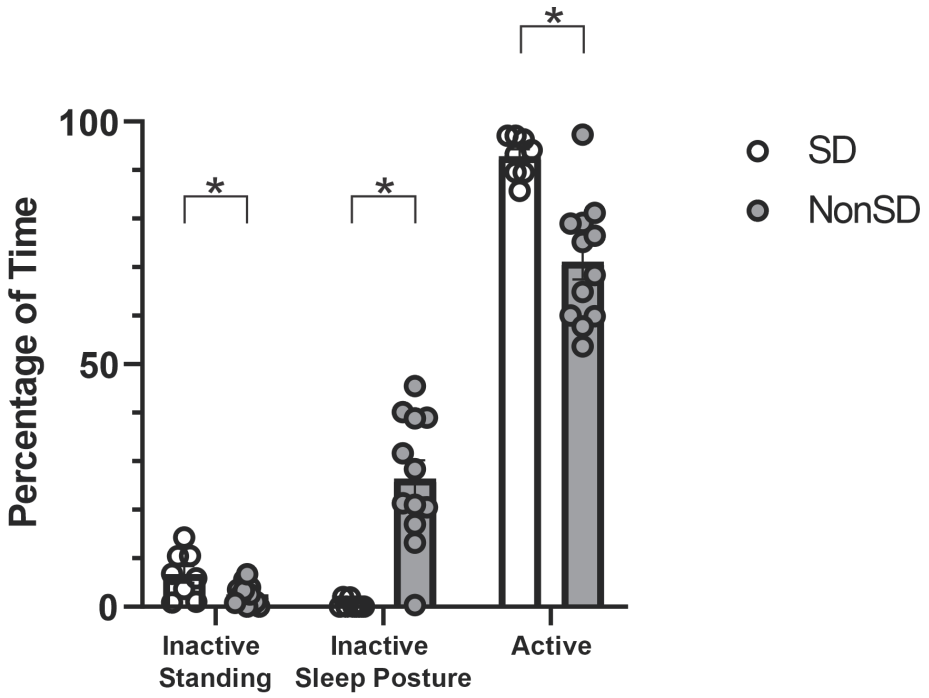

Figure 3.4 Behavioural activity during the pre-experimental condition (Day 2, T: 0-6 hours).

The percentage of time spent in each behavioural state of all animals during the 6 h pre-experimental condition. Each individual animal is shown as a representative dot. The sleep deprived group is shown in white-filled circles and the non-sleep deprived group in grey-filled circles. The bars report the mean, and the error bars represent SEM. Note that one animal in the NonSD-wake condition was active for 97% of the time, but was not designated as sleep deprived for analysis because it wouldn't have impacted the subsequent experimental period of enforced wakefulness. This was later confirmed to be the case since it had comparable c-Fos patterns to the other animals in the nonSD-wake group. Animals in the sleep-deprived group spent significantly less time in sleeping posture (Sleep-deprived: 0.48 ± 0.32%; non-sleep deprived: 26.40 ± 3.82%; $t(18)=5.47$, $p=1.01\times10^{-4}$), with significantly more time in inactive but standing (sleep deprived:

6.69 ± 1.70%; non-sleep deprived: 2.53 ± 0.63%; t(18)=1.58, p=0.02) and active (sleep deprived: 92.83 ± 1.48%; non-sleep deprived: 71.09 ± 3.63%; t(18)=4.69, p=3.66 $x10^{-4}$).

3.5.2 Experimental conditions (Day 2, T=6-8 h)

Irrespective of pre-experimental conditions (SD-urethane or nonSD-urethane), rats that received anesthetic doses of urethane remained inactive and unresponsive for the entire 2 h recovery period. As shown in Figure 3.5, the animals in the SD-saline group spent 78.0 ± 1.2% of the time inactive in a sleeping posture, 1.6 ± 0.7% of the time inactive but standing and the remainder of the time (20.4 ± 1.3%) active. Rats in the nonSD-saline group spent 67.5 ± 3.4% of the time inactive in a sleeping posture, 4.5 ± 0.8% of the time inactive but standing and the remainder of the time (28.0 ± 3.2%) active. The nonSD-wake group rats spent on average 97.7 ± 0.87% of the time active, with the remainder of the time inactive but standing (2.3 ± 0.87%).

A two-way ANOVA was conducted and a statistically significant difference was found in both time spent in a specific state within experimental groups ($F(1.220, 10.98) = 464.0$, $p<1x10^{-4}$), and between groups ($F(4, 18) = 399.6$, $p<1x10^{-4}$). Post-hoc tests showed that the nonSD-wake group spent significantly more time active (SD-saline: $t(5.22)=69.26$, $p<1x10^{-4}$; nonSD-saline: $t(3.45)=30.03$, $p=2x10^{-4}$), and less time inactive in a sleeping posture (SD-saline: $t(3.00)=89.92$, $p<1x10^{-4}$; nonSD-saline: $t(3.00)=28.43$, $p=6x10^{-4}$) than the SD-saline and nonSD-saline groups. No other significant differences were observed.

Of note, and as represented in Figure 3.6, the SD-saline group rats spent on average 29.54 ± 6.3 continuous minutes per episode of sleep posture, in contrast to the nonSD-saline group which spent an average of 11.38 ± 1.9 continuous minutes per episode of sleep posture. This represents a significant difference in duration per sleep posture episode (Mann-Whitney $U=102$, $p=1.9x10^{-2}$, two-tailed). This significant difference was also observed in the number of sleep-

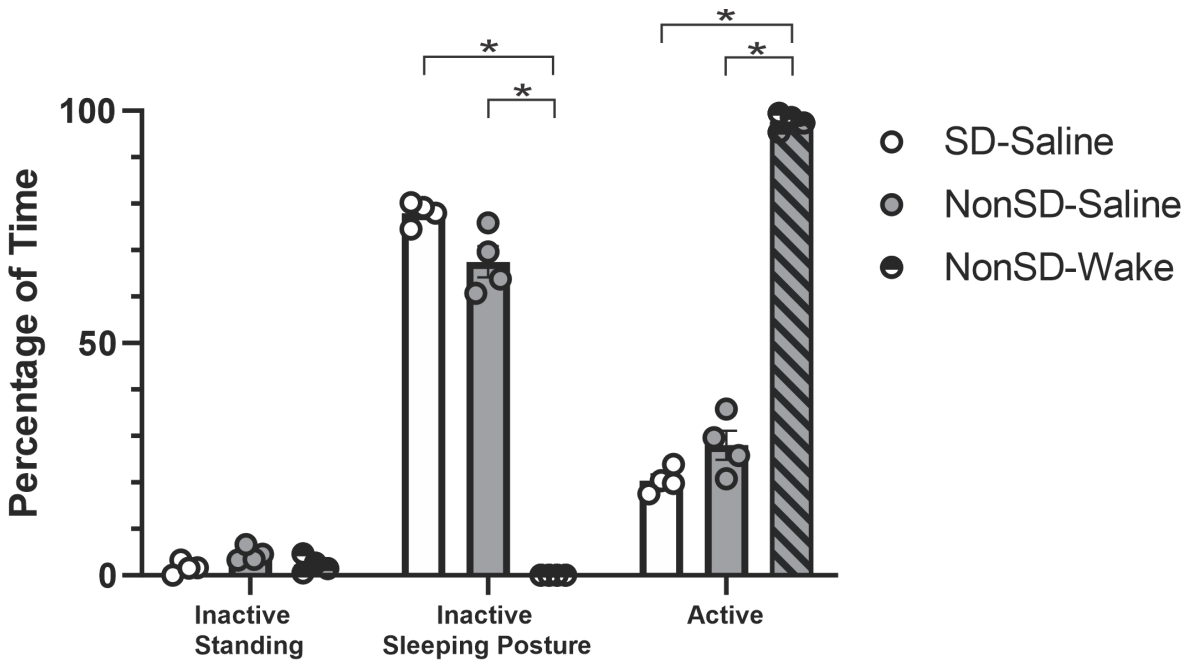

Figure 3.5 Behavioural activity during the experimental condition (Day 2, T = 6-8 hours).

The percentage of time spent in each state of all the animals during the 2 h experimental period. Each individual experiment is shown as a dot. The SD-saline group is shown in white-filled dots and bars. The nonSD-saline group is shown in grey-filled dots and bars, and the nonSD-wake in half black-filled dots and black-striped grey bar. The bars report the mean, and the error bars represent SEM. Animals in the SD-Saline (78.0 ± 1.2%) and nonSD-Saline (67.5 ± 3.4%) groups spent significantly more time inactive in a sleeping posture compared to the NonSD-Wake (0%; SD-saline: $t(3.00)=89.92$, $p<1x10^{-4}$; nonSD-saline: $t(3.00)=28.43$, $p=6x10^{-4}$). Similarly, animals in the SD-Saline (20.4 ± 1.3%) and NonSD-Saline (28.0 ± 3.2%) groups spent significantly less time active compared to the NonSD-Wake group (97.7 ± 0.87%; SD-saline: $t(5.22)=69.26$, $p<1x10^{-4}$; nonSD-saline: $t(3.45)=30.03$, $p=2x10^{-4}$). No other significant differences were noted.

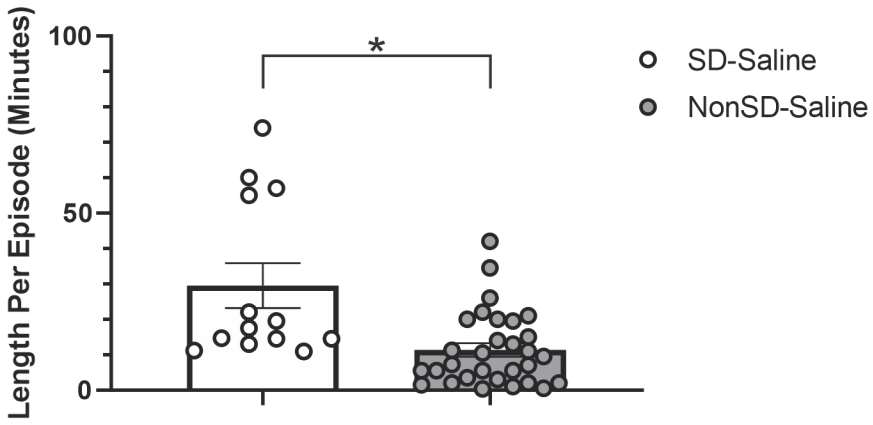

Figure 3.6 Sleep posture bout length.

The average duration per sleep posture episode during the experimental period. Each individual experiment is shown as a dot. The SD-saline group is shown in white-filled dots and bars and the nonSD-saline group in grey-filled dots and bars. The bars report the overall mean, and the error bars represent SEM. Animals in the SD-Saline group had significantly longer average bouts of sleep posture (29.54 ± 6.3 continuous minutes per episode of sleep posture) compared to the NonSD-Saline group (11.38 ± 1.9 continuous minutes per episode of sleep posture; Mann-Whitney $U=102$, $p=1.9\times10^{-2}$, two-tailed).

posture epochs, with nonSD-saline rats having on average 7.5 ± 1.6 epochs compared to the 3.0 ± 0.4 epochs in the SD-saline group ($t(6)=2.5$, $p=4.4x10^{-2}$).

3.5.3 c-Fos immunoreactivity

Ten different nuclei involved in endogenous sleep-wake circuitry were identified and imaged for each animal (Figure 3.2). Prior to imaging any ROI, the cerebellum was assessed as a negative control to verify a lack of c-Fos immunoreactivity (IR) and used to scale for detection of NeuN IR. Similarly, the preBötC was imaged as a positive control to verify predicted c-Fos IR. Cell counts are reported herein as the proportion of NeuN positive cells that expressed c-Fos. We also normalized the number of c-Fos positive cells to the area imaged, however, since area and number of NeuN cells were significantly correlated in all circumstances (Pearson r test, $r(20) = 0.4463$ to 0.662, $p<0.05$), we have only reported normalizations to NeuN counts. Please see Table 3.3 for a full breakdown of Pearson r tests of each pair of measures across each ROI. Indeed, the pattern of our results was nearly identical using both normalization techniques. Raw cell counts of the number of c-Fos and NeuN-expressing cells can be found in Tables 3.4 and 3.5.

As a nucleus predominantly active during wakefulness, the TMN showed the weakest c-Fos expression in the non-wake experimental groups (Ko et al., 2003; Takahashi et al., 2006). As shown in Figure 3.7, the SD-saline group had the lowest percentage of NeuN-cFos double-labeled cells (2.08 ± 0.33%). The SD-urethane (3.83 ± 0.23%), nonSD-saline (4.17 ± 0.26%), and nonSD-urethane (4.31 ± 0.56%) groups all had highly comparable (and similarly low) percentages of double-labelling in the TMN. Conversely, the nonSD-wake group had the highest

Nucleus	Pearson R Test
TMN	r(20) = 0.65, p=00.17
VLPO	r(20) = 0.47, p=0.0376
LHb	r(20) = 0.53, p=0.0154
vlPAG	r(20) = 0.61, p=0.0045
LDT	r(20) = 0.45, p=0.0485
PPT	r(20) = 0.47, p=0.0374
LH	r(20) = 0.57, p=0.0089
LC	r(20) = 0.44, p=0.0013
DR	r(20) = 0.52, p=0.0197
BF	r(20) = 0.46, p=0.0406

Table 3.3 Pearson R test results.

Full results for the Pearson R Test results for all ROI, showing correlation between area and NeuN count.

Nucleus	SD-Saline	SD-Urethane	NonSD-Saline	NonSD-Urethane	NonSD-Wake
TMN	12.25 ± 1.75	21.50 ± 0.96	22.75 ± 2.18	24.50 ± 3.30	113.5 ± 3.93
VLPO	111.5 ± 5.38	67.50 ± 9.50	62.50 ± 8.06	54.00 ± 7.80	6.50 ± 0.65
LHb	67.50 ± 11.03	22.75 ± 1.97	30.25 ± 2.29	31.50 ± 2.26	10.25 ± 0.85
vlPAG	77.5 ± 4.17	38.50 ± 0.65	53.00 ± 7.15	42.75 ± 4.15	9.00 ± 1.08
LDT	33.25 ± 4.68	51.50 ± 10.28	56.50 ± 6.40	53.50 ± 8.11	119.8 ± 5.69
PPT	66.50 ± 8.97	78.50 ± 5.11	85.50 ± 12.31	83.75 ± 5.59	168.3 ± 18.33
LH	20.50 ± 0.50	23.00 ± 1.87	27.25 ± 2.46	30.25 ± 3.57	95.00 ± 3.54
LC	65.25 ± 2.96	47.50 ± 2.87	58.75 ± 5.02	68.50 ± 6.29	67.50 ± 2.18
DR	54.00 ± 7.53	31.25 ± 1.65	52.00 ± 8.05	56.75 ± 7.43	112.0 ± 4.30
BF	16.75 ± 0.75	100.8 ± 13.21	38.50 ± 1.56	45.00 ± 3.56	169.3 ± 5.17

Table 3.4 Raw c-Fos labeled cell counts.

Summary of c-Fos cell counts in all ROI in all groups. The means for each group are reported alongside the SEM and the range for each group.

Nucleus	SD-Saline	SD-Urethane	NonSD-Saline	NonSD-Urethane	NonSD-Wake
TMN	588.8 ± 25.29	561.3 ± 14.82	545.0 ± 23.94	568.3 ± 37.05	556.3 ± 16.34
VLPO	512.8 ± 24.51	531.8 ± 11.76	547.0 ± 21.91	488.3 ± 15.70	454.8 ± 13.23
LHb	485.8 ± 25.53	550.8 ± 25.14	564.5 ± 34.77	558.3 ± 27.84	563.0 ± 27.97
vlPAG	555.3 ± 10.84	553.0 ± 11.78	493.8 ± 21.08	585.0 ± 31.90	562.8 ± 14.97
LDT	564.5 ± 10.65	553.3 ± 38.73	542.8 ± 27.79	597.3 ± 67.28	591.8 ± 29.56
PPT	511.5 ± 27.20	346.5 ± 26.12	377.5 ± 24.82	383.5 ± 36.10	350.8 ± 7.087
LH	584.5 ± 22.41	608.0 ± 13.74	528.3 ± 14.67	529.8 ± 20.96	525.3 ± 11.54
LC	583.8 ± 19.22	504.5 ± 39.70	521.3 ± 13.26	613.3 ± 28.37	595.0 ± 12.34
DR	550.8 ± 15.89	542.0 ± 35.54	544.5 ± 25.45	583.5 ± 11.96	572.0 ± 10.75
BF	507.3 ± 17.24	589.5 ± 23.54	487.0 ± 14.97	559.8 ± 14.97	485.8 ± 25.85

Table 3.5 Raw NeuN labeled cell counts.

Summary of cell count of NeuN labeled cells in all ROI in all groups. The means for each group are reported alongside their SEM and the range for each group.

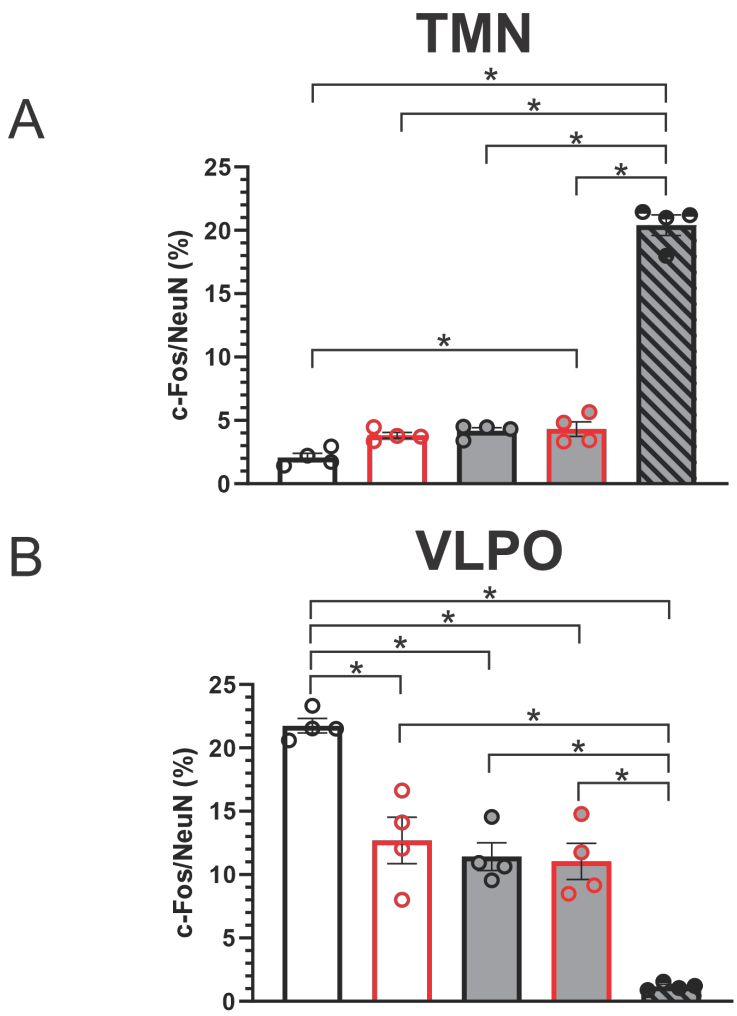

Figure 3.7 VLPO and TMN cell counts.

The proportion of NeuN-cFos-IR cells for all experiments within the (A) TMN, tubomammillary nucleus and (B) VLPO, ventrolateral preoptic area. Each individual experiment is shown as a dot. The SD-saline group is shown in black-white, the SD-urethane group in red-white, the nonSD-saline group in black-grey, the nonSD-urethane group in red-grey, and the nonSD-wake group in blue-grey. The bars report the mean, with SEM error bars.

percentage of NeuN-cFos double-labeled cells within the TMN at 20.41 ± 0.82%. Statistical analysis indicated significant differences between the groups as determined by a one-way ANOVA ($F(4,15) = 235.9$, $p<1x10^{-4}$), with a Tukey pos-hoc test indicating the SD-saline group had significantly lower percentage of NeuN-cFos double-labeled TMN cells compared to the nonSD-urethane group ($p<4.0x10^{-2}$), while the nonSD-wake group had significantly higher expression compared to all other groups (All: $p<1x10^{-4}$). A full summary of all significant comparisons for all ROI can be found in Table 3.6.

Conversely, as a sleep-promoting nucleus with high levels of activity during slow-wave sleep, the VLPO showed the greatest percentage of NeuN-cFos double-labeled cells in the SD-saline group (21.74 ± 0.57%; Figure 3.7). The SD-urethane (12.70 ± 1.83%), nonSD-saline (11.42 ± 1.09%), and nonSD-urethane (11.05 ± 1.43%) groups all had comparable percentages of NeuN-cFos double-labeled cells. The nonSD-wake group had the lowest percentage of NeuN-cFos double-labeled cells within the VLPO at only 1.18 ± 0.14%. A one-way ANOVA showed significant differences between the groups ($F(4,15) = 38.53$, $p<1x10^{-4}$), with a post-hoc test revealing that the SD-saline group had a significantly higher percentage of NeuN-cFos double-labeled cells than all other groups (SD-urethane: $p=6x10^{-4}$, nonSD-saline: $p=1x10^{-4}$, nonSD-urethane: $p<1x10^{-4}$, nonSD-wake: $p<1x10^{-4}$). Conversely, the nonSD-wake group had a significantly lower percentage of NeuN-cFos double-labeled cells compared to all other groups (SD-saline: $p<1x10^{-4}$, SD-urethane: $p<1x10^{-4}$, nonSD-saline: $p=2x10^{-4}$, nonSD-urethane: $p=2x10^{-4}$).

As expected, the percentage of NeuN-cFos double labeled cells in the TMN and VLPO for the two most contrasting behavioural groups in our study, SD-saline and nonSD-wake showed opposing results to each other. Consistent with previous research assessing recovery

	SD-Saline	*SD-Urethane*	*NonSD-Saline*	*NonSD-Urethane*	*NonSD-Wake*
SD-Saline		**VLPO:** t(15)=7.695 **LHb:** t(15)=12.28 **vlPAG:** t(15)=9.713 **BF:** t(15)=8.299	**VLPO:** t(15)=8.785 **LHb:** t(15)=10.73 **vlPAG:** t(15)=4.460 **PPT:** t(15)=5.250	**TMN:** t(15)=4.534 **VLPO:** t(15)=9.099 **LHb:** t(15)=10.38 **vlPAG:** t(15)=9.238 **PPT:** t(15)=4.817 **LH:** t(15)=5.583	**TMN:** t(15)=37.19 **VLPO:** t(15)=17.49 **LHb:** t(15)=15.18 **vlPAG:** t(15)=17.14 **LDT:** t(15)=12.99 **PPT:** t(15)=19.07 **LH:** t(15)=36.91 **DR:** t(15)=8.908 **BF:** t(15)=19.00
SD-Urethane	**VLPO:** p=0.0006 **LHb:** p<0.0001 **vlPAG:** p<0.0001 **BF:** p=0.0003		**vlPAG:** t(15)=5.253 **BF:** t(15)=5.532	**LH:** t(15)=4.887 **BF:** t(15)=5.447	**TMN:** t(15)=33.63 **VLPO:** t(15)=9.798 **vlPAG:** t(15)=7.426 **LDT:** t(15)=9.921 **PPT:** t(15)=15.42 **LH:** t(15)=36.22 **DR:** t(15)=12.61 **BF:** t(15)=10.70
NonSD-Saline	**VLPO:** p=0.0001 **LHb:** p<0.0001 **vlPAG:** p=0.0442 **PPT:** p=0.0152	**vlPAG:** p=0.0152 **BF:** p=0.0103		**vlPAG:** t(15)=4.778	**TMN:** t(15)=32.93 **VLPO:** t(15)=8.707 **LHb:** t(15)=4.459 **vlPAG:** t(15)=12.68 **LDT:** t(15)=8.910 **PPT:** t(15)=13.82 **LH:** t(15)=32.72 **DR:** t(15)=9.140 **BF:** t(15)=16.23
NonSD-Urethane	**TMN:** p=0.0401 **VLPO:** p<0.0001 **LHb:** p<0.0001 **vlPAG:** p<0.0001 **PPT:** p=0.0274 **LH:** p=0.0096	**LH:** p=0.0249 **BF:** p=0.0116	**vlPAG:** p=0.0289		**TMN:** t(15)=32.65 **VLPO:** t(15)=8.394 **LHb:** t(15)=4.801 **vlPAG:** t(15)=7.901 **LDT:** t(15)=10.22 **PPT:** t(15)=14.26 **LH:** t(15)=31.33 **DR:** t(15)=8.984 **BF:** t(15)=16.15
NonSD-Wake	**TMN:** p<0.0001 **VLPO:** p<0.0001 **LHb:** p<0.0001 **vlPAG:** p<0.0001 **LDT:** p<0.0001 **PPT:** p<0.0001 **LH:** p<0.0001 **DR:** p=0.0001 **BF:** p<0.0001	**TMN:** p<0.0001 **VLPO:** p<0.0001 **vlPAG:** p=0.0008 **LDT:** p<0.0001 **PPT:** p<0.0001 **LH:** p<0.0001	**TMN:** p<0.0001 **VLPO:** p=0.0002 **LHb:** p=0.0443 **vlPAG:** p<0.0001 **LDT:** p=0.0001 **PPT:** p<0.0001 **LH:** p<0.0001 **DR:** p<0.0001 **BF:** p<0.0001	**TMN:** p<0.0001 **VLPO:** p=0.0002 **LHb:** p=0.0280 **vlPAG:** p=0.0004 **LDT:** p<0.0001 **PPT:** p<0.0001 **LH:** p<0.0001 **DR:** p=0.0001 **BF:** p<0.0001	

	DR: p<0.0001 **BF:** p<0.0001

Table 3.6 Post-hoc Tukey test significant results.

Summary results for Tukey Post-Hoc testing for all ROI, showing only significant results.

sleep after sleep deprivation (Gong et al., 2004), c-Fos expression for animals in the SD-saline group was high in the VLPO, and very low in the TMN. In contrast, animals in the nonSD-wake group had very low c-Fos expression in the sleep-related VLPO, and very high expression in the wake-related TMN; consistent with the behavioural state (Figure 3.7).

In the LHb, the SD-saline group again exhibited the highest percentage of NeuN-cFos double-labeled cells (Figure 3.8; 13.90 ± 1.68%). The SD-urethane (4.13 ± 0.25%), nonSD-saline (5.36 ± 0.32%), and nonSD-urethane (5.64 ± 0.38%) groups all showed comparable expression, and the nonSD-wake group had the lowest percentage of NeuN-cFos double-labeled cells within the LHb (1.82 ± 0.16%). A one-way ANOVA across groups showed significant differences of the means ($F(4,15) = 33.08$, $p<1x10^{-4}$). Post-hoc testing showed that the SD-saline group had a significantly higher percentage of NeuN-cFos double-labeled cells compared to all other groups (All: $p<1x10^{-4}$), while the nonSD-wake group had a significantly lower percentage of NeuN-cFos double-labeled cells compared to all groups (SD-sleep: $p<1x10^{-4}$, nonSD-sleep: $p=0.0443$, nonSD-urethane: $p=2.8x10^{-2}$) except the SD-urethane group ($p=0.29$; Figure 3.8).

As with both the VLPO and LHb, the percentage of vlPAG NeuN-cFos double-labeled cells were greatest in the SD-saline group (13.96 ± 0.99%). The SD-urethane group averaged 6.96 ± 0.17%, while the nonSD-saline group averaged 10.74 ± 1.04%, and nonSD-urethane group averaged 7.30 ± 0.67%. The nonSD-wake group had the lowest percentage of NeuN-cFos double-labeled cells (1.60 ± 0.22%). ANOVA showed significant differences in the means ($F(4,15) = 41.11$, $p<1x10^{-4}$). The SD-saline group had a significantly higher percentage of NeuN-cFos double-labeled vlPAG cells compared to all other groups (SD-urethane: $p<1x10^{-4}$, nonSD-saline: $p=0.0442$, nonSD-urethane: $p<1x10^{-4}$, nonSD-wake: $p<1x10^{-4}$), while the nonSD-wake

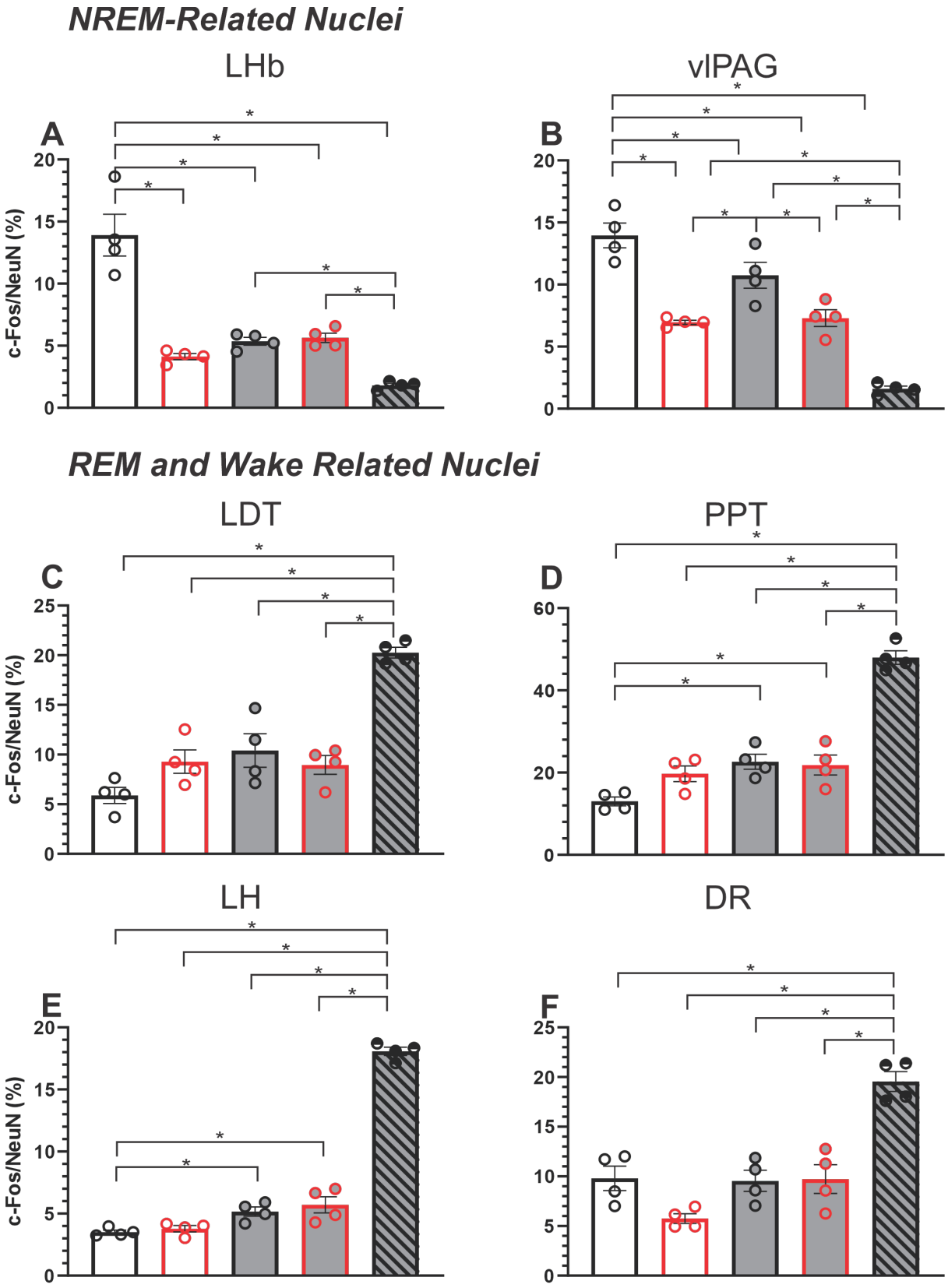
NREM-Related Nuclei
LHb
vlPAG
A
B
c-Fos/NeuN (%)
REM and Wake Related Nuclei
LDT
PPT
C
D
LH
DR
E
F

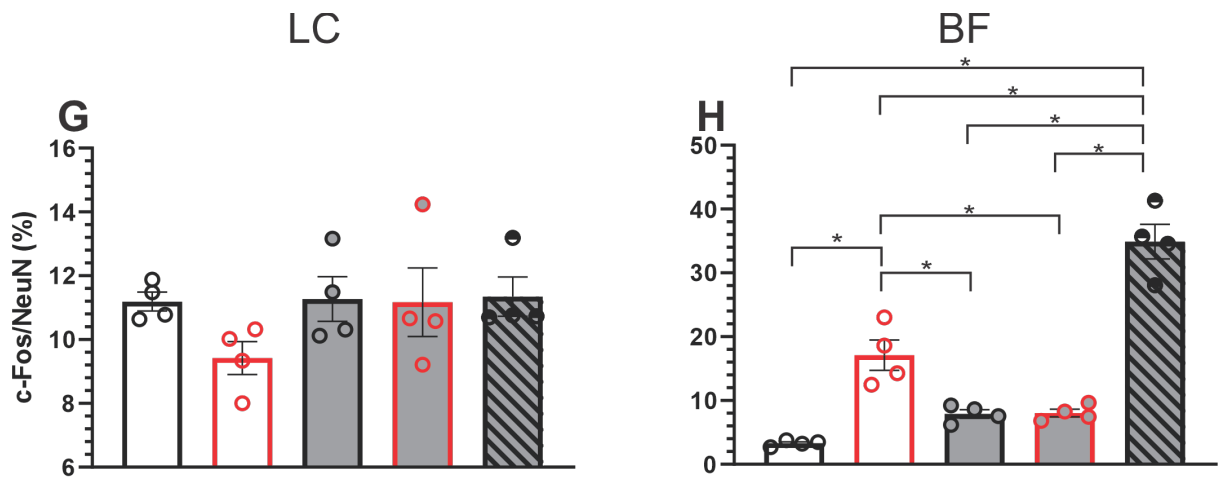

Figure 3.8 ROI Double-labeled cell counts.

The proportion of NeuN-cFos-IR cell for all experiments in remain ROI. Each individual experiment is shown as a dot. The SD-saline group is shown in black-white, the SD-urethane group in red-white, the nonSD-saline group in black-grey, the nonSD-urethane group in red-grey, and the nonSD-wake group in grey with black stripes. The bars report the mean, with error bars representing SEM. (A) LHb, Lateral Habenula; (B) vlPAG, Ventrolateral Periaqueductal Grey; (C) LDT, Laterodorsal Tegmental Nucleus ; (D) PPT, Pedunculopontine Nucleus; (E) LH, Perifornical Area of the Lateral Hypothalamus; (F) DR, Dorsal Raphe; (G) LC, Locus Coeruleus; and (H) BF, Basal Forebrain.

group had a significantly lower percentage of NeuN-cFos double-labeled cells compared to all other groups (SD-saline: $p<1x10^{-4}$, SD-urethane: $p=8x10^{-4}$, nonSD-saline: $p<1x10^{-4}$, nonSD-urethane: $p<4x10^{-4}$). In addition, the nonSD-saline group had a significantly larger percentage of NeuN-cFos double-labeled cells compared to the SD-urethane ($p=1.52x10^{-2}$) and nonSD-urethane ($p=2.89x10^{-2}$) groups (Figure 3.8).

The LDT, PPT and LH nuclei that are known to be more active during both wakefulness and REM sleep, were also sampled for c-Fos expression (Figure 3.8). In the LDT, the SD-saline group had a moderate amount of NeuN-cFos double-labeled cells (5.89 ± 0.81%). The SD-urethane (9.30 ± 1.18%), nonSD-saline (10.41 ± 1.69%), and nonSD-urethane (8.96 ± 0.95%) groups all had similar percentages of NeuN-cFos double-labeled cells within the LDT. Finally, the nonSD-wake group showed the greatest percentage of NeuN-cFos double-labeled cells in the LDT at 20.27 ± 0.54%. A one-way ANOVA showed significant differences ($F(4,15) = 24.39$, $p<1x10^{-4}$), with post hoc testing revealing that the nonSD-wake group showed significantly greater expression compared to all other groups (All: $p<1x10^{-4}$).

In the PPT the SD-saline group had the lowest percentage of NeuN-cFos double-labeled cells (13.01 ± 1.09%), with the SD-urethane (19.71 ± 1.91%), nonSD-saline (22.63 ± 1.84%), and nonSD-urethane (21.84 ± 2.43%) had relatively comparable expression levels between the three groups. The nonSD-wake group had the highest percentage of NeuN-cFos double-labeled cells at 47.98 ± 1.65%. A one-way ANOVA showed significant differences ($F(4,15) = 24.39$, $p<1x10^{-4}$), and post-hoc testing determined the SD-saline group had significantly lower percentages of NeuN-cFos double-labeled cells compared to all groups (nonSD-saline: $p=1.52x10^{-2}$, nonSD-urethane: $p=2.74x10^{-2}$, nonSD-wake: $p<1x10^{-4}$), except the SD-urethane

group (p=0.12). The nonSD-wake group had significantly greater percentage of NeuN-cFos double-labeled cells compared to all other groups (All: $p<1x10^{-4}$).

As illustrated in Figure 3.8, the LH showed comparable results between the SD-saline (3.51 ± 0.17%) and SD-urethane (3.78 ± 0.25%) groups, while the nonSD-saline (5.16 ± 0.66%), and nonSD-urethane (5.71 ± 0.66%) also showed near parallel results. In contrast, the nonSD-wake group had a higher percentage of NeuN-cFos double-labeled cells in the LH (18.07 ± 0.34%). Significant differences between the groups were detected using a one-way ANOVA ($F(4,15) = 240.7$, $p<1x10^{-4}$). Post-hoc testing revealed the nonSD-wake group had a significantly greater percentage of NeuN-cFos double-labeled cells compared to all other groups (All: $p<1x10^{-4}$), and that the nonSD-urethane group had a higher percentage of NeuN-cFos double-labeled cells compared to the SD-saline ($p=9.6 x10^{-3}$) and SD-urethane groups ($p=2.49x10^{-2}$).

Within the DR, the SD-saline (9.81 ± 1.23%), nonSD-saline (9.55 ± 1.07%), and nonSD-urethane (9.72 ± 1.44%) groups all had similar percentages of NeuN-cFos double-labeled cells. The SD-urethane group showed a slightly lower percentage of NeuN-cFos double-labeled cells (5.76 ± 4.89%), while in comparison, the nonSD-wake group showed approximately double the percentage of NeuN-cFos double-labeled cells as compared to all other groups (19.56 ± 1.00%). There was a significant difference between the means ($F(4,15) = 22.07$, $p<1x10^{-4}$) for double-labeled cells in the DR. The nonSD-wake group had significantly higher percentage of NeuN-cFos double-labeled cells compared to all other groups (All: $p<1x10^{-4}$), but no other significant differences were observed (Figure 3.8).

Interestingly, although the LC was expected to have demonstrated increased c-Fos IR during wakefulness, the percentages of NeuN-cFos double-labeled cells demonstrated a lack of

significant differences across the five groups. LC double labelling across groups was highly similar: SD-saline (11.19 ± 0.29%), SD-urethane (9.42 ± 0.52%), nonSD-saline (11.27 ± 0.70%), nonSD-urethane (11.17 ± 1.08%), and the nonSD-wake group (11.34 ± 0.61%). The LC showed no significant differences between the means ($F(4,15) = 1.41$, $p = 0.27$; Figure 3.8).

The BF, which is a heterogenous population of neurons involved in both wakefulness and sleep, also presented some unexpected results. The SD-saline group demonstrated the lowest percentage counts of NeuN-cFos double-labeled cells (3.30 ± 0.23%). The nonSD-saline (7.90 ± 0.67%) and nonSD-urethane groups (8.04 ± 0.61%) had relatively comparable proportions of NeuN-cFos double-labeled cells in the BF. The SD-urethane group had a higher percentage of NeuN-cFos double-labeled cells (17.1 ± 2.36%), while the nonSD-wake group (34.90 ± 2.72%) had the largest percentage of NeuN-cFos double-labeled cells. A one-way ANOVA indicated significant differences between the means ($F(4,15) = 57.24$, $p<1x10^{-4}$). A Tukey post-hoc test showed that the SD-urethane group had significantly higher c-Fos expression in the BF compared to the SD-saline ($p=3x10^{-4}$), the nonSD-saline ($p=1.03x10^{-2}$), and the nonSD-urethane groups ($p=1.16x10^{-2}$). The nonSD-wake group had significantly higher c-Fos expression compared to all other groups (All: $p<1x10^{-4}$), including the SD-urethane group (Figure 3.8).

3.6 Discussion

The pattern of neural activation as measured by the expression of the immediate early gene product c-Fos within endogenous sleep-wake circuitry during urethane anesthesia exhibits a striking correspondence with that of unpressured sleep, regardless of whether or not the rats that received urethane were previously sleep deprived. Of the ten ROI investigated, only two nuclei

had significant differences in c-Fos expression between the unpressured sleep experimental group (nonSD-saline) and either of the urethane groups, suggesting that urethane anesthesia and unpressured sleep converge upon a preponderance of shared neural targets within endogenous sleep-wake circuitry. This is further evidence of the suitability of urethane as a model for the brain mechanisms of natural sleep.

3.6.1 Pressured and unpressured sleep

In accordance with previous studies using a similar DOW total sleep deprivation protocol (Chang et al., 2006a), rats in the sleep deprivation groups were successfully sleep deprived during the 6 hour pre-experimental phase. Rats in the sleep deprived groups spent less than 1% of the pre-experimental phase in a sleeping posture, and also spent significantly more time active than rats in the non-sleep deprived groups. Furthermore, during the 2 hour experimental phase, rats in the sleep deprived groups had significantly longer sleep bouts (as measured by time spent in a sleep posture) than those in the non-sleep deprived groups, which is typically associated with recovery sleep following total sleep deprivation (Friedman et al., 1979). Consequently, the c-Fos data collected from the SD-saline group is a characteristic representation of neural activation during pressured sleep, in line with previous evidence (Ledoux et al., 1996; Gong et al., 2004).

Interestingly, although the nonSD-saline group were not sleep deprived during the pre-experimental phase, they also spent the majority of the experimental phase in a sleep posture. Indeed, other than the sleep posture bout duration, nonSD-saline rats did not differ significantly from SD-saline rats in terms of the distribution of time spent in any behavioural condition during the 2-hour experimental period. Perhaps not surprisingly in this regard, both SD-saline and

nonSD-saline groups showed significant differences in neural activation patterns as compared to rats in the nonSD-wake group in 9 of the 10 sleep-wake nuclei examined for c-Fos expression, indicating that both the SD-saline and nonSD-saline groups were likely sleeping and unconscious for the majority of the 2-hour experimental period. Thus, while EEG measures were not collected in this study, we conclude from both the behavioural data and the patterns of neural activation, that the c-Fos data collected from the nonSD-saline animals is representative of neural activation during unpressured sleep.

This interpretation is further supported by significantly greater c-Fos expression in the SD-saline group compared to the nonSD-saline group in both the VLPO and LHb. Both of these nuclei are associated with the generation, maintenance and consolidation of NREM sleep, and are therefore necessary for generating slow-wave activity (SWA), which serves as an indicator of homeostatic sleep need (Borbély, 1982; Gong et al., 2004; Rodriguez et al., 2016; Gelegen et al., 2018). Accordingly, the tripartite stratification of c-Fos expression between pressured sleep (SD-saline), unpressured sleep (nonSD-saline), and wake (nonSD-wake) in our results allowed us to further refine our comparison of urethane and natural sleep within sleep-wake circuitry based on any differences in the pattern of neural activation during urethane anesthesia that occurred due to homeostatic sleep pressure.

3.6.2 Influence of sleep pressure on urethane anesthesia

Intriguingly, we observed no significant differences in c-Fos expression between the SD-urethane and nonSD-urethane groups in 9 of the 10 ROI we assessed. This suggests that, unlike natural sleep, the neural activity produced during urethane anesthesia remains relatively

unaffected by homeostatic sleep pressure. The consistency of neural activation we observed in the sleep deprived and non-sleep deprived urethane anesthesia groups is presumably a product of both the stereotyped cycling of forebrain state that is characteristic of urethane (Clement et al., 2008; Pagliardini et al., 2013b), and the long-lasting physiological stability of the anesthetic (Maggi and Meli, 1986; Field et al., 1993).

Only the basal forebrain (BF) region exhibited differential c-Fos expression due to sleep pressure across the two urethane groups. Specifically, SD-urethane had significantly more c-Fos expression in the BF than nonSD-urethane, SD-saline, and nonSD-saline groups, although all groups had significantly lower c-Fos immunoreactivity in the BF compared to nonSD-wake (Figure 3.8). The high levels of activity in the BF in the nonSD-wake group were anticipated, as the BF has well-established cholinergic outputs that are integral to cortical activation during wakefulness (Greco et al., 2000a; Jones, 2005). Moreover, the BF also suppresses SWA by promoting cortical fast activity (Han et al., 2014; Arrigoni and Fuller, 2019). Although we are not sure why there was increased c-Fos immunoreactivity of the BF in the SD-urethane group, we hypothesize that increased sleep pressure may have resulted in compensatory BF activity in order to produce the stereotyped brain state alternations typically observed in urethane anesthesia. However, due to the heterogeneous neurochemical nature of the BF, future experiments localized to this region will be required to confirm whether this effect is precipitated through cholinergic pathways, or through another neurochemically distinct group of neurons (Gritti et al., 2006).

3.6.3 Urethane c-Fos expression parallels that of unpressured sleep

Unpressured sleep (nonSD-saline) had significant differences between one or both urethane groups in only 1 out of 10 ROI, whereas pressured sleep (SD-saline) had significant differences between one or both urethane groups in 6 of the 10 ROI investigated. This, coupled with the similar patterns of c-Fos expression between SD-urethane and nonSD-urethane, suggests that urethane and unpressured sleep exhibit parallel patterns of neural activity, irrespective of prior exposure to sleep deprivation in urethane. It is also important to note that both SD-urethane and nonSD-urethane had significantly different levels of c-Fos expression compared to nonSD-wake in the same sleep-comparable ROIs (9 of 10), in the same direction that was observed in both the pressured (SD-saline) and unpressured (nonSD-saline) sleep groups, indicating an analogous neural pattern of unconsciousness.

The only exception to the correspondence between urethane and unpressured sleep was observed in the vlPAG, where the nonSD-saline group had significantly higher c-Fos expression than both SD-urethane and nonSD-urethane groups. Increased firing of GABAergic neurons in the vlPAG consolidates NREM sleep while suppressing REM, which ultimately plays a role in the timing of alternations between REM and NREM (Weber et al., 2018a). Subsequently, a higher level of vlPAG activity would align with an increased amount of time spent in NREM, which is typically observed both following SD, and early in a sleep cycle, diminishing as the sleep cycle progresses (Carskadon and Dement, 2005; Simasko and Mukherjee, 2009; Rodriguez et al., 2016). Accordingly, since urethane anesthesia is characterized by stereotyped cycles with a consistent ratio of REM-like and NREM-like activity, and no changes in ultradian rhythm *per se*, we hypothesize that the significantly higher vlPAG activity in both SD-saline and nonSD-saline compared to the urethane anesthetized groups could be due to increased NREM pressure (Clement et al., 2008). However, since EEG measures were beyond the scope of this study,

future experiments characterizing the period and alternations in brain states during sleep and urethane anesthesia, in conjunction with experiments localized to the vlPAG will be needed to conclusively delineate the differences in c-Fos expression observed.

Only 3 ROI showed practically identical patterns of expression between pressured sleep, unpressured sleep and urethane groups – the LDT, DR and LC (Figure 3.8C, F, G). The LDT and the DR are associated with being most active during wakefulness, and exhibiting low activity or quiescence during NREM, and REM, respectively (Saper et al., 2010). This conforms with significantly higher levels of c-Fos expression we observed in nonSD-wake compared to all other groups in both the LDT and DR. Surprisingly, although the LC is also associated with being most active during wakefulness, we did not observe any significant differences in c-Fos expression between any of the groups, including the nonSD-wake group (Aston-Jones and Bloom, 1981). One of the contributing factors to this outcome may be that while the LC does not fundamentally affect sleep-wake architecture, it is essential for sustained wakefulness in response to novel environmental stimuli (Gompf et al., 2010). Since all animals in our study were habituated to the disk-over-water apparatus for 3 hours on the day prior to the experiment, this particular context was not novel and may have attenuated any LC response in the nonSD-wake group. Furthermore, LC activity plays a role in suppressing REM-on cells during NREM, which could account for similar levels of expression across all the unconscious states (Pace-Schott and Hobson, 2002). However, further electrophysiological experiments focused within the LC will be required to delineate differences in online patterns of activity sleep and urethane anesthesia.

3.6.4 Limitations and future directions

It has already been well established that urethane anesthesia has extensive neurobiological commonalities with natural sleep, in terms of: spontaneous alternations between an activated (REM-like) and deactivated (NREM-like) brain state, the periodicity of these alternations, and the accompanying fluctuations in peripheral physiology, such as heart and respiration rates (Clement et al 2008; Pagliardini et al 2013; Ward-Flanagan et al 2022). Consequently, the aim of our present study was to determine whether similar commonalities between sleep and urethane anesthesia would be observed when measuring c-Fos activation across a broad assortment of nuclei associated with the expression of sleep/wakefulness.

We reasoned that this study would be an appropriate first step in disseminating the potential mechanistic overlaps and divergences of sleep and urethane anesthesia. As such, we endeavoured to determine which, if any, sleep-wake nuclei exhibited a consistent pattern of activation during sleep and urethane anesthesia, and additionally whether sleep deprivation – which is a common tool in studies of natural sleep – affected neural activity under urethane. While we did not conduct EEG/EMG recordings in this study, we did bias brain state using behavioural methods: NREM is typically dominant and prolonged during recovery sleep which would correspond with increased synchronized slow-wave activity (Dijk, 2009), whereas wake produces a desynchronized brain state.

We have shown that urethane anesthetized animals exhibit c-Fos activity in the sleep-wake circuit most akin to that observed under unpressured (non-recovery) natural sleep, and extremely different from that of wake. Having conducted this broad comparison, it is now possible to narrow our focus, with this study serving as a foundation for the next steps required

to investigate potential convergent mechanisms between sleep and urethane. For instance, future studies could avoid sleep-deprivation as a tool in order to ensure a fairer comparison between sleep and urethane, and they should use EEG/EMG to probe the differences we observed between pressured sleep and urethane/unpressured sleep. Additionally, future studies should investigate specific heterogeneous nuclei (such as the basal forebrain) to determine the contributions of individual cell-types to the convergent patterns of activation we observed between urethane anesthesia and unpressured sleep. We are confident that our study will contribute to designing future experiments with greater precision.

3.6.5 Conclusion

Here, we have demonstrated that urethane anesthesia and unpressured sleep exhibit highly similar and parallel patterns of neural activation within endogenous sleep-wake nuclei, regardless of prior exposure to sleep deprivation preceding urethane administration. Our results conform with the previous consistencies reported between urethane and natural sleep in terms of behavioural, electrographic and physiological elements (Clement et al., 2008; Pagliardini et al., 2013a; Ward-Flanagan and Dickson, 2019). As such, in addition to allowing researchers the experimental advantage of manipulations that are not technically or ethically feasible during sleep, urethane represents an unparalleled pharmacological model for unpressured, natural sleep.

4 Intravenous chloral hydrate anesthesia provides appropriate analgesia for surgical interventions in male Sprague-Dawley rats

Rachel Ward-Flanagan[1] & Clayton T. Dickson[1,2,3,4]

[1] Neuroscience and Mental Health Institute, University of Alberta, Canada, T6G 2E1

[2] Department of Psychology, University of Alberta, Canada, T6G 2R3

[3] Department of Physiology, University of Alberta, Canada, T6G 2H7

[4] Department of Anesthesiology and Pain Medicine, University of Alberta, Canada, T6G 2G3

Acknowledgements: This work was supported by a Natural Sciences and Engineering Research Council of Canada (NSERC) Discovery grant 2016-06576 to C.T.D. R.W-F was supported by an NSERC Doctoral Postgraduate Scholarship, as well as an Alberta Graduate Excellence Scholarship. We would like to thank Nicholas R.G. Silver, B.Sc. for his assistance in collecting the withdrawal latency data. We would also like to thank the most fabulous Dr. Karim Fouad for the use of the Hargreaves infrared nociceptive apparatus.

https://doi.org/10.1371/journal.pone.0286504

4.1 Abstract

Background: The use of chloral hydrate as a sole maintenance anesthetic agent in rodent research has been controversial due to information in reference literature conflicting with that of primary research studies regarding its analgesic efficacy, and because of its associated tissue damage when administered intraperitoneally.

Objective: Our aim was to assess the analgesic efficacy of chloral hydrate using an intravenous (i.v.) route of administration, in order to prevent the local tissue irritation or ileus that has been previously reported using intraperitoneal (i.p.) routes.

Methods: We measured tail withdrawal latencies to a nociceptive thermal stimulus (infrared beam) in Sprague-Dawley rats – first when awake (unanesthetized), and then subsequently during i.v. chloral hydrate anesthesia. During anesthesia we also measured ongoing heart and respiration rates.

Results: Withdrawal latencies during chloral hydrate anesthesia were significantly higher, and often maximal, indicating a robust analgesic effect. Importantly, both respiration and heart rate remained unchanged following exposure to the nociceptive stimulus, and were comparable to values observed under other anesthetics and during natural sleep.

Conclusions: Together with previous studies, these results demonstrate that i.v. chloral hydrate provides excellent anesthetic depth and analgesic efficacy for surgical manipulations in rats.

4.2 Introduction

For both clinical and research applications, general anesthesia is characteristically composed of several discrete endpoints, including: a reversible loss of consciousness, akinesia, amnesia, and analgesia (Brown et al., 2010). By this definition, the use of chloral hydrate in animal research has been contraindicated due to assertions it that does not provide adequate analgesia to meet the requirements of a sole anesthetic agent for induction or maintenance (Silverman and Muir, 1993; Baxter et al., 2009). Furthermore, chloral hydrate has other complications related to local tissue irritation and ileus when administered via intraperitoneal (i.p.) injection (Fleischman et al., 1977).

Troublingly, the most common claims of insufficient analgesia during chloral hydrate anesthesia appear in reference textbooks where these statements are made without citations to any experimental studies (Hall, 2001; Flecknell, 2016b). In direct contrast, our review of the primary neurobiological literature found studies that directly contradicted these claims. For example, comparative studies have demonstrated that the anesthesia and analgesia produced by chloral hydrate is comparable to other commonly used research anesthetics, such as ketamine-xylazine, pentobarbital, and urethane (Field et al., 1993; Rodrigues et al., 2006). In addition, the active metabolite of chloral hydrate, 2,2,2-trichloroethanol, has been demonstrated to modulate membrane currents and subsequently inhibit pain transmission in mammalian dorsal root ganglion neurons (Gruss et al., 2002; Fischer et al., 2003), suggesting a direct means of attenuating pain sensation at the level of the spinal cord itself. Furthermore, when nuclei implicated in the modulation of descending endogenous antinociception (such as the ventrolateral periaqueductal gray, or A5-7 noradrenergic cell groups) are chemically lesioned, analgesia is attenuated (as measured by a decrease in tail flick latency to a thermal nociceptive

stimuli) in rats anesthetized with either ketamine or chloral hydrate (Lu et al., 2008). Taken together, these studies show that chloral hydrate not only exhibits analgesic effects at the cellular level, but is comparable to other commonly used research anesthetics in terms of supraspinal targets and behavioural effects and as such is an equally appropriate anesthetic for surgical procedures.

However, while other studies have also found that chloral hydrate produced appropriate depth of anesthesia and analgesia for surgical tolerance, there have been valid criticisms due to the post-surgical development of peritonitis and corresponding pathological complications (i.e weight loss and increased stress hormones) when it is administered intraperitoneally (Hüske et al., 2016). Consequently, our aim was to use a modern and standardized methodology to assess the efficacy of analgesia during intravenous (i.v.) chloral hydrate anesthesia in male Sprague-Dawley rats, and thereby determine whether chloral hydrate is suitable for use as a sole anesthetic agent for maintenance of anesthesia in rodent research. To that end, we measured withdrawal responses in rats to noxious thermal stimuli both while unanesthetized and while anesthetized with chloral hydrate, using an i.v. delivery of chloral hydrate in order to both circumvent the immunological complications associated with the traditional i.p. method and to allow for a more consistent plane of anesthesia. We hypothesized that i.v. chloral hydrate would provide adequate analgesia and increase tail withdrawal latencies to a noxious thermal stimuli, in congruence with previous studies showing that chloral hydrate provides excellent depth of anesthesia and analgesia.

4.3 Materials and methods

4.3.1 Subjects

Data were collected from 7 naïve male Sprague-Dawley rats (Charles River; CD 001) weighing on average 319.9 ± 6.0 g (mean ± SEM). Prior to experimentation, rats were kept on a 12-hour light/dark cycle at 20 ± 1ºC, in polycarbonate shoebox-shaped 42 x 25.5 x 18 cm ventilated cages (Tecniplast, Buguggiate VA, Italy), containing no more than 4 rats per cage. Cages were lined with aspen chip bedding (Living World, Rolf C. Hagen Inc, Baie d'Urfé, QC, Canada) and also contained a plastic tube for enrichment, and standard rat chow (5001, LabDiet, St. Louis, MO) and water (demineralized) were provided *ad libitum*. Welfare checks were performed daily prior to experiments. All methods used in this study conform to the animal use protocol (protocol number: 092) approved by the Biological Sciences Animal Care and Use Committee of the University of Alberta, in accordance with the guidelines established by the Canadian Council on Animal Care. In an effort to reduce our overall number of animals used, a subset of these animals (n=5) were used in subsequent experiments that are not reported here.

4.3.2 Baseline withdrawal assessment

Rats were initially placed in a Hargreaves apparatus (Ugo Basile, Gemonio, VA, Italy) for 15 minutes in order to acclimate to the chamber and reduce movement. Upon acclimation, tail withdrawal latencies to thermal stimulation were recorded by applying an infrared (IR) beam to the approximate middle of the tail at an intensity level of 57 (arbitrary units). The intensity chosen was based on a pilot study with 2 naïve rats, since it produced an average tail withdrawal latency of ~10 seconds (Austin et al., 2012). We recorded 5 separate trials of tail withdrawal latency per animal, allowing for recovery for a minimum of one minute between each trial. As

the intensity of the IR beam increases during the trial, each trial was limited to a maximum of 30 seconds (3x the average baseline withdrawal latency) to ensure no dermal damage occurred from trial to trial (Le Bars et al., 2001).

4.3.3 Surgery and anesthesia

Following tail withdrawal tests, rats were anesthetized in a plexiglass anesthetic chamber using 4% isoflurane in medical (100%) oxygen. Once the animal exhibited a loss of righting reflexes, it was transferred to a nosecone and maintained at 1.5 – 2.5% isoflurane and implanted with a flexible silicone jugular catheter (Silastic 508-004, Dow Corning, Midland, MI). Isoflurane was then discontinued and the animal was switched to chloral hydrate anesthesia (Sigma-Aldrich, Oakville, ON; (≥98% MQ200; 0.1 g/mL in phosphate-buffered saline) using an i.v. bolus dose of 200 mg/kg (0.64±0.01 mL based on the previously reported average weight). The rat was then moved to a servo-driven heating pad (TR-100; Fine Sciences Tools, Vancouver, BC) to maintain core body temperature at ~37°C (36.8±0.3°C, n=7), and placed on a continuous i.v. infusion of chloral hydrate at a rate of 150 mg/kg per hour (0.48±0.01 mL based on the previously reported average weight). We chose this concentration to attenuate the total volume of fluid administered, on average the animals received 1.60±0.03 mL over the course of 2 hours. Animals were then secured in a stereotaxic frame and monitored for any adverse reaction to ensure they were at a surgical plane of anesthesia (Kopf Instruments, Tujunga, CA, USA). If any reaction (i.e paw movement, head shake) was observed, the animal was given an additional small bolus (<0.05 mL/<5 mg) of chloral hydrate until a surgical plane was attained and the animal

could be secured within the stereotaxic frame without any reactionary movement. These boluses were recorded with any other pre-trial period boluses, as outlined below.

Heart rate (HR) and respiratory rate (RR) were continuously monitored using a pulse pressure transducer (AD Instruments, Colorado Springs, CO) connected to the left hind paw, and a thermocouple wire (30 gauge Type K; Thermo Electric Co., Inc.; Brampton, ON, Canada) placed in front of the right nasal passage. Any indication of loss of a surgical plane of anesthesia (increased HR and RR, confirmed with a hindlimb withdrawal to toe-pad pressure) was followed quickly by administration of small (<0.05 mL/<5 mg) bolus increments of chloral hydrate until a clinical plane was restored as defined by a loss of reflexive withdrawal to a hind paw pinch. Small boluses (<0.05 mL/<5 mg) were also administered when the syringe body was refilled to account for the interruption of the continuous infusion, and the majority of all boluses for both maintenance of anesthetic plane and syringe refills were administered prior to any trials for nociception. The total additional chloral hydrate administered during the pre-trial period was ~12% of the continuous dose per hour (0.18±0.01 mL/18±1 mg, n=7). Only 2 animals received boluses during the trial period, and only for refill purposes, not due to a loss of surgical plane (0.04±0.01 mL/4±1 mg, n=2).

4.3.4 Anesthetized withdrawal assessment

Rats received a continuous infusion of chloral hydrate for a minimum of 1 hour prior to testing for analgesia, to ensure complete metabolism of any residual isoflurane. Using the same protocol as in the baseline withdrawal assessment, we applied an IR beam at the same intensity level and recorded 5 separate trials of tail withdrawal latency per animal, allowing for recovery

for at least one minute between each trial. As before, each trial was limited to a maximum of 30 seconds to ensure no dermal damage occurred trial to trial. Following termination of the experiment, rats were deeply anesthetized using urethane (Sigma-Aldrich; ≥99% MQ200; 1.7 g/kg), and then exsanguinated by transcardial perfusion with saline.

4.3.5 Data processing and statistical analyses

Thermocouple signals were amplified at a gain of 1000 and then filtered between 0.1 and 500 Hz using an AC amplifier (Model 1700, A-M Systems Inc.) and sampled at 1000 Hz. All signals were recorded using a PowerLab AD board in conjunction with LabChart Pro (AD Instruments). Average respiration rate and heart rate were computed from 40-minute baseline recordings taken prior to any IR stimuli trials, and were analyzed using custom scripts for MATLAB (Mathworks; Natick, MA), which processed the signals in spectral time windows 30-seconds in duration, with a frequency resolution of 0.167 Hz.

Due to the complication of movement artefacts in the heart and respiratory signals that often arose during the IR trials from positioning the tail on the IR beam, pair-wise comparisons of pre-IR and IR heart and respiration rate were analyzed for 3 trials per animal where there were no movement artefacts. These physiological analyses were computed by using the peak analysis function in LabChart to assess the instantaneous (cycle-by-cycle) period of heart and respiration rate. The threshold for peak detection was adjusted for pair-wise comparisons to account for any noise in the signal, with an average threshold of 1.84±0.09 standard deviations (SD) from baseline for respiration analyses, and an average threshold of 1.87±0.04 SD from baseline for

heart rate analyses. One animal was excluded from respiration analyses due to complete signal dropout.

Arithmetic means were computed for individual data for each animal within both conditions being compared: baseline unanesthetized and anesthetized for withdrawal latencies, and the 30 seconds pre-IR and during IR for respiration and heart rate during anesthesia. Overall means were then computed for each condition along with SEM. Statistical tests included a Shapiro-Wilk test for normality on both baseline (unanesthetized) and anesthetized, and pre-IR and IR datasets, followed by a paired t-test to compare both conditions within-subjects. These statistical tests were performed using Prism 8 (GraphPad Prism Software Inc, San Diego, CA), using a significance level of $\alpha=0.05$. Power analysis was computed post-hoc for latency data and we determined that maximal power was obtained with a minimum group size of 4. Additionally, we determined that the minimum detectable difference for these data was 5.18 seconds.

4.4 Results

During chloral hydrate anesthesia, the average HR was 384±24.0 beats per minute (n=7), and the average RR was 108±5.40 breaths per minute (n=7), which fall between values previously reported for urethane anesthetized rats (~444.0 beats per minute HR; ~126 breaths per minute RR) and naturally sleeping rats during slow-wave sleep (~330 beats per minute HR; ~96.0 breaths per minute RR), and as such are consistent with unconsciousness (Viczko et al., 2014; Silver et al., 2021).

Compared to unanesthetized values, tail withdrawal latencies were significantly longer under chloral hydrate anesthesia in 6 of the 7 rats tested, as determined by a Student's t-test for each animal. Furthermore, in 3 of the 7 animals tested, and across 57% of all anesthetized trials, no withdrawal took place within the 30 second limit (Figure 4.1). A Shapiro-Wilk test showed that both unanesthetized ($W(6)=0.9043$, $p=0.3580$) and anesthetized ($W(6)=0.8684$, $p=0.1798$) data sets were normal, and a paired t-test revealed that this increase in withdrawal latency was highly significant ($t(6)=7.711$, $p=0.0002$).

Moreover, there were no changes in either heart or respiration rates in response to the nociceptive thermal IR stimulus (Figure 4.2). A paired t-test comparison of the 30 seconds immediately preceding an IR stimulus (pre-IR) to the 30 second period during which the IR beam was delivered yielded no significant differences in the respiration rate ($t(5)=1.070$, $p=0.334$) following a Shapiro-Wilk test for normality which showed that both unanesthetized ($W(5)=0.9467$, $p=0.7137$) and anesthetized ($W(5)=0.9642$, $p=0.8517$) data sets were normal. Similarly, in measuring heart rate, both unanesthetized ($W(6)=0.8472$, $p=0.1158$) and anesthetized ($W(6)=0.8527$, $p=0.1302$) data sets were normal and no significant changes in the heart rate ($t(6)=2.061$, $p=0.085$) were observed when comparing the 30s pre-IR to IR. Even when we compared the distribution of the instantaneous (cycle-by-cycle) cardiac and respiration periods across individual trials, no systematic differences were observed (Figure 4.3A,B). This was confirmed by assessing the linear fit for the instantaneous heart rate and breathing rate during IR exposure, which revealed: 1) no significant changes in heart rate in any of the trials, and 2) only 2 of 18 trials had a significant change in breathing rate, both of which were a negative slope, indicating a decrease in breathing rate, rather than an expected increase in reaction to a nociceptive stimuli (Figure 4.3C,D).

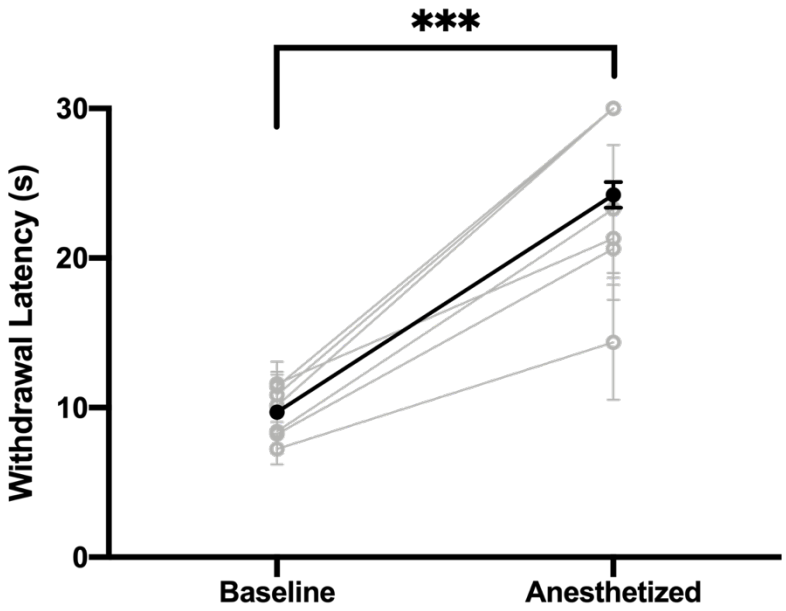

Figure 4.1 Chloral hydrate anesthesia significantly increases latency of tail withdrawal from a nociceptive stimulus.

Within-subject comparison of tail withdrawal latencies to a nociceptive stimulus while unanesthetized and while subsequently anesthetized with chloral hydrate anesthesia (200mg/kg initial bolus; 150 mg/kg per hour continuous intravenous infusion). Withdrawal latencies increased significantly during chloral hydrate anesthesia in every rat tested (individual values represented in grey; average represented in black). ***$p<0.0001$

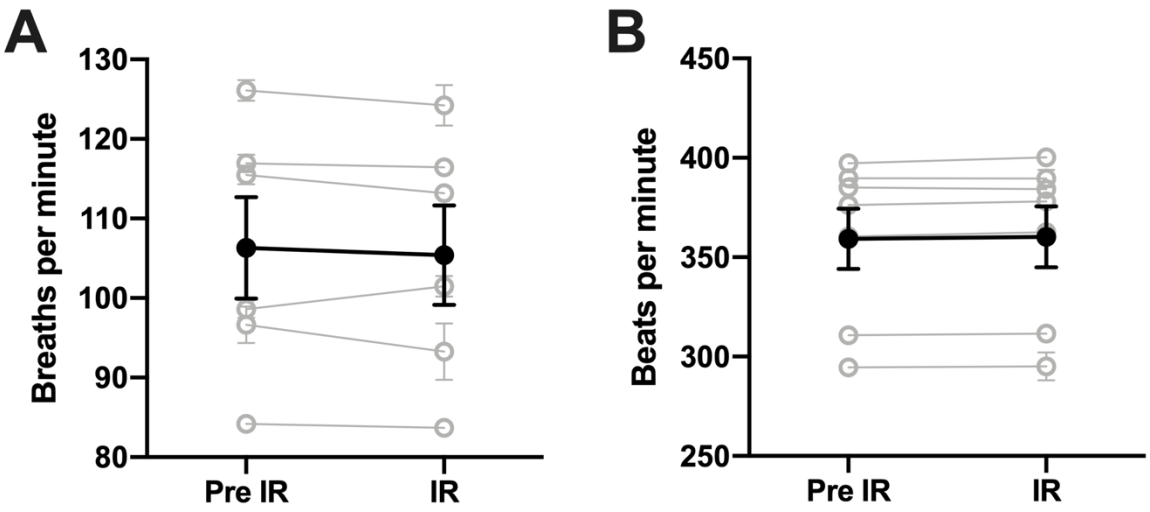

Figure 4.2 Heart and respiratory rate remain unchanged during nociceptive stimulation under chloral hydrate anesthesia.

(A) Within-subjects comparison of respiration rate 30 seconds pre-IR stimulus and during IR stimulus averaged over 3 separate trials (individual averages are represented in grey, grand average of all animals is represented in black). (B) Within-subjects comparison of heart rate 30 seconds pre-IR stimulus and during IR stimulus averaged over 3 separate trials (individual averages are represented in grey, grand average of all animals is represented in black).

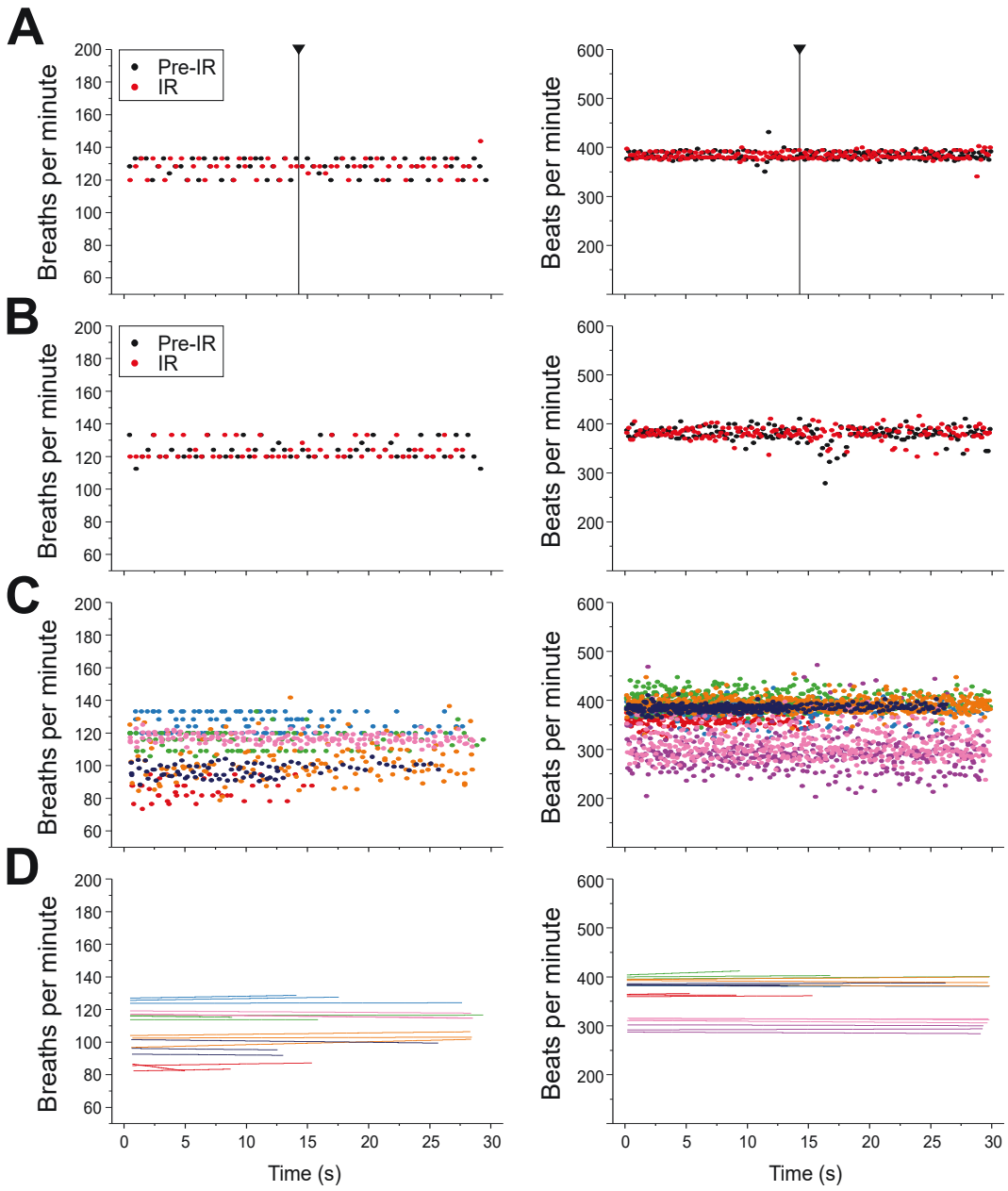

Figure 4.3 Heart and respiratory rate remain unchanged with or without tail flick response during nociceptive stimulation under chloral hydrate anesthesia.

Figure 4.3 Heart and respiratory rate remain unchanged with or without tail flick response during nociceptive stimulation under chloral hydrate anesthesia.

(A) Within-subject comparison of instantaneous (cycle-by-cycle) respiration rate (left) and heart rate (right) 30 seconds pre-IR stimulus (in black) and during IR stimulus (in red). Nociceptive thermal stimulation during IR is cut off at 14.5s (denoted by a black line) due to a tail flick reaction. (B) Within-subject comparison of the same animal in A showing instantaneous (cycle-by-cycle) respiration rate (left) and heart rate (right) 30 seconds pre-IR stimulus (in black) and during IR stimulus (in red). Nociceptive thermal stimulation is not cut off during IR as the animal did not react within the 30s. (C) Instantaneous (cycle-by-cycle) respiration rate (left) and heart rate (right) during IR for all trials (i.e 3 trials per rat). Each animal is denoted by a single colour to show variation across subjects. (D) Linear fit of each trial during IR. Each animal is denoted by a single colour.

4.5 Discussion

Our data demonstrate that there is a significant increase in the latency of withdrawal responses, together with no changes in ongoing basic physiological responses such as respiration or heart rate in response to a nociceptive thermal stimulus under continuous i.v. chloral hydrate anesthesia. These results are consistent with prior reports from the primary literature that chloral hydrate provides excellent anesthetic depth, including analgesia, for surgical manipulations in rats (Field et al., 1993; Rodrigues et al., 2006).

While the assessment of nociception can be a difficult task due to the many inter-related physiological factors that can influence behavioural outcomes (Le Bars et al., 2001), we endeavoured to mitigate these confounds by using a within-subjects design to compare the naïve baseline to the anesthetized state, on the same day, at the same IR intensity across all subjects, and at the same location on the tail. Though a relatively simple protocol, our approach accounts for much of the variance that can often affect thermal nociceptive measures (i.e ambient room temperature, stimulation site, and intensity, etc.) (Le Bars et al., 2001; Deuis et al., 2017). Our within-subjects design also informed our choice to analyze our data as the change of raw latency values from baseline for each animal, rather than as a percentage of the maximum latency, which would be dependent on our arbitrary cut-off, and which would lead to the statistical fallacy of comparing percentages of percentages (Le Bars et al., 2001). Thus, we are confident that our data is a fair representation of the analgesic effect of chloral hydrate on the tail flick response to a nociceptive stimuli in rats.

The occurrence of tail withdrawals under chloral hydrate in our results are a further indication that the effect observed is due to analgesia, rather than an artefact of immobility

causing an inability to move while the animal may still be perceiving pain. Furthermore, while the tail flick withdrawal is typically considered a spinal reflex, lower intensity stimuli which produce a delayed baseline withdrawal (>5s) are generally thought to engage higher-order supraspinal structures in order to process pain and execute the withdrawal behaviour (Jensen and Yaksh, 1986; Le Bars et al., 2001; Deuis et al., 2017). This line of evidence, when taken together with the study showing that chemical lesions to the vlPAG or descending noradrenergic neurons (both of which are thought to modulate endogenous antinociception) significantly decreases tail flick latency under chloral hydrate anesthesia (Lu et al., 2008), suggests that the analgesic effect we observed is mediated via supraspinal structures.

Yet, we acknowledge that our study has limitations. Though we have shown i.v. administration of chloral hydrate provides an appropriate depth of anesthesia and analgesia necessary to achieve a surgical plane, further experiments will be required to determine if i.v. administration alleviates the post-surgical physiological side effects associated with i.p. routes (Hüske et al., 2016). In addition, the scope of nociceptive stimuli in our study is limited to a thermal IR stimulus. However, when considered in the context of previous primary literature, our data adds to and is consistent with reports of that the anesthesia and analgesia provided by chloral hydrate is appropriate for surgical manipulations (Field et al., 1993; Rodrigues et al., 2006; Hüske et al., 2016; Ward-Flanagan et al., 2022), and thus are in stark contrast to widespread claims that chloral hydrate should only be considered as a hypnotic with poor analgesic properties (Silverman and Muir, 1993; Hall, 2001; Flecknell, 2016b).

We stress that our argument is not that analgesics should never be used in conjunction with chloral hydrate anesthesia, but that chloral hydrate provides sufficient analgesia for experimental paradigms which require a surgical plane of anesthesia and aim to minimize

confounding factors that multiple drugs can introduce. Although chloral hydrate has been under-utilized mainly due to the erroneous assertion of inadequate analgesia, it appears that when delivered intravenously in rats, it meets the requirements of a sole anesthetic agent for maintenance of anesthesia and should be considered more often by researchers when using the protocol we have outlined here.

5 Sleep-like alternations of brain state under chloral hydrate anesthesia

Rachel Ward-Flanagan[1], Nicholas Silver[1] & Clayton T. Dickson[1,2,3,4]

[1] Neuroscience and Mental Health Institute, University of Alberta, Canada, T6G 2E1

[2] Department of Psychology, University of Alberta, Canada, T6G 2R3

[3] Department of Physiology, University of Alberta, Canada, T6G 2H7

[4] Department of Anesthesiology and Pain Medicine, University of Alberta, Canada, T6G 2G3

Acknowledgements: This work was supported by a Natural Sciences and Engineering Research Council of Canada (NSERC) Discovery grant 2016-06576 to C.T.D. R.W-F was supported by an NSERC Doctoral Postgraduate Scholarship, as well as an Alberta Graduate Excellence Scholarship.

5.1 Abstract

Though sleep is a ubiquitous, phylogenetically conserved behaviour, which is vital for survival, its core function remains a mystery. One of the main contributing factors to this lack of progress is the fragile nature of sleep, which limits possible experimental paradigms due to technical and ethical considerations. Pharmacological models of natural sleep can alleviate many of the issues that would otherwise prohibit experimentation, however, few pharmacological models can reproduce the complex neurophysiology of natural sleep. Currently, urethane anesthesia produces the most accurate replication of sleep-like alternations of brain state and concomitant changes in peripheral physiology, but it is also limited to acute experimental protocols. Consequently, we endeavoured to investigate chloral hydrate, which is not limited to acute preparations, as a potential alternative to urethane to model sleep.

We found that chloral hydrate produced a neurophysiological profile that was incredibly similar to sleep and urethane anesthesia in terms of individual brain states of forebrain activation and deactivation, timing of alternations between these brain states, and sensitivity to bidirectional cholinergic neuromodulation. Furthermore, respiratory rate, respiratory variability and the incidence of sighs all increased during states of forebrain activation under chloral hydrate, which is analogous to respiration in natural sleep and urethane. However, heart rate and temperature were not comparable to sleep. Taken together, our results suggest that urethane remains a more comprehensive pharmacological model of sleep, but that when experimental flexibility is required that chloral hydrate can serve as a model of sleep-like brain states, and their alternations.

5.2 Introduction

The most precise, and obvious way to study sleep-related neurobiology is to perform experiments during sleep itself. However, natural sleep is plagued by a host of experimental challenges, both in terms of technical obstacles (e.g., getting subjects to actually sleep), and ethical limitations (e.g., the inability to perform otherwise painful monitoring and manipulations). By using a pharmacological model of sleep, researchers can not only alleviate the majority of these issues, but can also achieve a greater degree of experimental control (Ward-Flanagan and Dickson, 2019). This is perhaps best exemplified by urethane anesthesia, which produces both an extremely stable surgical plane of anesthesia, as well as highly stereotyped and cyclical brain state alternations resembling the rapid eye movement (REM) and non-REM (NREM) cycle in natural sleep (Clement et al., 2008; Silver et al., 2021).

In addition to sleep-like brain states, peripheral physiological measures under urethane also exhibit brain state-related fluctuations consistent with those observed during natural sleep, including changes in: respiratory rate and variability, heart rate, body temperature, EMG tone, pupillary size and urodynamic function (Clement et al., 2008; Whitten et al., 2009; Pagliardini et al., 2012; Blasiak et al., 2013; Crook and Lovick, 2016). Consequently, urethane has been an invaluable tool for many discoveries that have subsequently been confirmed in natural sleep. Such discoveries include: the cortical and hippocampal slow oscillation (Steriade et al., 1993; Wolansky et al., 2006); the hyperoxic promotion of NREM (Hauer et al., 2018), and the involvement of astrocytes in cortical synchronization during NREM (Poskanzer and Yuste, 2016; Vaidyanathan et al., 2021). However, despite its robust parallels with natural sleep, urethane remains limited as a model, as it is contraindicated for use in recovery experiments due to long-term pathological and carcinogenic effects (Maggi and Meli, 1986).

Recently, in an attempt to find an alternate model, we performed a direct comparison of urethane and five other common research anesthetics to assess if any other agents could produce sleep-like brain state alternations consistent with those of urethane, and critically, at a surgical plane of anesthesia (Ward-Flanagan et al., 2022). Of the anesthetics tested, we found that three anesthetics produced a coma-like state of burst-suppression (pentobarbital, isoflurane, and propofol), one produced a unitary NREM-like state of slow-wave activity (ketamine-xylazine), and that only chloral hydrate and urethane allowed for cyclical, spontaneous brain state alternations between a REM-like state of forebrain activation, and a NREM-like state of deactivation (Ward-Flanagan et al., 2022). This finding suggested that chloral hydrate had the potential to serve as an alternate pharmacological model for sleep, and unlike urethane, one that would not necessarily be limited to acute experimental paradigms (Field et al., 1993).

Thus, our aim in the present study was to assess the propriety of chloral hydrate as an alternative to urethane as a pharmacological model of sleep. To that end, we systematically characterized various neurophysiological measures under chloral hydrate anesthesia that are known to correspond across natural sleep and urethane anesthesia. Here we report that the spontaneous electrophysiological activity observed under chloral hydrate maps well onto that observed under natural sleep as well as urethane anesthesia in terms of constituent brain states, the timing of alternations, and sensitivity to cholinergic neuromodulation. However, while respiration under chloral hydrate appears analogous to sleep and urethane, other peripheral physiological measures do not entirely correspond and subsequently are not representative of natural sleep. Overall, while chloral hydrate may provide a more experimentally flexible model for sleep-like alternations of brain state, urethane remains a more comprehensive model of the neurophysiology of natural sleep.

5.3 Methods

5.3.1 Subjects

Data were collected from a total of 39 naïve male Sprague-Dawley rats, obtained from Charles River (CD 001) through Sciences Animal Support Services at University of Alberta. Data from ten of these subjects has been reported in two previous publications, 5 in (Ward-Flanagan et al, 2022) and 5 in (Ward-Flanagan & Dickson, in revision). All experiments reported in this study involved acute anesthesia. At the time of experimentation rats weighed an average of 319.38±6.03 g. Prior to testing, rats were housed in polycarbonate shoebox-shaped ventilated cages (Tecniplast, Buguggiate VA, Italy), containing a 10 cm diameter PVC cylinder for enrichment, and were housed with no more than 4 rats per cage. Rats were kept on a 12-hour light/dark cycle at 20±1ºC, and received standard rat chow (5001, LabDiet, St. Louis, MO, USA) and demineralized tap water *ad libitum*. All procedures conformed to the animal use protocol (092) approved by the Biological Sciences Animal Care and Use Committee of the University of Alberta, and were in accordance with the guidelines established by the Canadian Council on Animal Care.

5.3.2 Anesthesia and surgery

Rats were initially anesthetized in an enclosed plexiglass chamber using isoflurane (4%) in 100% medical oxygen. Following a loss or righting reflexes, animals were implanted with a flexible, silicone jugular catheter (Silastic 508-004, Dow Corning, Midland, MI, USA), while being maintained on isoflurane (1.5-2.5%) via a nose cone. Isoflurane was then discontinued, as

the animal was switched to intravenous (i.v.) chloral hydrate anesthesia (Sigma-Aldrich, Oakville, ON, Canada; ≥98% MQ200; 0.1 g/mL in phosphate-buffered saline), using a bolus dose (200 mg/kg) delivered over a period of less than 2 minutes. Following the bolus, chloral hydrate anesthesia was maintained at a rate of 150 $mg \cdot kg^{-1} \cdot hr^{-1}$ using a continuous infusion pump (KDS100, KD Scientific Inc., Holliston, MA, USA) for the duration of the experiment, unless specified below. The rat was then transferred to, and secured within a stereotaxic frame (Kopf Instruments, Tujunga, CA, USA). Core body temperature was maintained at ~37°C by servo-driven heating pad (TR-100, Fine Sciences Tools, Vancouver, BC, Canada). Prior to incision, 0.5 ml of lidocaine (2%) was injected along the midline of the scalp, followed by a single incision to expose the skull. The skull was then leveled by adjusting the rats head until bregma and lambda were at the same horizontal plane.

Anesthetic depth was monitored throughout the experiment by observing for sustained changes in heart rate recorded via a pulse pressure transducer connected to the left hind paw (AD Instruments, Colorado Springs, CO, USA), or vibrissae movement. If either of these changes were observed anesthetic plane was assessed by checking for a reflexive withdrawal to a hind paw pinch. Any indication of a loss of surgical plane was quickly corrected by administration of small (<0.05 mL) bolus increments of CH until a surgical plane was restored. Typically, supplemental doses were administered near the beginning of the experiment, and on average, the total supplemental bolus dose administered was 0.06±0.01 mL (N=39).

5.3.3 Stereotaxic procedures

The placement of bipolar recording electrodes was determined by using bregma as a reference for stereotaxic coordinates. Two bipolar electrodes, constructed of two lengths of Teflon-coated stainless steel wire twisted together (bare diameter 125 um: A-M Systems Inc., Sequim, WA, USA), were implanted in each rat in order to serve as an index of forebrain state, one in the frontal neocortex (AP: +2.8, ML: +2.0, DV (tip of long electrode): -1.0 to -1.2 mm), and one in the contralateral hippocampus (AP: -3.5, ML: -2.5, DV: -2.2 to -3.5 mm). Electrodes were fixed in place using dental acrylic fixed to a jeweler's screw anchored in the skull. Following experiment termination, rats were euthanized either by transcardial perfusion under deep anesthesia, or by a lethal overdose of urethane anesthesia.

5.3.4 Recording procedures and manipulations

Characterization of continuous local field potentials during i.v. chloral hydrate anesthesia

A total of 30 animals were used to characterize spontaneous neurophysiological states under chloral hydrate anesthesia. Local field potential (LFP) activity was recorded at cortical and hippocampal sites for a minimum of 40 minutes. These signals were differentially amplified at a gain of 1000, and filtered between 0.1 and 500 Hz using an AC-coupled amplifier (Model 1700, A-M Systems). Once amplified, LFPs were sampled at 1000 Hz with additional anti-alias filtering at 500 Hz, and recorded using a PowerLab AD board in conjunction with LabChart Pro (AD Instruments) running on a PC computer.

Characterization of additional bolus doses, and temporary discontinuation of anesthesia

In a subset of animals (n=3), we assessed the effects of bolus doses (15 mg per bolus) of chloral hydrate in addition to the continuous infusion at the standard rate of 150 $mg \cdot kg^{-1} \cdot hr^{-1}$. The effect of each bolus on LFP activity was observed for two full cycles before any additional bolus doses of chloral hydrate were administered. In the same animals, we observed the effects of chloral hydrate metabolism in the absence of continuous infusion of chloral hydrate. The infusion pump was turned off and the animals were monitored closely for any shifts in anesthetic plane. The infusion pump was immediately restarted once any shift in anesthetic plane was observed.

Analgesia across brain state fluctuations

Prior to anesthesia and surgery, a subgroup of rats (n=5) were acclimated to a Hargreaves apparatus (Ugo Basile, Gemonio, VA, Italy) for 15 minutes. Following this period, a nociceptive thermal stimulus (infrared beam) was applied to the approximate middle of the tail at an intensity level of 57 (arbitrary units). Tail withdrawal latencies were recorded over 5 separate trials per animal, with a minimum of a one-minute recovery period between each trial. To ensure animals did not sustain any dermal damage, trials were limited to a maximum of 30 seconds due to the maximum intensity of the nociceptive stimulus. These rats then underwent surgery, anesthesia, and stereotaxic procedures as described above. Before the second, anesthetized Hargreaves test of nociception, rats received a continuous infusion of chloral hydrate for a minimum of one hour. Using the same stimulus intensity as used during the un-anesthetized baseline trials, tail withdrawal latencies were assessed across both activated and deactivated brain states (see results) for a total of 10 trials (5 per state) per animal (n=5).

Physiological correlates of brain state

In a subset of animals (n=13), cortical and hippocampal LFPs, respiration, heart rate, and body temperature were measured simultaneously in order to compare these physiological measures with fluctuations in brain state. LFPs were recorded as described above. Respiration rate was monitored by placing a thermocouple wire (30 gauge Type K; Thermo Electric Co., Inc.; Brampton, ON, Canada) in front of the right nasal passage, to continuously measure the changes in temperature caused by inspiration (decreased temperature) and expiration (increased temperature). Thermocouple signals were amplified using the same procedure as for LFPs: at a gain of 1000, and filtered between 0.1 and 500 Hz using an AC-coupled amplifier (Model 1700, A-M Systems). Heart rate was monitored via a pulse transducer (AD Instruments), and core body temperature was continuously recorded via a rectal probe (Harvard Apparatus Holliston, MA, USA). As with LFP signals, all amplified physiological measures were then sampled at 1000 Hz (with anti-alias filtering at 500 Hz), using a PowerLab AD board and digitally recorded with LabChart Pro (AD Instruments).

Pharmacological manipulations

Following baseline recordings, pharmacological manipulations were administered systemically in order to assess the influence of cholinergic signalling under chloral hydrate anesthesia. Animals received either: 1) the muscarinic receptor antagonist atropine sulfate alone (AtSO4; 50 mg/kg; n=4), or 2) the muscarinic agonist m-oxotremorine (OXO; 4 mg/kg),

followed by atropine sulfate (50 mg/kg; n=5). Animals in the second condition were pre-treated with a muscarinic antagonist atropine methyl nitrate (0.5 mg/kg), which does not cross the blood-brain barrier, in order to suppress salivary secretions, and stabilize respiration when OXO was administered. This was done a minimum of 20 minutes prior to the administration of OXO drugs. AtSO4 was made fresh on the day of each experiment, and OXO was either prepared fresh on the day of the experiment, or in a batch solution and stored frozen in individual aliquots for each experiment to avoid repeated freeze/thaw. Frozen OXO was limited to use within a 3 month window (Oxotremorine, 2023).

Within-subjects comparison of chloral hydrate and urethane anesthesia

In order to directly compare chloral hydrate and urethane, spontaneous LFP activity was recorded in 9 rats under both choral hydrate and urethane anesthesia. Following baseline recordings under urethane anesthesia as described above, the infusion pump was stopped and chloral hydrate was discontinued for ~5 minutes. Urethane was then administered very slowly in small boluses (<0.05 mL) via either a tail vein catheter, or jugular catheter (1.7 g/kg; >15 minutes). This was done while monitoring for any changes in anesthetic depth, as determined by heart rate and brain state – if the animal was very deep, urethane was administered more slowly over longer intervals, and if the animal exhibited a lessening of anesthetic depth urethane was administered over shorter intervals. Spontaneous LFP activity under urethane was assessed after an average of 74.44±11.39 minutes following the discontinuation of chloral hydrate.

5.3.5 Data processing and analysis

Raw signals were initially examined visually using LabChart Pro (AD Instruments) to segment data for further analyses using a combination of custom MATLAB code (version R2017b, Mathworks; Natick, MA), and Origin Pro (Microcal Software Inc.; Northampton, MA). Spectral power was computed with data segments consisting of a series of 6-second Hanning-windowed samples, with a 2-second overlap using Welch's periodogram method. Spectrograms which visualize the change in power at a range of frequencies over a longer duration were computed using a sliding 30-second window moving across the data segment in 6-second increments.

The timing of brain state alternations was assessed by characterizing changes in specific frequencies of cortical and hippocampal power measures from spectrograms calculated over long durations. In either cortical or hippocampal signals, high power of slow (~1Hz) frequencies denoted the presence of deactivated states, while high power of the theta bandwidth (2.5-4Hz) in the hippocampal signal denoted the activated state. To accentuate brain state alternations, a slow/theta power ratio was calculated and plotted as a function of time. In order to pinpoint state-switching, a threshold value was determined by characterizing the saddle point of the resulting bimodal distribution of power values, with deactivated states above threshold, and activated states below.

In experiments where we evaluated the effects of bolus infusions of chloral hydrate and the temporary discontinuation of ongoing chloral hydrate infusions, the percentage of time spent in activated states was calculated per cycle as described above. Arithmetic means were calculated for 2 cycles prior to the first bolus dose, and for each bolus dose over a total of 3

boluses. This was done to ensure that a stable change was observed over more than just one cycle before administering another bolus. For a consistent comparison, the same approach was used in the assessment of metabolism, with the percentage of activated per cycle averaged over 2 cycles prior to the temporary discontinuation of chloral hydrate then compared with the average of 2 cycles during the infusion discontinuation.

For experiments assessing analgesia, arithmetic means for tail withdrawal latencies were computed for individual data within each animal for all 3 conditions being compared (baseline-unanesthetized, deactivated-anesthetized, activated-anesthetized). Between-subject means for each condition were subsequently computed along with error (SEM). Data sets for each condition were tested for normality using a Shapiro-Wilk test, followed by a repeated measures one-way ANOVA, followed by Tukey's post-hoc analyses for multiple comparisons to compare changes in withdrawal latency within-subjects across conditions. All analgesia statistical analyses were performed using a significance level of $\alpha=0.05$ in Prism 8 (GraphPad Prism Software Inc, San Diego, CA).

Breathing and heart rate frequency were computed by extracting the period from peak to peak using the peak analysis module in LabChart Pro (AD Instruments), set at a detection threshold of 2.5 SD. Mean frequency, and the coefficient of variance for these measures were determined for each brain state per cycle based on the state change threshold crosses in SO/Theta power ratio as described above. Continuous temperature data was extracted from LabChart, and values were adjacent averaged in 30s windows which shifted over the data in 10s increments. Sighs were identified by a characteristic high-amplitude distinctive waveform, with a delay until the next inspiration. Arithmetic means and error (SEM) for breathing rate, heart rate, temperature

and sighs was then plotted for the activated and deactivated states per animal, and across animals, and compared using paired t-tests.

Analysis of the influence of cholinergic pharmacological manipulations was performed by comparing equal durations of the SO/Theta ratio in baseline, against OXO and/or AtSO4 conditions. We began analyzing OXO and AtSO4 conditions at the immediate onset of any drug effect, which was defined by the first noticeable change in SO/Theta power alternations. This both allowed us to compute an onset for the drug effect and also to fairly interpret the types of changes evoked by both drugs. The percentage of time in the deactivated state of the whole section was computed, and compared using a paired t-test in the AtSO4 alone experiments, and a repeated measures one-way ANOVA with Tukey's multiple comparisons for the OXO+AtSO4 experiments.

Comparisons of LFP activity and alternation dynamics across chloral hydrate and urethane anesthesia within subjects were performed by comparing sections of equal duration with a minimum of 3 full cycles. The period of brain state alternations was calculated using the SO/Theta ratio as described above, and peak frequencies were derived from the observable maximal power values from spectral power plots for each activated and deactivated state for each animal and for each drug. The arithmetic means and error (SEM) for peak frequencies were then plotted for each animal, and across animals for both anesthetic conditions. Paired t-tests were used to compare changes across the anesthetics.

5.4 Results

Spontaneous, rhythmic, and sleep-like brain state alternations under chloral hydrate anesthesia

Over long recording periods (>40 minutes) under chloral hydrate anesthesia, we observed spontaneous, cyclical alternations of forebrain state in the spontaneous LFP traces at both cortical and hippocampal sites (Figure 5.1A-C). These alternations were stereotyped, alternating between: 1) a deactivated (nonREM-like) state, characterized by large amplitude slow-oscillatory (SO) activity in both cortical (~1Hz) and hippocampal (~0.5Hz) sites versus 2) an activated (REM-like) state, characterized by suppression of SO activity at both cortical and hippocampal sites and a prominent theta rhythm (2.5-4 Hz) in the hippocampus. On average, cortical SO exhibited a peak frequency of 0.80±0.01 Hz, hippocampal theta exhibited a peak frequency of 3.18±0.07 Hz, and hippocampal SO exhibited a peak frequency of 0.48±0.04 Hz (n=30; Figure 5.1E).

By plotting the power fluctuations of the peak cortical SO and hippocampal theta over time from the spectrographic analysis, we were able to systematically characterize the rhythmical periodicity of the state alternations, as defined by the time that elapses for one full cycle across both brain states (Figure 5.1C,F). The periodicity of state changes was highly consistent from cycle to cycle within-subjects, with a calculation of the linear fit of 3-6 cycles resulting in non-significant slopes for 29 out of 30 animals ($p>0.05$; Figure 5.1F,G). On average, one full cycle lasted 10.63±0.33 minutes. Across all animals, the activated state contributed to an average of 3.90±0.22 minutes (36.38±1.43%) per cycle whereas the deactivated state made up the remainder: 6.73±0.25 minutes (63.62±1.43%) per cycle (Figure 5.1G,H). Taken together, these results are indicative of a stable, and consistent alternation of forebrain state under chloral hydrate anesthesia.

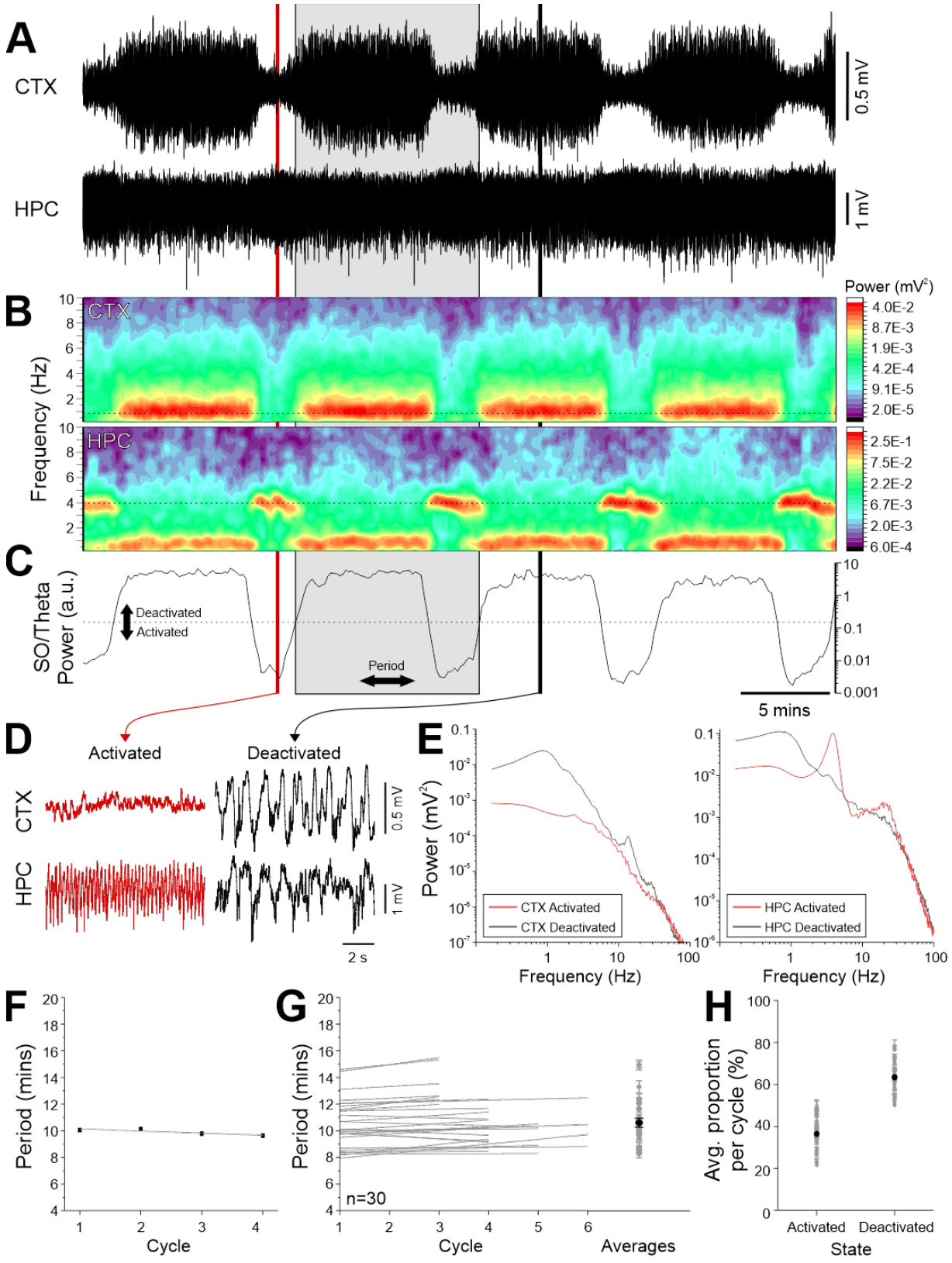

Figure 5.1 Consistent cyclical alternations of brain state under chloral hydrate anesthesia.

Figure 5.1 Consistent cyclical alternations of brain state under chloral hydrate anesthesia. **A)** Raw cortical (CTX) and hippocampal (HPC) LFP traces from a continuous long-term recording (>40min) under chloral hydrate anesthesia. **B)** Time-locked spectrograms of the same activity in CTX and HPC. Peak frequencies for CTX slow oscillation (SO; 0.83 Hz) and HPC theta (4 Hz) are denoted with a dashed black line **C)** Power fluctuations of the peak SO/theta power ratio are plotted over time. The state change threshold (the saddle of the bimodal power distribution) is denoted by a dashed line. Values above the threshold correspond to a deactivated state, and values below correspond to an activated state. A representative period consisting of one full cycle is denoted by the grey box **D)** Representative 10s CTX and HPC LFP traces during an activated state (in red) and a deactivated stated (in black). These selections were taken from the corresponding red and black boxes in A-C **E)** Power spectra of CTX (left) and HPC (right) activity during activated (red) and deactivated (black) states. The CTX SO peak frequency (0.83 Hz) can be observed in the deactivated CTX spectra, and the HPC theta peak frequency (4 Hz) can be observed in the HPC activated spectra **F)** Scatter plot of alternation period by cycle for C. The exemplar period in C corresponds to cycle 2. Linear fit (in grey) shows that the slope is not significantly different from zero ($p=0.10$) **G)** The left panel shows the aggregate linear fits of period across time for state cycling (for 3-6 cycles) across all 30 experiments. The slope was not significantly different from zero in 29 of the 30 experiments ($p>0.05$). The right panel shows the individual averages of period (in grey), and the grand average (in black) of 10.63±0.33 minutes ($n=30$) **H)** Individual averages (in grey) of the proportion of time spent in the activated and deactivated state per cycle, and the grand average (in black) of 36.38±1.43% in activated and 63.62±1.43% in deactivated.

Changes in chloral hydrate dosage affect the proportions of time spent in either brain state, but not periodicity of state changes

Though we reasoned that the continuous delivery of chloral hydrate should ensure a stable depth of anesthesia, we wanted to assess whether changes in anesthetic dosage were a potential cause of the observed alternations in brain state. To this end, we first assessed the effects of supplemental i.v. doses of chloral hydrate by administering three separate 15 mg boluses of chloral hydrate in addition to the continuous infusion of 150 $mg \cdot kg^{-1} \cdot hr^{-1}$. As previously reported in Ward-Flanagan et al. (2022), each supplemental bolus decreased the proportion of time spent in the activated state per cycle by an average of 16.65±4.14% to a floor of 0% (Figure 5.2A; n=3), correspondent with an inverse increase in the time spent in deactivated patterns per cycle. Each point in Figure 5.2 is averaged over 2 cycles to ensure the stability of the changes observed. However, while the proportion of time spent in either state changed with the dosage of chloral hydrate, the periodicity of the alternations themselves remained stable from cycle to cycle (Figure 5.2A; n=3). A similar, but reverse effect was observed when continuous infusion was paused, with the time spent in activated patterns per cycle increasing by 12.47±3.68%, but again no changes to the periodicity of state alternations was observed (Figure 5.2B; n=3). The stability of the periodicity despite the changes in the proportion of time spent in either state per cycle suggests that state alternations are not a result of fluctuating anesthetic dosage.

Cyclical forebrain activation during chloral hydrate anesthesia is not the result of a reduction in anesthetic depth

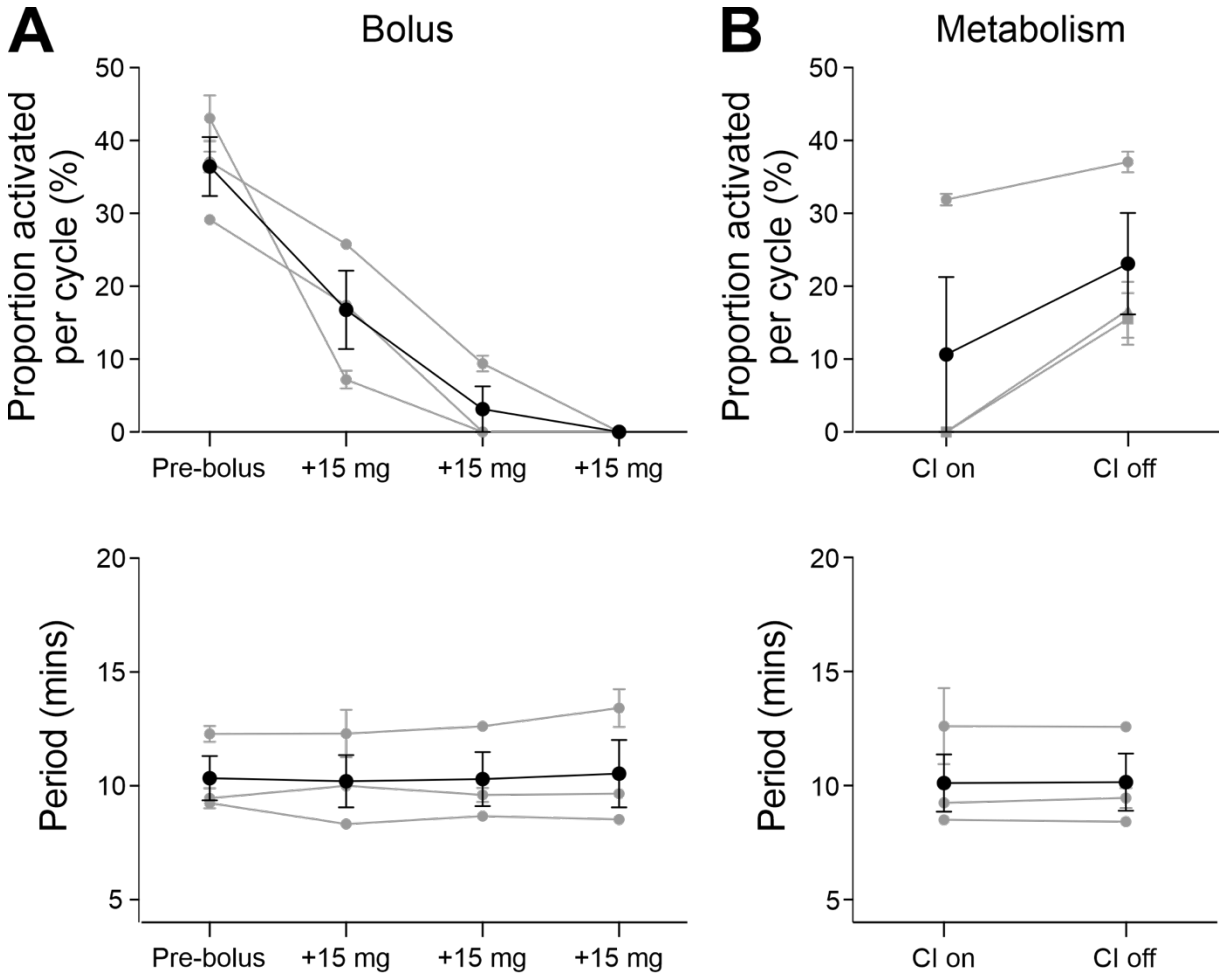

Figure 5.2 Forebrain activation, but not periodicity, changes as a function of chloral hydrate dosage.

A) The top panel shows the percentage proportion of time spent in an activated state per cycle as a function of additional 15 mg bolus doses of chloral hydrate in addition to the continuous infusion of 150 $mg \cdot kg^{-1} \cdot hr^{-1}$. The bottom panel shows the period of the corresponding cycles. Each point for both individual experiments (in grey), and the grand average (in black) is the average±SEM for 2 cycles to ensure a stable effect before proceeding with another bolus **B)** The top panel shows the percentage proportion of time spent in an activated state per cycle during continuous infusion for 2 cycles, and when continuous infusion is paused for 2 cycles. The bottom panel shows the

period for the corresponding cycles. Each point for both individual experiments (in grey), and the grand average (in black) is the average±SEM for 2 cycles.

Although we have previously confirmed that chloral hydrate anesthesia provides significant analgesia (Ward-Flanagan and Dickson, in revision), we wanted to confirm that state changes were not a functional variation in anesthetic depth. In order to quantitatively assess the plane of anesthesia across both the activated and deactivated brain states, we performed a within-subject behavioural assay of latency to tail withdrawal from a nociceptive (ramped infrared thermal) stimulus. This test was also administered pre-anesthesia in a freely moving awake condition in the same rats. A Shapiro-Wilk test showed that the data sets for all 3 conditions: unanesthetized-wake ($W(4)=0.8991$, $p=0.4048$), CH-activated ($W(4)=0.8090$, $p=0.0958$), and CH-deactivated ($W(4)=0.9642$, $p=0.8368$) were distributed normally. A repeated-measures one-way ANOVA showed a statistically significant difference between conditions (Figure 5.3; $F(2, 8)=56.77$, $p<0.0001$). Post-hoc analyses for multiple comparisons using Tukey's test revealed a significant increase in tail withdrawal latency when comparing unanesthetized-wake to CH-activated ($p<0.0001$, 95% CI=[-22.45 to -12.72]) and unanesthetized-wake to CH-deactivated ($p=0.002$, 95% CI=[-17.51 to -7.78]). Interestingly, tail latencies were longest during CH-activated, and were even significantly higher than those observed during CH-deactivated ($p=0.047$, 95% CI=[0.08 to 9.80]). Thus, anesthetic depth was deepest during CH-activated, and therefore brain state activation does not appear to be due to a shift toward a lowered plane of anesthesia.

Under chloral hydrate, respiration, but not cardiovascular or temperature measures are sleep-like

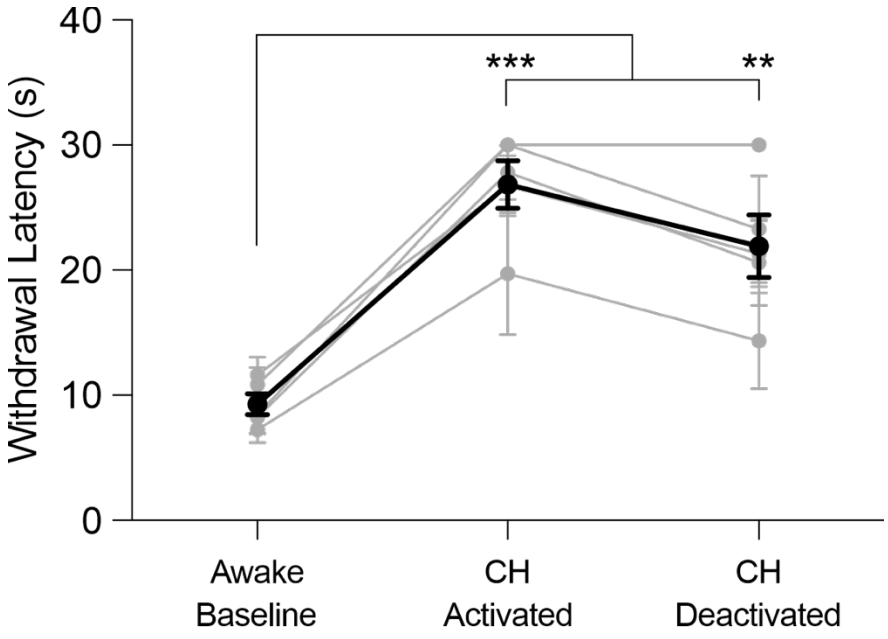

Figure 5.3 Tail withdrawal latencies are significantly increased during both forebrain activation and deactivation under chloral hydrate anesthesia.

A within-subjects comparison of tail withdrawal latencies to a nociceptive thermal stimulus during unanesthetized (baseline), and both activated and deactivated brain states under chloral hydrate anesthesia. Tail latencies were significantly longer under chloral hydrate anesthesia in both the activated state ($p<0.0001$, 95% CI=[-22.45 to -12.72]) and the deactivated state ($p=0.002$, 95% CI=[-17.51 to -7.78]) when compared to baseline unanesthetized tail withdrawal latencies. Within the unconscious anesthetized state, tail withdrawal latencies during the activated state were also significantly longer when compared to the deactivated state ($p=0.047$, 95% CI=[0.08 to 9.80]).

Peripheral physiological measures of are known to co-vary with brain state during both natural sleep and urethane anesthesia (Clement et al., 2008; Datta, 2010). Brain state fluctuations are characterized by increases in heart rate, breathing rate, respiratory variability and sighs during REM and the REM-like activated state during urethane anesthesia (Whitten et al., 2009; Pagliardini et al., 2012; Pagliardini et al., 2013a).

Breathing rate was significantly increased during the activated state (1.84±0.06 Hz) as compared to the deactivated state (1.79±0.06 Hz) as confirmed by a paired t-test (Figure 5.4A; $t(12)=2.32$, $p=0.039$). By measuring the coefficient of variance (CoV), we assessed the stability of the rhythmic signal, and found that respiratory variability was significantly higher during the activated state (0.13±0.03 CoV) than during the deactivated state (0.10±0.02 CoV) when compared using a paired t-test (Figure 5.4B; $t(12)=2.43$, $p=0.032$). Similar to both breathing rate and variability, the incidence of sighs during the activated state (2.82±0.33 sighs) compared to the deactivated state (0.95±0.08 sighs) was also significantly higher (Figure 5.4C; $t(12)=6.62$, $p<0.0001$).

In terms of heart rate, we did not observe any changes as a function of brain state. Heart rate remained stable across activated (6.66±0.15 Hz) and deactivated (6.70±0.18 Hz) brain states, with no significant changes (Figure 5.4D; $t(12)=0.69$, $p=0.50$). The variability of heart rate across brain states also remained unchanged between the activated (0.07±0.02 CoV) and deactivated (0.05±0.01 CoV) states (Figure 5.4E; $t(12)=1.21$, $p=0.25$). Core temperature under chloral hydrate changed as a function of brain state (Figure 5.4F). Curiously though, the directionality of this effect was the opposite of what we expected, as core temperature was significantly higher during

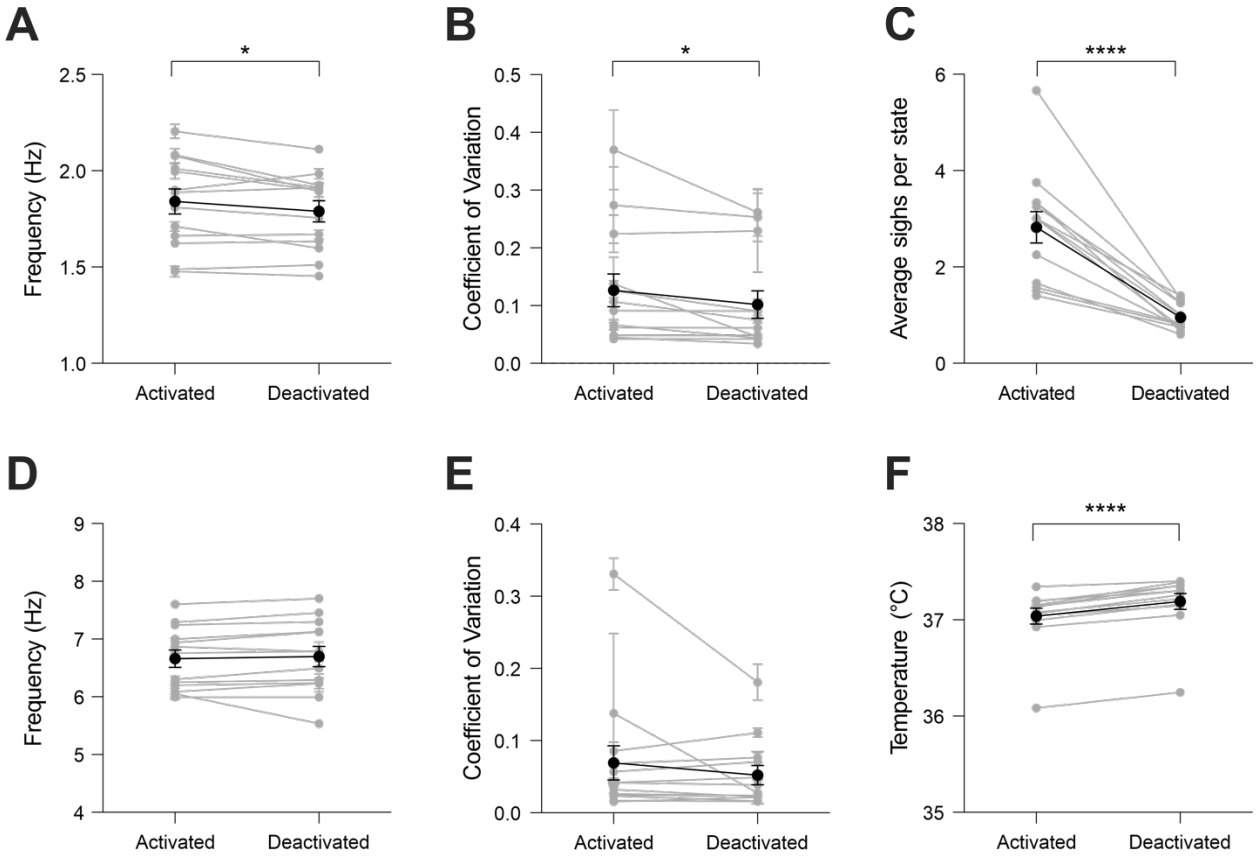

Figure 5.4 Measures of physiology as a function of brain state under chloral hydrate.

A) Average breathing rate per brain state for individual animals (in grey) and the grand average across animals (in black). Breathing rate is significantly higher in the activated state ($p=0.039$). **B)** Respiratory variability per brain state for individual animals (in grey) and the grand average across animals (in black). The activated state has significantly greater respiratory variability ($p=0.032$). **C)** Number of sighs per brain state for individual animals (in grey) and the grand average across animals (in black). The incidence of sighs is significantly higher during forebrain activation ($p<0.0001$). **D)** Heart rate per brain state for individual animals (in grey) and the grand average across animals (in black). There is no significant change in heart rate across states. **E)** Heart rate variability per brain state for individual animals (in grey) and the grand average across animals (in black). There is no significant change in variability across states. **F)** Average temperature as a

function of brain state, for both individual animals (in grey) and the grand average across animals (in black). Temperature is significantly increased in the deactivated state ($p<0.0001$).

the deactivated state (37.19±0.08°C), when compared to the activated state (37.04±0.08°C), as determined by a paired t-test ($t(12)=11.17$, $p<0.0001$).

State alternations under chloral hydrate are sensitive to cholinergic manipulations

As the brain state alternations in both natural sleep and urethane anesthesia are known to be dependent upon endogenous cholinergic neuromodulation (Clement et al., 2008; Arrigoni and Fuller, 2019), we reasoned that changes in brain state under chloral hydrate may also be sensitive to manipulations that pharmacologically target central cholinergic receptors. Consequently, we endeavoured to assess the effects of administering a cholinergic agonist (OXO; 4mg/kg) and antagonist ($AtSO_4$; 50 mg/kg) upon the spontaneous brain state cycling observed under chloral hydrate. To assess this, we measured the overall percentage of time spent in the deactivated state using equal duration comparison windows for baseline, OXO and $AtSO_4$ conditions in each animal (49.83±1.26 mins, n=5).

We found that both cholinergic manipulations significantly affected alternations of brain state (Figure 5.5A-C), which was confirmed by a repeated measures one-way ANOVA ($F(2, 8)=14.65$, $p=0.0021$). Similar to both sleep and urethane anesthesia (Clement et al., 2008; Arrigoni and Fuller, 2019), under chloral hydrate anesthesia, cholinergic agonism promoted an activated (REM-like) state while cholinergic antagonism promoted a deactivated (nonREM-like) state. The average latency to the onset of the agonistic effect of OXO was 9.17±4.43 mins (n=5). The activated state promoted by OXO was characterized by increased power and duration of theta activity in the hippocampus, and suppression of slow-oscillation power in both the cortex and the hippocampus (Figure 5.5A-C). Post-hoc analyses for multiple comparisons using Tukey's test revealed that overall average time spent in the deactivated state was significantly

less (p=0.019, 95% CI=[8.30 to 79.72]) during the OXO condition (14.05±6.84% deactivated, n=5) compared to baseline (58.06±5.34% deactivated, n=5; Figure 5.5D). Additionally, though we observed individual shifts in the frequency of theta during the OXO condition (Figure 5.5A), overall these changes were not systematic across animals (t(4)=0.00, p>0.99).

In contrast to OXO, $AtSO_4$ administration profoundly suppressed activated patterns while promoting the deactivated state. The average latency to the antagonistic effects of $AtSO_4$ administered after OXO was 13.78±5.30 minutes, n=5. As shown in Figure 5.5(A-C) following $AtSO_4$ administration slow-oscillatory power was promoted and theta power was greatly decreased. In fact, state threshold crosses were completely abolished within 20.51±8.70 minutes from injection of $AtSO_4$ (n=5). The total time in deactivated was significantly higher in the $AtSO_4$ condition (80.54±11.97% deactivated, n=5) as compared to the OXO condition (14.05±6.84% deactivated), as determined by Tukey's test for multiple comparisons (Figure 5.5D; p=0.0018, 95% CI=[-102.20 to -30.78]). However, the difference between baseline and $AtSO_4$ was not significant when OXO was administered first (p=0.23, 95% CI=[-58.19 to 13.23]).

To test the effects of $AtSO_4$ alone on brain state cycling under chloral hydrate, we used a similar approach of measuring the overall time spent in the deactivated state as a percentage of windows of equal duration in both baseline and $AtSO_4$ conditions. We found that, when administered alone, $AtSO_4$ significantly increased the percentage of time spent in the deactivated state (98.08±1.11% deactivated, n=4) as compared to baseline (66.58±3.82% deactivated, n=4) when compared using a paired t-test (Figure 5.5E; t(3)=10.41, p=0.0019). Additionally, when administered alone, $AtSO_4$ had a slightly shorter onset (9.91±5.47 minutes, n=4), and abolished

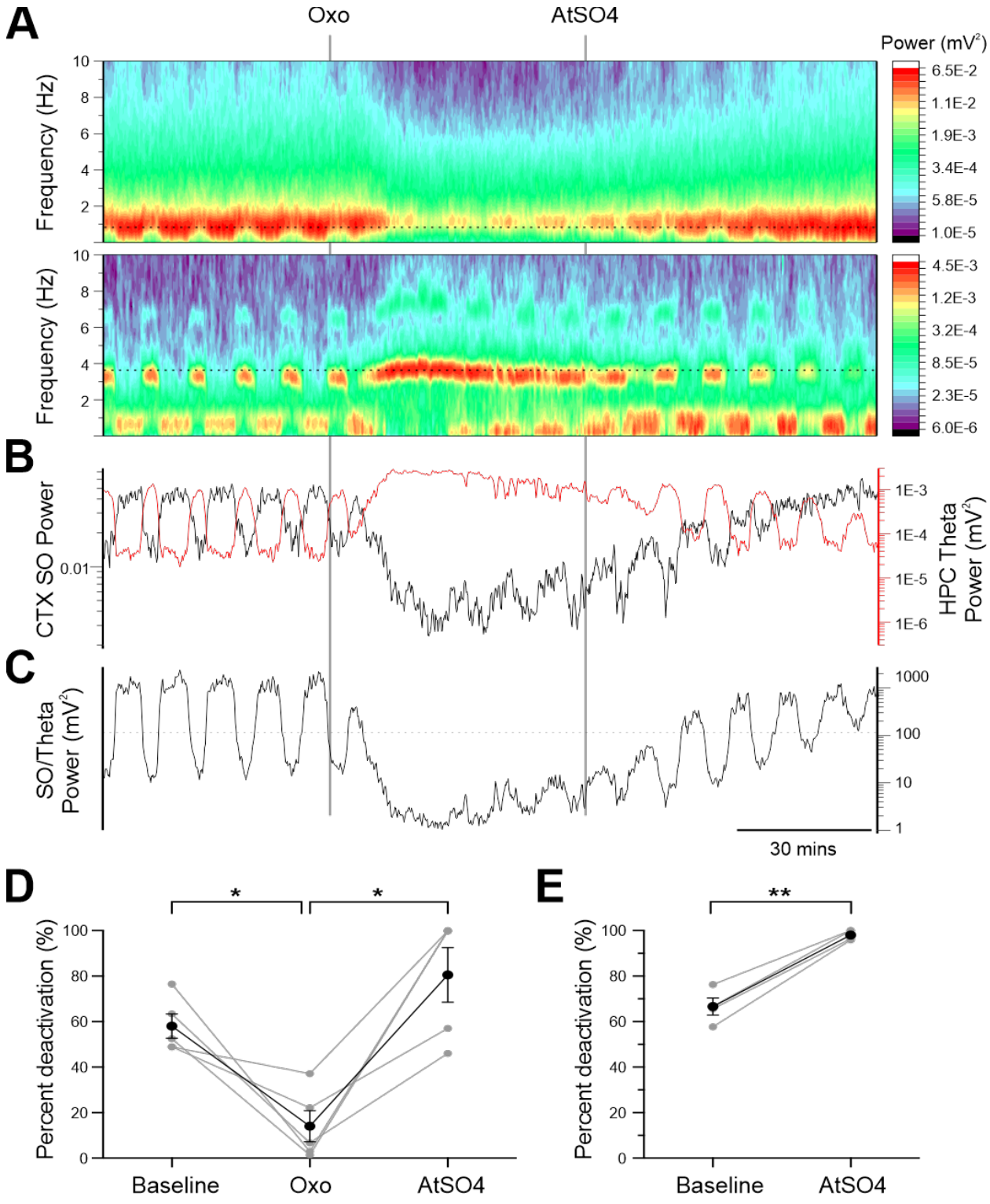

Figure 5.5 Brain state under chloral hydrate is sensitive to cholinergic manipulations.

Figure 5.5 Brain state under chloral hydrate is sensitive to cholinergic manipulations.

A) Cortical (CTX; top) and hippocampal (HPC; bottom) spectrograms of activity during baseline, and following administration of OXO and $AtSO_4$ (denoted by grey lines behind spectrograms). **B)** Average CTX slow-oscillatory power (SO; 3 pt average centered on 0.83 Hz), and average HPC theta power (5 pt average centered on 3.67 Hz), showing changes in power over time, and time-locked to the spectrograms above. **C)** Time-locked power fluctuations of the average peak SO/theta power ratio plotted over time. The state change threshold (the saddle of the bimodal power distribution) is denoted by a dashed line. Values above the threshold correspond to a deactivated state, and values below correspond to an activated state. **D)** Aggregate data of within-subjects comparison of the total time in the deactivated state (%) per condition (baseline, OXO and $AtSO_4$, n=5). Forebrain deactivation is significantly decreased during the OXO condition compared to baseline (p=0.019, 95% CI=[8.30 to 79.72]) and significantly increased in $AtSO_4$ as compared to OXO (p=0.0018, 95% CI=[-102.20 to -30.78]). **E)** A separate group of experiments comparing baseline to $AtSO_4$ alone (n=4). Forebrain deactivation is significantly increased during $AtSO_4$ compared to baseline (**p=0.0019).

the activated state in all animals (n=4) in approximately half the amount of time (10.67±5.25 minutes) in comparison with administrations following OXO treatments.

Chloral hydrate in comparison to urethane anesthesia

The only other anesthetic that is known to produce sleep-like brain state alternations at a surgical plane of anesthesia is urethane (Clement et al., 2008; Ward-Flanagan et al., 2022). In order to compare the brain states produced under these anesthetics as directly as possible, we performed a within-subjects comparison, by recording the spontaneous brain state alternations first under chloral hydrate and then followed by urethane after chloral hydrate washout. While we were unable to counter-balance the order of administration of these anesthetics due to the extremely slow pharmacokinetics of urethane (Sotomayor and Collins, 1990), we allowed for an extended washout/clearance time before assessing brain state under urethane (74.44±11.39 minutes, n=9).

During the deactivated state, we found that the peak frequency of the cortical slow-oscillation remains the same across chloral hydrate and urethane, as evidenced by the dashed line across the cortical spectrograms in Figure 5.6A. The similarities of slow-oscillations under chloral hydrate and urethane are apparent in the spectral plots for cortical and hippocampal power during the deactivated state (Figure 5.6B). Despite some variability across animals, a paired t-test showed that the overall peak frequency did not significantly change for cortical SO ($t(8)=1.99$, $p=0.08$), nor for hippocampal SO ($t(8)=0.22$, $p=0.83$) from chloral hydrate to urethane anesthesia (Figure 5.6C). Similarly, the period of alternation cycles remained the same despite the change in anesthesia, when compared using a paired t-test ($t(8)=0.63$, $p=0.54$; Figure 5.6C).

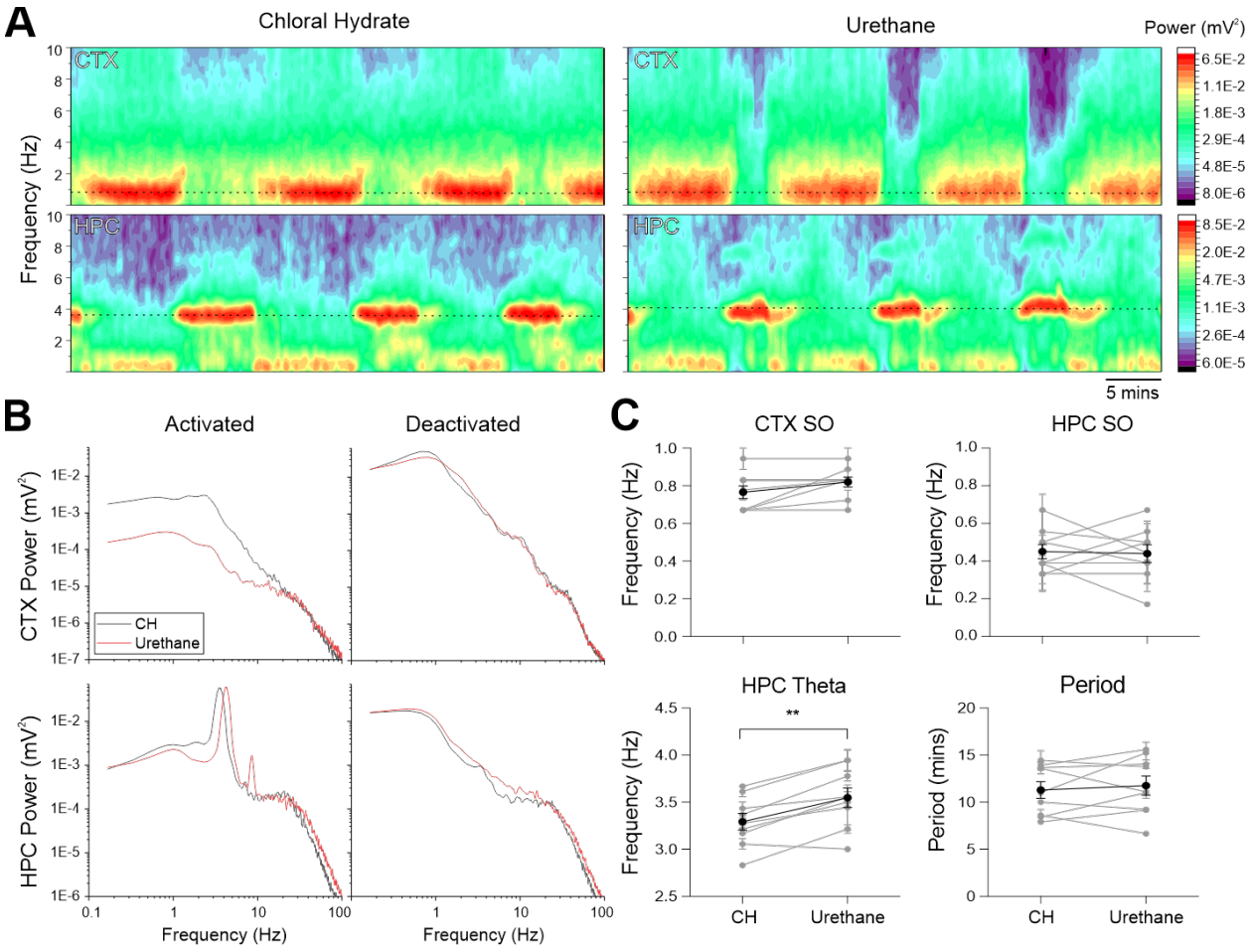

Figure 5.6 Comparison of chloral hydrate and urethane within-subjects.

A) Spectrograms of CTX (top) and HPC (bottom) activity in chloral hydrate (left) and urethane (right). The peak frequency for CTX slow oscillation (SO; denoted with a black dashed line in CTX) remain the same across the change in anesthetics, but the peak frequency for HPC theta (denoted with a black dashed line in HPC) increases in urethane. **B)** Spectra for CTX power (top) and HPC power (bottom) during activated (left) and deactivated (right) states. Cortical power is more suppressed in urethane (red) than chloral hydrate (black) during forebrain activation, but is similar in power and peak (0.83 Hz) in deactivated. HPC theta is shifted left in chloral hydrate HPC activation, indicating a slowing of theta. **C)** SO peak frequencies (top) are not significantly different across chloral hydrate and urethane in either the CTX (left) or HPC (right). HPC theta

(bottom left) is significantly higher in urethane (**p=0.001). Period (bottom right) is unchanged across chloral hydrate and urethane.

However, we did observe some differences across the two anesthetics; for instance, while both anesthetics showed suppressed cortical power during the activated state, this suppression appeared to be more profound under urethane (Figure 5.6A,B). The most notable change however, was a systematic increase in the peak frequency of hippocampal theta from an average of 3.29±0.05 Hz (n=9) under chloral hydrate to 3.55±0.06 Hz (n=9) under urethane (Figure 5.6A-C). This increase was observed in 8 of the 9 animals tested and a paired t-test revealed that the shift was significant ($t(8)=5.02$, $p=0.001$; Figure 5.6C).

5.5 Discussion

We have previously shown that out of six common research anesthetics, only urethane and chloral hydrate produce sleep-like alternations in forebrain state at a surgical plane of anesthesia (Ward-Flanagan et al., 2022). Our results in the present study: 1) replicate the brain state alternations previously observed under chloral hydrate, and 2) further demonstrate that these alternations bear a striking resemblance to both natural sleep and urethane anesthesia, in terms of individual EEG components, cycle timing, and sensitivity to cholinergic manipulations (Clement et al., 2008; Pagliardini et al., 2013a). However, despite fluctuations in the respiratory signal consistent with those observed during natural sleep and urethane, such parity was not present across all peripheral physiological measures. Taken together, these overlaps suggest that both chloral hydrate and urethane may serve as pharmacological models of sleep not only for individual brain states but also the cyclical dynamics thereof, but that at present, urethane appears to provide a more comprehensive pharmacological model for the associated peripheral physiological variations of natural sleep.

5.5.1 Comparable sleep-like brain state alternations under chloral hydrate and urethane

The spontaneous electrophysiological activity we observed under chloral hydrate was highly comparable to what has been previously characterized in both natural sleep and urethane anesthesia (Clement et al., 2008). Surgical anesthesia under continuous intravenous chloral hydrate produces stereotyped, cyclical alternations between two heterogenous brain states: 1) REM-like forebrain activation, characterized by rhythmic hippocampal theta (2.5-4 Hz) and a suppression of cortical slow-oscillations, and 2) NREM-like forebrain deactivation characterized by large-amplitude slow-oscillatory cortical (~1 Hz) and hippocampal (~0.5 Hz) activity. The average period of these alternations under chloral hydrate anesthesia (~11 minutes) was identical to the period previously reported for urethane (Clement et al., 2008), and also well within the distribution of the typical REM/NREM cycle duration (9.5-13.5 minutes) during natural sleep (Borbély, 1976).

Under typical anesthetics, forebrain activation typically coincides with a loss of surgical plane, and an imminent return of reflexive responding (Ward-Flanagan et al., 2022), however, the phenomenon of a spontaneous desynchronized cortical LFP under choral hydrate in the absence of any signs of a return to consciousness has been previously described, albeit briefly, by others before us (Puig et al., 2010; Ushimaru and Kawaguchi, 2015). In agreement with these prior observations, the activated state we observed under chloral hydrate does not appear to be a result of a reduction in anesthetic depth. Our results systematically demonstrate that the activated state under chloral hydrate paradoxically coincides with a significantly increased threshold for nociception, rather than a decrease in anesthetic depth. This parallels the incongruous nature of

REM sleep, which is also known as “paradoxical sleep” due to the contradictory coupling of wake-like EEG patterns of forebrain activation, with an increased threshold for behavioural arousal (Jouvet, 1965; Datta, 2010). Furthermore, the alternations between forebrain activation and deactivation were not a result of fluctuations in the depth of anesthesia, as chloral hydrate was delivered continuously, and as bolus doses of chloral hydrate supplemental to the continuous infusion did not abolish state alternations (Clement et al., 2008; Ward-Flanagan et al., 2022). Therefore, the forebrain activation under chloral hydrate appears to be representative of an unconscious REM-like, rather than a wake-like state of brain activity.

Forebrain deactivation under chloral hydrate also appears to map extremely well onto the synchronous, slow-oscillatory activity observed during the deactivated state in urethane anesthesia (Figure 5.6C) and during slow-wave sleep (Wolansky et al., 2006; Clement et al., 2008). This similarity to slow-wave sleep is perhaps unsurprising, as chloral hydrate has not only been used to model the Up/Down dynamics of cortical slow-waves (Ushimaru and Kawaguchi, 2015), but also exhibits similar patterns of cell-specific neuronal firing across the slow-oscillation to those observed in natural sleep (Niethard et al., 2018; Moody et al., 2021). Moreover, chloral hydrate has been shown to elicit c-Fos activation in the lateral habenula, a neuroanatomical node of the sleep-wake system known play a key role in both the sedative component of propofol anesthesia, and in consolidating the NREM state during natural sleep (Lu et al., 2008; Gelegen et al., 2018). However, it is of note that the activation of the lateral habenula observed under chloral hydrate is less than that of other anesthetics, which is consistent with the cyclical alternations between forebrain activation and deactivation that we observed in the present study, rather than a solitary state of NREM-like slow-waves under other anesthetics, such as ketamine-xylazine (Lu et al., 2008; Sharma et al., 2010; Ward-Flanagan et al., 2022).

It is well-established that cholinergic neuromodulation biases brain state in natural sleep, with muscarinic agonists promoting REM, while muscarinic antagonists block REM and promote NREM (Jouvet and Michel, 1960; Mouret et al., 1967; Arrigoni and Fuller, 2019). Brain state alternations under chloral hydrate (Figure 5.5) and urethane exhibit the same sensitivity to cholinergic manipulation as natural sleep (Clement et al., 2008). This shared means of brain state modulation in tandem with the remarkable similarities of electrophysiological components and their timing suggests that further mechanistic overlaps between chloral hydrate, urethane and natural sleep may exist.

5.5.2 Sleep-like respiration, but not heart rate or temperature under chloral hydrate

In congruence with the parallels of brain state described above, we also saw changes in the respiratory signal under chloral hydrate analogous to those observed during natural sleep. Specifically, during the REM-like activated state under chloral hydrate, we observed an increase in: 1) the rate of respiration, 2) respiratory variability and 3) the incidence of sighs. These indicators of respiratory fragility have long been regarded as hallmarks of REM sleep, where respiratory disturbances most commonly occur, and are also observed under urethane anesthesia during forebrain activation (Aserinsky, 1965; Krieger, 2000; Pagliardini et al., 2012). These commonalities suggest that chloral hydrate may serve as a model sleep-like changes in respiration, though further investigation into the specifics of respiratory-related muscle (e.g abdominal, genioglossus muscles), and brain stem nuclei (e.g pre-bötzinger complex) recruitment under chloral hydrate will be necessary to fully assess any potential caveats (Pagliardini et al., 2013a; Alsahafi et al., 2015; Andrews and Pagliardini, 2015).

However, heart rate under chloral hydrate did not co-vary with brain state, with no differences in heart rate or heart rate variability across activated or deactivated states. This is in direct contrast with the increase in heart rate due to increased signal irregularity during forebrain activation that is observed in natural sleep, and during urethane anesthesia (Clement et al., 2008; Datta, 2010). We believe that this discrepancy is most likely a product of pharmacological differences between chloral hydrate (Butler, 1948; Krasowski and Harrison, 2000) and urethane (Hara and Harris, 2002; Sceniak and MacIver, 2006), leading to differences in the expression of sleep-like physiological measures. Specifically, urethane is known to cause minimal depression of the autonomic nervous system (Maggi and Meli, 1986; Dringenberg and Vanderwolf, 1995), while chloral hydrate is known to cause cardiovascular and respiratory depression (Field et al., 1993). This is also apparent in the respiratory signal, for although we observed significant changes in breathing rate as a function of brain state, these changes are less marked under chloral hydrate (deactivated: 1.79 Hz to activated: 1.84 Hz) than typically observed during natural sleep (deactivated: ~1.6 to activated:~1.9) (Stephenson et al., 2001; Zeng et al., 2012), or under urethane anesthesia (deactivated: 1.67 Hz to activated: 2.0 Hz) (Silver et al., 2021). Since the state-related differences in heart rate under urethane are even less than those observed in respiration (Silver et al., 2021), it therefore follows that under chloral hydrate any changes in heart rate in association with brain state would either be too minor to resolve, or may be depressed entirely. Future experiments using more sensitive cardiovascular measures, such as an electrocardiogram may better elucidate the origin of this discrepancy between chloral hydrate and sleep.

Another physiological inconsistency with sleep that we observed under chloral hydrate was the relationship of core temperature to brain state. In sleep, NREM is correlated with a

decrease in both brain and core body temperature, whereas REM is associated with a disruption of body temperature regulation and an increase in brain temperature (Harding et al., 2020). Under chloral hydrate, we observed an opposite coupling effect, where temperature was consistently increased during the deactivated NREM-like state, and decreased during forebrain activation. One potential explanation for this unexpected effect is that manipulation of skin temperature by external stimuli modulates brain state, as demonstrated by both the relationship of ambient temperature to natural sleep (Szymusiak and Satinoff, 1981; Cerri et al., 2017; Harding et al., 2018), and the bidirectional relationship of temperature stimuli to brain state under urethane, with warming stimuli eliciting forebrain activation and vice versa (Whitten et al., 2009). Consequently, in our study, the activated brain state may be associated with cooler body temperature due, as the trough in core body temperature is when the heating pad would be on. Therefore, future experiments will be required to assess the relationship of temperature and brain state under chloral hydrate in greater detail.

5.5.3 Viability of chloral hydrate as a pharmacological model of sleep

When using a model there are always limitations that researchers should take into account when designing experiments and interpreting their results. As anesthetics, both chloral hydrate and urethane differ from natural sleep in three fundamental ways, namely that sleep is: a spontaneously occurring endogenous process, homeostatically regulated, and reversible by gentle external stimuli (i.e subjects can be roused) (Tung and Mendelson, 2004; Mashour and Pal, 2012). However, while these differences are important considerations, they are also often serious obstacles to the collection of data. In this respect, chloral hydrate and urethane afford both

greater experimental control, as well as a wider variety of possible experimental manipulations that would be impossible in naturally sleeping animals (Ward-Flanagan and Dickson, 2019). Furthermore, since natural sleep in rodents is often highly fragmented, with transitions potentially occurring under 30s (Benington et al., 1994), the highly stereotyped brain state alternations under chloral hydrate and urethane provide a more consistent baseline from which to measure change (Pagliardini et al., 2012).

However, as a model for sleep chloral hydrate does have a few specific limitations researchers will need to keep in mind. For instance, there is a significant slowing of hippocampal theta during the activated state in chloral hydrate (~3.3 Hz) as compared to urethane (~4 Hz) and especially compared to natural sleep (~6-9 Hz) (Bland, 1986; Buzsaki, 2002; Clement et al., 2008). Additionally, as discussed in the previous section, there is a greater depression of both cardiovascular and respiratory measures under chloral hydrate than under urethane anesthesia (Maggi and Meli, 1986; Field et al., 1993; Dringenberg and Vanderwolf, 1995), and the relationship of brain state and thermoregulation will require further investigation in future studies.

Yet, chloral hydrate has the distinct advantage as an experimental model of not being restricted to acute experimental preparations (Flecknell, 2016c). As a result, chloral hydrate offers entirely unique opportunities to perform experiments that would be impossible in either sleep or urethane, or both. For instance, we are excited to see whether, like propofol, chloral hydrate can attenuate total sleep debt (Tung et al., 2004). Consequently, our conclusion is that chloral hydrate and urethane both offer reliable models of sleep-like brain state alternations, albeit with opposing strengths. Urethane remains the most complete model of sleep, other than

sleep itself, but chloral hydrate provides a useful alternative when greater experimental flexibility is required.

6

Discussion

Discussion

As the fundamental “hard problem”, how (un)consciousness occurs poses one of the most fascinating riddles in existence, and thus is a question that many of the greatest philosophers and scientists have devoted their lives to answering. Consequently, while the driving ambition behind this thesis was to add my own contribution toward answering the tripartite question of how unconsciousness is initiated, maintained, and reversed - I understood that my part would be incremental in this monumental task. Zooming in, I focused upon investigating pharmacological models of sleep, with the intention to build upon previous work from our lab which characterized the robust parallels between urethane anesthesia and natural sleep in terms of spontaneous neural activity, alternation timing, peripheral physiology, and sensitivity to neuromodulation (Clement et al., 2008; Whitten et al., 2009; Pagliardini et al., 2013a).

What may not be immediately apparent is that urethane is somewhat of an oddity, even within sleep and anesthesia research. As highlighted in the introduction, over the last thirty years the prevailing theory of how anesthetics with disparate pharmacological mechanisms produce unconsciousness is through co-opting endogenous sleep circuits (Lydic and Biebuyck, 1994; Franks, 2008; Jiang-Xie et al., 2019). However, the validity of this shared-circuit hypothesis is currently a matter of debate (Eikermann et al., 2020), and one of the main criticisms, even by those who support the idea of shared mechanisms, is that there are no anesthetics that mimic REM sleep (Franks and Wisden, 2021). It is likely that despite its compelling overlaps with natural sleep, urethane is usually overlooked, or in some cases even unknown to clinical researchers due to being restricted to acute animal research applications (Maggi and Meli, 1986; Flecknell, 2016c). In light of this limitation, the omission of urethane is understandable to an

extent, as the range of potential experimental applications, as well as the ease of translating results to a clinical setting is hindered in this capacity.

However, it is unfortunate that urethane is not more widely known, because although it is not a perfect replication of natural sleep, it provides the closest pharmacological model to natural sleep possible – essentially acting as a "missing link" between typical, widely used anesthetics such as propofol, and natural sleep (Ward-Flanagan et al., 2023). As such, understanding what makes urethane so similar to natural sleep, and what makes it different from other anesthetics may provide crucial insights into the endogenous mechanisms of both sleep and anesthetic unconsciousness. With both this and the limitations of urethane in mind, my specific goals with this thesis were to: 1) assess whether urethane anesthesia was the only anesthetic that could produce sleep-like neurophysiology at a surgical plane, and 2) evaluate if the neurophysiological overlaps of urethane and natural sleep were due to similar activation of sleep-wake nuclei in the brain. I have shown that, in addition to urethane, chloral hydrate anesthesia produces sleep-like neurophysiological alternations of brain state. Furthermore, I have demonstrated that urethane produces patterns of specific neuronal activity comparable to unpressured natural sleep in sleep-wake brain circuitry. Consequently, both urethane and chloral hydrate can provide unique pharmacological models of natural sleep, albeit with their own specific caveats, and will serve as invaluable tools in unravelling the mechanisms of unconsciousness.

6.1 Urethane and chloral hydrate produce sleep-like brain state alternations at a surgical plane of anesthesia

In Chapter 2, I performed a direct comparison of the spontaneous electrophysiological recordings under six commonly used research anesthetics using identical recording conditions, while maintaining animals at a surgical plane of anesthesia (Ward-Flanagan et al., 2022). Much like humans, even rats of the same species and similar weight can have variable needs in terms of anesthesia (Flecknell, 2016a). Thus, it was important to compare animals at a surgical plane of anesthesia not only because it is useful for a range of experimental applications that would be impossible in natural sleep, but also because it allowed us to compare each anesthetic at a relatively equivalent state, and importantly, one which could be confirmed behaviourally.

At that depth of surgical anesthesia, I demonstrated that pentobarbital, isoflurane and propofol all produced a coma-like brain state of burst-suppression (Brown et al., 2010), whereas ketamine-xylazine produced synchronized, slow-oscillatory activity more akin to slow-wave sleep (Chauvette et al., 2011). Surprisingly, not only urethane, but also chloral hydrate anesthesia produced the sleep-like spontaneous alternations between a state of forebrain activation and deactivation. Critically, the forebrain activation under chloral hydrate and urethane was not associated with a lessening of anesthetic depth, whereas any instances of forebrain activation in pentobarbital, isoflurane, propofol or ketamine-xylazine were all accompanied by a loss of the surgical plane of anesthesia.

This was an unexpected outcome, especially since chloral hydrate is typically classified as a GABAergic anesthetic, like pentobarbital and propofol (Akaike et al., 1990; Hara et al., 1993; Lovinger et al., 1993); whereas the primary pharmacological mechanism of urethane is to potentiate resting potassium conductance, thereby decreasing membrane input resistance and hyperpolarizing central neurons (Sceniak and MacIver, 2006). More recently, chloral hydrate has also been demonstrated to act at several K_{2P} channels, including TASK-3 which has been

implicated in both the consolidation of natural sleep and the generation of type II (i.e atropine sensitive) theta (Pang et al., 2009), which may account for some of its sleep-like properties (Luethy et al., 2017). Furthermore, since chloral hydrate is first metabolized into 2,2,2-tricholoethanol before it can exert its anesthetic effects (Butler, 1948), and urethane is also metabolized into ethanol and carbamic acid (Maggi and Meli, 1986), it is possible that the shared sleep-like brain states in chloral hydrate and urethane arise from a common metabolic by-product, namely ethanol. However, this has yet to be investigated, as to my knowledge, this was the first time that sleep-like spontaneous, cyclical alternations of brain state were demonstrated under chloral hydrate anesthesia. Importantly, this discovery also served to emphasize how both choice of anesthesia, and brain state monitoring are crucial considerations for researchers when designing neurophysiological experiments (Piccitto, 2018).

6.2 Urethane promotes c-Fos activity in sleep-wake nuclei analogous to unpressured sleep

As reviewed in the introduction, various anesthetic agents have been demonstrated to act on endogenous sleep-wake nuclei in agent-specific permutations (Lu et al., 2008; Ward-Flanagan and Dickson, 2019), and these overlaps have even led to discoveries of new endogenous sleep-promoting roles for nuclei such as the lateral habenula (Gelegen et al., 2018). Thus, it was clear that elucidating where in the brain sleep and urethane intersect would be an important foundation to direct future investigations. Based on the already extensively documented overlaps of neurophysiology between urethane anesthesia and natural sleep (Clement et al., 2008; Pagliardini et al., 2013a), I hypothesized that urethane would engage endogenous sleep-wake nuclei in a similar manner to natural sleep.

In order to test this, we compared the expression of a neural marker of activation (c-Fos) across ten known sleep-wake nuclei following five separate conditions: sleep-deprived rats engaging in recovery sleep (i.e pressured sleep), non-sleep deprived rats normally sleeping (i.e unpressured sleep), sleep-deprived rats anesthetized with urethane, non-sleep deprived rats anesthetized with urethane, and animals held in wake for the sleeping/anesthetized window.

The patterns of c-Fos expression across the selected sleep-wake nuclei was most alike between the urethane anesthesia and unpressured sleep conditions, supporting the idea that the unconscious state produced by urethane is due, at least in part, to acting on endogenous sleep-wake nuclei. This similarity is supported by the observations of a previous study assessing c-Fos expression in autonomic-related regions under urethane anesthesia (Krukoff et al., 1992). This study showed that urethane promotes activity in both the supraoptic nuclei, which is a hypothalamic area that has been revealed as an important centre for mediating NREM-sleep and anesthetic unconsciousness (Jiang-Xie et al., 2019), and the ventrolateral medulla, which has recently been demonstrated to have a subpopulation of glutamatergic neurons that are necessary and sufficient for wake to NREM transitions (Teng et al., 2022). Taken together, these results suggest that urethane produces a sleep-like state in terms of neuroanatomical targets as well as in the resulting neurophysiological state. Consequently, future research assessing brain-wide nuclei that are activated during urethane anesthesia may unveil hitherto unknown sleep-wake areas, and further assessment of the overlapping nuclei described in Chapter 3 using techniques with finer spatio-temporal resolution, in addition to chemically identified neurons may provide new insights into how a sleep-like state of unconsciousness is manifested in the brain.

However, Chapter 3 also demonstrated a key difference between sleep and urethane in that prior exposure to sleep-deprivation did not greatly change the patterns of neural activation

under urethane, whereas increased sleep need affected the patterns of c-Fos expression in naturally sleeping animals. This suggests that urethane differs from sleep, producing the same stereotyped alternations in brain state irrespective of sleep pressure, rather than a rebound resulting in the increased propensity and power of slow-wave sleep typically observed at the beginning of recovery sleep (Dijk, 2009). Yet, this difference is arguably a strength for urethane as a model of unpressured sleep, as researchers can be sure that the sleep pressure of individual animals will not affect experimental outcomes. It is also important to note, that while I did not perform EEG measurements of online brain states in this study, there were significant differences in the activity across sleep-wake nuclei between the wake condition and all of the unconscious conditions, which supports that the differences observed across sleep and urethane conditions were not due to arousal.

6.3 Chloral hydrate provides significant analgesia

When initially testing chloral hydrate in Chapter 2, I came across a controversy regarding its analgesic efficacy, wherein veterinary reference material asserted that chloral hydrate alone does not provide adequate analgesia for surgical interventions (Silverman and Muir, 1993; Baxter et al., 2009), but the results of primary neurobiological studies directly contradicted these claims (Field et al., 1993; Rodrigues et al., 2006). Thus, in order to evaluate the utility of chloral hydrate as pharmacological model for sleep, it was first necessary to assess its analgesic efficacy. To that end, in Chapter 4, I assessed tail withdrawal latency from a noxious thermal stimuli within subjects, comparing unanesthetized baseline withdrawal latencies to those under chloral hydrate anesthesia.

In congruence with previous reports of appropriate analgesia under chloral hydrate (Lu et al., 2008), I found that tail withdrawal latency was significantly increased, while heart rate and respiration remained unchanged during exposure to a nociceptive stimuli under chloral hydrate anesthesia. Furthermore, in Chapter 5, I showed that tail withdrawal latency was significantly increased during states of REM-like forebrain activation, as compared to the NREM-like deactivated state. Our results are in agreement with previous studies showing analgesic effects of chloral hydrate in ascending pain pathways at the level of the dorsal root ganglion (Gruss et al., 2002; Fischer et al., 2003), in descending pain pathways such as the ventrolateral periaqueductal gray and A5-7 noradrenergic cell groups (Lu et al., 2008), as well as those showing chloral hydrate has comparable analgesic effects to other anesthetics (Field et al., 1993; Rodrigues et al., 2006). When taken together the collective results of both our study and previous primary studies indicate that chloral hydrate provides sufficient analgesia for us as a sole maintenance anesthetic.

6.4 Chloral hydrate provides a flexible pharmacological model of sleep-like brain state alternations

Building upon the initial discovery of sleep-like brain state alternations under chloral hydrate (Chapter 2; Ward-Flanagan et al, 2022), and the confirmation of sufficient analgesia (Chapter 4), I characterized a number of neurophysiological and neurobiological measures under chloral hydrate anesthesia in order to assess its utility as a pharmacological model of sleep (Chapter 5). Chloral hydrate produced electrophysiological measures comparable to both natural sleep and urethane in terms of individual brain states, alternation timing and sensitivity to bidirectional central cholinergic manipulations (Clement et al., 2008; Arrigoni and Fuller, 2019).

Critically, neither the alternations of brain, nor the REM-like state of forebrain activation were due to changes in anesthetic dose or plane, as supplementary doses of chloral hydrate changed the proportion of time in either state, but did not abolish the alternations (Ward-Flanagan et al., 2022), and the activated state paradoxically increased the threshold for nociception. This also aligns with the increased threshold for behavioural arousal observed in physiological REM sleep (Datta, 2010). Furthermore, in terms of peripheral physiological measures, chloral hydrate produced an increase in breathing rate, respiratory variability and the incidence of sighs during REM-like forebrain activation, identical to sleep and urethane anesthesia (Krieger, 2000; Pagliardini et al., 2012; Pagliardini et al., 2013b).

Despite these similarities, there are a few inconsistencies between sleep and chloral hydrate, namely: a much slower hippocampal theta rhythm during forebrain activation, and a lack of heart rate fluctuations as a function of brain state (Bland, 1986; Silver et al., 2021). Additionally, although temperature co-varied with brain state under chloral hydrate, it was in an inverse direction to what is typically observed during natural sleep (Harding et al., 2020), or urethane (Whitten et al., 2009), with temperature increases occurring during the NREM-like deactivated state instead of the expected REM-like activated state. These inconsistencies warrant further investigation, and future studies using more sensitive measures such as brain temperature, or an electrocardiogram, should help elucidate the origin of these discrepancies. However, when these caveats are accounted for in an experimental design, chloral hydrate provides a new, experimentally versatile model for assessing both sleep-like changes in brain state and associated respiration. As an alternate to urethane which is limited to acute experiments, chloral hydrate will be especially useful in light of the recent shift in the field towards focusing on shared mechanisms of arousal and anesthetic emergence (Moody et al., 2021).

6.5 Future directions

While I have touched upon a few potential directions above, I feel that sleep and anesthesia research is at the cusp of a great many new discoveries, and that there is an overwhelming abundance of potential research questions that can build upon this work. In particular, in light of the sleep-like brain activity under chloral hydrate it would be interesting to see if anesthesia under chloral hydrate can attenuate total sleep debt. To my knowledge, this has only ever been shown in propofol anesthesia (Tung et al., 2004), whereas other anesthetics have only been shown to attenuate NREM sleep debt (Pal et al., 2011), and it would demonstrate whether the REM-like state of forebrain activation observed under chloral hydrate can serve a similar homeostatic function to physiological REM sleep. If so, this could inform a novel direction for research into the development of medications for sleep disorders, as well as potential interventions in clinical settings where sleep loss is detrimental to health outcomes (Skrobik et al., 2018).

While the relationship of thermoregulation and brain state under chloral hydrate will require further investigation, whatever the outcome is will be of interest in modeling sleep. For if, as it currently appears, the relationship of temperature and brain state is inverse to that observed during natural sleep, then chloral hydrate would provide a unique model to explore the effects, and potential mechanisms of uncoupling temperature and brain state, as these homeostatic processes are usually tightly linked (Harding et al., 2020). However, if brain state under chloral hydrate is biased towards activation by the external application of heat, as it is under urethane (Whitten et al., 2009), then chloral hydrate could serve as an extremely tractable

model for biasing sleep-like brain states in behavioural studies. For instance, in a study assessing the individual contributions of forebrain activation or deactivation to memory consolidation chloral hydrate could be used in place of traditional methods such as REM-sleep deprivation, which are associated with elevated stress, thus providing a more ethical method of biasing brain state (Nollet et al., 2020).

Furthermore, chloral hydrate could provide an avenue to assess discoveries made under urethane regarding the functional circuitry of these sleep-like alternations on behavioural outcomes. For instance, the nucleus reuniens, a midline thalamic nucleus, was recently demonstrated to have an important role in coordinating hippocampal and neocortical slow-oscillations during the NREM-like deactivated state under urethane (Hauer et al., 2019), and a subsequent lesion study confirmed that the RE plays a role in memory consolidation (Quet et al., 2020). In this type of context, more precise stimulation, or entrainment protocols which are possible in urethane anesthesia are often limited in behavioural studies by technical or ethical considerations. Sometimes specialized equipment can contravene these issues, but frequently such equipment is prohibitively expensive. Consequently, chloral hydrate may provide an elegant solution allowing for greater experimental control, and the assessment of behavioural outcomes, while also being both widely accessible and compatible with pre-existing neurophysiological experimental protocols.

While there are numerous applications for chloral hydrate in behavioural paradigms, there are also many questions to explore regarding the intersection of chloral hydrate and urethane anesthesia in pharmacologically producing a sleep-like brain state. Such as, does chloral hydrate produce a similar profile of c-Fos immunoreactivity in sleep-wake nuclei to natural sleep and urethane? It seems to me that any neuroanatomical sites that are active during urethane,

chloral hydrate and natural sleep are likely intrinsic for producing unconsciousness. Moreover, do these anesthetics have a shared pharmacological mechanism driving the sleep-like brain states they produce? At present, even though both chloral hydrate and urethane act at K_{2P} channels, they appear to have different specific targets, as chloral hydrate modulates TREK-1, and TASK-3 (Harinath and Sikdar, 2004; Luethy et al., 2017), and urethane does not (Sceniak and MacIver, 2006). However, both chloral hydrate (via 2,2,2-trichloroethanol) and urethane (via carbamic acid and ethanol) share ethanol as a metabolic by-product, which may prove to have a role in their similar sleep-like neurophysiology (Butler, 1948; Maggi and Meli, 1986). Probing the shared targets of chloral hydrate and urethane may also reveal important circuits beyond sleep, as anesthesia has recently become a novel tool for finding endogenous targets for pain-suppression (Hua et al., 2020). Thus, finding a mechanistic overlap across chloral hydrate and urethane may yield promising new therapeutic targets, which may aid in the development of safer anesthetic protocols, and improved interventions for sleep disorders.

6.6 Conclusion

In the work described within this thesis, I have demonstrated the unique sleep-like neurophysiological characteristics of chloral hydrate and urethane anesthesia, and their respective strengths and drawbacks as pharmacological models for the complexities of natural sleep. It is my hope that this work serves as a foundation for further investigations into the intricacies of the unconscious brain, and the integral role that it plays in the processes required for the optimal functioning of our conscious selves.

While the question of consciousness is almost as old as science itself, it is only within the last hundred years that sleep has been recognized as an active process (Aserinsky and Kleitman, 1953), and we are undoubtedly only beginning to understand how the brain may give rise to our conscious thoughts. At the heart of science is a unquenchable curiosity about the world we live in, and the brain provides a seemingly infinite source of mystery – the more we seek to understand it, and the more we quantify its behaviour and mechanisms, the more questions we inevitably raise. I feel incredibly lucky to participate in this maddening, confounding but ultimately joyful process, for like many other scientists before me, nothing could be more exciting to me than trying to answer a seemingly impossible question. I look forward to seeing what discoveries the next generation of scientists uncover.

References

Abel JH, Badgeley MA, Meschede-Krasa B, Schamberg G, Garwood IC, Lecamwasam K, Chakravarty S, Zhou DW, Keating M, Purdon PL (2021) Machine learning of EEG spectra classifies unconsciousness during GABAergic anesthesia. Plos one 16:e0246165.

Adamantidis AR, Zhang F, Aravanis AM, Deisseroth K, de Lecea L (2007) Neural substrates of awakening probed with optogenetic control of hypocretin neurons. Nature 450:420-424.

Adapa R (2017) Consciousness and Anesthesia. In: Total Intravenous Anesthesia and Target Controlled Infusions: A Comprehensive Global Anthology (Absalom AR, Mason KP, eds), pp 63-78. Cham: Springer International Publishing.

Aggarwal A, Brennan C, Shortal B, Contreras D, Kelz MB, Proekt A (2019) Coherence of Visual-Evoked Gamma Oscillations Is Disrupted by Propofol but Preserved Under Equipotent Doses of Isoflurane. Frontiers in Systems Neuroscience 13.

Akaike N, Tokutomi N, Ikemoto Y (1990) Augmentation of GABA-induced current in frog sensory neurons by pentobarbital. Am J Physiol 258:C452-460.

Akeju O, Brown EN (2017) Neural oscillations demonstrate that general anesthesia and sedative states are neurophysiologically distinct from sleep. Curr Opin Neurobiol 44:178-185.

Akrawi WP, Drummond JC, Kalkman CJ, Patel PM (1996) A comparison of the electrophysiologic characteristics of EEG burst-suppression as produced by isoflurane, thiopental, etomidate, and propofol. J Neurosurg Anesthesiol 8:40-46.

Alam MN, McGinty D, Szymusiak R (1995) Neuronal discharge of preoptic/anterior hypothalamic thermosensitive neurons: relation to NREM sleep. Am J Physiol 269:R1240-1249.

Alam MN, Gong H, Alam T, Jaganath R, McGinty D, Szymusiak R (2002) Sleep-waking discharge patterns of neurons recorded in the rat perifornical lateral hypothalamic area. J Physiol 538:619-631.

Alkire MT, McReynolds JR, Hahn EL, Trivedi AN (2007) Thalamic microinjection of nicotine reverses sevoflurane-induced loss of righting reflex in the rat. Anesthesiology 107:264-272.

Alsahafi Z, Dickson CT, Pagliardini S (2015) Optogenetic excitation of preBötzinger complex neurons potently drives inspiratory activity in vivo. The Journal of Physiology 593:3673-3692.

Altevogt BM, Colten HR (2006) Sleep disorders and sleep deprivation: an unmet public health problem: National Academies Press.

Anaclet C, Parmentier R, Ouk K, Guidon G, Buda C, Sastre JP, Akaoka H, Sergeeva OA, Yanagisawa M, Ohtsu H, Franco P, Haas HL, Lin JS (2009) Orexin/hypocretin and histamine: distinct roles in the control of wakefulness demonstrated using knock-out mouse models. J Neurosci 29:14423-14438.

Andrews CG, Pagliardini S (2015) Expiratory activation of abdominal muscle is associated with improved respiratory stability and an increase in minute ventilation in REM epochs of adult rats. Journal of applied physiology (Bethesda, Md : 1985) 119:968-974.

Arrigoni E, Fuller PM (2019) The Circuit, Cellular, and Synaptic Bases of Sleep-Wake Regulation. In: Handbook of Behavioral Neuroscience (Dringenberg HC, ed), pp 65-88: Elsevier.

Arrigoni E, Mochizuki T, Scammell TE (2010) Activation of the basal forebrain by the orexin/hypocretin neurones. Acta Physiol (Oxf) 198:223-235.

Aserinsky E (1965) Periodic respiratory pattern occurring in conjunction with eye movements during sleep. Science 150:763-766.

Aserinsky E, Kleitman N (1953) Regularly occurring periods of eye motility, and concomitant phenomena, during sleep. Science 118:273-274.

Aston-Jones G, Bloom FE (1981) Activity of norepinephrine-containing locus coeruleus neurons in behaving rats anticipates fluctuations in the sleep-waking cycle. J Neurosci 1:876-886.

Austin PJ, Wu A, Moalem-Taylor G (2012) Chronic constriction of the sciatic nerve and pain hypersensitivity testing in rats. J Vis Exp:3393.

Baker R, Gent TC, Yang Q, Parker S, Vyssotski AL, Wisden W, Brickley SG, Franks NP (2014) Altered activity in the central medial thalamus precedes changes in the neocortex during transitions into both sleep and propofol anesthesia. J Neurosci 34:13326-13335.

Bao W-W, Xu W, Pan G-J, Wang T-X, Han Y, Qu W-M, Li W-X, Huang Z-L (2021) Nucleus accumbens neurons expressing dopamine D1 receptors modulate states of consciousness in sevoflurane anesthesia. Current Biology 31:1893-1902. e1895.

Barr G, Jakobsson JG, Owall A, Anderson RE (1999) Nitrous oxide does not alter bispectral index: study with nitrous oxide as sole agent and as an adjunct to i.v. anaesthesia. BJA: British Journal of Anaesthesia 82:827-830.

Bastos AM, Donoghue JA, Brincat SL, Mahnke M, Yanar J, Correa J, Waite AS, Lundqvist M, Roy J, Brown EN, Miller EK (2021) Neural effects of propofol-induced unconsciousness and its reversal using thalamic stimulation. eLife 10:e60824.

Baxter Mark G, Murphy Kathy L, Taylor Polly M, Wolfensohn Sarah E (2009) Chloral Hydrate Is Not Acceptable for Anesthesia or Euthanasia of Small Animals. Anesthesiology 111:209-209.

Benington JH, Kodali SK, Heller HC (1994) Scoring Transitions to REM Sleep in Rats Based on the EEG Phenomena of Pre-REM Sleep: An Improved Analysis of Sleep Structure. Sleep 17:28-36.

Bergmann BM, Kushida CA, Everson CA, Gilliland MA, Obermeyer W, Rechtschaffen A (1989) Sleep deprivation in the rat: II. Methodology. Sleep 12:5-12.

Berridge CW, Waterhouse BD (2003) The locus coeruleus-noradrenergic system: modulation of behavioral state and state-dependent cognitive processes. Brain Res Brain Res Rev 42:33-84.

Blake H, Gerard RW (1937) Brain potentials during sleep. American Journal of Physiology-Legacy Content 119:692-703.

Blanco-Centurion C, Gerashchenko D, Shiromani PJ (2007) Effects of saporin-induced lesions of three arousal populations on daily levels of sleep and wake. J Neurosci 27:14041-14048.

Bland BH (1986) The physiology and pharmacology of hippocampal formation theta rhythms. Prog Neurobiol 26:1-54.

Blasiak T, Zawadzki A, Lewandowski MH (2013) Infra-slow oscillation (ISO) of the pupil size of urethane-anaesthetised rats. PLoS One 8.

Bodizs R, Kantor S, Szabo G, Szucs A, Eross L, Halasz P (2001) Rhythmic hippocampal slow oscillation characterizes REM sleep in humans. Hippocampus 11:747-753.

Bonhomme V, Staquet C, Montupil J, Defresne A, Kirsch M, Martial C, Vanhaudenhuyse A, Chatelle C, Larroque SK, Raimondo F, Demertzi A, Bodart O, Laureys S, Gosseries O (2019) General Anesthesia: A Probe to Explore Consciousness. Frontiers in Systems Neuroscience 13.

Borbély AA (1976) Sleep and motor activity of the rat during ultra-short light-dark cycles. Brain Res 114:305-317.

Borbély AA (1982) A two process model of sleep regulation. Hum neurobiol 1:195-204.

Brown EN, Lydic R, Schiff ND (2010) General anesthesia, sleep, and coma. N Engl J Med 363:2638-2650.

Brown EN, Purdon PL, Van Dort CJ (2011) General Anesthesia and Altered States of Arousal: A Systems Neuroscience Analysis. Annual Review of Neuroscience 34:601-628.

Brown EN, Solt K, Purdon PL, Akeju O, Eriksson L, Fleisher L, Wiener-Kronish J, Cohen N, Young W (2014) Monitoring brain state during general anesthesia and sedation. Miller's anesthesia 1:1524-1540.

Brown R, Lam AD, Gonzalez-Sulser A, Ying A, Jones M, Chou RC-C, Tzioras M, Jordan CY, Jedrasiak-Cape I, Hemonnot A-L, Abou Jaoude M, Cole AJ, Cash SS, Saito T, Saido T, Ribchester RR, Hashemi K, Oren I (2018) Circadian and Brain State Modulation of Network Hyperexcitability in Alzheimer's Disease. eNeuro 5:ENEURO.0426-0417.2018.

Brown RE, Basheer R, McKenna JT, Strecker RE, McCarley RW (2012) Control of sleep and wakefulness. Physiol Rev 92:1087-1187.

Butler TC (1948) The metabolic fate of chloral hydrate. Journal of Pharmacology and Experimental Therapeutics 92:49-58.

Buzsaki G (2002) Theta oscillations in the hippocampus. Neuron 33:325-340.

Cai S, Tang AC, Luo TY, Yang SC, Yang H, Liu CX, Shu Y, Pan YC, Zhang Y, Zhou L (2021) Effect of basal forebrain somatostatin and parvalbumin neurons in propofol and isoflurane anesthesia. CNS Neuroscience & Therapeutics 27:792-804.

Campagna JA, Miller KW, Forman SA (2003) Mechanisms of actions of inhaled anesthetics. N Engl J Med 348:2110-2124.

Cantero JL, Atienza M, Stickgold R, Kahana MJ, Madsen JR, Kocsis B (2003) Sleep-dependent theta oscillations in the human hippocampus and neocortex. J Neurosci 23:10897-10903.

Carskadon MA, Dement WC (2005) Chapter 2 - Normal Human Sleep: An Overview. In: Principles and Practice of Sleep Medicine (Fourth Edition), pp 13-23. Philadelphia: W.B. Saunders.

Carter ME, Brill J, Bonnavion P, Huguenard JR, Huerta R, de Lecea L (2012) Mechanism for Hypocretin-mediated sleep-to-wake transitions. Proc Natl Acad Sci U S A 109:E2635-2644.

Carter ME, Yizhar O, Chikahisa S, Nguyen H, Adamantidis A, Nishino S, Deisseroth K, de Lecea L (2010) Tuning arousal with optogenetic modulation of locus coeruleus neurons. Nat Neurosci 13:1526-1533.

Casely E, Laycock H (2022) Opioids in pain medicine. Anaesthesia & Intensive Care Medicine 23:384-390.

Cerri M, Luppi M, Tupone D, Zamboni G, Amici R (2017) REM sleep and endothermy: potential sites and mechanism of a reciprocal interference. Frontiers in Physiology 8:624.

Chang H-M, Wu U-I, Lin T-B, Lan C-T, Chien W-C, Huang W-L, Shieh J-Y (2006a) Total sleep deprivation inhibits the neuronal nitric oxide synthase and cytochrome oxidase reactivities in the nodose ganglion of adult rats. Journal of Anatomy 209:239-250.

Chang HM, Wu UI, Lin TB, Lan CT, Chien WC, Huang WL, Shieh JY (2006b) Total sleep deprivation inhibits the neuronal nitric oxide synthase and cytochrome oxidase reactivities in the nodose ganglion of adult rats. J Anat 209:239-250.

Chaudhuri A (1997) Neural activity mapping with inducible transcription factors. Neuroreport 8:v-ix.

Chaudhuri A, Zangenehpour S, Rahbar-Dehgan F, Ye F (2000) Molecular maps of neural activity and quiescence. Acta Neurobiol Exp (Wars) 60:403-410.

Chauvette S, Crochet S, Volgushev M, Timofeev I (2011) Properties of slow oscillation during slow-wave sleep and anesthesia in cats. J Neurosci 31:14998-15008.

Chemali Jessica J, Van Dort Christa J, Brown Emery N, Solt K (2012) Active Emergence from Propofol General Anesthesia Is Induced by Methylphenidate. Anesthesiology 116:998-1005.

Chen L, Yang Z-l, Cheng J, Zhang P-p, Zhang L-s, Liu X-s, Wang L-c (2019) Propofol decreases the excitability of cholinergic neurons in mouse basal forebrain via GABAA receptors. Acta Pharmacologica Sinica 40:755-761.

Choudhary RC, Khanday MA, Mitra A, Mallick BN (2014) Perifornical orexinergic neurons modulate REM sleep by influencing locus coeruleus neurons in rats. Neuroscience 279:33-43.

Chung S, Weber F, Zhong P, Tan CL, Nguyen TN, Beier KT, Hormann N, Chang WC, Zhang Z, Do JP, Yao S, Krashes MJ, Tasic B, Cetin A, Zeng H, Knight ZA, Luo L, Dan Y (2017) Identification of preoptic sleep neurons using retrograde labelling and gene profiling. Nature 545:477-481.

Cirelli C, Pompeiano M, Tononi G (1995) Sleep deprivation and c-fos expression in the rat brain. J Sleep Res 4:92-106.

Cirelli C, Pompeiano M, Tononi G (1996) Neuronal gene expression in the waking state: a role for the locus coeruleus. Science 274:1211-1215.

Clement EA, Richard A, Thwaites M, Ailon J, Peters S, Dickson CT (2008) Cyclic and sleep-like spontaneous alternations of brain state under urethane anaesthesia. PLoS One 3:e2004.

Clement O, Sapin E, Libourel PA, Arthaud S, Brischoux F, Fort P, Luppi PH (2012) The lateral hypothalamic area controls paradoxical (REM) sleep by means of descending projections to brainstem GABAergic neurons. J Neurosci 32:16763-16774.

Correa-Sales C, Rabin BC, Maze M (1992) A hypnotic response to dexmedetomidine, an alpha 2 agonist, is mediated in the locus coeruleus in rats. Anesthesiology 76:948-952.

Crook J, Lovick T (2016) Urodynamic function during sleep-like brain states in urethane anesthetized rats. Neuroscience 313:73-82.

Datta S (2010) Cellular and chemical neuroscience of mammalian sleep. Sleep Medicine 11:431-440.

Datta S, Patterson EH, Siwek DF (1997) Endogenous and exogenous nitric oxide in the pedunculopontine tegmentum induces sleep. Synapse 27:69-78.

Derbyshire AJ, Rempel B, Forbes A, Lambert E (1936) The effects of anesthetics on action potentials in the cerebral cortex of the cat. American Journal of Physiology-Legacy Content 116:577-596.

Descartes R (1984) The Philosophical Writings of Descartes: Volume 2: Cambridge University Press.

Détári L, Vanderwolf CH (1987) Activity of identified cortically projecting and other basal forebrain neurones during large slow waves and cortical activation in anaesthetized rats. Brain Research 437:1-8.

Deuis JR, Dvorakova LS, Vetter I (2017) Methods Used to Evaluate Pain Behaviors in Rodents. Frontiers in Molecular Neuroscience 10.

Devor M, Zalkind V (2001) Reversible analgesia, atonia, and loss of consciousness on bilateral intracerebral microinjection of pentobarbital. Pain 94:101-112.

Dijk DJ (2009) Regulation and functional correlates of slow wave sleep. J Clin Sleep Med 5:S6-15.

Dragunow M, Faull R (1989) The use of c-fos as a metabolic marker in neuronal pathway tracing. Journal of Neuroscience Methods 29:261-265.

Dringenberg HC, Vanderwolf CH (1995) Some general anesthetics reduce serotonergic neocortical activation and enhance the action of serotonergic antagonists. Brain Research Bulletin 36:285-292.

Eikermann M, Akeju O, Chamberlin NL (2020) Sleep and Anesthesia: The Shared Circuit Hypothesis Has Been Put to Bed. Current Biology 30:R219-R221.

Espana RA, Berridge CW (2006) Organization of noradrenergic efferents to arousal-related basal forebrain structures. J Comp Neurol 496:668-683.

Ferron J-F, Kroeger D, Chever O, Amzica F (2009a) Cortical inhibition during burst suppression induced with isoflurane anesthesia. Journal of Neuroscience 29:9850-9860.

Ferron JF, Kroeger D, Chever O, Amzica F (2009b) Cortical inhibition during burst suppression induced with isoflurane anesthesia. J Neurosci 29:9850-9860.

Field KJ, White WJ, Lang CM (1993) Anaesthetic effects of chloral hydrate, pentobarbitone and urethane in adult male rats. Lab Anim 27:258-269.

Fischer W, Wirkner K, Weber M, Eberts C, Köles L, Reinhardt R, Franke H, Allgaier C, Gillen C, Illes P (2003) Characterization of P2X3, P2Y1 and P2Y4 receptors in cultured

HEK293-hP2X3 cells and their inhibition by ethanol and trichloroethanol. Journal of neurochemistry 85:779-790.

Flecknell P (2016a) Chapter 5 - Anaesthesia of Common Laboratory Species: Special Considerations. In: Laboratory Animal Anaesthesia (Fourth Edition) (Flecknell P, ed), pp 193-256. Boston: Academic Press.

Flecknell P (2016b) Chapter 2 - Managing and Monitoring Anaesthesia. In: Laboratory Animal Anaesthesia (Fourth Edition) (Flecknell P, ed), pp 77-108. Boston: Academic Press.

Flecknell P (2016c) Chapter 3 - Special Techniques. In: Laboratory Animal Anaesthesia (Fourth Edition) (Flecknell P, ed), pp 109-140. Boston: Academic Press.

Fleischman RW, McCracken D, Forbes W (1977) Adynamic ileus in the rat induced by chloral hydrate. Lab Anim Sci 27:238-243.

Fleischmann A, Pilge S, Kiel T, Kratzer S, Schneider G, Kreuzer M (2018) Substance-Specific Differences in Human Electroencephalographic Burst Suppression Patterns. Frontiers in Human Neuroscience 12.

Fong R, Khokhar S, Chowdhury AN, Xie KG, Wong JH, Fox AP, Xie Z (2017) Caffeine accelerates recovery from general anesthesia via multiple pathways. J Neurophysiol 118:1591-1597.

Franks NP (2008) General anaesthesia: from molecular targets to neuronal pathways of sleep and arousal. Nat Rev Neurosci 9:370-386.

Franks NP, Wisden W (2021) The inescapable drive to sleep: Overlapping mechanisms of sleep and sedation. Science 374:556-559.

Friedman L, Bergmann BM, Rechtschaffen A (1979) Effects of Sleep Deprivation on Sleepiness, Sleep Intensity, and Subsequent Sleep in the Rat. Sleep 1:369-391.

Fu B, Yu T, Yuan J, Gong X, Zhang M (2017) Noradrenergic transmission in the central medial thalamic nucleus modulates the electroencephalographic activity and emergence from propofol anesthesia in rats. J Neurochem 140:862-873.

Fujita A, Bonnavion P, Wilson MH, Mickelsen LE, Bloit J, de Lecea L, Jackson AC (2017) Hypothalamic Tuberomammillary Nucleus Neurons: Electrophysiological Diversity and Essential Role in Arousal Stability. J Neurosci 37:9574-9592.

Fuller PM, Sherman D, Pedersen NP, Saper CB, Lu J (2011) Reassessment of the structural basis of the ascending arousal system. J Comp Neurol 519:933-956.

Garcia PS, Kolesky SE, Jenkins A (2010) General anesthetic actions on GABA(A) receptors. Curr Neuropharmacol 8:2-9.

Garner AR, Rowland DC, Hwang SY, Baumgaertel K, Roth BL, Kentros C, Mayford M (2012) Generation of a synthetic memory trace. Science 335:1513-1516.

Gelegen C, Miracca G, Ran MZ, Harding EC, Ye Z, Yu X, Tossell K, Houston CM, Yustos R, Hawkins ED, Vyssotski AL, Dong HL, Wisden W, Franks NP (2018) Excitatory Pathways from the Lateral Habenula Enable Propofol-Induced Sedation. Curr Biol 28:580-587 e585.

Gent TC, Adamantidis A (2017) Anaesthesia and sleep: Where are we now? Clinical and Translational Neuroscience 1.

Gerashchenko D, Chou TC, Blanco-Centurion CA, Saper CB, Shiromani PJ (2004) Effects of lesions of the histaminergic tuberomammillary nucleus on spontaneous sleep in rats. Sleep 27:1275-1281.

Gerashchenko D, Kohls MD, Greco M, Waleh NS, Salin-Pascual R, Kilduff TS, Lappi DA, Shiromani PJ (2001) Hypocretin-2-saporin lesions of the lateral hypothalamus produce narcoleptic-like sleep behavior in the rat. J Neurosci 21:7273-7283.

Gilsbach R, Roser C, Beetz N, Brede M, Hadamek K, Haubold M, Leemhuis J, Philipp M, Schneider J, Urbanski M, Szabo B, Weinshenker D, Hein L (2009) Genetic dissection of alpha2-adrenoceptor functions in adrenergic versus nonadrenergic cells. Mol Pharmacol 75:1160-1170.

Gloor P (1969) Hans Berger on Electroencephalography. American Journal of EEG Technology 9:1-8.

Goldman AM, Buchanan G, Aiba I, Noebels JL (2017) SUDEP Animal Models In: Models of Seizures and Epilepsy (Second edition) (Buckmaster PS, Galanopoulou AS, Moshé SL, eds), pp 1007-1018: Academic Press.

Gompf HS, Mathai C, Fuller PM, Wood DA, Pedersen NP, Saper CB, Lu J (2010) Locus ceruleus and anterior cingulate cortex sustain wakefulness in a novel environment. J Neurosci 30:14543-14551.

Gong H, McGinty D, Guzman-Marin R, Chew KT, Stewart D, Szymusiak R (2004) Activation of c-fos in GABAergic neurones in the preoptic area during sleep and in response to sleep deprivation. J Physiol 556:935-946.

Gonzalez-Rueda A, Pedrosa V, Feord RC, Clopath C, Paulsen O (2018) Activity-Dependent Downscaling of Subthreshold Synaptic Inputs during Slow-Wave-Sleep-like Activity In Vivo. Neuron 97:1244-1252 e1245.

Gottesmann C (2001) The golden age of rapid eye movement sleep discoveries. 1. Lucretius--1964. Prog Neurobiol 65:211-287.

Greco MA, Lu J, Wagner D, Shiromani PJ (2000a) c-Fos expression in the cholinergic basal forebrain after enforced wakefulness and recovery sleep. NeuroReport 11.

Greco MA, Lu J, Wagner D, Shiromani PJ (2000b) c-Fos expression in the cholinergic basal forebrain after enforced wakefulness and recovery sleep. Neuroreport 11:437-440.

Greene SA, Thurmon JC (1988) Xylazine--a review of its pharmacology and use in veterinary medicine. J Vet Pharmacol Ther 11:295-313.

Gritti I, Henny P, Galloni F, Mainville L, Mariotti M, Jones BE (2006) Stereological estimates of the basal forebrain cell population in the rat, including neurons containing choline acetyltransferase, glutamic acid decarboxylase or phosphate-activated glutaminase and colocalizing vesicular glutamate transporters. Neuroscience 143:1051-1064.

Gruss M, Hempelmann G, Scholz A (2002) Trichloroethanol alters action potentials in a subgroup of primary sensory neurones. Neuroreport 13:853-856.

Guo M, Wang J, Yuan Y, Chen L, He J, Wei W, Xu F, Liu Q, Peng M (2023) Role of adenosine A2A receptors in the loss of consciousness induced by propofol anesthesia. Journal of Neurochemistry 164:684-699.

Haack M, Simpson N, Sethna N, Kaur S, Mullington J (2020) Sleep deficiency and chronic pain: potential underlying mechanisms and clinical implications. Neuropsychopharmacology 45:205-216.

Hall AC, Lieb WR, Franks NP (1994) Stereoselective and non-stereoselective actions of isoflurane on the GABAA receptor. British journal of pharmacology 112:906-910.

Hall C, Trim (2001) Veterinary anaesthesia, 10th edition. Edinburgh: Saunders.

Han Y, Shi Y-f, Xi W, Zhou R, Tan Z-b, Wang H, Li X-m, Chen Z, Feng G, Luo M, Huang Z-l, Duan S, Yu Y-q (2014) Selective Activation of Cholinergic Basal Forebrain Neurons Induces Immediate Sleep-wake Transitions. Current Biology 24:693-698.

Hans P, Dewandre P-Y, Brichant JF, Bonhomme V (2004) Comparative effects of ketamine on Bispectral Index and spectral entropy of the electroencephalogram under sevoflurane anaesthesia. BJA: British Journal of Anaesthesia 94:336-340.

Hara K, Harris RA (2002) The anesthetic mechanism of urethane: the effects on neurotransmitter-gated ion channels. Anesth Analg 94:313-318, table of contents.

Hara M, Kai Y, Ikemoto Y (1993) Propofol activates GABAA receptor-chloride ionophore complex in dissociated hippocampal pyramidal neurons of the rat. Anesthesiology 79:781-788.

Harding EC, Franks NP, Wisden W (2020) Sleep and thermoregulation. Current Opinion in Physiology 15:7-13.

Harding EC, Yu X, Miao A, Andrews N, Ma Y, Ye Z, Lignos L, Miracca G, Ba W, Yustos R, Vyssotski AL, Wisden W, Franks NP (2018) A Neuronal Hub Binding Sleep Initiation and Body Cooling in Response to a Warm External Stimulus. Current Biology 28:2263-2273.e2264.

Harinath S, Sikdar S (2004) Trichloroethanol enhances the activity of recombinant human TREK-1 and TRAAK channels. Neuropharmacology 46:750-760.

Harrison NL, Simmonds MA (1985) Quantitative studies on some antagonists of N-methyl D-aspartate in slices of rat cerebral cortex. British Journal of Pharmacology 84:381-391.

Hassani OK, Henny P, Lee MG, Jones BE (2010) GABAergic neurons intermingled with orexin and MCH neurons in the lateral hypothalamus discharge maximally during sleep. Eur J Neurosci 32:448-457.

Hauer BE, Pagliardini S, Dickson CT (2019) The Reuniens Nucleus of the Thalamus Has an Essential Role in Coordinating Slow-Wave Activity between Neocortex and Hippocampus. eNeuro 6:ENEURO.0365-0319.2019.

Hauer BE, Negash B, Chan K, Vuong W, Colbourne F, Pagliardini S, Dickson CT (2018) Hyperoxia enhances slow-wave forebrain states in urethane-anesthetized and naturally sleeping rats. Journal of Neurophysiology 120:1505-1515.

Hemmings HC, Riegelhaupt PM, Kelz MB, Solt K, Eckenhoff RG, Orser BA, Goldstein PA (2019) Towards a Comprehensive Understanding of Anesthetic Mechanisms of Action: A Decade of Discovery. Trends in Pharmacological Sciences 40:464-481.

Herold KF, Hemmings Jr HC (2012) Sodium channels as targets for volatile anesthetics. Frontiers in pharmacology 3:50.

Herrera CG, Cadavieco MC, Jego S, Ponomarenko A, Korotkova T, Adamantidis A (2016) Hypothalamic feedforward inhibition of thalamocortical network controls arousal and consciousness. Nat Neurosci 19:290-298.

Horner RL (2008) Neuromodulation of hypoglossal motoneurons during sleep. Respir Physiol Neurobiol 164:179-196.

Hsieh KC, Gvilia I, Kumar S, Uschakov A, McGinty D, Alam MN, Szymusiak R (2011) c-Fos expression in neurons projecting from the preoptic and lateral hypothalamic areas to the ventrolateral periaqueductal gray in relation to sleep states. Neuroscience 188:55-67.

Hu J-J, Liu Y, Yao H, Cao B, Liao H, Yang R, Chen P, Song X-J (2023) Emergence of consciousness from anesthesia through ubiquitin degradation of KCC2 in the ventral posteromedial nucleus of the thalamus. Nature Neuroscience:1-14.

Hua T, Chen B, Lu D, Sakurai K, Zhao S, Han B-X, Kim J, Yin L, Chen Y, Lu J, Wang F (2020) General anesthetics activate a potent central pain-suppression circuit in the amygdala. Nature Neuroscience 23:854-868.

Hudetz AG (2012) General anesthesia and human brain connectivity. Brain Connect 2:291-302.

Huh Y, Cho J (2013) Urethane anesthesia depresses activities of thalamocortical neurons and alters its response to nociception in terms of dual firing modes. Front Behav Neurosci 7:141.

Hüske C, Sander SE, Hamann M, Kershaw O, Richter F, Richter A (2016) Towards optimized anesthesia protocols for stereotactic surgery in rats: Analgesic, stress and general health effects of injectable anesthetics. A comparison of a recommended complete reversal anesthesia with traditional chloral hydrate monoanesthesia. Brain research 1642:364-375.

Iranzo A (2016) Sleep in Neurodegenerative Diseases. Sleep Med Clin 11:1-18.

Irwin MR, Olmstead R, Carroll JE (2016) Sleep Disturbance, Sleep Duration, and Inflammation: A Systematic Review and Meta-Analysis of Cohort Studies and Experimental Sleep Deprivation. Biological Psychiatry 80:40-52.

Jacobs BL, Fornal CA (1991) Activity of brain serotonergic neurons in the behaving animal. Pharmacol Rev 43:563-578.

Jasper JR, Lesnick JD, Chang LK, Yamanishi SS, Chang TK, Hsu SA, Daunt DA, Bonhaus DW, Eglen RM (1998) Ligand efficacy and potency at recombinant alpha2 adrenergic

receptors: agonist-mediated [35S]GTPgammaS binding. Biochem Pharmacol 55:1035-1043.

Jensen TS, Yaksh TL (1986) III. Comparison of the antinociceptive action of mu and delta opioid receptor ligands in the periaqueductal gray matter, medial and paramedial ventral medulla in the rat as studied by the microinjection technique. Brain research 372:301-312.

Jiang-Xie L-F, Yin L, Zhao S, Prevosto V, Han B-X, Dzirasa K, Wang F (2019) A Common Neuroendocrine Substrate for Diverse General Anesthetics and Sleep. Neuron 102:1053-1065.e1054.

Jones BE (2005) Basic mechanisms of sleep-wake states. In: Principles and practice of sleep medicine, pp 136-153: Elsevier.

Jones BE (2017) Principal cell types of sleep–wake regulatory circuits. Current Opinion in Neurobiology 44:101-109.

Jones BE (2020) Arousal and sleep circuits. Neuropsychopharmacology 45:6-20.

Jouvet M (1965) Paradoxical Sleep — A Study of its Nature and Mechanisms. In: Progress in Brain Research (Akert K, Bally C, Schadé JP, eds), pp 20-62: Elsevier.

Jouvet M, Michel F (1960) New research on the structures responsible for the "paradoxical phase" of sleep. J Physiol (Paris) 52:130-131.

Jung S, Zimin PI, Woods CB, Kayser E-B, Haddad D, Reczek CR, Nakamura K, Ramirez J-M, Sedensky MM, Morgan PG (2022) Isoflurane inhibition of endocytosis is an anesthetic mechanism of action. Current Biology 32:3016-3032.e3013.

Kaputlu I, Sadan G, Ozdem S (1998) Exogenous adenosine potentiates hypnosis induced by intravenous anaesthetics. Anaesthesia 53:496-500.

Kawashima T, Okuno H, Bito H (2014) A new era for functional labeling of neurons: activity-dependent promoters have come of age. Front Neural Circuits 8:37.

Kelz MB, Mashour GA (2019) The biology of general anesthesia from Paramecium to primate. Current Biology 29:R1199-R1210.

Kelz MB, García PS, Mashour GA, Solt K (2019) Escape From Oblivion: Neural Mechanisms of Emergence From General Anesthesia. Anesthesia & Analgesia 128.

Kelz MB, Sun Y, Chen J, Cheng Meng Q, Moore JT, Veasey SC, Dixon S, Thornton M, Funato H, Yanagisawa M (2008) An essential role for orexins in emergence from general anesthesia. Proc Natl Acad Sci U S A 105:1309-1314.

Kenny JD, Westover MB, Ching S, Brown EN, Solt K (2014) Propofol and sevoflurane induce distinct burst suppression patterns in rats. Frontiers in Systems Neuroscience 8.

Khanday MA, Mallick BN (2015) REM sleep modulation by perifornical orexinergic inputs to the pedunculo-pontine tegmental neurons in rats. Neuroscience 308:125-133.

Ko EM, Estabrooke IV, McCarthy M, Scammell TE (2003) Wake-related activity of tuberomammillary neurons in rats. Brain Res 992:220-226.

Koch C, Massimini M, Boly M, Tononi G (2016) Neural correlates of consciousness: progress and problems. Nature Reviews Neuroscience 17:307-321.

Kohler C, Swanson LW, Haglund L, Wu JY (1985) The cytoarchitecture, histochemistry and projections of the tuberomammillary nucleus in the rat. Neuroscience 16:85-110.

Kovacs LA, Schiessl JA, Nafz AE, Csernus V, Gaszner B (2018) Both Basal and Acute Restraint Stress-Induced c-Fos Expression Is Influenced by Age in the Extended Amygdala and Brainstem Stress Centers in Male Rats. Front Aging Neurosci 10:248.

Koyama Y, Hayaishi O (1994) Firing of neurons in the preoptic/anterior hypothalamic areas in rat: its possible involvement in slow wave sleep and paradoxical sleep. Neurosci Res 19:31-38.

Krasowski MD, Harrison NL (2000) The actions of ether, alcohol and alkane general anaesthetics on GABAA and glycine receptors and the effects of TM2 and TM3 mutations. British journal of pharmacology 129:731-743.

Krasowski MD, Koltchine VV, Rick CE, Ye Q, Finn SE, Harrison NL (1998) Propofol and Other Intravenous Anesthetics Have Sites of Action on the γ-Aminobutyric Acid Type A Receptor Distinct from That for Isoflurane. Molecular Pharmacology 53:530.

Krieger J (2000) Respiratory physiology: breathing in normal subjects. Principles and practice of sleep medicine.

Kroeger D, Amzica F (2007) Hypersensitivity of the anesthesia-induced comatose brain. Journal of Neuroscience 27:10597-10607.

Kroeger D, Absi G, Gagliardi C, Bandaru SS, Madara JC, Ferrari LL, Arrigoni E, Münzberg H, Scammell TE, Saper CB, Vetrivelan R (2018) Galanin neurons in the ventrolateral preoptic area promote sleep and heat loss in mice. Nature Communications 9:4129.

Krukoff TL, Morton TL, Harris KH, Jhamandas JH (1992) Expression of c-fos protein in rat brain elicited by electrical stimulation of the pontine parabrachial nucleus. Journal of Neuroscience 12:3582-3590.

Kushikata T, Yoshida H, Kudo M, Kudo T, Kudo T, Hirota K (2011) Role of coerulean noradrenergic neurones in general anaesthesia in rats. Br J Anaesth 107:924-929.

Lakhlani PP, MacMillan LB, Guo TZ, McCool BA, Lovinger DM, Maze M, Limbird LE (1997) Substitution of a mutant alpha2a-adrenergic receptor via "hit and run" gene targeting

reveals the role of this subtype in sedative, analgesic, and anesthetic-sparing responses in vivo. Proc Natl Acad Sci U S A 94:9950-9955.

Lanir-Azaria S, Meiri G, Avigdor T, Minert A, Devor M (2018) Enhanced wakefulness following lesions of a mesopontine locus essential for the induction of general anesthesia. Behav Brain Res 341:198-211.

Le Bars D, Gozariu M, Cadden SW (2001) Animal Models of Nociception. Pharmacological Reviews 53:597.

LeDoux JE, Wilson DH, Gazzaniga MS (1977) A divided mind: Observations on the conscious properties of the separated hemispheres. Annals of Neurology: Official Journal of the American Neurological Association and the Child Neurology Society 2:417-421.

LeDoux JE, Michel M, Lau H (2020) A little history goes a long way toward understanding why we study consciousness the way we do today. Proceedings of the National Academy of Sciences 117:6976-6984.

Ledoux L, Sastre JP, Buda C, Luppi PH, Jouvet M (1996) Alterations in c-fos expression after different experimental procedures of sleep deprivation in the cat. Brain Res 735:108-118.

Lee MG, Hassani OK, Jones BE (2005a) Discharge of identified orexin/hypocretin neurons across the sleep-waking cycle. J Neurosci 25:6716-6720.

Lee MG, Hassani OK, Alonso A, Jones BE (2005b) Cholinergic basal forebrain neurons burst with theta during waking and paradoxical sleep. J Neurosci 25:4365-4369.

Lee SH, Dan Y (2012) Neuromodulation of brain states. Neuron 76:209-222.

Leung LS, Luo T, Ma J, Herrick I (2014) Brain areas that influence general anesthesia. Prog Neurobiol 122:24-44.

Leung LS, Petropoulos S, Shen B, Luo T, Herrick I, Rajakumar N, Ma J (2011) Lesion of cholinergic neurons in nucleus basalis enhances response to general anesthetics. Exp Neurol 228:259-269.

Levey AI, Hallanger AE, Wainer BH (1987) Cholinergic nucleus basalis neurons may influence the cortex via the thalamus. Neurosci Lett 74:7-13.

Lewis LD, Ching S, Weiner VS, Peterfreund RA, Eskandar EN, Cash SS, Brown EN, Purdon PL (2013) Local cortical dynamics of burst suppression in the anaesthetized brain. Brain 136:2727-2737.

Li J, Yu T, Shi F, Zhang Y, Duan Z, Fu B, Zhang Y (2018) Involvement of Ventral Periaqueductal Gray Dopaminergic Neurons in Propofol Anesthesia. Neurochemical Research 43:838-847.

Lian X, Lin Y, Luo T, Yuan H, Chen Y (2020) Comparison of dexmedetomidine with chloral hydrate as sedatives for pediatric patients: A systematic review and meta-analysis. Medicine 99.

Liang Y, Shi W, Xiang A, Hu D, Wang L, Zhang L (2021) The NAergic locus coeruleus-ventrolateral preoptic area neural circuit mediates rapid arousal from sleep. Current Biology 31:3729-3742.e3725.

Lin JS, Sakai K, Vanni-Mercier G, Jouvet M (1989) A critical role of the posterior hypothalamus in the mechanisms of wakefulness determined by microinjection of muscimol in freely moving cats. Brain Res 479:225-240.

Lin JS, Anaclet C, Sergeeva OA, Haas HL (2011) The waking brain: an update. Cell Mol Life Sci 68:2499-2512.

Lincoln DW (1969) Correlation of unit activity in the hypothalamus with EEG patterns associated with the sleep cycle. Experimental Neurology 24:1-18.

Liu X, Zhu X-H, Zhang Y, Chen W (2010a) Neural Origin of Spontaneous Hemodynamic Fluctuations in Rats under Burst–Suppression Anesthesia Condition. Cerebral Cortex 21:374-384.

Liu YW, Li J, Ye JH (2010b) Histamine regulates activities of neurons in the ventrolateral preoptic nucleus. J Physiol 588:4103-4116.

Lovinger DM, Zimmerman SA, Levitin M, Jones MV, Harrison NL (1993) Trichloroethanol potentiates synaptic transmission mediated by gamma-aminobutyric acidA receptors in hippocampal neurons. Journal of Pharmacology and Experimental Therapeutics 264:1097-1103.

Lu J, Greco MA, Shiromani P, Saper CB (2000) Effect of lesions of the ventrolateral preoptic nucleus on NREM and REM sleep. J Neurosci 20:3830-3842.

Lu J, Sherman D, Devor M, Saper CB (2006) A putative flip-flop switch for control of REM sleep. Nature 441:589-594.

Lu J, Nelson LE, Franks N, Maze M, Chamberlin NL, Saper CB (2008) Role of endogenous sleep-wake and analgesic systems in anesthesia. J Comp Neurol 508:648-662.

Lubejko ST, Graham RD, Livrizzi G, Schaefer R, Banghart MR, Creed MC (2022) The role of endogenous opioid neuropeptides in neurostimulation-driven analgesia. Frontiers in Systems Neuroscience.

Luethy A, Boghosian JD, Srikantha R, Cotten JF (2017) Halogenated ether, alcohol, and alkane anesthetics activate TASK-3 tandem pore potassium channels likely through a common mechanism. Molecular pharmacology 91:620-629.

Luo M, Fei X, Liu X, Jin Z, Wang Y, Xu M (2023) Divergent neural activity in the VLPO during anesthesia and sleep. Advanced Science 10:2203395.

Luo T, Leung LS (2009) Basal forebrain histaminergic transmission modulates electroencephalographic activity and emergence from isoflurane anesthesia. Anesthesiology 111:725-733.

Luo T-Y, Cai S, Qin Z-X, Yang S-C, Shu Y, Liu C-X, Zhang Y, Zhang L, Zhou L, Yu T (2020) Basal forebrain cholinergic activity modulates isoflurane and propofol anesthesia. Frontiers in Neuroscience 14:559077.

Luppi P-H, Gervasoni D, Verret L, Goutagny R, Peyron C, Salvert D, Leger L, Fort P (2006) Paradoxical (REM) sleep genesis: The switch from an aminergic–cholinergic to a GABAergic–glutamatergic hypothesis. Journal of Physiology-Paris 100:271-283.

Lydic R, Biebuyck JF (1994) Sleep neurobiology: relevance for mechanistic studies of anaesthesia. Br J Anaesth 72:506-508.

Lydic R, Baghdoyan HA (2005) Sleep, anesthesiology, and the neurobiology of arousal state control. Anesthesiology 103:1268-1295.

Ma J, Leung LS (2006) Limbic system participates in mediating the effects of general anesthetics. Neuropsychopharmacology 31:1177-1192.

Maggi CA, Meli A (1986) Suitability of urethane anesthesia for physiopharmacological investigations in various systems Part 1: General considerations. Experientia 42:109-114.

Maloney KJ, Mainville L, Jones BE (1999) Differential c-Fos expression in cholinergic, monoaminergic, and GABAergic cell groups of the pontomesencephalic tegmentum after paradoxical sleep deprivation and recovery. J Neurosci 19:3057-3072.

Mashour GA, Pal D (2012) Interfaces of sleep and anesthesia. Anesthesiol Clin 30:385-398.

Mashour GA, Pal D, Brown EN (2022) Prefrontal cortex as a key node in arousal circuitry. Trends in Neurosciences 45:722-732.

Matsumoto M, Hikosaka O (2007) Lateral habenula as a source of negative reward signals in dopamine neurons. Nature 447:1111-1115.

McCarley RW (2007) Neurobiology of REM and NREM sleep. Sleep Med 8:302-330.

McCormick DA, Nestvogel DB, He BJ (2020) Neuromodulation of brain state and behavior. Annual review of neuroscience 43:391-415.

McGinty D, Szymusiak R, Thomson D (1994) Preoptic/anterior hypothalamic warming increases EEG delta frequency activity within non-rapid eye movement sleep. Brain Res 667:273-277.

McGinty DJ, Sterman MB (1968) Sleep suppression after basal forebrain lesions in the cat. Science 160:1253-1255.

McKenna JT, Cordeira JW, Jeffrey BA, Ward CP, Winston S, McCarley RW, Strecker RE (2009) c-Fos protein expression is increased in cholinergic neurons of the rodent basal forebrain during spontaneous and induced wakefulness. Brain Res Bull 80:382-388.

Mease RA, Metz M, Groh A (2016) Cortical Sensory Responses Are Enhanced by the Higher-Order Thalamus. Cell Rep 14:208-215.

Mesulam MM, Mufson EJ, Levey AI, Wainer BH (1983) Cholinergic innervation of cortex by the basal forebrain: cytochemistry and cortical connections of the septal area, diagonal band nuclei, nucleus basalis (substantia innominata), and hypothalamus in the rhesus monkey. J Comp Neurol 214:170-197.

Mileykovskiy BY, Kiyashchenko LI, Siegel JM (2005) Behavioral correlates of activity in identified hypocretin/orexin neurons. Neuron 46:787-798.

Minert A, Devor M (2016) Brainstem node for loss of consciousness due to GABA(A) receptor-active anesthetics. Exp Neurol 275 Pt 1:38-45.

Minert A, Yatziv SL, Devor M (2017) Location of the Mesopontine Neurons Responsible for Maintenance of Anesthetic Loss of Consciousness. J Neurosci 37:9320-9331.

Minert A, Baron M, Devor M (2020) Reduced Sensitivity to Anesthetic Agents upon Lesioning the Mesopontine Tegmental Anesthesia Area in Rats Depends on Anesthetic Type. Anesthesiology 132:535-550.

Moffitt JR, Bambah-Mukku D, Eichhorn SW, Vaughn E, Shekhar K, Perez JD, Rubinstein ND, Hao J, Regev A, Dulac C, Zhuang X (2018) Molecular, spatial, and functional single-cell profiling of the hypothalamic preoptic region. Science 362:eaau5324.

Mondino A, González J, Li D, Mateos D, Osorio L, Cavelli M, Castro-Nin JP, Serantes D, Costa A, Vanini G (2022) Urethane anaesthesia exhibits neurophysiological correlates of unconsciousness and is distinct from sleep. European Journal of Neuroscience.

Monti JM, Jantos H (2008) The roles of dopamine and serotonin, and of their receptors, in regulating sleep and waking. Prog Brain Res 172:625-646.

Moody OA, Zhang ER, Vincent KF, Kato R, Melonakos ED, Nehs CJ, Solt K (2021) The neural circuits underlying general anesthesia and sleep. Anesthesia and analgesia 132:1254.

Moore JT, Chen J, Han B, Meng QC, Veasey SC, Beck SG, Kelz MB (2012) Direct activation of sleep-promoting VLPO neurons by volatile anesthetics contributes to anesthetic hypnosis. Curr Biol 22:2008-2016.

Moruzzi G, Magoun HW (1949) Brain stem reticular formation and activation of the EEG. Electroencephalogr Clin Neurophysiol 1:455-473.

Mouret J, Delorme F, Jouvet M (1967) Lesions of the pontine tegmentum and sleep in rats. C R Seances Soc Biol Fil 161:1603-1606.

Mukamel EA, Pirondini E, Babadi B, Wong KF, Pierce ET, Harrell PG, Walsh JL, Salazar-Gomez AF, Cash SS, Eskandar EN, Weiner VS, Brown EN, Purdon PL (2014) A transition in brain state during propofol-induced unconsciousness. J Neurosci 34:839-845.

Munoz-Ortiz E, Diaz-Escarcega R, Meza-Andrade R, Munoz-Ortiz J, Garcia-Garcia F, Lopez-Meraz L, Beltran-Prrazal L, Morgado-Valle C (2017) Selective deprivation of rapid eye movement (REM) sleep for 24 h does not modify the

c-Fos immunoreactivity in the Ventral Respiratory Column (VRC) of rat. Devista eNeurobiologia 8.

Nagele P, Mendel J B, Placzek William J, Scott Barbara A, d'Avignon D A, Crowder C M (2005) Volatile Anesthetics Bind Rat Synaptic Snare Proteins. Anesthesiology 103:768-778.

Nakahiro M, Yeh JZ, Brunner E, Narahashi T (1989) General anesthetics modulate GABA receptor channel complex in rat dorsal root ganglion neurons. The FASEB Journal 3:1850-1854.

Nauta WJ (1946) Hypothalamic regulation of sleep in rats; an experimental study. J Neurophysiol 9:285-316.

Nelson AB, Faraguna U, Tononi G, Cirelli C (2010) Effects of Anesthesia on the Response to Sleep Deprivation. Sleep 33:1659-1667.

Nelson LE, Guo TZ, Lu J, Saper CB, Franks NP, Maze M (2002) The sedative component of anesthesia is mediated by GABA(A) receptors in an endogenous sleep pathway. Nat Neurosci 5:979-984.

Nelson LE, Lu J, Guo T, Saper CB, Franks NP, Maze M (2003) The alpha2-adrenoceptor agonist dexmedetomidine converges on an endogenous sleep-promoting pathway to exert its sedative effects. Anesthesiology 98:428-436.

Niethard N, Ngo H-VV, Ehrlich I, Born J (2018) Cortical circuit activity underlying sleep slow oscillations and spindles. Proceedings of the National Academy of Sciences 115:E9220-E9229.

Nollet M, Wisden W, Franks NP (2020) Sleep deprivation and stress: a reciprocal relationship. Interface focus 10:20190092.

Nomeir AA, Ioannou YM, Sanders JM, Matthews HB (1989) Comparative metabolism and disposition of ethyl carbamate (urethane) in male fischer 344 rats and male B6C3F1 mice. Toxicology and Applied Pharmacology 97:203-215.

Oishi Y, Suzuki Y, Takahashi K, Yonezawa T, Kanda T, Takata Y, Cherasse Y, Lazarus M (2017) Activation of ventral tegmental area dopamine neurons produces wakefulness through dopamine D2-like receptors in mice. Brain Structure and Function 222:2907-2915.

Opp MR, Toth LA (2003) Neural-immune interactions in the regulation of sleep. Front Biosci 8:d768-779.

Orestes P, Bojadzic D, Chow RM, Todorovic SM (2009) Mechanisms and functional significance of inhibition of neuronal T-type calcium channels by isoflurane. Molecular pharmacology 75:542-554.

Oxotremorine M (2023) Data Sheet: HY-101372A. In: https://www.medchemexpress.com/oxotremorine-m-iodide.html. NJ, USA: MedChemExpress.

Pace-Schott EF, Hobson JA (2002) The neurobiology of sleep: genetics, cellular physiology and subcortical networks. Nat Rev Neurosci 3:591-605.

Pagliardini S, Funk GD, Dickson CT (2013a) Breathing and brain state: urethane anesthesia as a model for natural sleep. Respir Physiol Neurobiol 188:324-332.

Pagliardini S, Gosgnach S, Dickson CT (2013b) Spontaneous sleep-like brain state alternations and breathing characteristics in urethane anesthetized mice. PLoS One 8:e70411.

Pagliardini S, Greer JJ, Funk GD, Dickson CT (2012) State-dependent modulation of breathing in urethane-anesthetized rats. J Neurosci 32:11259-11270.

Pal D, Mashour GA (2011) Sleep and Anesthesia: A Consideration of States, Traits, and Mechanisms. In: Sleep and Anesthesia: Neural Correlates in Theory and Experiment (Hutt A, ed), pp 1-20. New York, NY: Springer New York.

Pal D, Lipinski WJ, Walker AJ, Turner AM, Mashour GA (2011) State-specific effects of sevoflurane anesthesia on sleep homeostasis: selective recovery of slow wave but not rapid eye movement sleep. Anesthesiology 114:302-310.

Pang DSJ, Robledo CJ, Carr DR, Gent TC, Vyssotski AL, Caley A, Zecharia AY, Wisden W, Brickley SG, Franks NP (2009) An unexpected role for TASK-3 potassium channels in network oscillations with implications for sleep mechanisms and anesthetic action. Proceedings of the National Academy of Sciences 106:17546-17551.

Pelayo R, Dement WC (2017) Chapter 1 - History of Sleep Physiology and Medicine. In: Principles and Practice of Sleep Medicine (Sixth Edition) (Kryger M, Roth T, Dement WC, eds), pp 3-14.e14: Elsevier.

Petrovic J, Ciric J, Lazic K, Kalauzi A, Saponjic J (2013) Lesion of the pedunculopontine tegmental nucleus in rat augments cortical activation and disturbs sleep/wake state transitions structure. Exp Neurol 247:562-571.

Piccitto MR (2018) Recommendations for the Design and Analysis of In Vivo Electrophysiology Studies. J Neurosci 38:5837-5839.

Pillay S, Vizuete JA, McCallum JB, Hudetz AG (2011) Norepinephrine infusion into nucleus basalis elicits microarousal in desflurane-anesthetized rats. Anesthesiology 115:733-742.

Porkka-Heiskanen T, Strecker RE, Thakkar M, Bjorkum AA, Greene RW, McCarley RW (1997) Adenosine: a mediator of the sleep-inducing effects of prolonged wakefulness. Science 276:1265-1268.

Poskanzer KE, Yuste R (2016) Astrocytes regulate cortical state switching in vivo. Proc Natl Acad Sci U S A 113:E2675-2684.

Prys-Roberts C (1987) Anesthesia: a practical or impractical construct? British Journal of Anaesthesia 59:1341-1345.

Puig MV, Watakabe A, Ushimaru M, Yamamori T, Kawaguchi Y (2010) Serotonin Modulates Fast-Spiking Interneuron and Synchronous Activity in the Rat Prefrontal Cortex through 5-HT1A and 5-HT2A Receptors. The Journal of Neuroscience 30:2211.

Purdon PL, Sampson A, Pavone KJ, Brown EN (2015) Clinical Electroencephalography for Anesthesiologists: Part I: Background and Basic Signatures. Anesthesiology 123:937-960.

Purdon PL, Pierce ET, Mukamel EA, Prerau MJ, Walsh JL, Wong KF, Salazar-Gomez AF, Harrell PG, Sampson AL, Cimenser A, Ching S, Kopell NJ, Tavares-Stoeckel C, Habeeb K, Merhar R, Brown EN (2013) Electroencephalogram signatures of loss and recovery of consciousness from propofol. Proc Natl Acad Sci U S A 110:E1142-1151.

Quet E, Majchrzak M, Cosquer B, Morvan T, Wolff M, Cassel J-C, Pereira de Vasconcelos A, Stéphan A (2020) The reuniens and rhomboid nuclei are necessary for contextual fear memory persistence in rats. Brain Structure and Function 225:955-968.

Rechtschaffen A, Siegel JM (2000) Sleep and dreaming. In: Principles of Neural Science, 4th edition Edition (Kandell E, Schwartz JH, Jessell TM, eds), pp 936-947. New York: McGraw-Hill.

Rechtschaffen A, Bergmann BM, Everson CA, Kushida CA, Gilliland MA (2002) Sleep deprivation in the rat: X. Integration and discussion of the findings. 1989. Sleep 25:68-87.

Reijmers LG, Perkins BL, Matsuo N, Mayford M (2007) Localization of a stable neural correlate of associative memory. Science 317:1230-1233.

Reitz SL, Kelz MB (2021) Preoptic area modulation of arousal in natural and drug induced unconscious states. Frontiers in Neuroscience 15:644330.

Reitz SL, Wasilczuk AZ, Beh GH, Proekt A, Kelz MB (2021) Activation of preoptic tachykinin 1 neurons promotes wakefulness over sleep and volatile anesthetic-induced unconsciousness. Current Biology 31:394-405. e394.

Ren S et al. (2018) The paraventricular thalamus is a critical thalamic area for wakefulness. Science 362:429-434.

Robinson TE, Kramis RC, Vanderwolf CH (1977) Two types of cerebral activation during active sleep: relations to behavior. Brain Research 124:544-549.

Rodrigues SF, de Oliveira MA, Martins JO, Sannomiya P, de Cássia Tostes R, Nigro D, Carvalho MHC, Fortes ZB (2006) Differential effects of chloral hydrate- and ketamine/xylazine-induced anesthesia by the s.c. route. Life Sciences 79:1630-1637.

Rodriguez AV, Funk CM, Vyazovskiy VV, Nir Y, Tononi G, Cirelli C (2016) Why Does Sleep Slow-Wave Activity Increase After Extended Wake? Assessing the Effects of Increased Cortical Firing During Wake and Sleep. The Journal of Neuroscience 36:12436.

Sallanon M, Denoyer M, Kitahama K, Aubert C, Gay N, Jouvet M (1989) Long-lasting insomnia induced by preoptic neuron lesions and its transient reversal by muscimol injection into the posterior hypothalamus in the cat. Neuroscience 32:669-683.

Sanders RD, Tononi G, Laureys S, Sleigh JW (2012) Unresponsiveness not equal unconsciousness. Anesthesiology 116:946-959.

Saper CB, Fuller PM (2017) Wake-sleep circuitry: an overview. Curr Opin Neurobiol 44:186-192.

Saper CB, Scammell TE, Lu J (2005) Hypothalamic regulation of sleep and circadian rhythms. Nature 437:1257-1263.

Saper CB, Fuller PM, Pedersen NP, Lu J, Scammell TE (2010) Sleep state switching. Neuron 68:1023-1042.

Sapin E, Lapray D, Berod A, Goutagny R, Leger L, Ravassard P, Clement O, Hanriot L, Fort P, Luppi PH (2009) Localization of the brainstem GABAergic neurons controlling paradoxical (REM) sleep. PLoS One 4:e4272.

Saunier CF, Akaoka H, de La Chapelle B, Charlety PJ, Chergui K, Chouvet G, Buda M, Quintin L (1993) Activation of brain noradrenergic neurons during recovery from halothane anesthesia. Persistence of phasic activation after clonidine. Anesthesiology 79:1072-1082.

Sceniak MP, MacIver MB (2006) Cellular actions of urethane on rat visual cortical neurons in vitro. J Neurophysiol 95:3865-3874.

Scharf MT, Kelz MB (2013) Sleep and Anesthesia Interactions: A Pharmacological Appraisal. Curr Anesthesiol Rep 3:1-9.

Selman WR, Spetzler RF, Roessmann UR, Rosenblatt JI, Crumrine RC (1981) Barbiturate-induced coma therapy for focal cerebral ischemia: Effect after temporary and permanent MCA occlusion. Journal of neurosurgery 55:220-226.

Semba K (2000) Multiple output pathways of the basal forebrain: organization, chemical heterogeneity, and roles in vigilance. Behav Brain Res 115:117-141.

Seth AK, Bayne T (2022) Theories of consciousness. Nature Reviews Neuroscience 23:439-452.

Shafer A (1995) Metaphor and anesthesia. Anesthesiology 83:1331-1342.

Sharma AV, Wolansky T, Dickson CT (2010) A comparison of sleeplike slow oscillations in the hippocampus under ketamine and urethane anesthesia. J Neurophysiol 104:932-939.

Sherin JE, Shiromani PJ, McCarley RW, Saper CB (1996) Activation of ventrolateral preoptic neurons during sleep. Science 271:216-219.

Sherin JE, Elmquist JK, Torrealba F, Saper CB (1998) Innervation of histaminergic tuberomammillary neurons by GABAergic and galaninergic neurons in the ventrolateral preoptic nucleus of the rat. J Neurosci 18:4705-4721.

Sheroziya M, Timofeev I (2014) Global Intracellular Slow-Wave Dynamics of the Thalamocortical System. The Journal of Neuroscience 34:8875.

Shi F, Yu T, Fu B, Zhang Y (2017) Involvement of substantia nigra dopaminergic neurons in propofol anesthesia.

Shirasaka T, Yonaha T, Onizuka S, Tsuneyoshi I (2011) Effects of orexin-A on propofol anesthesia in rats. J Anesth 25:65-71.

Shouse MN, Siegel JM (1992) Pontine regulation of REM sleep components in cats: integrity of the pedunculopontine tegmentum (PPT) is important for phasic events but unnecessary for atonia during REM sleep. Brain Res 571:50-63.

Sigl JC, Chamoun NG (1994) An introduction to bispectral analysis for the electroencephalogram. Journal of clinical monitoring 10:392-404.

Silver NRG, Ward-Flanagan R, Dickson CT (2021) Long-term stability of physiological signals within fluctuations of brain state under urethane anesthesia. PLOS ONE 16:e0258939.

Silverman J, Muir WW, 3rd (1993) A review of laboratory animal anesthesia with chloral hydrate and chloralose. Lab Anim Sci 43:210-216.

Simasko SM, Mukherjee S (2009) Novel analysis of sleep patterns in rats separates periods of vigilance cycling from long-duration wake events. Behavioural brain research 196:228-236.

Skrobik Y, Duprey MS, Hill NS, Devlin JW (2018) Low-dose Nocturnal Dexmedetomidine Prevents ICU Delirium: A Randomized, Placebo-controlled Trial. Am J Respir Crit Care Med.

Sotomayor RE, Collins TFX (1990) Mutagenicity, Metabolism, and DNA Interactions of Urethane. Toxicology and Industrial Health 6:71-108.

Staines WA, Daddona PE, Nagy JI (1987) The organization and hypothalamic projections of the tuberomammillary nucleus in the rat: an immunohistochemical study of adenosine deaminase-positive neurons and fibers. Neuroscience 23:571-596.

Steininger TL, Gong H, McGinty D, Szymusiak R (2001) Subregional organization of preoptic area/anterior hypothalamic projections to arousal-related monoaminergic cell groups. J Comp Neurol 429:638-653.

Steininger TL, Alam MN, Gong H, Szymusiak R, McGinty D (1999) Sleep-waking discharge of neurons in the posterior lateral hypothalamus of the albino rat. Brain Res 840:138-147.

Stephenson R, Liao KS, Hamrahi H, Horner RL (2001) Circadian rhythms and sleep have additive effects on respiration in the rat. J Physiol 536:225-235.

Steriade M (2005) Sleep, epilepsy and thalamic reticular inhibitory neurons. Trends Neurosci 28:317-324.

Steriade M, McCarley RW (2005) Brain Stem Control of Wakefulness and Sleep.

Steriade M, Nunez A, Amzica F (1993) A novel slow (< 1 Hz) oscillation of neocortical neurons in vivo: depolarizing and hyperpolarizing components. J Neurosci 13:3252-3265.

Sulaman BA, Wang S, Tyan J, Eban-Rothschild A (2023) Neuro-orchestration of sleep and wakefulness. Nature Neuroscience 26:196-212.

Swank RL, Watson CW (1949) Effects of barbiturates and ether on spontaneous electrical activity of dog brain. Journal of Neurophysiology 12:137-160.

Szymusiak R, Satinoff E (1981) Maximal REM sleep time defines a narrower thermoneutral zone than does minimal metabolic rate. Physiology & behavior 26:687-690.

Szymusiak R, Gvilia I, McGinty D (2007) Hypothalamic control of sleep. Sleep Med 8:291-301.

Szymusiak R, Alam N, Steininger TL, McGinty D (1998) Sleep-waking discharge patterns of ventrolateral preoptic/anterior hypothalamic neurons in rats. Brain Res 803:178-188.

Szyndler J, Maciejak P, Turzynska D, Sobolewska A, Taracha E, Skorzewska A, Lehner M, Bidzinski A, Hamed A, Wislowska-Stanek A, Krzascik P, Plaznik A (2009) Mapping of c-Fos expression in the rat brain during the evolution of pentylenetetrazol-kindled seizures. Epilepsy Behav 16:216-224.

Takahashi K, Lin JS, Sakai K (2006) Neuronal activity of histaminergic tuberomammillary neurons during wake-sleep states in the mouse. J Neurosci 26:10292-10298.

Takahashi K, Lin JS, Sakai K (2009) Characterization and mapping of sleep-waking specific neurons in the basal forebrain and preoptic hypothalamus in mice. Neuroscience 161:269-292.

Taveras EM, Rifas-Shiman SL, Oken E, Gunderson EP, Gillman MW (2008) Short sleep duration in infancy and risk of childhood overweight. Arch Pediatr Adolesc Med 162:305-311.

Taylor NE, Van Dort CJ, Kenny JD, Pei J, Guidera JA, Vlasov KY, Lee JT, Boyden ES, Brown EN, Solt K (2016) Optogenetic activation of dopamine neurons in the ventral tegmental area induces reanimation from general anesthesia. Proc Natl Acad Sci U S A.

Teng S, Zhen F, Wang L, Schalchli JC, Simko J, Chen X, Jin H, Makinson CD, Peng Y (2022) Control of non-REM sleep by ventrolateral medulla glutamatergic neurons projecting to the preoptic area. Nature Communications 13:4748.

Teppema LJ, Baby S (2011) Anesthetics and control of breathing. Respiratory Physiology & Neurobiology 177:80-92.

Thakkar M, Portas C, McCarley RW (1996) Chronic low-amplitude electrical stimulation of the laterodorsal tegmental nucleus of freely moving cats increases REM sleep. Brain Res 723:223-227.

Thakkar MM (2011) Histamine in the regulation of wakefulness. Sleep Med Rev 15:65-74.

Tung A, Mendelson WB (2004) Anesthesia and sleep. Sleep Med Rev 8:213-225.

Tung A, Szafran MJ, Bluhm B, Mendelson WB (2002) Sleep deprivation potentiates the onset and duration of loss of righting reflex induced by propofol and isoflurane. Anesthesiology 97:906-911.

Tung A, Bergmann BM, Herrera S, Cao D, Mendelson WB (2004) Recovery from sleep deprivation occurs during propofol anesthesia. Anesthesiology 100:1419-1426.

Tung A, Herrera S, Szafran MJ, Kasza K, Mendelson WB (2005) Effect of sleep deprivation on righting reflex in the rat is partially reversed by administration of adenosine A1 and A2 receptor antagonists. Anesthesiology 102:1158-1164.

Ushimaru M, Kawaguchi Y (2015) Temporal Structure of Neuronal Activity among Cortical Neuron Subtypes during Slow Oscillations in Anesthetized Rats. The Journal of Neuroscience 35:11988.

Uygun DS, Ye Z, Zecharia AY, Harding EC, Yu X, Yustos R, Vyssotski AL, Brickley SG, Franks NP, Wisden W (2016) Bottom-Up versus Top-Down Induction of Sleep by Zolpidem Acting on Histaminergic and Neocortex Neurons. J Neurosci 36:11171-11184.

Vacas S, Kurien P, Maze M (2013) Sleep and Anesthesia - Common mechanisms of action. Sleep Med Clin 8:1-9.

Vaidyanathan TV, Collard M, Yokoyama S, Reitman ME, Poskanzer KE (2021) Cortical astrocytes independently regulate sleep depth and duration via separate GPCR pathways. eLife 10:e63329.

Van Dort CJ, Zachs DP, Kenny JD, Zheng S, Goldblum RR, Gelwan NA, Ramos DM, Nolan MA, Wang K, Weng FJ, Lin Y, Wilson MA, Brown EN (2015) Optogenetic activation of cholinergic neurons in the PPT or LDT induces REM sleep. Proc Natl Acad Sci U S A 112:584-589.

Van Ness PC (1990) Pentobarbital and EEG burst suppression in treatment of status epilepticus refractory to benzodiazepines and phenytoin. Epilepsia 31:61-67.

Vanini G, Bassana M, Mast M, Mondino A, Cerda I, Phyle M, Chen V, Colmenero AV, Hambrecht-Wiedbusch VS, Mashour GA (2020) Activation of Preoptic GABAergic or Glutamatergic Neurons Modulates Sleep-Wake Architecture, but Not Anesthetic State Transitions. Current Biology 30:779-787.e774.

Vazey EM, Aston-Jones G (2014) Designer receptor manipulations reveal a role of the locus coeruleus noradrenergic system in isoflurane general anesthesia. Proc Natl Acad Sci U S A 111:3859-3864.

Venner A, De Luca R, Sohn LT, Bandaru SS, Verstegen AMJ, Arrigoni E, Fuller PM (2019) An Inhibitory Lateral Hypothalamic-Preoptic Circuit Mediates Rapid Arousals from Sleep. Current Biology 29:4155-4168.e4155.

Vertes RP (1988) Brainstem afferents to the basal forebrain in the rat. Neuroscience 24:907-935.

Vertes RP, Kocsis B (1997) Brainstem-diencephalo-septohippocampal systems controlling the theta rhythm of the hippocampus. Neuroscience 81:893-926.

Viczko J, Sharma AV, Pagliardini S, Wolansky T, Dickson CT (2014) Lack of Respiratory Coupling with Neocortical and Hippocampal Slow Oscillations. The Journal of Neuroscience 34:3937.

von Economo C (1930) Sleep as a problem of localization. The Journal of Nervous and Mental Disease 71:249-259.

Voss LJ, Young BJ, Barnards JP, Sleigh J (2005) Differential anaesthetic effects following microinjection of thiopentone and propofol into the pons of adult rats: a pilot study. Anaesth Intensive Care 33:373-380.

Walczak M, Blasiak T (2017) Midbrain dopaminergic neuron activity across alternating brain states of urethane anaesthetized rat. Eur J Neurosci 45:1068-1077.

Wan X, Mathers DA, Puil E (2003) Pentobarbital modulates intrinsic and GABA-receptor conductances in thalamocortical inhibition. Neuroscience 121:947-958.

Wang Y-L, Wang L, Xu W, He M, Dong H, Shi H-Y, Chen Y-Q, Huang Z-L (2023) Paraventricular thalamus controls consciousness transitions during propofol anaesthesia in mice. British Journal of Anaesthesia.

Ward-Flanagan R, Dickson CT (2019) Neurobiological Parallels, Overlaps, and Divergences of Sleep and Anesthesia. In: Handbook of Behavioral Neuroscience, pp 223-236: Elsevier.

Ward-Flanagan R, Pagliardini S, Dickson CT (2023) Urethane provides an unparalleled anesthetic model for natural sleep: Commentary on Mondino et al, 2022. European Journal of Neuroscience n/a.

Ward-Flanagan R, Lo AS, Clement EA, Dickson CT (2022) A Comparison of Brain-State Dynamics across Common Anesthetic Agents in Male Sprague-Dawley Rats. International Journal of Molecular Sciences 23:3608.

Weber F, Dan Y (2016) Circuit-based interrogation of sleep control. Nature 538:51-59.

Weber F, Hoang Do JP, Chung S, Beier KT, Bikov M, Saffari Doost M, Dan Y (2018a) Regulation of REM and Non-REM Sleep by Periaqueductal GABAergic Neurons. Nature Communications 9:354.

Weber F, Hoang Do JP, Chung S, Beier KT, Bikov M, Saffari Doost M, Dan Y (2018b) Regulation of REM and Non-REM Sleep by Periaqueductal GABAergic Neurons. Nat Commun 9:354.

Weiser TG, Haynes AB, Molina G, Lipsitz SR, Esquivel MM, Uribe-Leitz T, Fu R, Azad T, Chao TE, Berry WR, Gawande AA (2015) Estimate of the global volume of surgery in 2012: an assessment supporting improved health outcomes. Lancet 385 Suppl 2:S11.

Whitten TA, Martz LJ, Guico A, Gervais N, Dickson CT (2009) Heat synch: Inter- and independence of body-temperature fluctuations and brain-state alternations in urethane-anesthetized rats. J Neurophysiol 102:1647-1656.

Wisden W, Yu X, Franks NP (2017) GABA Receptors and the Pharmacology of Sleep. Handb Exp Pharmacol.

Wolansky T, Clement EA, Peters SR, Palczak MA, Dickson CT (2006) Hippocampal slow oscillation: a novel EEG state and its coordination with ongoing neocortical activity. J Neurosci 26:6213-6229.

Xu M, Chung S, Zhang S, Zhong P, Ma C, Chang WC, Weissbourd B, Sakai N, Luo L, Nishino S, Dan Y (2015) Basal forebrain circuit for sleep-wake control. Nat Neurosci 18:1641-1647.

Yang QZ, Hatton GI (1997) Electrophysiology of excitatory and inhibitory afferents to rat histaminergic tuberomammillary nucleus neurons from hypothalamic and forebrain sites. Brain Research 773:162-172.

Yang Y, Lee JT, Guidera JA, Vlasov KY, Pei J, Brown EN, Solt K, Shanechi MM (2019) Developing a personalized closed-loop controller of medically-induced coma in a rodent model. Journal of neural engineering 16:036022.

Yin L, Li L, Deng J, Wang D, Guo Y, Zhang X, Li H, Zhao S, Zhong H, Dong H (2019) Optogenetic/chemogenetic activation of GABAergic neurons in the ventral tegmental area facilitates general anesthesia via projections to the lateral hypothalamus in mice. Frontiers in Neural Circuits 13:73.

Ying SW, Goldstein PA (2005) Propofol suppresses synaptic responsiveness of somatosensory relay neurons to excitatory input by potentiating GABA(A) receptor chloride channels. Mol Pain 1:2.

Ying SW, Werner DF, Homanics GE, Harrison NL, Goldstein PA (2009) Isoflurane modulates excitability in the mouse thalamus via GABA-dependent and GABA-independent mechanisms. Neuropharmacology 56:438-447.

Yoshida K, McCormack S, Espana RA, Crocker A, Scammell TE (2006) Afferents to the orexin neurons of the rat brain. J Comp Neurol 494:845-861.

Yu X, Franks NP, Wisden W (2018) Sleep and Sedative States Induced by Targeting the Histamine and Noradrenergic Systems. Front Neural Circuits 12:4.

Yu X, Li W, Ma Y, Tossell K, Harris JJ, Harding EC, Ba W, Miracca G, Wang D, Li L, Guo J, Chen M, Li Y, Yustos R, Vyssotski AL, Burdakov D, Yang Q, Dong H, Franks NP,

Wisden W (2019) GABA and glutamate neurons in the VTA regulate sleep and wakefulness. Nat Neurosci 22:106-119.

Zaborszky L, Duque A (2000) Local synaptic connections of basal forebrain neurons. Behav Brain Res 115:143-158.

Zaborszky L, Cullinan WE, Braun A (1991) Afferents to basal forebrain cholinergic projection neurons: an update. Adv Exp Med Biol 295:43-100.

Zant JC, Rozov S, Wigren HK, Panula P, Porkka-Heiskanen T (2012) Histamine release in the basal forebrain mediates cortical activation through cholinergic neurons. J Neurosci 32:13244-13254.

Zarhin D, Atsmon R, Ruggiero A, Baeloha H, Shoob S, Scharf O, Heim LR, Buchbinder N, Shinikamin O, Shapira I (2022) Disrupted neural correlates of anesthesia and sleep reveal early circuit dysfunctions in Alzheimer models. Cell Reports 38:110268.

Zecharia AY, Nelson LE, Gent TC, Schumacher M, Jurd R, Rudolph U, Brickley SG, Maze M, Franks NP (2009) The involvement of hypothalamic sleep pathways in general anesthesia: testing the hypothesis using the GABAA receptor beta3N265M knock-in mouse. J Neurosci 29:2177-2187.

Zecharia AY, Yu X, Gotz T, Ye Z, Carr DR, Wulff P, Bettler B, Vyssotski AL, Brickley SG, Franks NP, Wisden W (2012) GABAergic inhibition of histaminergic neurons regulates active waking but not the sleep-wake switch or propofol-induced loss of consciousness. J Neurosci 32:13062-13075.

Zeng T, Mott C, Mollicone D, Sanford LD (2012) Automated determination of wakefulness and sleep in rats based on non-invasively acquired measures of movement and respiratory activity. Journal of Neuroscience Methods 204:276-287.

Zhang LN, Li ZJ, Tong L, Guo C, Niu JY, Hou WG, Dong HL (2012) Orexin-A facilitates emergence from propofol anesthesia in the rat. Anesth Analg 115:789-796.

Zhang Z, Ferretti V, Guntan I, Moro A, Steinberg EA, Ye Z, Zecharia AY, Yu X, Vyssotski AL, Brickley SG, Yustos R, Pillidge ZE, Harding EC, Wisden W, Franks NP (2015) Neuronal ensembles sufficient for recovery sleep and the sedative actions of alpha2 adrenergic agonists. Nat Neurosci 18:553-561.

Zhong P, Zhang Z, Barger Z, Ma C, Liu D, Ding X, Dan Y (2019) Control of Non-REM Sleep by Midbrain Neurotensinergic Neurons. Neuron 104:795-809 e796.

Zhou F, Wang D, Li H, Wang S, Zhang X, Li A, Tong T, Zhong H, Yang Q, Dong H (2023) Orexinergic innervations at GABAergic neurons of the lateral habenula mediates the anesthetic potency of sevoflurane. CNS Neuroscience & Therapeutics 29:1332-1344.

Zhou X, Wang Y, Zhang C, Wang M, Zhang M, Yu L, Yan M (2015) The Role of Dopaminergic VTA Neurons in General Anesthesia. PLoS One 10:e0138187.